The modulation of autophagy by African swine fever virus

Gareth Shimmon

Thesis submitted in partial fulfilment of the requirements for the degree of Doctor of Philosophy

University of East Anglia

Norwich Medical School

Faculty of Medicine and Health Sciences

September 2019

Abstract

African swine fever (ASF) is a lethal haemorrhagic disease of domestic pigs caused by infection with African swine fever virus (ASFV). An outbreak in Russia in 2007 has since advanced into Europe and the Far East. With the spread of ASF expected to continue, the requirement for effective vaccines has become critical. The prospects for vaccine development are promising as infection with attenuated strains of ASFV can offer protection against closely related virulent strains.

Autophagy is an essential cell process that sequesters cytoplasmic cargo into double-membrane vesicles called autophagosomes for degradation via lysosomes. Autophagy regulates multiple pathways that are vital to mounting an effective immune response and viruses specifically target this pathway for modulation. Experiments have shown that inhibiting the ability of viruses to regulate autophagy can lead to enhanced immune responses. The work in this thesis shows that autophagy is actively inhibited by ASFV and is not required for virus replication. Further investigation revealed that ASFV activates Akt and mTORC1 which causes a block in autophagosome assembly. Pharmacological studies show that autophagy can be induced during the very early stages of viral replication but at later times, additional measures of modulation are implemented, most likely via virally encoded genes.

ASFV encodes A179L which binds to the key autophagy protein Beclin 1 leading to the inhibition of autophagosome formation. However, this work has demonstrated that additional protein modulators are also encoded. A gene library screen was conducted to identify these and unexpectedly, the results showed that some ASFV genes are able to stimulate elements of the autophagy pathway which was investigated further.

This research will expand our understanding of the interaction between ASFV and the autophagy pathway with the potential that a low virulent ASFV strain with an altered ability to modulate autophagy will provide enhanced immunity against virulent isolates.

Nothing in the world can take the place of persistence.

Talent will not; nothing is more common than unsuccessful men with talent.

Genius will not; unrewarded genius is almost a proverb.

Education will not; the world is full of educated derelicts.

Persistence and determination alone are omnipotent.

- *Calvin Coolidge*

Table of Contents

List of Figures

List of Tables

List of Appendices

Declaration of Authorship

I certify that the work contained in the thesis submitted by me for the degree of Doctor of Philosophy is my original work except where due reference is made to other authors, and has not been previously submitted by me for a degree at this or any other university.

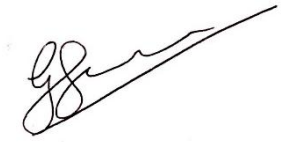

Gareth Shimmon

Acknowledgements

My gratitude is first and foremost given to my primary supervisor Dr Chris Netherton for his unwavering support, guidance and seemingly infinite patience throughout my PhD. During the numerous times I believed the project was ‘stuck’, Chris helped me to find an alternative way. I also appreciate all of the DIY advice along with our many shady car park dealings. I would like to thank my university supervisor Professor Tom Wileman who always provided a fresh perspective on the project and reminded me not to drown in the detail. Thank you to the ASF and ASF Vaccinology groups for providing feedback, advice, reagents and some laughs along the way.

My thanks also go to the bio-imaging department for the help that Dr Pippa Hawes provided with all things microscopy related and the endless times Jenny ‘magic fingers’ Simpson managed to fix the confocal microscope. I would also like to thank Jenny for her tea and lunchtime companionship where we were able to discuss the real things that matter in life such as scrunchers and folders.

I would like to extend a special thank you to my science and life mentor, Professor Terry Jackson who gave me the opportunity to start my science career. Little did you know that you had hired an employee for life. I look forward to continuing our science partnership in the field of homebrewing.

My sincerest gratitude also goes to my friends Dr Tim Harvey-Samuel and 2Lt Tom Nicholson for the unhealthy amounts of meat that we consumed and the epic weekends away in the Welsh rain. Tim provided a constant reminder that ‘none of this matters anyway’ and Tom embodied the notion that there is so much more to life than being in the lab.

I would like to thank my family for their support, particularly my parents who sacrificed so much to ensure that I received the best possible education and encouraged me to never shy away from my goals.

My greatest thanks go to Grace for your love, support and advice throughout the project. I apologise for the several occasions that the seemingly endless series of failed experiments led to anger, frustration and sadness. It remains questionable whether I would have a thesis to hand in without your encouragement. I am truly grateful.

Abbreviations

µg	Microgram
µl	Microlitre
µm	Micrometer
µM	Micromolar
× g	Centrifugal force
°C	Degrees Celsius
3-MA	3-methyladenine
4E-BP1	4E-binding protein 1
AdH5	Adenovirus human type 5
AMPK	5' AMP-activated protein kinase
ANOVA	Analysis of variance
ASF	African swine fever
ASFV	African swine fever virus
Atg	Autophagy-related gene
ATP	Adenosine triphosphate
Bcl-2	B-cell lymphoma 2
CD	Clusters of differentiation
CHOP	C/EBP homologous protein
CLEM	Correlative light electron microscopy
Cnx	Calnexin
CPE	Cytopathic effect
DAMP	Damage-associated molecular pattern
DAPI	4′,6-diamidino-2-phenylindole
DENV	Dengue virus
DMEM	Dulbecco's modified eagle's medium
DMSO	Dimethyl sulfoxide
DNA	Deoxyribonucleic acid
dNTP	Deoxynucleoside triphosphate
EBSS	Earle's balanced salt solution
EDTA	Ethylenediaminetetraacetic acid
EIF	Eukaryotic initiation factor

EM	Electron microscopy
ER	Endoplasmic reticulum
FCS	Foetal calf serum
GABARAP	γ-aminobutyric acid receptor-associated protein
GFP	Green fluorescent protein
HA	Human influenza hemagglutinin
HCMV	Human cytomegalovirus
HEPES	4-(2-hydroxyethyl)-1-piperazineethanesulfonic acid
HIV	Human immunodeficiency virus
HPI	Hours post-infection
HRP	Horseradish peroxidase
HSV	Herpes simplex virus
IAV	Influenza A virus
IBV	Infectious bronchitis virus
IF	Immunofluorescence
IFN	Interferon
IL	Interleukin
IP	Immunoprecipitation
ISG	Interferon-stimulated gene
JEV	Japanese encephalitis virus
KO	Knock-out
LAMP	Lysosome-associated membrane glycoprotein
LAP	LC3-associated phagocytosis
LB	Luria broth
LC3	Short for MAP1LC3
LC3-I	Non-lipidated LC3
LC3-II	Lipidated LC3
LIR	LC3-interacting region
MAP1LC3	Microtubule-associated protein 1 light chain 3
MEF	Mouse embryo fibroblasts
MES	2-ethanesulfonic acid
MGF	Multigene family

MHC	Major histocompatibility complex
MHV	Mouse hepatitis virus
ml	Millilitre
mm	Millimeter
mM	Millimolar
MOI	Multiplicity of infection
MOPS	3-(N-morpholino)propanesulfonic acid
MS	Mass spectrometry
MTOC	Microtubule-organizing centre
mTOR	Mammalian target of rapamycin
mTORC1	Mammalian target of rapamycin complex 1
ng	Nanogram
nM	Nanomolar
ORF	Open reading frame
p70-S6K	Ribosomal protein S6 kinase beta-1
PAGE	Polyacrylamide gel electrophoresis
PAMP	Pathogen-associated molecular pattern
PAS	Pre-autophagosomal structure
PBS	Phosphate-buffered saline
PCR	Polymerase chain reaction
PDI	Protein disulfide-isomerase
PDK1	Phosphoinositide-dependent protein kinase 1
PE	Phosphatidylethanolamine
PFA	Paraformaldehyde
PI3K	Phosphoinositide 3-kinase
PKB/Akt	Protein kinase B
PKR	Protein kinase R
PRR	Pattern recognition receptors
PTDINS3P	Phosphatidylinositol 3-phosphate
PTEN	Phosphatase and tensin homolog
PV	Poliovirus
PVDF	Polyvinylidene fluoride

Rab	Ras-related protein
RNA	Ribonucleic acid
RPM	Revolutions per minute
RTK	Receptor tyrosine kinases
SDS	Sodium dodecyl sulfate
SOC	Super Optimal broth
SQSTM1	Sequestosome 1 (p62)
TBK1	TANK-binding kinase 1
TBS	Tris-buffered saline
TE	Tris-EDTA
TEM	Transmission electron microscopy
TFA	Trifluoroacetic
TIR	Tandem inverted repeat
TLR	Toll-like receptor
TNF	Tumour necrosis factor
TOR	Target of rapamycin
TSC2	Tuberous sclerosis complex 2
TVA	Tubulovesicular autophagosomes
ULK	Uncoordinated 51-like kinase
UPR	Unfolded protein response
VACV	Vaccinia virus
Vps34	Vacuolar protein sorting 34
WB	Western blot
WIPI	WD-repeat protein interacting with phosphoinositides
WT	Wild-type

1 Introduction

1.1 African swine fever

African swine fever (ASF) is an infectious disease of domestic pigs and wild boar. ASF can inflict severe economic losses due not only to livestock mortality but also to the enforcement of trade restrictions. Efforts to control the disease are challenging owing in part to its complex epidemiology. This has contributed to significant spread of ASF in sub-Saharan Africa, Europe and Asia. With the likelihood that the distribution of ASF will expand, the importance of conducting fundamental research on its biology is paramount.

1.1.1 Historical perspectives

ASF was provisionally identified in Kenya by RE. Montgomery in 1910, and first published later in 1921 (Montgomery, 1921). Montgomery noted that in most disease cases the presence of wild pig, chiefly the warthog (*Phacochoerus spp*) was known in the vicinity of affected farms. In describing the severity of the disease, he wrote, "…as available statistics show, an owner, should his herd contract infection, must be prepared for a practically total loss…" In addition, Montgomery determined that ASF was caused by a virus – African swine fever virus (ASFV). Work conducted in South Africa a few years later confirmed Montgomery's findings and proved that warthogs and bushpigs (*Potamochoerus spp*) were a reservoir for the virus (Plowright, 1986). Not long after, it was discovered that employing a strict stamping out policy was an effective control measure which led to the eradication of the disease from Cape Province in South Africa by 1939 (Pini and Hurter, 1975).

Although it was widely accepted that warthogs and bushpigs were the most likely culprits responsible for the emergence of disease in domestic pigs, it was also known that contact between domestic and wild pig populations was rare. Furthermore, experiments aimed at transmitting the virus from infected warthogs to the domestic host had not been successful (Parker et al., 1969). Major breakthroughs came in 1963 when ASFV was detected in a tick (*Ornithodoros erraticus*) in Spain (Sanchez-Botija, 1963) and in 1969 when Plowright and colleagues isolated ASFV from ticks (*Ornithodoros moubata*) that inhabited the burrows of warthogs (Plowright et al., 1969). Following these initial discoveries, it was determined that ASFV replicated in the tick (Plowright et al., 1970b), that both transovarial and sexual transmission of ASFV in ticks was possible (Plowright et al., 1974, Plowright et al., 1970a) and that infected ticks could transmit the disease to domestic pigs under experimental conditions (Plowright et al., 1970b). Additionally, it was proposed that ticks could harbour the virus for life and serve as a long term reservoir without repeated exposure to a viraemic host (Plowright et al., 1970b). This not only provided an explanation for the mechanism behind transfer of virus from the wild pig to its domestic counterpart but also served to explain how the disease suddenly re-appeared in regions that had since been declared free from disease.

1.1.2 Distribution and impact

ASF remains endemic in most of sub-Saharan Africa. The first spread of ASF outside of Africa occurred in 1957 when waste from airline flights was fed to pigs located near Lisbon airport (Boinas et al., 2011). Although the disease was rapidly eradicated, its re-introduction into Portugal in 1960 preceded a 30-year period of outbreaks within the Iberian Peninsula (Costard et al., 2009). In Sardinia, the disease has remained endemic since 1978 (EFSA, 2010). ASF was also reported in The Americas in the 1960's, however was eradicated during the 1980's (Sanchez-Vizcaino et al., 2012). In April 2007, ASF emerged in the Caucasus region near the port of Poti on the Black Sea (Rowlands et al., 2008). Believed to have been introduced through infected meat products transported on international ships, the disease has since spread into the Russian Federation, China, Vietnam, Laos, Mongolia and much of Eastern Europe. ASF was detected for the first time in Western Europe in September 2018 in wild boar located in Belgium. Figure 1.1 shows the distribution of ASF outbreaks as reported by the World Organisation for Animal Health (OIE).

At least twenty-two distinct genotypes of ASF have been defined, each of which are not uniformly geographically distributed (Dixon et al., 2013). Genotype I comprises viruses sampled from Europe, South America, the Caribbean and West Africa. Analysis revealed that it was virus belonging to genotype I that spread from Africa to Portugal in 1957 and 1960 (Bastos et al., 2003). Virus introduced to the Caucasus in 2007 belongs to genotype II which circulates in south-eastern Africa (Rowlands et al., 2008).

ASF is considered one of the most important diseases of swine due to the severe socioeconomic consequences of an outbreak. Depending on the infecting strain, mortality rates can be as high as 100% (Hubalek et al., 2014). An estimated 296 000 pigs were destroyed in the North Caucasus and Russian Federation between 2007 and 2012 as part of disease control measures (Gogin et al., 2013) and in Vietnam more than 1.2 million pigs, 4% of the national herd, have now died or been killed (Normile, 2019). Due to their complex nature, eradication programs are costly. An estimated $92 million was spent by the Spanish authorities during the final five years alone of an eradication program that lasted ten years (Arias and Sánchez-Vizcaíno, 2002a, Arias and Sánchez-Vizcaíno, 2002b). ASF is an OIE notifiable disease and as such, countries experiencing an outbreak or countries considered to be ASF endemic are subject to trade restrictions on swine and swine products. Countries that are free from ASF take significant precautions against introducing the disease. Many countries in Africa, Eastern Europe and Asia have a high proportion of small-scale and subsistence farmers whose livelihoods depend on the sale and consumption of products from tiny herds. The death or destruction of their animals, in most cases in the absence of financial compensation, is particularly devastating.

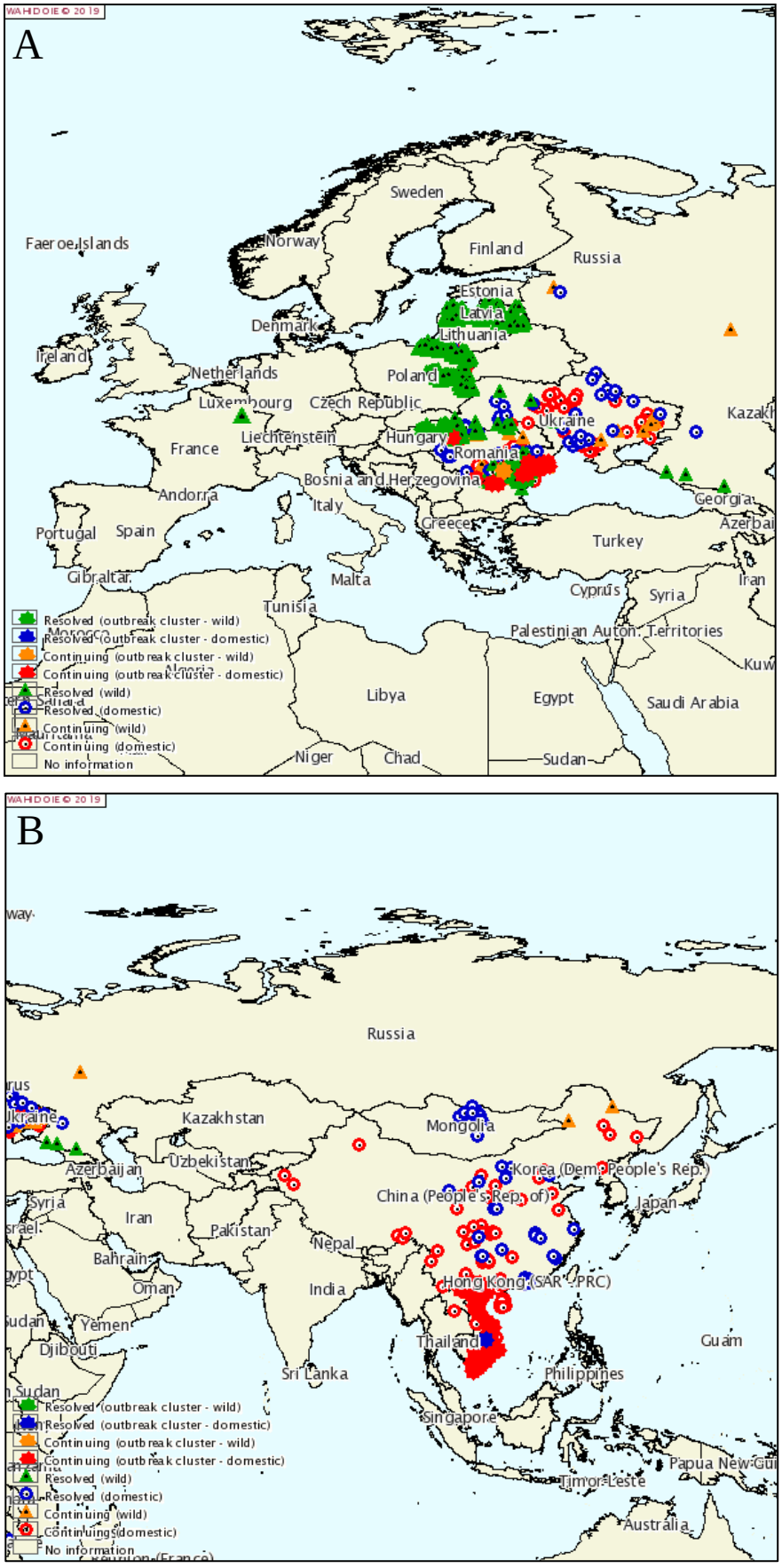

Figure 1.1 Distribution of ASF outbreaks

Distribution of ASF outbreaks reported to the OIE in Europe (Panel A) and Asia (Panel B) from January to July 2019. (Obtained from www.oie.int/)

1.1.3 Clinical features

The incubation period, clinical presentations and pathological findings of ASF vary significantly depending on the infecting virus strain, the route and dose of infection as well as host characteristics (Sanchez-Vizcaino et al., 2015). ASFV is classified according to virulence. In general, highly virulent strains cause the peracute and acute forms of ASF while moderately virulent strains lead to the acute and sub-acute forms. In addition, chronic forms are usually caused from moderate-to-low virulent strains. The acute form has an incubation period of 3-4 days but in other forms of ASF this can be up to 20 days (Sanchez-Vizcaino et al., 2015). Typical haemorrhagic clinical signs of the peracute and acute forms of ASF have led to its description as a haemorrhagic disease. Haemorrhaging can be widespread including petechiae, epistaxis and lesions of lymphoid and non-lymphoid organs (Rodriguez et al., 1996). Other presentations of disease seen in the chronic and aclinical forms have been described that exclude this characteristic feature. In fact, in most cases non-specific clinical signs are seen such as loss of appetite, vomiting, diarrhoea, depression, huddling and fever (Sanchez-Vizcaino et al., 2015). Duration of illness varies considerably with subacute forms lasting 5-30 days. Chronic forms can develop over 15 months in some cases. As ASF is clinically similar to other diseases such as classical swine fever and salmonellosis, laboratory testing is essential for definitive diagnosis. In warthogs and bushpigs, a transient viraemia is detected but these animals do not show any clinical disease (Jori and Bastos, 2009).

1.1.4 Transmission and pathogenesis

In domestic populations, ASF is mainly spread via the oro-nasal route. Transmission can also occur by consumption of contaminated material such as swill, by contact with materials and fomites contaminated with the excreta from infected animals and by bites from infected ticks (Guinat et al., 2016). Infected pigs may shed virus up to 48 hours before the onset of clinical signs (Penrith and Vosloo, 2009). One study has reported the mechanical transmission of ASF by large biting flies experimentally (Mellor et al., 1987) but there have been no reports of this in the field. Airborne transmission is possible but over very short distances and is likely to only be a problem in intensive farming units (Wilkinson et al., 1977). There is no reliable evidence pointing to trans-placental transmission. Recent research has shown that recovered pigs were able to transmit the virus to susceptible populations three months after infection, suggesting a role for carrier animals in the maintenance of disease in endemic regions (Gallardo et al., 2015).

In the vertebrate host, ASFV predominantly infects monocytes and macrophages (Gomez-Villamandos et al., 2013), however in later stages of disease several other cell types including lymphocytes and neutrophils can also be infected (Carrasco et al., 1996a, Carrasco et al., 1996b). In the case of oro-nasal transmission, primary infection occurs in monocytes and macrophages of the tonsils and mandibular lymph nodes (Greig, 1972). From there, it spreads to target organs via the

blood and draining lymph nodes. As the principal sites of secondary replication, this includes bone marrow, liver, lungs, spleen, kidneys and lymphatic tissue (Blome et al., 2013). Upon infection, several macrophage subpopulations demonstrate secretory and phagocytic activation. This leads to a dramatic increase in pro-inflammatory cytokine release, in particular IL-1, IL-6 and TNF-α which coincides with fever and vascular damage (Salguero et al., 2002). Indeed, it is generally accepted that haemorrhagic lesions result from cytokine interactions rather than by virus-induced cell damage (Blome et al., 2013).

1.1.5 Control of ASF

ASF is regarded as one of the most complex infectious diseases of swine. The fact that ASF exists in an ancient sylvatic cycle means that the virus is maintained in regions in which warthogs and ticks co-exist. Therefore, preventing the spread of disease into domestic pig populations is centred on eliminating contact with wild suids and the ticks in contact with them. In regions with wild boar populations such as Europe, additional considerations need to be made on the potential for comparatively long distance disease dissemination. In fact the recent spread of ASF into domestic pigs in the Russian Federation is attributed to direct contact between wild boar and free-ranging pigs (Gogin et al., 2013). In addition, ASFV is remarkably stable in protein environments, consequently virus has been detected in a number of meat products (McKercher et al., 1978). Collectively, these factors contribute to making the control of ASF a challenging task.

Effective control of ASF can however be achieved through a combination of slaughter, quarantine and stringent biosecurity measures. For example, this can include limiting the movement of vehicles and people between premises and banning the feeding of swill to livestock. These and other strict sanitary measures were instrumental in the eradication of ASF from Spain in 1995 (Arias and Sánchez-Vizcaíno, 2002b). Currently, there is no commercial ASF vaccine available although many researchers consider the prospects for vaccine development to be promising. While inactivated virus does not confer protection (Blome et al., 2014), low virulent strains can provide a degree of protection against closely related virulent strains (King et al., 2011, Leitao et al., 2001). In the past, a number of vaccine strategies have been tested including the use of live-attenuated vaccines (O'Donnell et al., 2015, Reis et al., 2016) and several types of subunit vaccine (Argilaguet et al., 2012, Ivanov et al., 2011, Neilan et al., 2004, Netherton et al., 2019). While many of these candidate vaccines have shown potential, none have advanced to commercial production. This is partly due to a lack of complete understanding of the required elements for immune protection in the host.

The role of antibodies in protection against ASF is keenly debated (Escribano et al., 2013). Research has shown that neutralisation of virulent isolates can be achieved in vitro using convalescent pig serum or monoclonal antibodies raised against neutralizing epitopes (Borca et al., 1994, Zsak et al., 1993). However, exploiting this as a means of immunity in the in vivo setting has

not been reliably demonstrated (Barderas et al., 2001, Neilan et al., 2004, Onisk et al., 1994). This would indicate that taken in isolation, the humoral response is not sufficient to confer protection. Indeed, the cellular immune response including natural killer cells and cytotoxic T lymphocytes has been shown to be undoubtedly important (Oura et al., 2005, Takamatsu et al., 2013).

1.2 African swine fever virus

1.2.1 Classification

ASFV was initially classified as a myxovirus (Andrewes, 1963, Breese and DeBoer, 1966) then later, based on the icosahedral morphology of the capsid, reclassified as a member of the Iridoviridae (Kelly and Robertson, 1973). However, further research revealed that in several important aspects such as genome structure, ASFV more closely resembled poxviruses (Dixon, 1986). In 2001 the virus was reclassified for a second time as the only known member of the family Asfarviridae in the genus Asfivirus (Fauquet and Mayo, 2001). The Asfarviridae family belongs to the nucleo-cytoplasmic large DNA virus super-family (NCLDV) which also includes Poxviridae, Iridoviridae, Phycodnaviridae, Mimiviridae and other giant virus families (Iyer et al., 2006). Phylogenetic analysis reveals that ASFV is located in a distinct clade between the Poxviridae and Iridoviridae (Raoult et al., 2004).

At present, ASFV is the only known true DNA arbovirus. Despite some evidence for the role of Ixodid ticks in the transmission of lumpy skin disease virus (Tuppurainen et al., 2013, Tuppurainen et al., 2011), replication within the tick host is yet to be demonstrated (Tuppurainen et al., 2015).

1.2.2 Morphology

The ASFV virion is icosahedral in shape and approximately 200 nm in diameter (Breese and DeBoer, 1966, Carrascosa et al., 1984). The triangulation number of the capsid is 189-217, corresponding to 1892-2172 capsomers (Carrascosa et al., 1984). The virion comprises at least 68 proteins arranged into four concentric domains, named as the nucleoid; matrix/core; inner envelope and capsid (Alejo et al., 2018, Salas and Andres, 2013). Additionally, each virion acquires an external envelope upon budding through the plasma membrane (Breese and DeBoer, 1966). Figure 1.2 depicts a graphical representation of the ASFV virion structure.

The B646L gene product p72 is considered the major capsid protein and constitutes one third of the virion mass (Andres et al., 1997). Beneath the protein capsid lies the inner lipid membrane. Initially this was believed to be a double membrane (Andres et al., 1998, Rouiller et al., 1998) however, using a novel method of sample preparation for electron microscopy, Hawes and colleagues showed a single lipid bilayer formed from the collapse of the endoplasmic reticulum (ER) cisternae (Hawes et al., 2008). Another structural protein - p54 (J13L) is present within the inner envelope and is thought to be an important factor in the mechanism of ER collapse (Windsor et al., 2012). The protein products from the cleavage of two polyproteins – pp220 and pp62, form a protein layer

approximately 30 nm in size referred to as the matrix/core shell. Collectively, these protein products account for 32% of the virion mass (Andres et al., 2002). Cleavage of the polyproteins is carried out by the viral protease – pS273R, also located in the matrix/core shell (Andres et al., 2001a). The nucleoid is a dense region of approximately 80 nm in size and contains the viral genome (Andres et al., 1997), nucleoproteins and transcriptional machinery including RNA polymerase and early transcription factors (Salas and Andres, 2013).

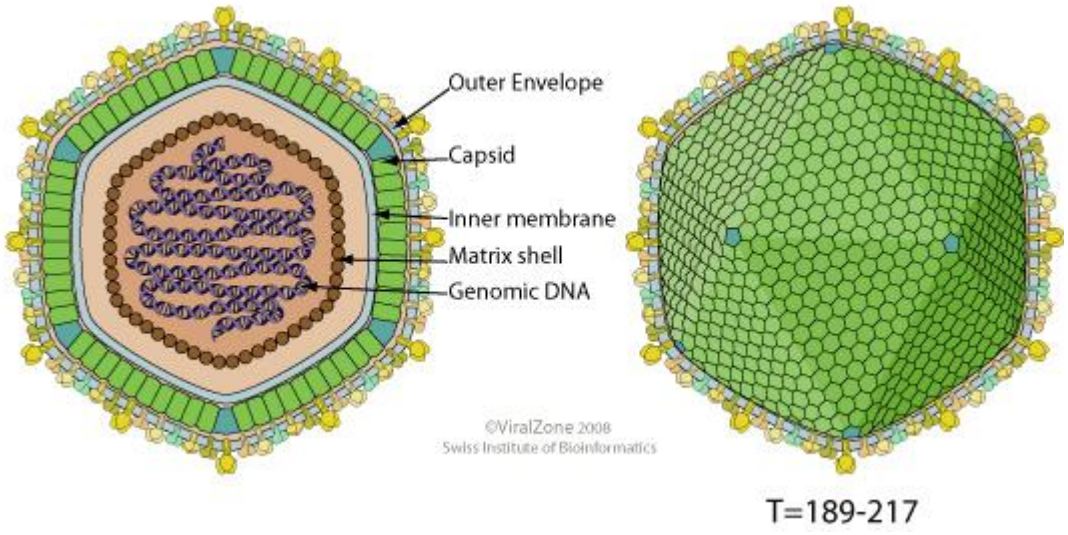

Figure 1.2 Virion structure of ASFV

Image displays the morphology of the ASFV virion - approximately 200 nm in diameter. Arranged into four concentric domains, starting from the centre - the nucleoid containing the condensed viral DNA; the matrix/core shell; the inner membrane derived from the ER; the p72 capsid and finally the outer envelope acquired from budding through the plasma membrane. The triangulation number of the icosahedral capsid is 189-217, corresponding to 1892-2172 capsomers. Obtained from ViralZone, Swiss Institute of Bioinformatics (ViralZone, 2019).

1.2.3 Genome organisation

The ASFV genome comprises a single linear, double-stranded AT rich DNA molecule that varies in length from approximately 170 to 193 kbp depending on the virus isolate (Chapman et al., 2008, de Villiers et al., 2010, Yanez et al., 1995). Between 151 and 167 closely spaced open reading frames (ORFs) are encoded in both directions (Yanez et al., 1995). The majority of these genes have no known or predicted function at present (Chapman et al., 2008). In similarity to poxvirus DNA, the ends of the ASFV genome contain hairpin loops which are inverted and complimentary to each other (Goebel et al., 1990, Gonzalez et al., 1986). In further resemblance to poxviruses, these hairpin loops are adjacent to tandem inverted repeats (TIR) (Sogo et al., 1984, Yanez et al., 1995). The dissimilarity in genome length between ASFV isolates can be due to variation in the number of TIRs (Blasco et al., 1989, Dixon et al., 1990) however, variation is predominantly due to the loss or gain of members of the five multigene families (MGFs); MGF 100, 110, 300, 360 and

505/530 which are positioned towards the terminal ends of the genome (Chapman et al., 2008, de la Vega et al., 1990, Portugal et al., 2015). In addition, some genes that do not belong to MGFs such as DP96R and E66L demonstrate a variable isolate-specific presence. These two genes are present in Ba71V but not Malawi Lil20/1 (Yanez et al., 1995). Some genes such as DP71L can exist as a long form (184AA) or a short form (71AA) which also contributes to changes in genome length (Goatley et al., 1999). The presence or absence of members of MGF360 and MGF505/530 significantly influences the observed differences in pathogenicity between isolates (Neilan et al., 2002, Portugal et al., 2015).

1.2.4 Replication and infection cycle

Viral replication of ASFV is a highly orchestrated process. ASFV displays a tropism for cells of the monocyte-macrophage lineage both in vivo and in vitro (Fernandez et al., 1992, Malmquist and Hay, 1960). In order to initiate an infection, viruses are required to bind to the surface of a target cell, transverse the plasma membrane and gain entry to the relevant cell compartment to begin replication. Receptor-mediated endocytosis is believed to be a major route of entry for ASFV (Alcami et al., 1989), however the precise receptor(s) used are yet to be determined. Work conducted by Galindo and colleagues pointed to proteins as the major class of receptor as opposed to lipids or carbohydrates (Galindo et al., 1997). Other studies have linked cell permissiveness with the presence of specific cell surface markers, including CD203a+ (McCullough et al., 1999); porcine CD163 (Sanchez-Torres et al., 2003) and CD45 and MHCII (Lithgow et al., 2014). While these molecules may have a role as receptors, it remains unknown if they are essential for infection.

One of multiple investigations into the entry of ASFV has revealed a dependence on dynamin and presents clathrin-mediated endocytosis as the most likely entry mechanism (Hernaez and Alonso, 2010). In contrast, ASFV infection was impaired following treatment of cells with a sodium/proton exchange inhibitor which is regarded as a hallmark of macropinocytosis (Sanchez et al., 2012). Further to this, work carried out by Basta and colleagues implicated phagocytosis as the primary means of ASFV entry into macrophages (Basta et al., 2010). Following these studies there has been no conclusive evidence to exclusively support one hypothesis over another although a recent investigation concluded that ASFV uses both clathrin-mediated endocytosis and macropinocytosis (Hernaez et al., 2016). Hernaez and colleagues found that macropinocytosis was not specifically stimulated by the virus suggesting that internalisation of the virus via this route was more likely the result of constitutive sampling of the environment by the cell.

Despite the existence of multiple theories on virus entry, it is believed that only virus which enters the endocytic pathway results in a productive infection as intraluminal acidification of endosomes is essential for virus un-coating (Cuesta-Geijo et al., 2012). Similarly, a loss of integrity of the endocytic pathway, inhibiting the maturation of early endosomes into late endosomes results in reduced infectivity (Cuesta-Geijo et al., 2012). After capsid un-coating the viral inner membrane

fuses with the endosomal membrane and delivers the viral core particle into the cytosol (Hernaez et al., 2016).

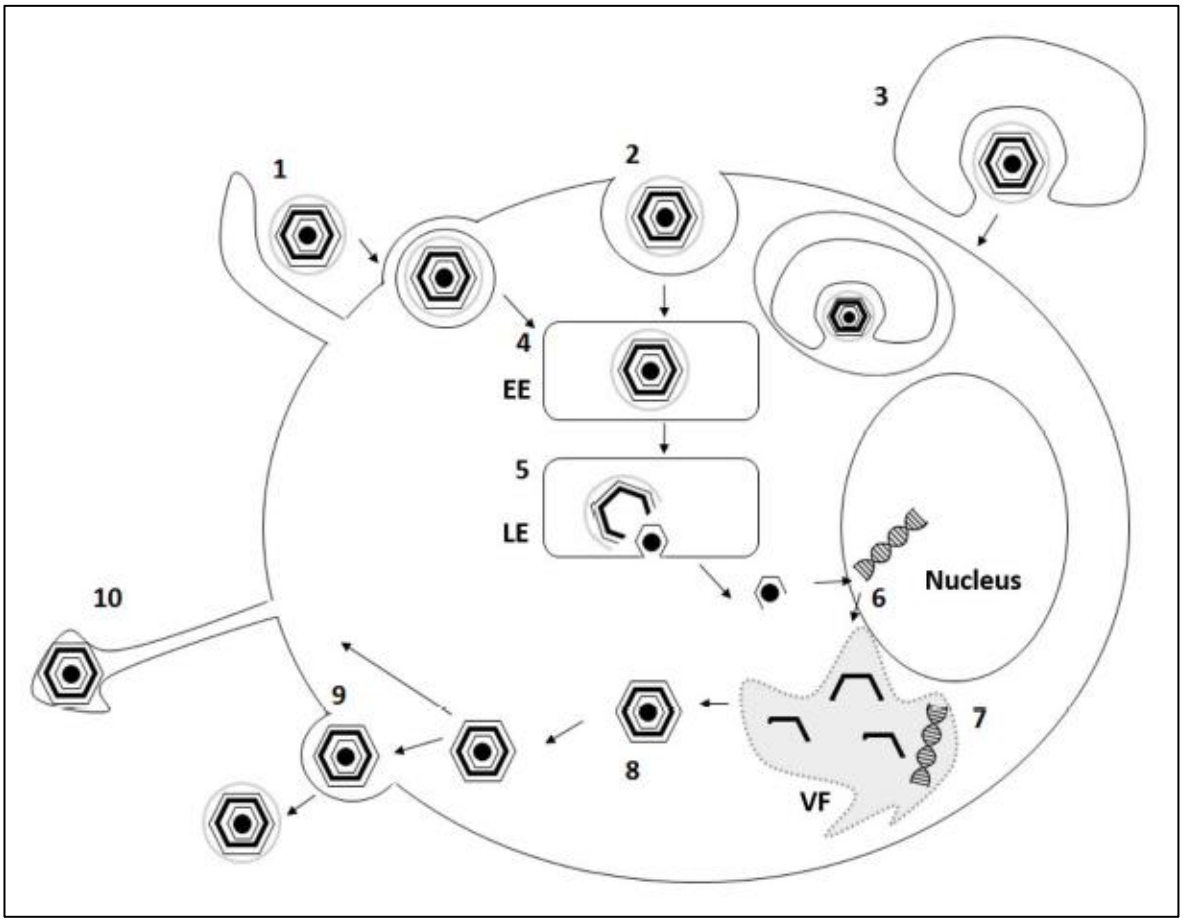

Figure 1.3 ASFV replication cycle

ASFV enters susceptible host cells by (1) macropinocytosis, (2) clathrin mediated endocytosis or (3) phagocytosis and enters the early endosome (EE) (4). Maturation of the early endosome produces the late endosome (LE) (5) where dis-encapsidation occurs followed by release of the partially uncoated core particle by fusion of the inner membrane and endosomal membrane. Early transcription begins in the partially uncoated core whilst the initial phase of DNA replication occurs in the nucleus (6). Later in infection, replication and assembly of the virion occurs in the virus factory (VF) (7). Fully assembled virus particles are transported to the cell surface along microtubules (8) and are released either by budding (9) or travelling along actin projections (10). (Obtained from Dr Claire Barber, (Barber, 2015))

Following release into the cytosol, the core relocates to within close proximity of the microtubule organising centre (MTOC) in the perinuclear region (Hernaez et al., 2006). This relies on the interaction between the structural protein p54 and dynein motor proteins to facilitate transport along the microtubule network (Alonso et al., 2001). Viral DNA replication occurs in two phases. The first is a nuclear phase which produces short DNA fragments which can be seen budding into the cytoplasm (Garcia-Beato et al., 1992). The second phase is cytoplasmic resulting in longer DNA fragments which are the precursor molecules of mature viral DNA (Rojo et al., 1999).

Production of genomic DNA occurs in a similar manner to poxviruses through the formation of head to head concatemeric subunits which are then resolved into units of genomic length (Moss, 2013, Rojo et al., 1999). The exact purpose of the nuclear phase of replication remains unclear. Destabilisation of the nuclear membrane is a bystander effect which may aid access to the host RNA polymerase II which is inactivated and degraded by the virus (Ballester et al., 2011).

ASFV gene expression is divided into distinct phases of transcription in the viral replication cycle (Rodriguez and Salas, 2013). Genes are classified as immediate-early, early, intermediate and late. The classes are based on experimental conditions rather than time per se. Immediate-early transcripts are synthesised in the presence of cycloheximide and so do not require protein synthesis. Early transcripts are not sensitive to DNA synthesis inhibitors whereas both intermediate and late are. Transcription and DNA replication are closely co-ordinated with a decline in early gene expression observed at the onset of DNA replication (Rodriguez and Salas, 2013) although there are two types of early transcripts, those that are turned off after DNA replication begins and those that are not. The ASFV virion contains sufficient transcriptional machinery, thought to be at least 20 genes, to synthesise mature transcripts with transcription commencing at AT rich promotor sequences upstream of each gene (Rodriguez and Salas, 2013). In contrast, ASFV is entirely reliant on the host translational machinery for viral protein production as is the case for most viruses. Infection leads to increased assembly of the host translation complex EIF4F (Castello et al., 2009). Interestingly, the virus has developed strategies to favour the synthesis of viral proteins for example by impairing the nuclear export of cellular mRNA's (Castello et al., 2009). ASFV also encodes a gene (DP71L) that ensures global protein synthesis is maintained in the face of cellular innate immune responses by dephosphorylating EIF2α (Zhang et al., 2010).

Assembly of virions takes place in structures called virus factories located close to the MTOC and first observed in the cell at 8 hpi (Brookes et al., 1996). The microtubule network has a significant role in the formation of these structures by facilitating the transport of various essential components (Rojo et al., 1998, Stefanovic et al., 2005). Each viral factory consists of structural proteins, viral membranes, immature and mature virions and viral DNA enclosed in a vimentin cage (Cobbold et al., 1996, Rouiller et al., 1998, Stefanovic et al., 2005). To the periphery are an abundant number of mitochondria (Rojo et al., 1998). Also recruited to the viral factories is EIF4F and other elements of the host translation machinery (Castello et al., 2009). In the absence of p54, viral factories are generated that lack membrane precursors (Rodriguez et al., 2004). Indeed, p54 is essential in the recruitment of structural proteins as well as ER membranes to the viral factory and therefore represents a key factor in the morphogenesis of ASFV.

Morphogenesis begins with the modification of ER membrane to form the precursors of the inner envelope. These are initially observed as laminar structures upon which the protein core is assembled on the concave face and the capsid on the convex surface creating immature polyhedral virions (Andres et al., 1997, Garcia-Escudero et al., 1998). A number of viral proteins play

important roles in the production of mature virions. Capsid-associated protein 80 (CAP80), the B602L gene product is a chaperone protein required for the conformational maturation of the major capsid protein p72 (Cobbold et al., 2001). Formation of capsid vertices is reliant on the structural protein pB438L which is a crucial component to attaining the correct icosahedral capsid structure (Epifano et al., 2006) while the virus core is formed from products resulting from the processing of the polyproteins p220 and p62 (Andres et al., 2002). The concluding steps of ASFV morphogenesis occur when viral DNA condenses outside of, and adjacent to empty particles to form a pronucleoid before being inserted into the maturing capsid (Brookes et al., 1996). Closure of the capsid vertex and condensation of the particle completes the process (Brookes et al., 1996). Mature virions are transported to the plasma membrane along microtubules in a conventional kinesin-dependent manner (Jouvenet et al., 2004), a process in which the viral protein pE120R is essential (Andres et al., 2001b). Egress of the virus primarily occurs through budding of the plasma membrane (Breese and DeBoer, 1966), however at later time points in infection cells may undergo lysis (Breese and DeBoer, 1966).

1.3 Autophagy

In the early 1960's, researchers began to describe observations of a mechanism in living cells of bulk segregation and digestion of portions of the cells' own cytoplasm (De Duve and Wattiaux, 1966). The term 'autophagy' was coined in 1963 by Christian de Duve (De Duve, 1963) and derives from the Greek word meaning self-eating. In distinguishing this from proteasomal degradation, autophagy specifically refers to the catabolic process that leads to elimination of cytosolic cell constituents by delivery to mammalian lysosomes or plant and yeast vacuoles (Boya et al., 2013). Products resulting from this breakdown are re-used to manufacture new macro-molecules or provide an energy source to maintain metabolism under nutrient deprivation.

To date, three distinct types of autophagy have been described. Microautophagy involves inward invagination, protrusion or septation of the lysosomal membrane which leads to engulfment of cytoplasmic contents for degradation (Li et al., 2012). Chaperone-mediated autophagy relies on the use of chaperone proteins to mediate the passage of proteins across the lysosomal membrane and into the lysosomal lumen (Cuervo, 2011). Microautophagy and chaperone-mediated autophagy are processes in which comparatively smaller cytoplasmic objects or molecules are degraded. In contrast, macroautophagy was the designation suggested by Mortimore *et al* to distinguish bulk segregation of cytoplasm as originally described by de Duve from other mechanisms of autophagy (De Duve, 1963, Mortimore et al., 1983). The process of macroautophagy (hereafter referred to as autophagy) is centred on the incorporation of cargo into specialised vesicular organelles called autophagosomes. These migrate to and fuse with lysosomes containing acid hydrolases that carry out breakdown of the cargo which can include damaged organelles, long-lived proteins, and even invasive pathogens.

1.3.1 Macroautophagy

Autophagosomes, although not named as such at the time, were first visualised by electron microscopy in the late 1950's (Clark, 1957, Novikoff et al., 1956). Clark described in mouse kidney cells vacuoles containing dense inclusions which 'may possess the structural characteristics of mitochondria'. Since then, autophagy has been reported in a wide array of cells in animals, plants and fungi suggesting that autophagy is a highly conserved pathway through evolution. Autophagy is a complex process involving at least 30 autophagy-related (Atg) gene products (Mizushima et al., 2011). In contrast to most other intracellular trafficking pathways, induction of autophagy involves de novo formation of double-membrane vesicles (autophagosomes) i.e. vesicles that do not bud from a pre-existing organelle although there is evidence to suggest that several organelles can contribute membrane including mitochondria (Hailey et al., 2010), Golgi apparatus (Geng and Klionsky, 2010) and the ER (Yla-Anttila et al., 2009). The autophagy process is summarised in Figure 1.4 and can be broadly divided into three events – initiation; vesicle elongation (forming the complete autophagosome) and maturation (fusion with the lysosome). In yeast, autophagosomes are formed by elongation of the isolation membrane in a process that takes place at the pre-autophagosomal structure (PAS) (Suzuki and Ohsumi, 2010). In mammals, autophagosomes are nucleated within a membrane compartment called the omegasome that is dynamically connected to the ER (Axe et al., 2008). Described below are two protein complexes and two conjugation systems which are critical to the autophagy pathway.

1.3.1.1 Target of rapamycin

The target of rapamycin (TOR) protein plays a major regulatory role in autophagy induction (Sengupta et al., 2010). The mammalian homolog is known as mTOR. TOR forms a protein complex that under nutrient-rich conditions is active and inhibits autophagy whereas under nutrient deprivation or rapamycin treatment, TOR is inhibited allowing for an increase in autophagic activity (Noda and Ohsumi, 1998). This function is mediated through interaction with the Atg1-Atg13-Atg17 kinase complex possibly in combination with other Atg proteins such as Atg11; Atg20; Atg24; Atg29 and Atg30. More specifically, TOR regulates the phosphorylation state of Atg13 (Kamada et al., 2000). Upon inactivation of TOR, Atg13 is rapidly dephosphorylated resulting in increased affinity for Atg1 and Atg17. The interaction of Atg1 with Atg13 and Atg17 triggers activation of Atg1 kinase activity. The kinase activity of Atg1 is essential for autophagy although its exact downstream functions remain unclear (Cheong et al., 2008). The functionally equivalent mammalian homologs of yeast Atg1 are the uncoordinated 51-like kinases 1 and 2 (ULK1 and ULK2). Knockdown of ULK1 inhibits autophagy in a step downstream of mTOR (Chan et al., 2007).

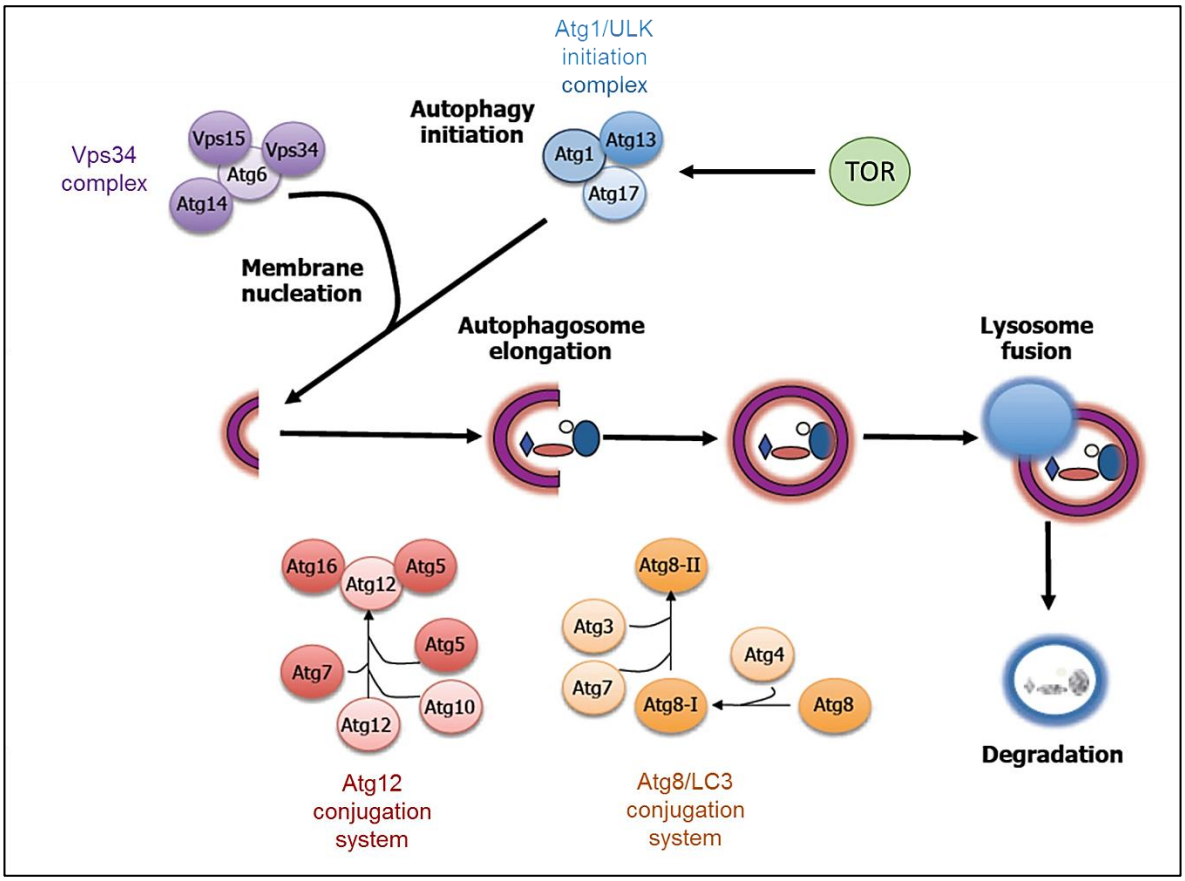

Figure 1.4 Autophagy pathway

Regulation of autophagy occurs via a set of autophagy-related proteins (Atg proteins). Nutrient deprivation leads to inactivation of TOR resulting in activation of downstream Atg proteins. In combination with other factors, these events are required for initiation, membrane nucleation and elongation and finally, maturation and fusion of the autophagosome with the lysosome leading to degradation of cargo. Adapted from Gelino and Hansen (2012).

1.3.1.2 Vacuolar protein sorting 34

The vacuolar protein sorting 34 (Vps34) lipid kinase complex is also essential in the autophagy pathway (Funderburk et al., 2010). Vps34 comprises a class III phosphatidylinositol 3 kinase complexed with Vps30/Atg6; Vps15 and Atg14. The mammalian homologs of Vps30/Atg6 and Vps15 are Beclin 1 and h150 respectively. The function of Beclin 1 is controlled by Bcl-2 (B-cell lymphoma/leukemia-2), an anti-apoptotic protein that binds to and sequesters Beclin 1 to inhibit autophagy under nutrient-replete conditions. Dissociation of Bcl-2 from Beclin 1 is required for autophagy induction (He and Klionsky, 2009). The Vps34 complex generates phosphatidylinositol 3-phosphate (PtdIns3P) which is crucial for the biogenesis of the autophagosome (Petiot et al., 2000). A possibility is that production of PtdIns3P recruits PtdIns3P-binding proteins which in turn recruit additional downstream effector proteins to the site of autophagosome assembly. One such effector protein in humans is the WD-repeat protein interacting with phosphoinositides (WIPI) which is considered important in the lipidation of LC3 (see below for LC3 lipidation process)

(Proikas-Cezanne et al., 2015). Of the four human WIPI members, WIPI1, 2 and 4 have been shown to be essential for autophagosome formation while the function of WIPI3 remains unknown.

1.3.1.3 The Atg12 conjugation system

The Atg12 conjugation system is responsible for the covalent attachment of Atg12 to Atg5 which is catalysed by Atg7 and Atg10. Atg7 hydrolyses ATP leading to activation of Atg12 via formation of a high energy bond. Subsequently, the activated Atg12 is transferred directly to Atg10 and then finally to Atg5 to form the final conjugate. With Atg5 further bound non-covalently to Atg16, this conjugation results in an Atg12-Atg5-Atg16 multimeric structure (Atg16 complex). This complex is functionally vital for autophagy and specifies the site of LC3 lipidation (Fujita et al., 2008).

1.3.1.4 The Atg8/LC3 lipidation system

The mammalian homologs of Atg8 constitute a family of proteins that are subdivided into two major subfamilies: microtubule-associated protein 1 light chain 3 (MAP1LC3 or LC3) and γ-aminobutyric acid receptor-associated protein (GABARAP). Both are essential to the autophagy pathway where LC3 functions in the elongation of the autophagosome membrane and GABARAP functions in autophagosome maturation (Weidberg et al., 2010). Multiple isoforms of LC3 have been described including LC3A, B, B2 and C which exhibit variable tissue distributions (He et al., 2003). Newly synthesised LC3 (LC3-I) is conjugated to a membrane lipid, phosphatidylethanolamine (PE) to form LC3-II (Ichimura et al., 2000). LC3-I is first protealytically cleaved by Atg4 exposing a glycine residue at amino acid position 120. This glycine residue is then bound to Atg7 before being transferred to Atg3. Finally, an amide bond is formed between the same glycine residue and PE.

During autophagosome formation, both the Atg16 complex and LC3-II are localised to the PAS and are intimately associated with the expanding autophagosome (Suzuki et al., 2001). While the Atg16 complex can be identified on the outer surface of the membrane (Mizushima et al., 2003), LC3-II is found on both the inner and outer surfaces (Kabeya et al., 2000). The Atg16 complex is released into the cytoplasm around the time of autophagosome completion as the outer LC3-II is also cleaved off. The LC3-II on the inner surface remains intact and is degraded following fusion of the autophagosome and lysosome. LC3 is often used to monitor autophagic activity and in mammals, LC3B is the most prevalent and well-established autophagosome marker (Klionsky et al., 2016). LC3-I is predominantly cytosolic but upon activation of autophagy, the conversion to LC3-II is accompanied by a redistribution into punctate structures representative of autophagosomes.

1.3.2 The PI3K/Akt/mTOR axis

Autophagy can be activated in response to a number of cell stressors including but not limited to nutrient deprivation, ER stress, oxidative stress and pathogen infection. As described above, TOR

is a central regulator of autophagy. In mammalian cells, mTOR exists as two functionally distinct complexes, mTORC1 and mTORC2 (Sengupta et al., 2010). It has been proposed that mTORC1 directly senses and is phosphorylated in response to nutrient signals (Long et al., 2005), although a role for Rag proteins in mTORC1 activation has also been described (Kim et al., 2008).

Another major route of mTORC1 activation is via the PI3K/Akt signalling cascade in response to growth factors, cytokines and hormones such as insulin (Chan et al., 1999). Upon binding of these molecules to receptor tyrosine kinases (RTKs) at the cell surface, recruitment and binding of class I PI3K results in the generation of phosphatidylinositol (3,4,5)-trisphosphate (PIP_3) from phosphatidylinositol (4,5)-bisphosphate (PIP_2). Accumulation of PIP_3 leads to the recruitment of both protein kinase B (PKB)/Akt and its activator phosphoinositide-dependent protein kinase 1 (PDK1) which is responsible for the phosphorylation and activation of Akt at residue T308. Phosphorylation at residue S473 of Akt by mTORC2 is required for its complete activation (Sarbassov et al., 2005). Activated Akt promotes the phosphorylation and inactivation of the tuberous sclerosis complex 2 (TSC2) protein which is a negative regulator of mTORC1 leading to mTORC1 activation and the inhibition of autophagy. When hormones are absent, mTORC1 is inactivated allowing for the activation of autophagy. Additionally, the 3′-phosphoinositide phosphatase PTEN reverses the PIP_2 to PIP_3 reaction which decreases downstream Akt signalling and positively regulates autophagy (Arico et al., 2001). The PI3K/Akt pathway not only influences the induction of autophagy but also protein translation via the mTORC1 mediated activation of p70-S6K, a translation activator, and the mTORC1 mediated suppression of 4E-BP1, a translation repressor (Ma and Blenis, 2009). Finally, it is important to highlight that Akt can inhibit autophagy independently of mTORC1 via the phosphorylation and inactivation of Beclin 1 (Wang et al., 2012) and that Akt can also inhibit the activation of TSC2 by suppressing the activity of 5′-AMP-activated protein kinase (AMPK) during low cellular energy status (Hahn-Windgassen et al., 2005, Inoki et al., 2003). The PI3K/Akt/mTOR axis is presented schematically in Figure 1.5.

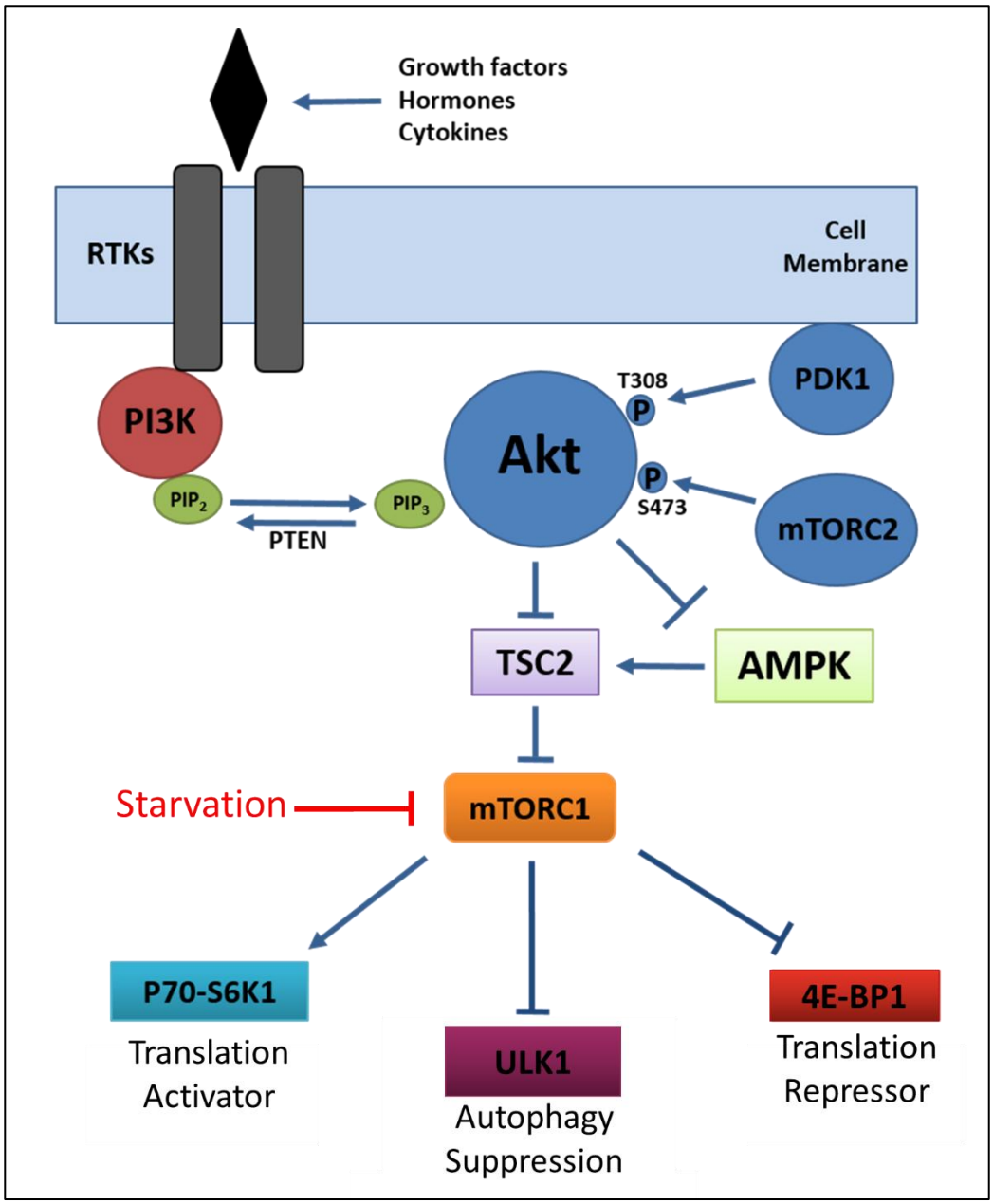

Figure 1.5 PI3K/Akt/mTOR axis

Binding of signalling molecules such as insulin to receptor tyrosine kinases (RTKs) at the cell surface leads to the downstream recruitment of PI3K which catalyses the conversion of PIP_2 to PIP_3. Accumulation of PIP_3 results in the translocation of Akt to the plasma membrane where it is activated via phosphorylation at T308 and S473 by PDK1 and mTORC2 respectively. Active Akt leads to activation of mTORC1 via phosphorylation and inactivation of the mTORC1 repressor, TSC2. The activation of mTORC1 results in the inhibition of autophagy via the ULK1 complex and the promotion of protein translation via p70-S6K and 4E-BP1. Inactivation of mTORC1 can be achieved by starvation or activation of TSC2 via AMPK. Adapted from Batra (2016).

1.4 Virus/host interactions

1.4.1 Autophagy and immunity

Research on autophagy has uncovered an array of diverse functions that go beyond turnover of long-lived organelles or responding to nutrient deprivation. Autophagy has also been implicated in cell development and differentiation (Li et al., 2015) and is even thought to play a role in life span extension (Madeo et al., 2015). In addition, the role of autophagy in neurodegenerative diseases such as Alzheimers and Parkinsons (Kiriyama and Nochi, 2015) as well as cancer (Ozpolat and Benbrook, 2015) is the subject of increasing interest. Traditionally, autophagy has been considered to be a non-selective pathway, however recent findings have challenged this thinking. A vital function of autophagy is the clearance of aggregated proteins and cytosolic ubiquitinated substrates. Studies suggest that this degradative process is also selective and mediated through the mammalian protein p62/sequestosome 1 (Bjorkoy et al., 2005). Ubiquitinated cargo is bound by p62 via its ubiquitin-associated domain which is then targeted to autophagosomes by the binding of p62 to LC3 located on the inner surface of the autophagosome (Pankiv et al., 2007). Binding of p62 to LC3 occurs via its LC3-interacting region (LIR) motif and LIR motifs have been identified in several other autophagy receptor molecules (Birgisdottir et al., 2013). The selective degradation of damaged or superfluous mitochondria via the autophagy pathway, known as mitophagy, is mediated by the Atg32 receptor (Okamoto et al., 2009) and bacterial pathogens are known to be targeted by the autophagy receptors NDP52 and optineurin (Thurston et al., 2009, Wild et al., 2011).

One of the first indications that autophagy is used by cells to degrade pathogens was the observation by Smith and colleagues of herpes simplex virus (HSV) and human cytomegalovirus (HCMV) located inside autophagosomes (Smith and de Harven, 1978). Since then, a tremendous amount of research has been conducted on this subject which is referred to as xenophagy – the degradation of foreign entities including viruses, bacteria and parasites (Gomes and Dikic, 2014). In fact, studies have revealed that autophagy is implicated in diverse aspects of immunity, functioning in both the innate and adaptive immune responses.

In its most basic form, autophagy acts as an intrinsic defence mechanism by degrading cytosolic or vacuole-containing microbes (Levine, 2005). Alternatively, following cell invasion by microbes, pattern recognition receptors such as toll-like receptors (TLRs) recognize molecules called DAMPs (damage-associated molecular patterns) and PAMPs (pathogen-associated molecular patterns). DAMPs are cell-derived molecules able to generate signals following cell stress or damage while PAMPs are pathogen derived molecules that are encountered during infection. Recognition of these molecules by TLRs activates pro-inflammatory responses in some cases accompanied by interferon production (Janeway and Medzhitov, 2002). Research conducted by Shi and colleagues demonstrated that TLR4 activation led to the release of Beclin 1 from Bcl-2 via binding to TLR

adaptor proteins which initiated an autophagy response (Shi and Kehrl, 2008). Additionally, evidence suggests that considerable cross-talk exists between autophagy and the interferon response (Tian et al., 2019). For example, expression of RNA-dependent eIF2α protein kinase (PKR), an important interferon-stimulated gene (ISG) product is essential for autophagic degradation of HSV-1 (Talloczy et al., 2006). Collectively, studies such as these demonstrate an integral role of autophagy in innate immunity.

The function of autophagy in adaptive immunity has also been extensively examined. Cytosolic proteins have been shown to be constitutively delivered to multi-vesicular MHC class II-loading compartments via fusion with autophagosomes. In this way, targeting of the influenza matrix protein 1 to autophagosomes led to strongly enhanced MHC class II presentation to CD4+ T cell clones (Schmid et al., 2007). Autophagy can also influence MHC class I presentation and was shown to enhance the presentation of endogenous viral antigens during HSV-1 infection (English et al., 2009). The role that autophagy plays in immunity is summarised in Figure 1.6.

It is important to note that autophagy proteins such as LC3 may have anti-viral functions which are independent of their function in canonical autophagy. Indeed, evidence of LC3 lipidation on other macroendocytic vacuole membranes has been described and is required for lysosomal-mediated degradation of engulfed cargo (Florey and Overholtzer, 2012). Non-canonical autophagy refers to the process of targeting LC3 to a single membrane in contrast to the double membrane of the autophagosome (Florey and Overholtzer, 2012). An example of this is LC3 lipidation at single-membrane phagosomes in a process called LC3-associated phagocytosis (LAP) following the engulfment of pathogens (Sanjuan et al., 2007, Sanjuan et al., 2009). Depending on cell type, LAP can promote a more rapid maturation of the phagosome in response to TLR signalling leading to accelerated loading and presentation on MHC-II (Sanjuan et al., 2009, Schille et al., 2018).

1.4.2 Modulation of autophagy by viruses

With such an important role in the host response to infection, it is unsurprising that autophagy is modulated by numerous viruses. Viruses are known to encode genes that specifically inhibit the autophagy pathway. Some of these inhibitors act on stimulatory cell signal pathways, for example the HSV-1 Us11 protein has been shown to inhibit PKR-mediated induction of autophagy (Lussignol et al., 2013). Other inhibitors have a direct interaction with the autophagy machinery - the ICP34.5 protein of HSV-1 was the first to be described (Orvedahl et al., 2007). ICP34.5 is able to bind to the key autophagy protein Beclin 1 and inhibit its autophagy function. Beclin 1 is a common target for virus modulation, indeed ASFV also encodes a Beclin 1 binding protein called A179L which has a high degree of sequence homology to the proto-oncogene Bcl-2, an apoptosis antagonist (Hernaez et al., 2013, Kroemer, 1997, Neilan et al., 1993). Beclin 1 is a Bcl-2 interacting protein and denotes an important point of convergence between the apoptosis and autophagy pathways perhaps making it a particularly useful target for inhibition by viruses (Liang et al.,

1998). ASFV seems to exploit this cross-over as exogenous expression of A179L leads to the inhibition of both apoptosis and the formation of autophagosomes (Hernaez et al., 2013, Revilla et al., 1997).

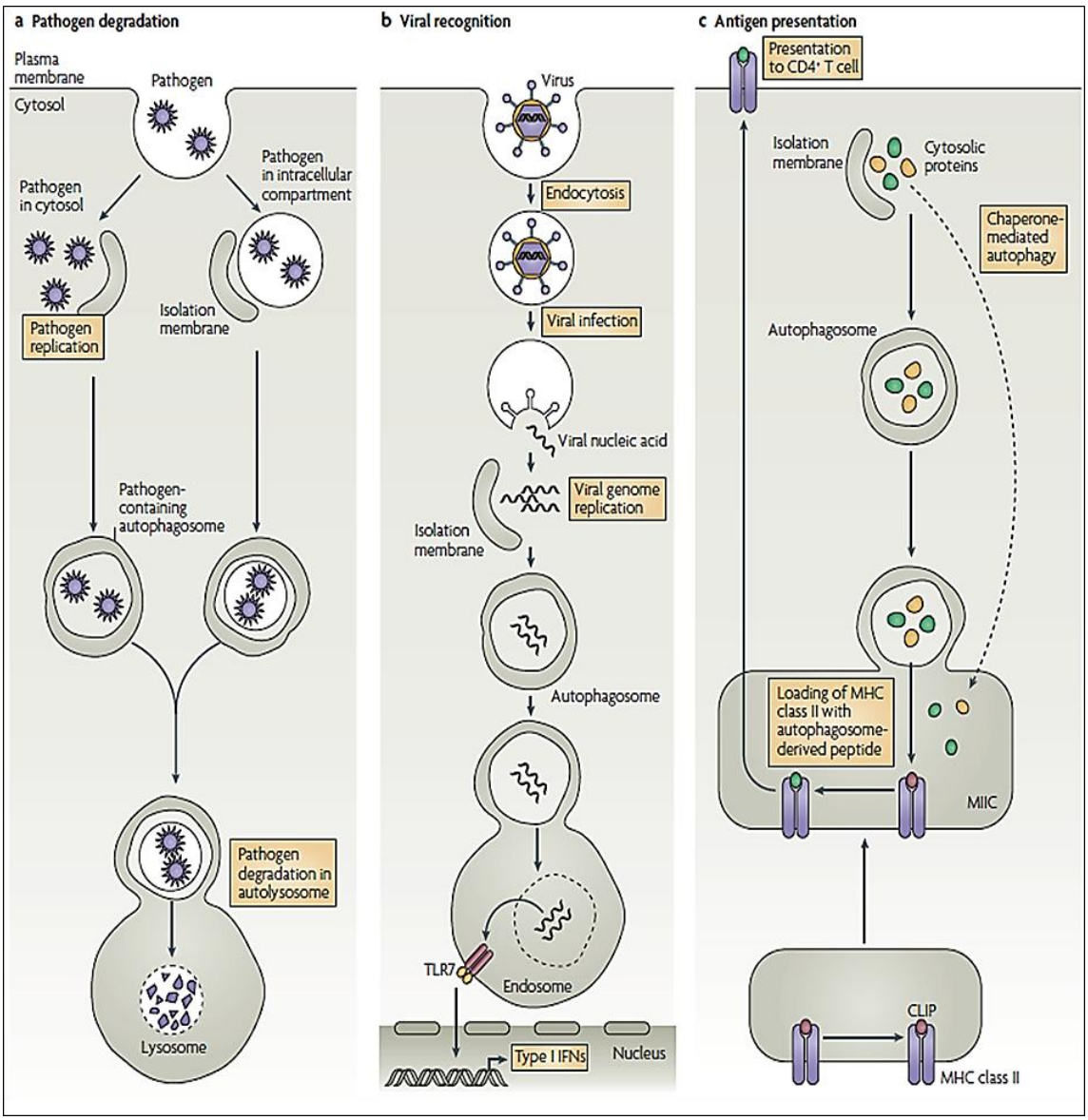

Figure 1.6 The role of autophagy in the innate and adaptive immune responses

a) Intracellular pathogens (viruses, bacteria and parasites) that are either free inside the cytosol or contained within intracellular compartments such as phagosomes are engulfed into autophagosomes and degraded following fusion with lysosomes. b) Autophagy is used to transport viral nucleic acids to intracellular compartments containing Toll-like receptor 7 (TLR7) which signals the production of Type I interferon. c) Following engulfment into autophagosomes, antigens are delivered to MHC class II molecules by fusion of the autophagosome with late endosomes (MIIC's). Antigens can then be presented to CD4+ T cells. Cytosolic antigens can also be directly imported into MIIC's by chaperone mediated autophagy. Taken from Levine and Deretic (2007).

In the context of infectious disease, it is likely that in most circumstances, induction of autophagy would favour the immune response. Nevertheless, there are instances in which certain microorganisms benefit from increased autophagic activity (Kirkegaard et al., 2004). In the case of viral infections, autophagy can act as a source of intracellular membrane that serves as a scaffold for the generation of viral replication complexes (Kirkegaard, 2009). For this reason, knockdown of autophagy related gene products results in reduced viral yields of poliovirus (Jackson et al., 2005) and mouse hepatitis virus (Prentice et al., 2004). Parvovirus-B19 has been shown to activate autophagy which mediates prolonged survival of infected cells, potentially allowing more time for viral replication (Nakashima et al., 2006). Autophagy can also be exploited for viral release as poliovirus has been shown to exit infected cells using a non-lytic mechanism that is autophagy dependent (Bird et al., 2014). It is important to highlight that in many cases the stimulation of autophagy during virus infection does not necessarily lead to progression through the entire pathway. For example, influenza virus triggers autophagosome formation but inhibits the fusion of autophagosomes with lysosomes presumably to limit any anti-viral effects (Zhang et al., 2014).

The PI3K/Akt signalling cascade which is intimately connected to the autophagy pathway and involved in multiple cell functions including metabolism, growth, survival and proliferation is also commonly targeted by viruses (Dunn and Connor, 2012, Hemmings and Restuccia, 2012). With such far-reaching influence in the cell, PI3K/Akt signalling can be crucial for viral replication. Viral growth in response to PI3/Akt activation is likely to be directly linked to mTORC1 activity due to the role that mTORC1 plays in protein translation via the downstream effectors p70-S6K and 4E-BP1. For this reason, viruses that rely on cap-dependent translation such as mammalian DNA viruses require active mTORC1 to maintain protein translation. Indeed, the activation of the PI3K/Akt pathway by vaccinia virus (VACV) was shown to be required for viral growth although this was also linked to the inhibition of apoptosis (Soares et al., 2009). Similarly, Flaviviruses such as dengue virus (DENV) and Japanese encephalitis virus (JEV) activate the PI3K/Akt pathway which has an anti-apoptotic effect, as a block in this activation induced apoptotic cell death in the early stages of infection (Lee et al., 2005). Human Papillomavirus has been shown to activate the PI3K/Akt pathway, leading to the activation of mTORC1 and the inhibition of autophagy which benefits viral replication (Surviladze et al., 2013).

Modifying the ability of viruses to control the autophagy response can significantly alter the outcome of infection. For example, stimulation of autophagy using rapamycin results in significant reductions of virus titre during DENV infection of monocytic cells (Panyasrivanit et al., 2011). Using a genetic approach, an HSV-1 mutant virus lacking the Beclin 1-binding domain of ICP34.5 was shown to lose the ability to control autophagy (Orvedahl et al., 2007). Infection of mice with the aforementioned mutant virus resulted in reduced mortality, demonstrating the potential for exploiting autophagy as a means of viral attenuation. The basis of this attenuation may be linked to an altered host immune response, as a separate study using this virus showed that infection resulted

in a significantly stronger CD4+ T-cell response as well as increased gamma interferon and interleukin-2 production (Leib et al., 2009). Interestingly, gamma interferon is an important correlate of protection against ASFV (King et al., 2011) and therefore methods aimed at increasing secretion levels in response to vaccination may prove to be important. For example, the immunogenicity of vaccine strain viruses could be enhanced by limiting the ability of the virus to modulate autophagy which may lead to increased antigen presentation and a greater T-cell response.

1.5 Research Aims

African swine fever is a significant disease of livestock that negatively impacts livelihoods and economies. In the face of continued spread into new regions including Europe and Asia, the requirement for commercially offered vaccines has now reached a critical level. Thus far, research has been conducted to delineate the intricacies of the host response to ASFV in an effort to harness this interaction for use as a vaccine model. This has been accompanied by an elevated interest in rationally attenuated vaccines (Borca et al., 1998, Lewis et al., 2000, Zsak et al., 1998). Within the vaccine design process, methods aimed at enhancing the host immune response will prove to be particularly useful. A potential barrier to this approach is the lack of knowledge surrounding the sizeable repertoire of ASFV genes and their functions.

Induction of autophagy during ASFV entry reduces viral replication (Hernaez et al., 2013), but the importance of autophagy in the ASFV life cycle is unclear. ASFV replication has not been reported to induce autophagosome formation during infection (Hernaez et al., 2013), and pre-treatment of cells with 3-methyladenine that inhibits autophagy does not greatly affect viral replication (Basta et al., 2010). The purpose of this project is firstly to characterise the modulation of the ubiquitous cell process of autophagy by ASFV and secondly to investigate which viral mechanisms are involved. This includes screening for virally encoded autophagy modulators, the identification of which may offer an opportunity to alter modulatory outcomes for the purpose of improving vaccine efficacy. Low virulent strains of ASFV that lack autophagy modulators may provide enhanced immunity against virulent isolates of the virus. This research could therefore contribute to rational vaccine design and offer an approach to accelerating acquirement of effective ASFV vaccines.

2 Materials and methods

2.1 Cell culture

Vero cells (ECACC 84113001) were maintained in tissue culture flasks in Dulbecco's Modified Eagle's Medium (DMEM-GlutaMAX™, ThermoFisher Scientific) supplemented with 10% (v/v) heat inactivated Foetal Calf Serum (FCS, Life Science Production) and Penicillin (100 U/ml)-Streptomycin (100 µg/ml) (ThermoFisher Scientific). Porcine bone marrow derived macrophages were maintained in Earle's Balanced Salt Solution (EBSS; ThermoFisher Scientific) supplemented with 4 mM HEPES (ThermoFisher Scientific), 10% (v/v) porcine serum (Biosera) and Penicillin (100 U/ml)-Streptomycin (100 µg/ml). Mouse embryo fibroblast cells (MEFs) were maintained in DMEM supplemented with non-essential amino acids (Sigma) and Penicillin (100 U/ml)-Streptomycin (100 µg/ml). HEK293 (ECACC 85120602) cells were maintained in DMEM supplemented with 10% (v/v) FCS and Penicillin (100 U/ml)-Streptomycin (100 µg/ml). All cells were kept at 37°C with 5% CO_2.

Vero cells were passaged by removing the growth medium and washing the cells twice with phosphate buffered saline without CaMg (PBS [-]; ThermoFisher Scientific) before incubating with trypsin EDTA (ThermoFisher Scientific) at 37°C for approximately 5 minutes to allow cell detachment. Cells were then transferred to a 30 ml universal tube containing growth medium and centrifuged at 340 × *g* for 5 minutes. The supernatant was then removed and cells were resuspended in growth medium before transferring an appropriate volume of the cell suspension to a new flask containing fresh medium. Finally, cells were incubated at 37°C and grown until confluent.

For use in experiments, viable cells were identified using the trypan blue exclusion method, (trypan blue acquired from Sigma) and counted using a 0.2 mm depth improved Neubauer haemocytometer. Cells were subsequently seeded into 6-, 24- or 96-well tissue culture microtitre plates (Nunc) at an appropriate density.

To cryopreserve cells, the confluent cell layer was removed using trypsin EDTA as above and cells were centrifuged at 340 × *g* for 5 minutes. Cell pellets were resuspended in freezing medium consisting of 10% (v/v) DMSO (Sigma) and 90% (v/v) FCS. Finally, cells were transferred to cryo-freezing tubes (Nunc) and stored at -80°C.

Porcine bone marrow derived macrophages were harvested from the long bones of pigs. Bones were cut into small fragments and incubated in PBS supplemented with 1% (v/v) FCS and Penicillin (100 U/ml)-Streptomycin (100 µg/ml) at 35°C for 90 minutes. The bone marrow suspension was then filtered through muslin to remove the bone fragments and centrifuged at 350 × *g* for 10 minutes. Supernatant was discarded and the cell pellet was washed in PBS. After repeating the centrifugation step, the cell pellet which contained the bone marrow derived

macrophages plus additional cell types was resuspended in the appropriate cell medium and cells were counted and seeded into flasks.

To harvest blood derived macrophages, erythrocytes were sedimented from whole pig blood by incubation with an equal volume of 6% dextran (Sigma) solution for 30 minutes at 37°C. White blood cells were concentrated from the supernatant by centrifugation and washed several times with PBS before plating 2 x 10^7 cells per 6-well plate in DMEM supplemented with 30% (v/v) pig serum and Penicillin (100 U/ml)-Streptomycin (100 µg/ml). Cells were cultured overnight to allow monocytes to adhere and then the media was changed. Two days after this cells were used in experiments.

2.2 Growth, maintenance and titration of virus stocks

2.2.1 Virus isolates

The parental virus strain Ba71V and recombinant Ba71V virus lacking the A179L gene (A179L KO) (generated by Dr Claire Barber) were used to infect Vero cells. BA71V is a non-pathogenic tissue-culture adapted virus derived from a virulent parental strain isolated in 1971 from a pig near Badajoz, Spain (Enjuanes et al., 1976). The attenuated Uganda isolate was used to infect MEFs (Hess et al., 1965) and the virulent field isolate OURT88/1 (Boinas et al., 2004) was used to infect blood derived macrophages.

2.2.2 Growth of virus stocks

Vero cells were cultured in T175 flasks such that they reached approximately 80% confluence prior to inoculation with parental, recombinant Ba71V or attenuated Uganda. Flasks were then incubated for 3 - 5 days at 37°C in the presence of CO_2. The contents of the flask were transferred to a 50 ml Falcon tube (BD Falcon) and centrifuged at 3500 × *g* for 15 minutes before harvesting the supernatant. Clarified supernatant was stored at -80°C.

Growth of the OURT88/1 isolate was carried out on bone marrow derived macrophages. T175 flasks were seeded with 50-75 ml of cells at a concentration of approximately 1.6 x 10^7 cells/ml and incubated at 37°C in the presence of CO_2. After 3 days, inoculum was added and cells were incubated until at least 90% of cells had detached before harvesting. Cell debris was pelleted for 10 minutes at 1000 × *g* and clarified supernatant was removed. Cell pellet was vortexed and subjected to three freeze/thaw cycles at -80°C before a final centrifugation step. Supernatant was removed and combined with the previously harvested supernatant before storage at -80°C.

2.2.3 Virus infection of cells

The virus inoculum was diluted in 2% FCS or porcine serum media and then added to pre-plated cells or cells seeded onto glass coverslips at an appropriate multiplicity of infection (MOI). Virus was left to adsorb for 1 hour at 37°C with CO_2. The inoculum was subsequently removed and cells

washed in media. Cells were then incubated in 2% FCS or porcine serum media at 37°C with CO_2 for the required length of time.

2.2.4 Endpoint titration of virus

Vero cells were seeded onto 96 well plates (Nunc) in 100 µl of media containing 1 x 10^5 cells/ml in each well. The following day a ten-fold dilution series of the virus from 10^{-1} to 10^{-8} was prepared in 2% FCS culture medium and added to the cells in their existing culture media. This was applied in quadruplicate at 50 µl per well. The plate was sealed with a plate sealer and the plate incubated at 37°C with CO_2 for 3 days. The culture media/virus was removed and the cells were washed once with PBS (-) prior to fixation in 4% paraformaldehyde (PFA).

After 1 hour, cells were washed with PBS (-) and then incubated in PBS containing 0.2% Triton X-100 (Sigma) for 10 minutes. The PBS/Triton mix was discarded, and the plate incubated in block buffer consisting of 10% (v/v) TBS, 0.2% (v/v) NaN3 and 0.2% (v/v) fish skin gelatin (Sigma) for 30 minutes. The block buffer was discarded, and the cells incubated with primary antibody against viral protein p30 (clone C18, Pirbright Institute) diluted 1:1000 in block buffer for 1 hour. Following incubation with the primary antibody the plate was washed three times in PBS (-).

For evaluation by immunofluorescence cells were incubated for 1 hour in the presence of goat anti-mouse Alexa Fluor 488 (Life Technologies) diluted 1:500 in block buffer. Plates were subsequently washed three times in PBS (-) and the plates read using an inverted microscope.

The TCID50 was determined using the Spearman Kärber method (Kärber, 1931).

Titration of the Uganda and OURT88/1 strains was carried out essentially using the same method except that bone marrow derived macrophages were used instead of Vero cells. Additionally, plates were read by counting wells that demonstrated red blood cell rosettes instead of immunofluorescent labelling of the virus (Malmquist and Hay, 1960).

2.2.5 Virus purification

Ba71V virus stocks were grown in tissue culture roller bottles (Fisher Scientific) and harvested as per the method in section 2.2.2. Following this, clarified supernatants were centrifuged at 24 000 × *g* for 1.5 hours and the resulting virus pellets were then purified by two consecutive Percoll density gradients as described (Carrascosa et al., 1985). Purified virus stocks were titrated using the method in section 2.2.4. The purity of the virus preparation was analysed by negative stain electron microscopy.

2.3 DNA techniques

2.3.1 PCR

A179L was cloned into the pcDNA3.1 HA-N expression vector using PCR amplification of codon-optimised A179L (ordered from ThermoFisher Scientific). PCR reactions were carried out using an Eppendorf MasterCycler or Nexus thermal cycler. Primers used to amplify A179L were ordered from Sigma and encoded XhoI and PstI cut sites on the forward and reverse primers respectively (see Table 2.1). Components were assembled as follows; 100 - 150 ng of A179L template DNA, 5 µl of 10X PCR buffer for KOD Hot Start DNA Polymerase, 5 µl dNTPs, 3 µl 25 mM $MgSO_4$, 10 µl of Q-solution (Qiagen), primers to a final concentration of 100 nM and 1 µl of KOD Hot Start DNA Polymerase. The reaction volume was made up to 50 µl with nuclease-free water. The PCR program was carried out at 95°C for 4 minutes, followed by 30 cycles consisting of 95°C for 30 seconds, 50°C for 30 seconds, 70°C for 20 seconds, with a final step of 70°C for 5 minutes. Following PCR, samples were stored at -20°C or immediately analysed on an agarose gel.

Table 2.1 PCR primers

Primer	Sequence (5' – 3')
A179L FOR	AACCAACTCGAGCATGGAAGGCGAGGAACTGATCTACCAC
A179L REV	ACATACCTGCAGTCAGATCAGGTTGCAGTTCCGCAG

2.3.2 Restriction endonuclease digests and DNA purification and ligation

Restriction endonuclease digest of the A179L PCR amplicons was carried out in a total volume of 30 µl using NEB buffer 3 (New England Biolabs) according to the manufacturer's instructions. Restriction enzyme XhoI was supplied by New England Biolabs and PstI was supplied by Promega. Restriction digest of the pcDNA3.1 HA-N destination vector included 15 minute treatment with temperature sensitive alkaline phosphatase (Promega) to remove terminal phosphate groups. Samples were analysed by agarose gel electrophoresis before being purified using an illustra™ GFX™ PCR DNA and Gel Band Purification Kit (GE, UK) by following the manufacturer's protocol. DNA was eluted in 30 µl nuclease free water and stored at -20°C until needed. The A179L amplicon was ligated into the pcDNA3.1 HA-N destination vector in a total reaction volume of 10 µl using 0.5 µl T4 DNA ligase (Promega) in a T4 ligase buffer solution (Promega). This was carried out using a vector:insert molar ratio of 1:3, where the vector concentration was approximately 100 - 150 ng. Ligations were conducted at 16°C overnight and were subsequently used to transform chemically competent *E.coli*.

2.3.3 Transformation of competent cells and isolation of DNA

Frozen TOP10 competent cells were gently thawed on ice for 5 - 10 minutes. 50 ng of DNA was pipetted in to 50 µl of thawed cells and gently stirred, then left to incubate on ice for 20 minutes. The cells were then heat shocked in a water bath at 42°C for 35 seconds, and returned to ice for a further 2 minutes. 300 µl of SOC medium was added and the cells were incubated in an orbital incubator for 90 minutes at 37°C with continuous shaking at 200 rpm. Afterwards, the cells were plated on to Luria broth (LB) agar plates containing ampicillin at 100 µg/ml. The plates were then incubated overnight at 37°C until colonies were seen. Following this, either small scale (2.5 ml) or large scale (400 ml) bacterial cultures were set up in LB broth. DNA was extracted using either a QIAprep Spin Miniprep kit or Qiagen Plasmid Maxi Kit following the manufacturer's protocols. The concentration of eluted DNA was analysed using a Nanodrop 1000, which was set to measure the optical density of a given sample at 260 nm.

2.3.4 DNA Sequencing

Purified DNA was sequenced using a BigDye® Terminator v3.1 Cycle Sequencing Kit, (Applied Biosystems, UK) using the primers listed in Table 2.2. This system uses four-colour fluorophore conjugated dideoxy-nucleotides in a terminator cycle sequencing reaction. Sequencing reactions were ethanol precipitated, then re-suspended in 20 µl of HI-DI formamide. Samples were run on an ABI 3730 DNA analyser. Sequences were analysed using Vector NTI Advance (version 11.5.4).

Table 2.2 Sequencing primers

Primer	Sequence (5' – 3')
CMV FOR	GCAAATGGGCGGTAGGCGTG
BGH REV	TAGAAGGCACAGTCGAGG

2.3.5 A179L mutagenesis

Mutation of the A179L ligand binding groove was carried out using site-directed mutagenesis in sequential stages in which the valine residue at position 73 was first mutated to tyrosine followed by mutation of the glycine residue at position 89 also to tyrosine. Site-specific primers were designed using the QuickChange Primer Design webpage (Agilent) (see Table 2.3). Mutagenesis was carried out using 50 ng of the pcDNA3.1 HA-A179L construct as a template in a PCR reaction using the same conditions described in section 2.3.1. Following amplification, 1 µl of DpnI (New England Biolabs) was added to each reaction to digest the parental DNA template and to select for mutation-containing synthesized DNA. Constructs encoding mutant A179L were transformed into *E.coli* then isolated from bacterial cultures and sequenced as previously described in sections 2.3.3 and 2.3.4.

Table 2.3 A179L mutagenesis primers

Primer	Sequence (5' – 3')
V73Y FOR	CCCAGTTCACCGGCTACGTGACCGAGCTGT
V73Y REV	ACAGCTCGGTCACGTAGCCGGTGAACTGGG
G89Y FOR	GCTGAACACGATGAAGTAGCAGATCCGGCCCCAG
G89Y REV	CTGGGGCCGGATCTGCTACTTCATCGTGTTCAGC

2.3.6 Generation of adenovirus vectors

Adenovirus expressing wild-type (WT) A179L or mutant (YY) A179L were engineered using Gateway® Technology (ThermoFisher Scientific). Each gene was initially cloned into an entry vector using restriction digest. DNA encoding WT or YY A179L was excised from the pcDNA3.1 HA-N constructs (see section 2.3.1) using KpnI and PmeI (New England Biolabs). Similarly, the p2022 entry vector was cut using KpnI and StuI (New England Biolabs) and all digests were carried out using Cutsmart buffer (New England Biolabs). Digests were gel purified and samples were ligated using the methods described in section 2.3.2 followed by plasmid purification from bacterial culture as described in section 2.3.3.

To generate adenovirus expression clones, a recombination reaction was performed using the entry vector cloned above and a Gateway® destination vector (p664) encoding adenovirus human type 5 (AdH5). This system uses specific recombination sequences, att L sites in the entry vector and att R sites in the destination vector, and the proprietary enzyme mix 'LR Clonase' to catalyse the transfer of the gene of interest from the entry vector to the destination vector. Separate reactions for WT A179L and YY A179L were set up in 10 µl volumes that contained 150 ng of each of the entry and destination vectors in addition to 6 µl of TE buffer pH 8.0 and 2 µl of LR Clonase™ II Enzyme Mix (ThermoFisher Scientific). Reactions were incubated overnight at room temperature and the resulting constructs were used to transform *E.coli.* DNA was purified from bacterial cultures and sequenced as described in sections 2.3.3 and 2.3.4.

To prepare the AdH5 expression constructs for cell transfection, DNA was linearised using PacI (New England Biolabs) and Cutsmart buffer. Following this, samples were heated at 65°C for 25 minutes to inactivate the restriction enzyme. Transfections were carried out on HEK293 cells which is an immortalized line of primary human embryonic kidney cells transformed by sheared human AdH5 DNA. The cells harbour the E1A and E1B region of the adenoviral genome, that complement, in trans, the deletion of the E1 region in the recombinant adenovirus. Cells were cultured to a confluency of approximately 80% in 6 well plates prior to transfection using Lipofectamine™ 2000 (ThermoFisher Scientific) following the manufacturer's protocol. Cells

were incubated overnight at 37°C and then incubated in fresh cell media for a further 3 days. Cells were detached from the plate using TrypLE™ Express (ThermoFisher Scientific) and transferred into a T75 tissue culture flask and monitored for CPE. When greater than 80% CPE was evident, cells were harvested by pelleting at 1500 × *g* for 5 minutes. Cell pellets were resuspended in lysis buffer (10 mM Tris, 1 mM $MgCl_2$, pH 7.8) and subjected to three freeze/thaw cycles at -20°C to release cell-associated virus.

Master AdH5 stocks were prepared by inoculating a T175 flask of HEK293 cells with each of the A179L adenoviruses and harvesting the cells using the described method after complete CPE was evident. Finally, master stocks were tested for expression by transducing Vero cells and analysing the cells by confocal microscopy using an anti-HA tag antibody.

2.4 Protein methods

2.4.1 SDS-PAGE

Proteins from cell lysates were resolved by SDS-PAGE (sodium dodecyl sulfate polyacrylamide gel electrophoresis), using 10 - 15% resolving gels, overlaid with a 4% stacking gel on a Hoefer Mighty Small II electrophoresis unit. Cell lysates were harvested in sample preparation buffer containing loading buffer. Following denaturation at 98°C for 5 minutes, 10 - 20 µl of the sample was subsequently loaded onto the gel alongside a Full-Range Rainbow Molecular Weight Marker (GE Healthcare). Gels were run in NuPAGE MES running buffer (ThermoFisher Scientific) with the exception of LC3 analysing gels that were run in NuPAGE MOPS running buffer (ThermoFisher Scientific) at 100 V until the dye front reached the end of the gel.

2.4.2 Western blotting

Proteins were transferred onto nitrocellulose membranes (Hybond PVDF membrane, GE Healthcare) using Mini Protean II slab cell Western blot apparatus (Bio-Rad) by running at 100 V for 1 hour in transfer buffer (25 mM Trizma, 190 mM glycine, 20% methanol). The membrane was removed and incubated in blocking buffer consisting of TBS with 0.2% (v/v) Tween (TBS-T) and 5% (w/v) milk powder for 1 hour, prior to overnight incubation with primary antibody diluted in blocking buffer. Membranes were washed three times in TBS-T, prior to incubation with appropriate HRP-conjugated secondary antibodies, which had been diluted in blocking buffer, for 1 hour. Membranes were washed a further three times in TBS-T prior to detection of chemiluminescence by incubating the membrane with Pierce ECL western blotting substrate (ThermoFisher Scientific) for 3 minutes. Membranes were then imaged using a G:Box Chemi system (Syngene).

2.5 ASFV gene library

Plasmid libraries were supplied by Dr Claire Barber (The Pirbright Institute) and Dr Chris Netherton (The Pirbright Institute). 25 plasmids encoded genes from the Georgia 2007/1 isolate in pCMVi-LS (-H-P) CIM with a HA tag (YPYDVPDYA) at the 5' end and a Myc tag (EQKLISEEDL) at the 3' end. A further 25 genes from the OURT88/3 strain and the DP148R gene from the Benin 1997/1 strain had been cloned into pcDNA3.1zeo with a HA tag at the 3' end except for MGF110-4L and MGF110-5L that had no tags and R298L that had a HA tag at the 5' end. The adenovirus library was supplied by Dr Chris Netherton and consisted of 22 genes from the OURT88/3 strain and EP153R and MGF360-11L from the Benin1997/1 strain. All of these genes were cloned with a HA tag at 3' end except for CP196L that had no tag. The A179L plasmids and adenoviruses were cloned separately and contained a HA tag at the 5' end (see sections 2.3.1 to 2.3.6)

2.6 Transfection and transduction of mammalian cell lines

Cells were seeded at 2.5 x 10^4 cells/cm^2 on appropriate culture ware 16 hours prior to transfection as per the TransIT-LT1 transfection reagent protocol (Mirus). In brief, plasmid DNA and TransIT-LT1 reagent were added to OptiMEM (Gibco) at a ratio of 1 µg DNA to 3 µl transfection reagent. Following gentle agitation the mix was allowed to incubate for 25 minutes. The TransIT-LT1 reagent-DNA complex was added dropwise to cells that were gently rocked and returned to incubate at 37°C. To avoid tubulovesicular autophagosomes (TVAs) which are induced during the transfection process, cells were passaged after 24 hours and re-seeded onto coverslips. Cells were incubated at 37°C for 24 hours before starving and fixing.

To transduce cells using adenovirus, sufficient virus for MOI 100 was added directly to the cell media and incubated at 37°C for 24 hours to allow gene expression before starving and fixing.

2.7 Confocal microscopy

Cells were seeded at 2.5 x 10^4 cells/cm^2 onto glass coverslips (VWR) prior to infection, transfection or other relevant treatment. At the experimental end point, cells were washed with PBS and fixed and permeabilised with methanol for 6 minutes for assays analysing LC3 and WIPI except when GFP and LC3 were analysed in combination in which case cells were first fixed in 4% PFA for 30 minutes to preserve GFP signal followed by permeabilisation using methanol. Alternatively, experiments that did not include analysis of LC3 or WIPI were fixed using PFA only for 30 minutes and permeabilised for 10 minutes using PBS + 0.2% Triton X-100 (Sigma). Coverslips were washed three times with PBS then incubated for 1 hour in block buffer consisting of 10% (v/v) TBS, 0.2% (v/v) NaN3 and 0.2% (v/v) fish skin gelatin (Sigma). Coverslips were then incubated for a further hour in primary antibody diluted in block buffer and then washed three times for 5 minutes in PBS (-) to remove excess antibody. Next, coverslips were incubated for 1

hour with an appropriate Alexa Fluor (Life Technologies) secondary antibody diluted in block buffer and then washed three times in PBS (-) before incubation with DAPI nuclear stain (4', 6-Diamidino-2-Phenylindole, Dihydrochrolide, 10 mg/ml, Sigma) diluted 1:10 000 in ddH_2O for 10 minutes. Alternatively, nuclei were stained using TO-PRO-3 (ThermoFisher Scientific) diluted 1:8000 in PBS for 15 minutes. Finally, coverslips were washed twice in ddH_2O and then mounted in Vectashield (Vector Laboratories) on glass slides, and sealed using nail varnish.

Cells were visualised using a Leica confocal laser scanning microscope, and data analysed using LAS X (Leica Confocal Software).

2.8 Imaris analysis

To enumerate LC3 or WIPI puncta, confocal images were analysed in Imaris (version 9.2.1) using the 'Cells' analysis function. Cells were detected using either cytoplasmic LC3 staining, WIPI staining, or labelling of protein expression following infection or transduction. Detection thresholds were adjusted to cover each cell to the cell boundary. The software was set to detect puncta of approximately 0.5 µM in diameter and cells were visually inspected to ensure that the software had accurately identified visible puncta. Analysis was carried out for 30 cells per experimental condition and data was subsequently analysed in Graphpad Prism (version 7).

2.9 Electron microscopy

For analysis of purified virus preparations, virus was inactivated by 1:1 volume dilution in 2% glutaraldehyde in phosphate buffer (Agar Scientific) for 30 minutes at room temperature. A 7 µl sample of the fixed virus suspension was placed onto Formvar coated, glow discharged copper 200 mesh EM grids (Agar Scientific) and left to attach for 2 minutes at room temperature. Excess sample was then removed using filter paper. After a brief wash in ddH_2O, grids were placed on droplets of 3% aqueous uranyl acetate (Agar Scientific) for 1 minute before excess stain was removed with filter paper and grids were left to dry.

For analysis of transduced cells, Vero cells were seeded onto Thermanox coverslips (ThermoFisher Scientific) at 2.5×10^4 cells/cm^2 and incubated at 37°C until 90% confluence had been reached. Cells were transduced with AdH5 vectors encoding either E183L or E199L (MOI 100) and were incubated at 37°C for 24 hours to allow protein expression. Samples were fixed in 2% glutaraldehyde in phosphate buffer (Agar Scientific) for 1 hour before being fixed for a further hour in aqueous 1% osmium tetroxide (Agar Scientific). The samples were dehydrated in an ethanol series; 70% for 30 minutes, 90% for 15 minutes and 100% three times for 10 minutes each. A transitional step of 10 minutes in propylene oxide (Agar Scientific) was undertaken before the samples were infiltrated with a 50:50 mix of propylene oxide and epoxy resin (Agar Scientific) for 1 hour. After a final infiltration of 100% epoxy resin for 1 hour, the samples were embedded in

moulds and polymerised overnight at 60°C. Thin sections of 80 µm were cut, collected onto glow discharged copper 200 mesh EM grids (Agar Scientific) and grid stained using Leica EM AC20.

All samples were imaged at 100 kV in a FEI T12 TEM using a Tietz F214 CMOS camera.

2.10 Mass spectrometry

2.10.1 Sample preparation

Vero cells were seeded onto 90 mm petri dishes (Fisher Scientific) at 16.5 x 10^5 cells/dish and left to grow to 90% confluency. Cells were transduced using E199L-HA AdH5 at MOI 100 and incubated overnight at 37°C. Negative control samples were generated using non-transduced Vero cells that were maintained under the same conditions. Three replicate petri dishes were set up for each of the transduced and non-transduced samples. Cell media was removed and cells were washed twice in PBS. Cells were then suspended in 1 ml lysis buffer consisting of 10 mM Tris/Cl pH 7.5; 150 mM NaCl; 0.5 mM EDTA; 0.5% Igepal CA-630 and Halt protease and phosphatase inhibitor (ThermoFisher Scientific) before incubation on ice for 30 minutes. Samples were then centrifuged for 5 minutes at 16 000 × *g* and supernatants were transferred to separate tubes. To each tube containing the supernatant, 150 µl of anti-HA affinity matrix (Roche) was added and incubated overnight at 4°C on a tube rotator. Samples were pulse centrifuged for 20 seconds and supernatants were removed to waste. Next, samples were washed three times in wash buffer consisting of 10 mM Tris/Cl pH 7.5; 150 mM NaCl and 0.5 mM EDTA. Elution of proteins was carried out by adding 300 µl of glycine buffer, pH 2.5 and incubating for 10 minutes at room temperature. Samples were pulse centrifuged for 20 seconds and eluent was removed to a fresh tube containing 30 µl Tris buffer, pH 11. A total of four elutions was carried and eluents from each sample were pooled into a single tube. Finally, 24 µl of the eluted samples were analysed by western blot for the presence of E199L-HA. Eluent and affinity matrix from each sample was then processed for mass spectrometry analysis by Dr Stuart Armstrong at University of Liverpool.

2.10.2 Sample processing

IP analysis is similar to that described by García-Dorival (Garcia-Dorival et al., 2014). Eluted proteins were mixed with 50 mM ammonium bicarbonate in a 1:1 volume dilution. Proteins were reduced by addition of dithiothreitol (Sigma) (3 mM final concentration) and heated at 60°C for 10 minutes. The samples were returned to room temperature, and iodoacetamide (Sigma) (9 mM final concentration) was added for 30 minutes in the dark to alkylate the proteins. Proteins were digested with 0.2 µg of proteomic grade trypsin (Sigma) and left to incubate at 37°C overnight. The resulting peptide samples were then acidified with 1% (v/v) trifluoroacetic (TFA) acid. Peptides were concentrated and desalted using C18 Stage tips (ThermoFisher Scientific) and then samples dried using a centrifugal vacuum concentrator (Eppendorf). Peptides were re-suspended in 0.1% (v/v) trifluoroacetic acid and 5% (v/v) acetonitrile.

Affinity matrix (post glycine elution) was mixed with reducing sample buffer (LDS, ThermoFisher Scientific) in a 1:1 volume dilution and heated at 70°C for 10 minutes. Samples were separated on a 4 - 12% SDS PAGE gel (NuPAGE, ThermoFisher Scientific) and Coomassie stained. The entire lane was excised, avoiding antibody fragments and subjected to in-gel digestion with trypsin. Peptides were concentrated and desalted as above.

2.10.3 Mass spectrometry analysis

Peptides were analysed by on-line nanoflow liquid chromatography (LC) using the Ultimate 3000 nano system (Dionex/Thermo Fisher Scientific). Samples were loaded onto a trap column (Acclaim PepMap 100, 2 cm × 75 μm inner diameter, C18, 3 μm, 100 Å) at 5 μl.minute^{-1} with an aqueous solution containing 0.1% (v/v) TFA and 2% (v/v) acetonitrile. After 7 minutes, the trap column was set in-line an analytical column (Easy-Spray PepMap® RSLC 50 cm × 75 μm inner diameter, C18, 2 μm, 100 Å) fused to a silica nano-electrospray emitter (Dionex). The column was operated at a constant temperature of 30°C and the LC system coupled to a Q-Exactive HF mass spectrometer (Thermo Fisher Scientific). Chromatography was performed with a buffer system consisting of 0.1% formic acid (buffer A) and 80% acetonitrile in 0.1% formic acid (buffer B). The peptides were separated by a linear gradient of 3.8 - 50% buffer B over 30 minutes at a flow rate of 300 nl/minute. The Q-Exactive HF was operated in data-dependent mode with survey scans acquired at a resolution of 60 000 and scan range 350 - 2000 m/z. Up to the top ten most abundant isotope patterns with charge states +2 to +5 from the survey scan were selected with an isolation window of 2.0 Th and fragmented by higher energy collisional dissociation with normalized collision energies of 30. The maximum ion injection times for the survey scan and the MS/MS scans were 100 and 45 ms respectively, and the ion target value was set to 3E6 for survey scans and 1E5 for the MS/MS scans. MS/MS events were acquired at a resolution of 30 000. Repetitive sequencing of peptides was minimized through dynamic exclusion of the sequenced peptides for 20 seconds.

MS spectra data was analysed by label-free quantification (LFQ) using the MaxQuant software (v 1.6.1.0) (Cox et al., 2014) and searched against either a human protein database (Uniprot release-2017_10) or Chlorocebus sabaeus protein database (Uniprot release-2017_10) and the ASFV E199L bait protein sequence (Uniprot) using the Andromeda search engine. The false discovery rate (FDR) was set to 0.01, and a decoy database was included in the search to help identify false-positives. LFQ results were further processed with Perseus software (v 1.6.1.1) (Tyanova et al., 2016) to determine significance between resin alone compared to tagged E199L protein. Statistical t-test analysis was used to analyse intensity values. Proteins with a p-value <0.05 and a fold change >2 were considered statistically significant.

2.11 Statistics

Graphs were prepared in Graphpad Prism (version 7) and statistical analysis was performed in MiniTab (version 18) using analysis of variance (ANOVA), plus Tukey multiple comparison test to

determine statistical differences between groups. Data that did not fit a normal distribution was converted to $\log_{10}$ scale prior to conducting the statistical analysis.

2.12 Antibodies

Primary and secondary antibodies used for the detection of proteins by Western blot (WB) and immunofluorescence (IF)

Table 2.4 Antibodies

Name	Manufacturer	Clone/Product number	Species	Clonality	WB dilution	IF dilution
Primary Antibodies						
4E-BP1	Cell Signaling Technology	9452	Rabbit	Polyclonal	1:1000	
P-4E-BP1	Cell Signaling Technology	9459	Rabbit	Polyclonal	1:1000	
Akt	Cell Signaling Technology	4691	Rabbit	Monoclonal	1:1000	
P-Akt T308	Cell Signaling Technology	13038	Rabbit	Monoclonal	1:1000	
P-Akt S473	Cell Signaling Technology	4060	Rabbit	Monoclonal	1:2000	
Calnexin	Cell Signaling Technology	2679	Rabbit	Monoclonal	1:1000	
Calnexin	The Pirbright Institute	TW20	Rabbit	Monoclonal		1:500
CHOP	Cell Signaling Technology	2895	Mouse	Monoclonal	1:1000	
GFP	Abcam	ab290	Rabbit	Polyclonal	1:6000	
HA	Roche	11867423001	Rat	Monoclonal		1:1000
HA	Santa Cruz	SC-805	Rabbit	Polyclonal		1:500
HA-HRP	Roche	12013819001	Rat	Monoclonal	1:1000	
J18L	The Pirbright Institute	Anti-sera	Rabbit	Polyclonal	1:1000	
LC3B	Sigma	L7543	Rabbit	Polyclonal		1:1000
LC3B	Cell Signaling Technology	2775	Rabbit	Polyclonal	1:1000	
MGF110-4L/5L	The Pirbright Institute	TEW29	Rabbit	Monoclonal		1:500

Name	Manufacturer	Clone/Product number	Species	Clonality	WB dilution	IF dilution
p30	The Pirbright Institute	C18	Mouse	Monoclonal	1:1000	1:1000
p30	The Pirbright Institute	1D9	Mouse	Monoclonal		1:160
p62	Cell Signaling Technology	88588	Mouse	Monoclonal	1:500	
p70-S6K	Cell Signaling Technology	9202	Rabbit	Polyclonal	1:1000	
P-p70-S6K	Cell Signaling Technology	9205	Rabbit	Polyclonal	1:1000	
γ-tubulin	Sigma	T6557	Mouse	Monoclonal	1:2500	
ULK1	Cell Signaling Technology	8054	Rabbit	Monoclonal	1:1000	
P-ULK1	Cell Signaling Technology	14202	Rabbit	Monoclonal	1:1000	
WIPI2	Abcam	ab105459	Mouse	Monoclonal		1:1000
Secondary antibodies						
Mouse-HRP	Promega	W402B	Goat	Polyclonal	1:2000	
Rabbit-HRP	Santa Cruz	SC-2004	Goat	Polyclonal	1:2000	
mouse-488	ThermoFisher Scientific	A11029	Goat	Polyclonal		1:500
mouse-568	ThermoFisher Scientific	A11004	Goat	Polyclonal		1:500
mouse IgG1-568	ThermoFisher Scientific	A21124	Goat	Polyclonal		1:500
mouse IgG2A-488	ThermoFisher Scientific	A21131	Goat	Polyclonal		1:500
rabbit-405	ThermoFisher Scientific	A31556	Goat	Polyclonal		1:200
rabbit-488	ThermoFisher Scientific	A11034	Goat	Polyclonal		1:500
rabbit-568	ThermoFisher Scientific	A11036	Goat	Polyclonal		1:500
rat-568	ThermoFisher Scientific	A11077	Goat	Polyclonal		1:500

2.13 Pharmacological inhibitors

Pharmacological compounds used as inhibitors

Table 2.5 Pharmacological inhibitors

Name	Manufacturer	Product number	Target	Final concentration
Bafilomycin A1	Enzo	BML-CM110	vacuolar-type H+ ATPase	100 nM
LY294002	Sigma	L9908	PI3K	50 nM
MK-2206	Seleckchem	S1078	Akt1/2/3	5 µM
Torin1	Generon	A11587-10	mTOR	200 nM
Torin2	Sigma	SML1224	mTOR	1 µM
Tunicamycin	Sigma	T7765	N-glycosylation	20 µg/ml

3 Characterisation of the modulation of autophagy by ASFV

3.1 Introduction

Since the first descriptions of autophagy were published, extensive research has transformed our understanding of its purpose from what was exclusively regarded as a basic mechanism of maintaining adequate cell energy levels to one that is now multi-faceted. In the context of infection, autophagy has been shown to play important roles in host defence, from the fundamental intrinsic defence mechanism of engulfing cytoplasmic pathogens to the more advanced innate and adaptive immune responses (Gomes and Dikic, 2014). Research has also uncovered links between autophagy and host cell stress responses such as the unfolded-protein response (UPR) (Senft and Ronai, 2015) and apoptosis (Mukhopadhyay et al., 2014). Virus infection and replication inevitably lead to cell stress by disrupting and subverting multiple cell pathways to direct resources towards the benefit of virus replication. Consideration of its wide-ranging functions means that autophagy undoubtedly has a role to play in the cellular response to infection. The ability of the virus to propagate is in many ways dependent on its capacity to modulate these cellular stress responses including the autophagy response.

Infection of the cell by ASFV leads to the modification of several organelles in a highly orchestrated fashion including the cell cytoskeleton, nucleus, ER and mitochondria (Netherton and Wileman, 2013). Evidence of activation of caspase-12 and the ATF6 pathway of the UPR, regarded as key indicators of ER stress induction suggests that ASFV infection induces an ER stress response (Galindo et al., 2012). The activation of ER stress and the UPR by ASFV could also be an important factor in the induction of apoptosis. This is because signalling through caspase-12 and the ATF6 pathway of the UPR can trigger pro-apoptotic signals (Szegezdi et al., 2003, Szegezdi et al., 2006). Indeed, apoptosis is induced early on in ASFV infection, evidenced by the activation of caspase 3, most likely during virus entry or uncoating (Carrascosa et al., 2002). Critically, ASFV is able to delay the final execution step of the apoptotic pathway to allow time for virus replication by encoding several apoptosis modulators (Dixon et al., 2017). This includes A179L, a viral Bcl-2 homologue that has been shown to bind several proapoptotic Bcl-2 proteins including the key autophagy protein Beclin 1 (Banjara et al., 2017, Hernaez et al., 2013). Beclin 1, also a Bcl-2 interacting protein, is regarded as an important point of convergence between autophagy and apoptosis and has been shown to undergo caspase-mediated cleavage during apoptosis (Wirawan et al., 2010).

As alluded to above, there is an intricate synergy between autophagy, the UPR and apoptosis which has no doubt evolved to provide a potent defence against invading microbes and predictably, viruses employ a finely balanced strategy to successfully evade these defences. Herpes simplex virus type 1 (HSV-1) which is also a large double-stranded DNA virus, encodes multiple proteins that act on the autophagy pathway at different stages (Lussignol et al., 2013, Orvedahl et al., 2007).

Inhibition of autophagy is not only mandatory for viral neurovirulence but has also been shown to be involved in immune escape via the reduction of viral antigen presentation by dendritic cells (Gobeil and Leib, 2012). An engineered mutant of HSV-1 that had lost the ability to interact with Beclin 1 was cleared more rapidly by mice and stimulated stronger CD4 T-cell responses and enhanced levels of IFN-γ and IL-2 when compared to wild-type virus (Leib et al., 2009). This not only highlights the role of autophagy in the innate and adaptive immune response but also emphasises the potential importance of viral modulation of the autophagy response.

As with the regulation of the UPR and apoptosis response by ASFV, one would expect that autophagy is tightly controlled by the virus. Work carried out by Hernaez and colleagues has been the only contribution on the subject of autophagy in the context of ASFV infection (Hernaez et al., 2013). This work was mostly focused on characterising the novel interaction between A179L and Beclin 1 although the authors also concluded that ASFV does not induce autophagy in infected cells due to an observed absence of GFP-LC3 puncta and a non-elevated ratio of LC3-II to LC3-I. Gaining further understanding of the interaction between ASFV and autophagy will improve our knowledge of how the cell reacts to infection and how ASFV is able to evade the anti-microbial activity of autophagy. This may provide opportunities for therapeutic intervention or improved vaccine design.

The aim of this study was to determine whether autophagy occurred during ASFV infection and to identify whether the virus exerts an inducing or inhibitory effect on the autophagy pathway at the point of autophagosome formation. This was carried out using immunofluorescent microscopy and Western blot analysis of the key autophagic marker protein, LC3. Analysis of LC3-II by Western blot provides a useful global indication of any changes however, visually assessing intracellular changes in the infected cell by confocal microscopy eliminates any potential effects from the un-infected cell population. As, for example, the presence of the un-infected cell population within whole cell lysates could mask changes in LC3-II levels assayed by Western blot. Having said that, Western blot analysis is a convenient method of interrogating LC3 changes in cell types such as macrophages that are difficult to examine by fluorescent microscopy techniques. In addition to the modulation of autophagosome formation, the effect on autophagic flux by ASFV was examined using a p62 degradation assay.

This study also set out to determine whether infection perturbed or modulated autophagy pathways to help support replication. Studies included analysis of the virus life cycle comparing replication efficiency in autophagy competent and autophagy deficient cell lines. Finally, the potential for autophagy proteins to act in an autophagy-independent manner during ASFV infection was explored. The results and conclusions of these experiments were further aimed at forming a foundation of understanding from which to conduct downstream investigations into the mechanisms of autophagy modulation by ASFV which are described later in the thesis.

3.2 Results

3.2.1 ASFV inhibits the induction of autophagosomes in response to starvation

Starvation of cells in a balanced salt solution that is deficient of any form of energy source is an effective means of inducing autophagy. Starvation leads to the inactivation of the nutrient-sensing mTORC1 protein leading to the downstream formation of autophagosomes within the cell cytoplasm (Yang and Klionsky, 2009). As part of this process, LC3-I is converted to LC3-II, moving from a cytoplasmic pool to discreet LC3-II punctate structures as it becomes embedded within the expanding autophagosome membrane. This process is essential for autophagosome formation as LC3-II serves as a critical structural protein. Visualisation of these punctate structures by immunofluorescence is a key method of observing autophagosomes in the cell. Alternatively, increased cellular levels of LC3-II visualised by Western blot analysis can also be used to indicate the induction of autophagy (see results section 3.2.2).

To assess the effect of ASFV on autophagy, the number of autophagosomes in ASFV infected cells was visualised by confocal microscopy and compared to uninfected and mock infected cells in either nutrient replete (Figure 3.1.1) or starvation (Figure 3.1.2) conditions. Vero cells were infected for a total period of 4 hours during which cells were incubated for the last 2 hours in either complete cell media (non-starved) or Earle's balanced salt solution (EBSS) (starved) prior to being fixed and labelled for immunofluorescence. A 4 hour period of infection was chosen as by this stage early virus protein translation has begun and virus replication is commencing. Cells were either incubated with complete cell media only (uninfected), mock infected using Vero cell supernatant or infected with Ba71V (MOI 5).

LC3 labelling revealed a predominantly cytoplasmic signal with the occasional bright puncta in uninfected cells (Figure 3.1.1A). The puncta represent autophagosomes and the low numbers in these cells is typical of what would be expected under nutrient replete conditions. Similar results were seen in cells that had been infected with the mock inoculum, suggesting that Vero cell supernatant did not induce the formation of autophagosomes (Figure 3.1.1B). A similar pattern was observed in cells infected with Ba71V (Figure 3.1.1C). Labelling with the anti-p30 antibody identified cells expressing ASFV genes (Figure 3.1.1D), interestingly there were very few LC3 puncta in these cells. Taken together this showed that ASFV infection did not induce the formation of autophagosomes during the early stages of its replication cycle.

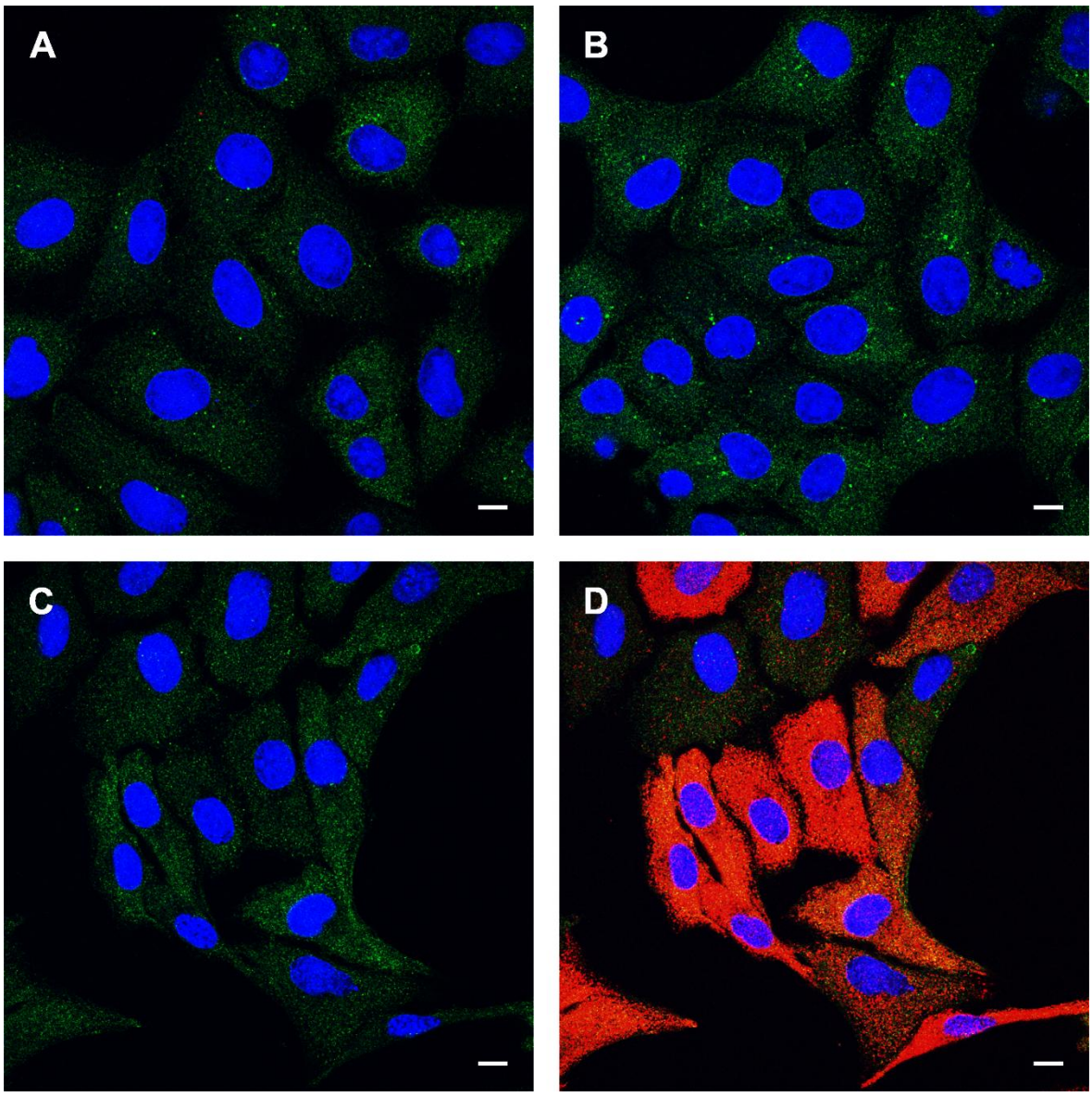

Figure 3.1.1 ASFV does not induce autophagosomes at 4 hpi

Vero cells were incubated with media alone (Panel A), mock inoculum (Panel B) or Ba71V (MOI 5) (Panels C and D) for 1 hour. Inocula were removed and cells were incubated for a total of 4 hours during which cells were non-starved in complete Vero cell media for the final 2 hours. Cells were then fixed and permeabilised in methanol before labelling LC3 shown in green, viral protein p30 shown in red and nuclei shown in blue. Panels A, B and D show labelling for p30. Panel C shows the same infected cells as Panel D but with the red channel removed to allow for clearer observation of LC3 staining. Scale bars represent 10 µM.

Higher numbers of autophagosomes were seen in both uninfected (Figure 3.1.2A) and mock infected cells (Figure 3.1.2B) after starvation when compared to cells under nutrient replete conditions (Figure 3.1.1). Comparable numbers of autophagosomes were observed in both uninfected and mock infected cells suggesting that Vero cell supernatant did not affect induction of autophagosomes under starvation conditions. The majority of the cells that had been infected with ASFV had cytoplasmic LC3 staining with very few puncta (Figure 3.1.2C). Labelling with anti-p30

showed that the cells that did contain puncta did not express viral proteins. This suggests that ASFV blocks the formation of starvation-induced autophagosomes at 4 hpi.

The number of autophagosomes per cell in 30 cells were enumerated using Imaris software for each experimental condition (Figure 3.1.3). A comparison between non-starved and starved cells revealed a statistically significant increase in the number of autophagosomes per cell following starvation in both the uninfected ($P < 0.001$) and mock infected ($P < 0.001$) cells, however no statistically significant difference was observed between these two conditions respectively ($P > 0.05$). A statistically significant decrease in the number of autophagosomes was observed in non-starved ASFV infected cells when compared to the non-starved uninfected ($P < 0.01$) and mock infected cells ($P < 0.01$). A statistically significant decrease in autophagosomes was also observed in starved ASFV infected cells when compared to starved uninfected ($P < 0.001$) and mock infected ($P < 0.001$) cells. These results therefore demonstrate the inhibitory effect of the virus on the formation of autophagosomes in resting cells under nutrient replete conditions and furthermore show that the inhibitory effect becomes more apparent in cells under starvation-induced stress.

3.2.2 ASFV inhibits accumulation of LC3-II in response to starvation in Vero cells

The confocal microscopy results described in section 3.2.1 suggests that ASFV does not induce the formation of autophagosomes and that ASFV blocks starvation-induced formation of autophagosomes at 4 hpi. To support these results LC3-II levels were assessed during early stages of the replication cycle by Western blot analysis.

LC3-I is conjugated to phosphatidylethanolamine (PE) to form LC3-PE (LC3-II) which is incorporated into the developing autophagosome (Yang and Klionsky, 2009). The relative amount of LC3-II is strongly correlated with the number of autophagosomes and an accumulation of LC3-II can be an indication of autophagosome accumulation (Kabeya et al., 2000). This is either the result of induction of autophagy for example by starvation or the result of a reduction in autophagosome turnover for example by blocking fusion with the lysosome. In the case of the former, greater LC3-II amounts are observed due to the rate of autophagosome degradation falling below the rate at which new autophagosomes are formed. Despite LC3-II having a greater mass in comparison to LC3-I, it shows faster electrophoretic mobility in PAGE gels, most likely due to increased hydrophobicity (Klionsky et al., 2016). The apparent molecular weight of LC3-I is approximately 16-18 kDa and LC3-II is approximately 14-16 kDa.

Levels of LC3-II were assessed at 4 hpi under nutrient rich and starvation conditions in uninfected, mock infected and ASFV infected Vero cells. Samples were then prepared from cells for analysis by immunoblotting and probed using anti-LC3 (which detects both LC3-I and LC3-II), anti-p30 viral protein and anti-γ tubulin antibodies.

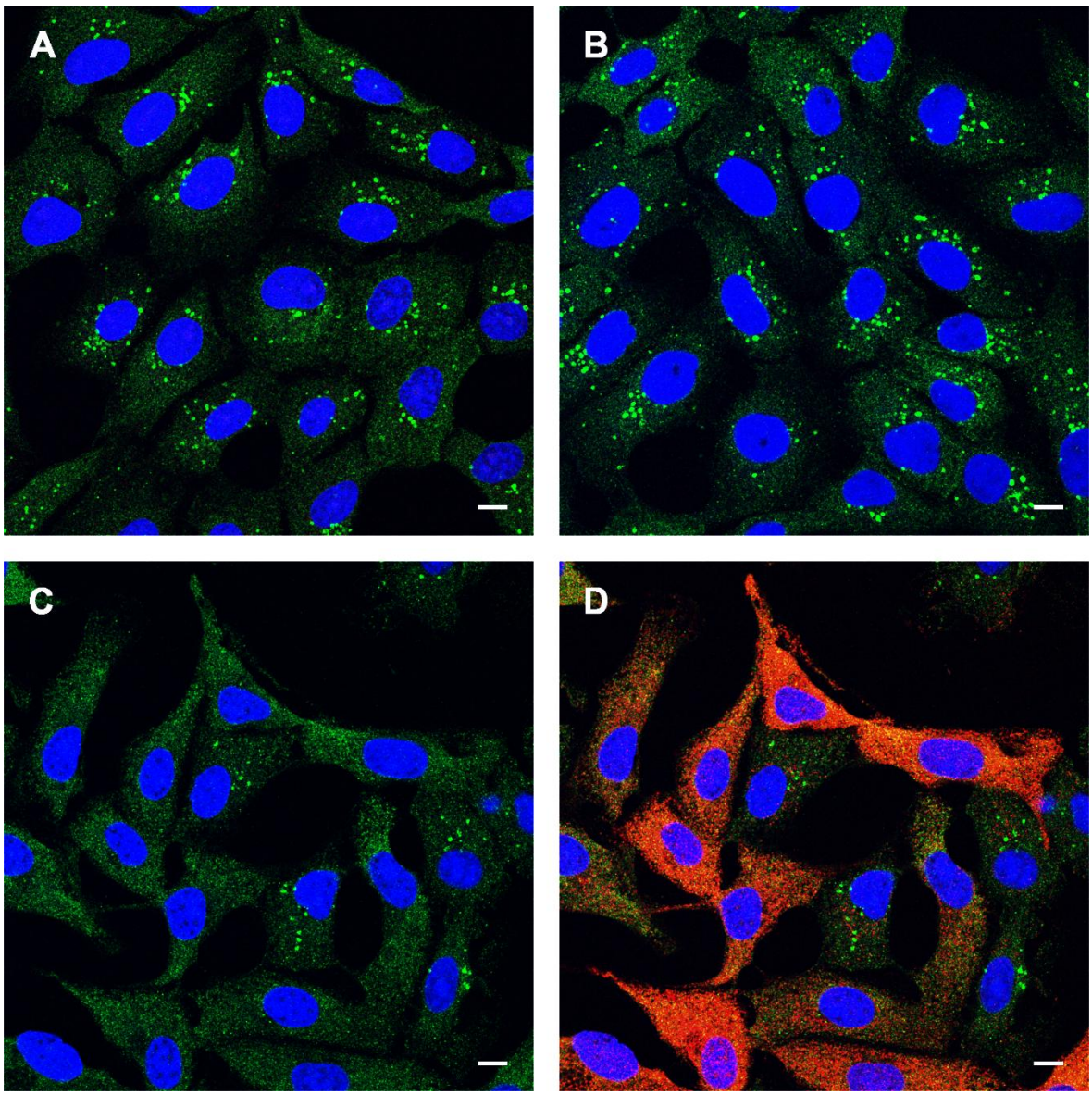

Figure 3.1.2 ASFV has an inhibitory effect on autophagy

Vero cells were incubated with media alone (Panel A), mock inoculum (Panel B) or Ba71V (MOI 5) (Panels C and D) for 1 hour. Inocula were removed and cells were incubated for a total of 4 hours during which cells were starved in EBSS for the final 2 hours. Cells were then fixed and permeabilised in methanol before labelling LC3 shown in green, viral protein p30 shown in red and nuclei shown in blue. Panels A, B and D show labelling for p30. Panel C shows the same infected cells as Panel D but with the red channel removed to allow for clearer observation of LC3 staining. Scale bars represent 10 µM.

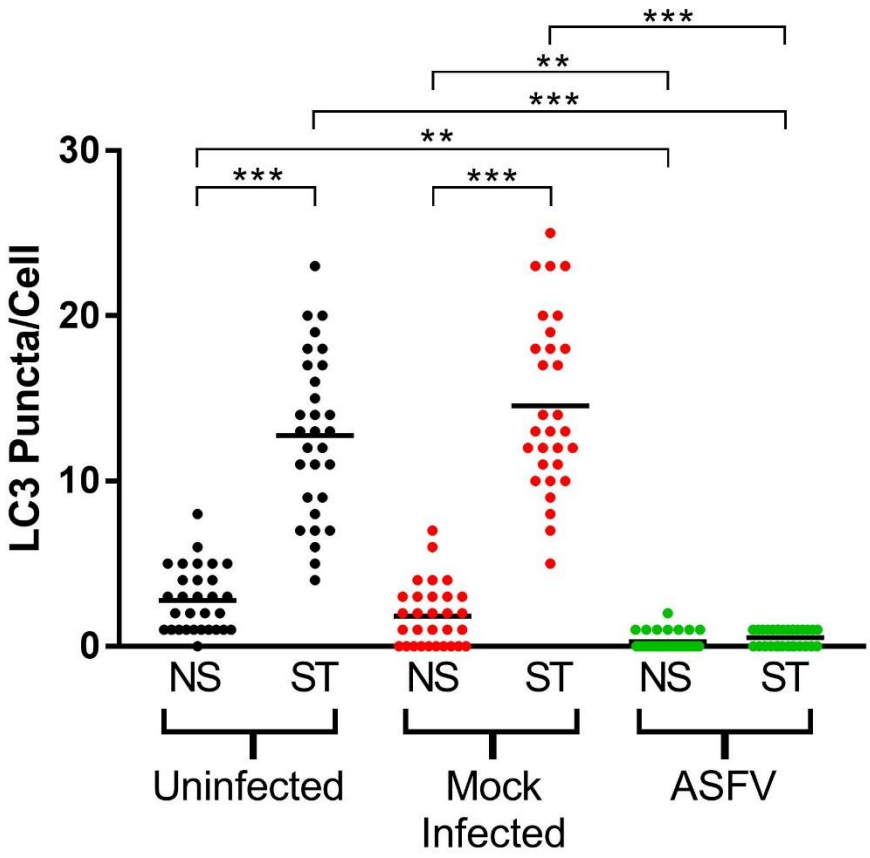

Figure 3.1.3 Imaris analysis confirms that ASFV inhibits the induction of autophagosomes in response to starvation

The number of LC3 puncta per cell for 30 individual cells per indicated experimental condition was quantified by Imaris analysis of confocal images. Vero cells were either uninfected, mock infected or infected with ASFV for a total of 4 hours. Prior to fixation, cells were either non-starved in complete cell media (NS) or starved in EBSS (ST) for 2 hours to induce autophagy. Centre lines show the medians. Statistical analysis was carried out in Minitab using analysis of variance with Tukey multiple comparisons test. Asterisks represent significant differences in value between NS and ST conditions and between the indicated infection status of the cells (** = P value of <0.01, *** = P value of <0.001).

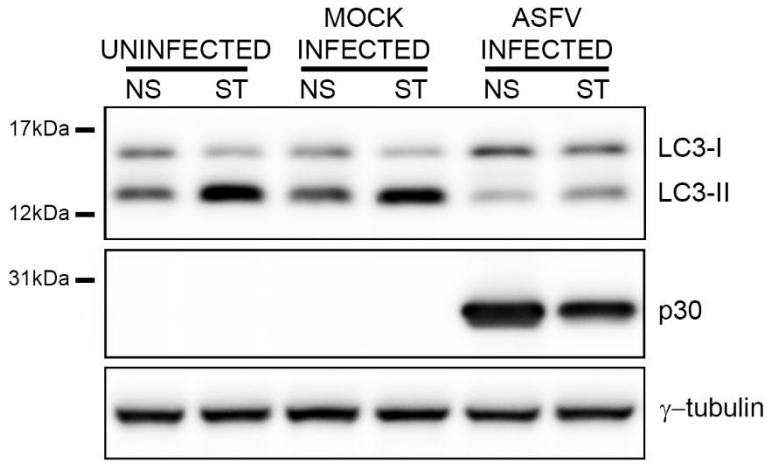

Figure 3.2 ASFV inhibits starvation-induced accumulation of LC3-II in Vero cells

Vero cells were incubated with media alone (uninfected), mock inoculum (mock infected) or Ba71V (MOI 5) for 1 hour. Inocula were removed and cells were incubated for a total of 4 hours during which cells were either non-starved (NS) in complete cell media or starved (ST) in EBSS for the final 2 hours. Cells were then lysed and samples prepared for resolution by bis-Tris PAGE before transfer to PVDF membrane. Finally, samples were probed with anti-LC3, anti-p30 and γ-tubulin antibodies followed by appropriate HRP-conjugated secondary antibodies. The positions of molecular mass markers are indicated to the left of the gels.

Expression of viral protein p30 was only detected in ASFV infected cells as expected, however, noticeably less protein was detected in starved cells when compared to non-starved cells, presumably due to reduced availability of amino acids for viral protein translation. The intensity of the band corresponding to LC3-II in the lanes containing samples from uninfected and mock infected cells under starvation conditions were much greater than those from non-starved cells demonstrating the induction of autophagy. Comparisons between non-starved cells showed less LC3-II in the ASFV infected cells compared to the uninfected and mock infected cells suggesting that ASFV did not induce LC3-II accumulation at 4 hpi. This was consistent with the absence of LC3 puncta in ASFV infected cells at 4 hpi (Figure 3.1.1). Under starvation conditions, the LC3-II band was much less intense in ASFV infected cells when compared with LC3-II levels in starved uninfected and starved mock infected cells which shows that starvation-induced LC3-II accumulation was inhibited by ASFV. This supports the confocal microscopy data that showed a block in starvation-induced formation of LC3 puncta at 4 hpi (Figure 3.1.2).

3.2.3 ASFV inhibits accumulation of LC3-II in response to drug treatment in porcine macrophages

As described previously, starvation is an effective method of inducing autophagosome formation via the inactivation of the nutrient sensing complex mTORC1. Using pharmacological inhibitors of mTORC1 is an alternative method of inducing the formation of autophagosomes with the concomitant accumulation of LC3-II. Torin2, a potent inhibitor of mTORC1 was developed to

overcome the rapamycin resistance of a significant subset of mTORC1 functionality (Liu et al., 2011, Thoreen et al., 2009).

ASFV inhibits accumulation of LC3-II in response to starvation in Vero cells using the Vero cell adapted strain of ASFV, Ba71V (3.2.2). However, porcine macrophages are the natural host cell of ASFV, and therefore the ability of the field strain virus OUR T88/1 to modulate autophagy in blood derived porcine macrophages was tested. Cells were either mock infected or infected with ASFV (MOI 5) for 6 hours. Separately, cells infected for 8 hours were incubated for the final 2 hours in complete cell media containing either DMSO (solvent control) or 1 μM Torin2 to induce LC3-II accumulation. Cell lysates were resolved by bis-Tris PAGE and immunoblotted with LC3 and anti-γ tubulin antibodies.

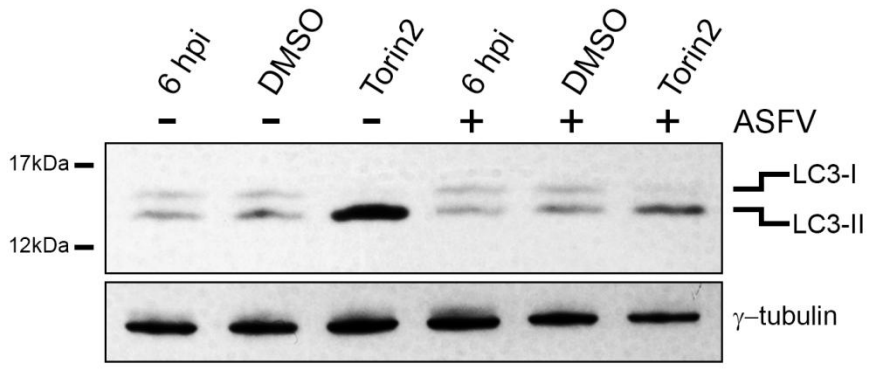

Figure 3.3.1 ASFV inhibits drug-induced accumulation of LC3-II in porcine macrophages

Blood derived porcine macrophages were either mock infected or infected with OUR T88/1 (MOI 5) for 6 hours (6 hpi). Separately, cells infected for a total of 8 hours were incubated for the final 2 hours in complete cell media containing DMSO or 1 μM Torin2 to induce an accumulation of LC3-II. Cells were then lysed and samples prepared for resolution by bis-Tris PAGE before transfer to PVDF membrane. Finally, samples were probed with anti-LC3 and γ-tubulin antibodies followed by appropriate HRP-conjugated secondary antibodies. The positions of molecular mass markers are indicated to the left of the gels. (This work was conducted by Dr Christopher Netherton)

The results showed similar amounts of LC3-II between the mock infected and ASFV infected cells at 6 hpi, demonstrating that the virus does not induce any accumulation of LC3-II above the level seen in mock infected cells. Cells that were incubated for a further 2 hours in the presence of DMSO did not show any appreciable difference in LC3-II band intensity indicating that the DMSO solvent alone has little effect on levels of LC3-II. A greater intensity of LC3-II was observed under Torin2 treatment of mock infected cells confirming that Torin2 had successfully stimulated the autophagy pathway. A comparison of LC3-II levels between mock infected and ASFV infected cells under Torin2 treatment showed much less LC3-II in ASFV infected cells demonstrating that ASFV had an inhibitory effect on Torin2-induced accumulation of LC3-II.

To quantify this effect, the integrated density of the LC3-II and γ-tubulin bands were determined using ImageJ. The relative densities of the LC3-II bands in the DMSO and Torin2 treatments were calculated by comparison to those at 6 hpi and finally the LC3-II values were normalised to those of γ-tubulin. Figure 3.3.2 shows the mean of three experiments where each of the three experiments used primary macrophages derived from a separate animal. The densitometry analysis showed there was less LC3-II after two hours stimulation with Torin2 in ASFV infected cells when compared to mock infected cells ($P < 0.001$) confirming the inhibitory effect by ASFV. This result combined with the results described in Figure 3.2 demonstrates that ASFV inhibits the accumulation of LC3-II in response to mTORC1 inactivation using a cell adapted strain or a virulent field strain and that this effect is seen in both Vero cells and macrophages.

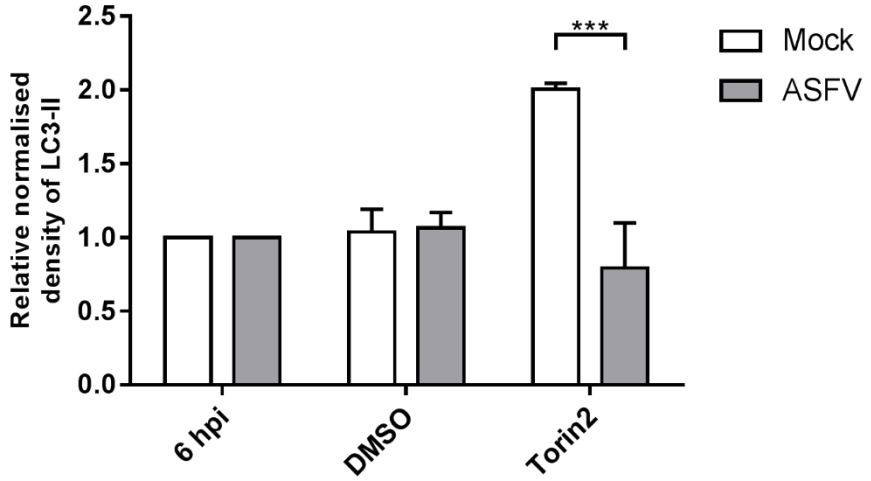

Figure 3.3.2 Densitometry analysis confirms that ASFV inhibits drug-induced accumulation of LC3-II in porcine macrophages

Densitometry analysis was carried out using ImageJ to determine the relative densities of the LC3-II bands from Western blot data shown in Figure 3.3.1. The relative densities of the LC3-II bands normalised to γ-tubulin in the DMSO and Torin2 treatments were calculated by comparison to those at 6 hpi. Data shown is the mean of three experiments and error bars indicate SEM. Statistical analysis was carried out in Minitab using analysis of variance with Tukey multiple comparisons test. Asterisks represent a significant difference in value between mock infected and ASFV infected cells (*** = P value of <0.001). (This work was conducted by Dr Christopher Netherton)

3.2.4 ASFV promotes formation of WIPI complexes

Sections 3.2.1 and 3.2.2 described the inhibition of starvation-induced LC3 puncta and the inhibition of starvation-induced accumulation of LC3-II by ASFV respectively. These results are both indicative of a block in the formation of autophagosomes by the virus. To further characterise this, a confocal microscopy experiment was conducted to investigate if the formation of WIPI

complexes is also inhibited by ASFV. WIPI forms an important effector protein complex upstream of autophagosome assembly that is vital for LC3 lipidation (Proikas-Cezanne et al., 2015).

Vero cells were either mock infected or infected with Ba71V for a period of 4 hours. During the final 2 hours, cells were incubated in either complete cell media (Figure 3.4.1) or EBSS starvation media (Figure 3.4.2) prior to being fixed and labelled for immunofluorescence. In this way, the inhibition or induction of WIPI complexes in mock infected or ASFV infected cells could easily be detected. Cells were labelled for WIPI and viral protein p30 to detect infected cells.

In mock infected cells, WIPI labelling revealed a mostly cytoplasmic signal with sporadic bright puncta that are representative of WIPI complexes (Figure 3.4.1A). The small quantity of puncta in these cells is typical of what would be expected under nutrient replete conditions. In cells infected with Ba71V (Figure 3.4.1B and C), a considerable number of WIPI complexes were detected in the vicinity of the nuclear periphery and in close proximity to each other. Anti-p30 labelling identified that the WIPI complexes were almost entirely detected in cells expressing ASFV genes (Fig 3.4.1C). Taken together this demonstrates that ASFV induces the formation of WIPI complexes at 4 hpi.

Considerably more WIPI complexes were seen in mock infected cells after starvation (Figure 3.4.2A) when compared to cells under nutrient rich conditions (Figure 3.4.1A). Visualisation of infected cells (Figure 3.4.2B and C) indicated a substantial number of WIPI complexes located in very close proximity to one another near the nuclear periphery. Labelling of p30 (Figure 3.4.2C) showed that a far greater number of WIPI complexes were detected in cells expressing p30 compared to those that were not, demonstrating that the WIPI puncta in ASFV infected cells were not exclusively formed in response to starvation. In addition, there was a clear contrast between the diffusely located WIPI complexes in mock infected cells and the aggregated complexes near the nuclear periphery in ASFV infected cells. Collectively, the results described in Figures 3.4.1 and 3.4.2 suggest that ASFV promotes the formation of WIPI complexes during the early stages of its replication cycle in a manner unaffected by nutrient availability.

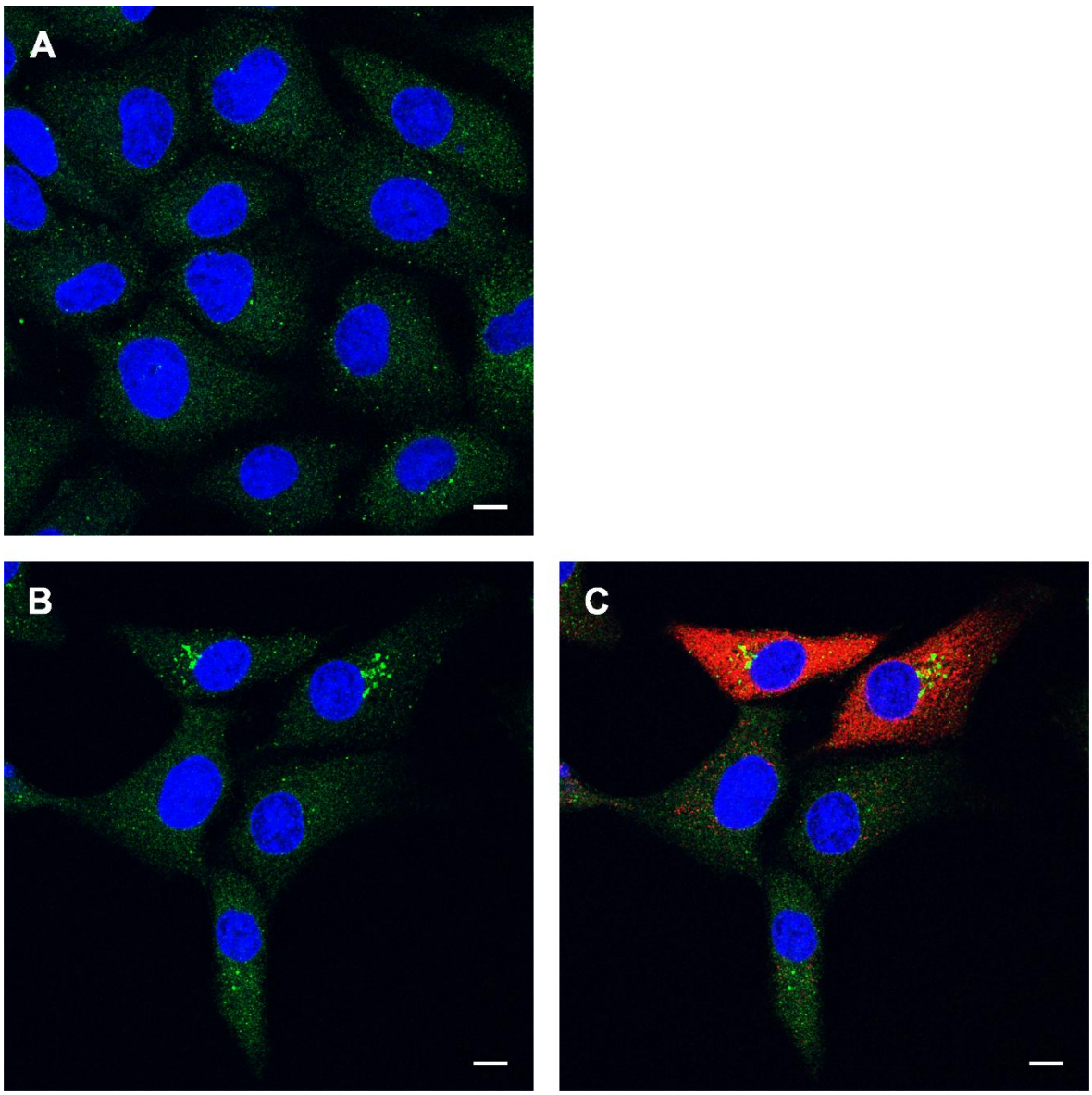

Figure 3.4.1 ASFV promotes the formation of WIPI complexes at 4 hpi under nutrient replete conditions

Vero cells were incubated with mock inoculum (Panel A) or Ba71V (MOI 5) (Panels B and C) for 1 hour. Inocula were removed and cells were incubated for a total of 4 hours during which cells were incubated in complete cell media for the final 2 hours. Cells were then fixed and permeabilised in methanol before labelling WIPI shown in green, viral protein p30 shown in red and nuclei shown in blue. Panels A and C show labelling for p30. Panel B shows the same infected cells as Panel C but with the red channel removed to allow for clearer observation of WIPI staining. Scale bars represent 10 µM.

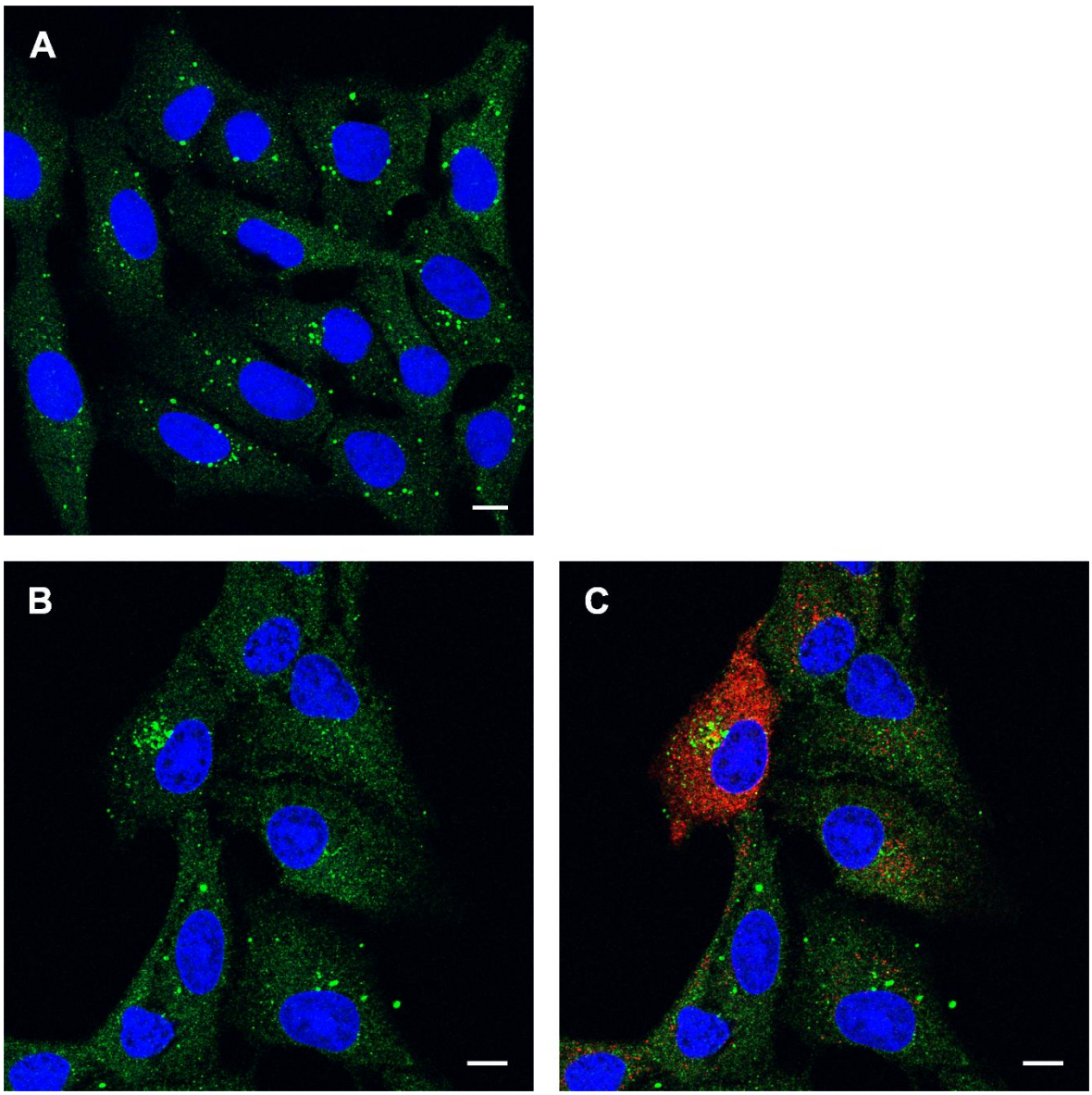

Figure 3.4.2 ASFV promotes the formation of WIPI complexes at 4 hpi under starvation conditions

Vero cells were incubated with mock inoculum (Panel A) or Ba71V (MOI 5) (Panels B and C) for 1 hour. Inocula were removed and cells were incubated for a total of 4 hours during which cells were starved in EBSS media for the final 2 hours. Cells were then fixed and permeabilised in methanol before labelling WIPI shown in green, viral protein p30 shown in red and nuclei shown in blue. Panels A and C show labelling for p30. Panel B shows the same infected cells as Panel C but with the red channel removed to allow for clearer observation of WIPI staining. Scale bars represent 10 µM.

3.2.5 ASFV inhibits starvation-induced degradation of p62

The results presented thus far have shown that although ASFV inhibits the formation of autophagosomes and inhibits the accumulation of LC3-II in response to inactivation of mTORC1, it is also able to stimulate the formation of WIPI complexes. The assembly of WIPI complexes is an essential step in the autophagy pathway that is required for the downstream formation of

autophagosomes. The induction of WIPI complexes in ASFV infected cells is therefore interesting considering that autophagosome formation is suppressed.

Using LC3-II as an autophagy marker is just one of several techniques that can be applied to interrogate the autophagy pathway (Klionsky et al., 2016). Autophagic activity is not only defined by the lipidation of LC3 during autophagosome generation, but also by flux through the whole system. Autophagic flux refers to the entire process of autophagy, including the formation of the autophagosome, fusion to the lysosome, breakdown of cargo and release of macro molecules back into the cytosol (Klionsky et al., 2016). Consequently, it is important to assess autophagic flux to gain a complete understanding of autophagic status of the cell. Increases in LC3-II or the appearance of autophagosomes, are not measures of autophagic flux as such, but can indicate the accumulation of autophagosomes due to stimulation of autophagy or inhibition of autophagosome clearance.

One method of evaluating autophagic flux is to quantify the rate of protein breakdown by autophagy. SQSTM1 also known as p62 is an autophagy receptor that contains a LIR motif as well as a ubiquitin binding domain, allowing it to bind both ubiquitinated substrates and LC3-II. In this way, p62 facilitates cargo docking inside the expanding autophagosome and is also incorporated into the completed autophagosome (Bjorkoy et al., 2009). Accordingly, p62 gets degraded in autolysosomes along with the cargo serving as a useful index of autophagic degradation. Activation of autophagy is strongly correlated with a decrease in p62 levels (Bjorkoy et al., 2009) and to test this Vero cells were either incubated in complete cell media, starved in EBSS or starved in EBSS in the presence of 100 nM bafilomycin A1 for 1 hour. Bafilomycin A1 acts by inhibiting vacuolar H+ ATPase (V-ATPase) which prevents fusion between autophagosomes and lysosomes (Yamamoto et al., 1998). In this way, bafilomycin A1 can be used to halt the degradation of p62. Following cell harvest, samples were probed with anti-p62 and γ-tubulin antibodies.

The intensity of the p62 band under starvation conditions appeared reduced when compared to cells that were incubated under nutrient replete conditions (Figure 3.5.1A). Densitometry analysis of three replicate experiments showed that starvation reduced the steady state levels of p62 by approximately one half (Figure 3.5.1B; $P < 0.05$). This demonstrated that autophagy was induced in the starved cells and p62 was degraded as a consequence. Levels of p62 after starvation in the presence of bafilomycin A1 were similar to cells incubated under nutrient replete conditions ($P > 0.05$) showing that starvation-induced degradation of p62 was blocked via the action of bafilomycin A1.

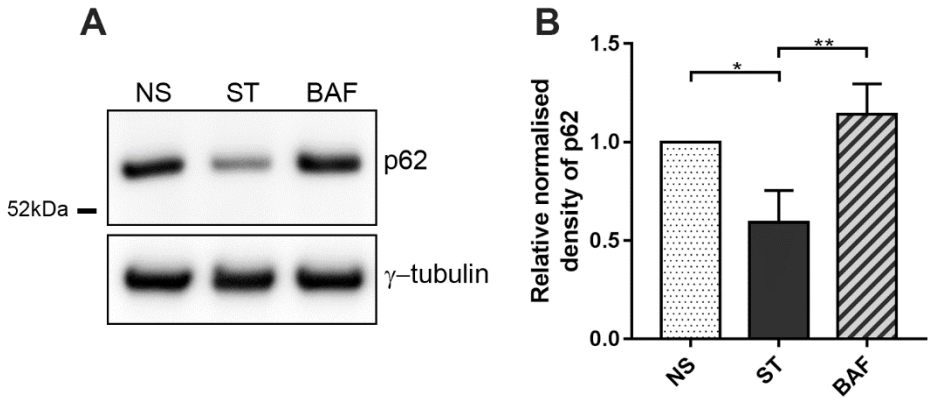

Figure 3.5.1 Activation of autophagy is strongly correlated with a decrease in p62

A) Vero cells were either incubated in complete cell media (NS), starved in EBSS (ST) or starved in EBSS in the presence of 100 nM bafilomycin A1 (BAF) for 1 hour. Cells were then lysed and samples prepared for resolution by bis-Tris PAGE before transfer to PVDF membrane. Finally, samples were probed with anti-p62 and γ-tubulin antibodies followed by appropriate HRP-conjugated secondary antibodies. The positions of molecular mass markers are indicated to the left of the gels. B) The relative densities of the p62 bands were calculated by comparison to that of the non-starved sample before being normalised to the values of γ-tubulin. Data shown is the mean of three experiments and error bars indicate SD. Statistical analysis was carried out in Minitab using analysis of variance with Tukey multiple comparisons test. Asterisks represent a significant difference in value between the indicated cell treatments (* = P value of <0.05 ** = P value of <0.01).

Following on from this, an experiment was conducted to determine if ASFV blocks starvation-induced degradation of p62. Vero cells were mock infected or infected with the Ba71V strain of ASFV (MOI 5) for a period of 4 hours or 12 hours. A 4 hour time point was chosen as previously inhibition of autophagosomes was seen at 4 hpi and 12 hours was chosen as by this stage the viral factory is well established and mature virions are beginning to appear. In this way, it could be tested whether p62 degradation is blocked by the virus at an early and late stage of the virus lifecycle. Prior to cell lysis, cells were either incubated in complete cell media or starved in EBSS for 2 hours to induce autophagy and the degradation of p62. Lastly, samples were probed with anti-p62 and γ-tubulin primary antibodies.

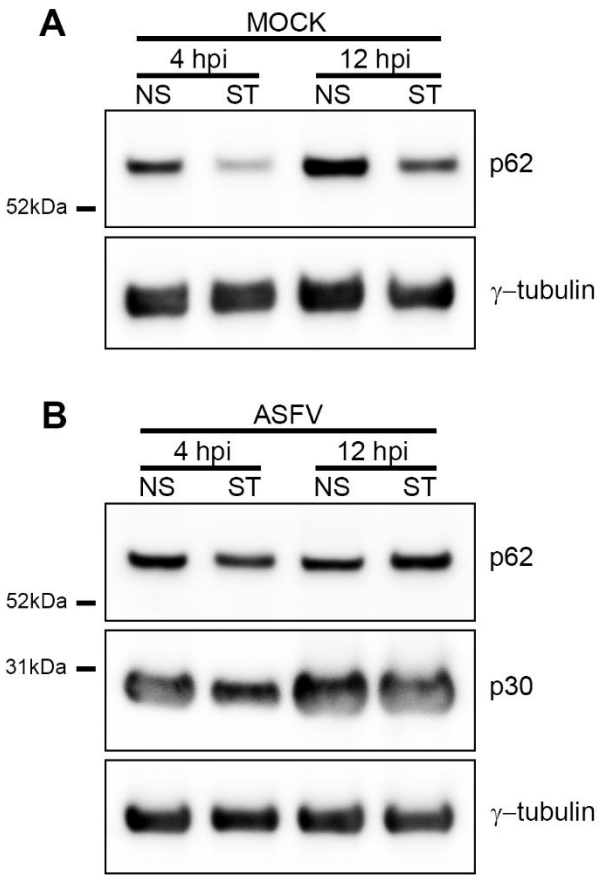

Figure 3.5.2 ASFV inhibits starvation-induced degradation of p62

Vero cells were incubated with mock inoculum (Panel A) or Ba71V (MOI 5) (Panel B) for 1 hour. Inocula were then removed and replaced with fresh 2% media. Cells were incubated for a total of 4 hours or 12 hours during which cells were either non-starved (NS) in complete cell media or starved (ST) in EBSS for the final 2 hours to induce autophagy and p62 degradation. Cells were lysed and samples prepared for resolution by bis-Tris PAGE before transfer to PVDF membrane. Finally, samples were probed with anti-p62, anti-p30 and γ-tubulin antibodies followed by appropriate HRP-conjugated secondary antibodies. The positions of molecular mass markers are indicated to the left of the gels.

Less p62 was seen in the samples derived from mock infected cells that had been starved at 4 hpi and 12 hpi when compared to the non-starved samples respectively (Figure 3.5.2A). In contrast, comparable levels of p62 were observed between cells that were starved and cells that were incubated under nutrient rich conditions at either 4 hpi or 12 hpi after infection with ASFV (Figure 3.5.2B). Immunoblotting with anti-p30 antibody showed expression of viral proteins in cells that were infected with ASFV. Densitometry analysis on three replicate experiments showed that the relative densities of the p62 bands in mock infected cells after starvation were roughly half that of cells that were non-starved (Figure 3.5.3).

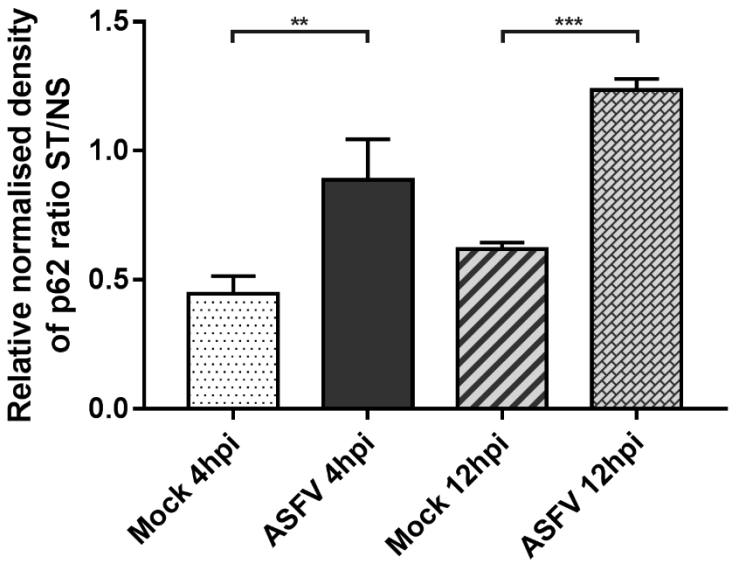

Figure 3.5.3 Densitometry analysis confirms that ASFV inhibits starvation-induced degradation of p62 at 4 hpi and 12hpi

Densitometry analysis was conducted using ImageJ to determine the relative densities of the p62 bands from Western blot data shown in Figure 3.5.2. The relative densities of the p62 bands were calculated by comparison to those of the 4 hpi non-starved sample before normalising the values to those of γ-tubulin. This was carried out separately on the mock infected and ASFV infected samples. Finally, the ratio of starved (ST) to non-starved (NS) values were calculated for mock infected and ASFV infected samples at 4 hpi and 12 hpi. Data shown is the mean of three experiments and error bars indicate SD. Statistical analysis was carried out in Minitab using analysis of variance with Tukey multiple comparisons test. Asterisks represent a significant difference in value between the mock infected and ASFV infected cells at 4 hpi and 12 hpi (** = P value of <0.01, *** = P value of <0.001).

Levels of p62 were relatively unchanged after starvation in ASFV infected cells at both 4 and 12 hpi and the difference in the ratio of starved to non-starved samples between mock infected and ASFV infected cells were significantly different at both 4 hpi ($P < 0.01$) and 12 hpi ($P < 0.001$). This clearly demonstrates that p62 is not degraded in ASFV infected cells at 4 hpi or 12 hpi as would usually be expected under starvation conditions. Together, the data showing that ASFV inhibits starvation-induced p62 degradation and that ASFV inhibits formation of autophagosomes, demonstrates that ASFV causes a block in autophagic flux at both early and late stages of infection. This suggests that the observed WIPI complexes in infected cells are not related to an induction of autophagy.

3.2.6 ASFV replication does not require the autophagy pathway

Having established that ASFV inhibits the formation of autophagosomes and blocks autophagic flux, it is tempting to speculate that ASFV does not depend on the process of autophagy for virus replication. To test this hypothesis, replication of ASFV was monitored following infection of

autophagy deficient cells with the attenuated Uganda strain. Generating mouse embryo fibroblasts (MEFs) with an Atg5$^{-/-}$ mutation renders them entirely autophagy deficient (Kuma et al., 2004). This is because the conjugation of Atg5 to Atg12 is critical to the targeting of LC3 to the isolation membrane and the elongation process during autophagosome formation (Mizushima et al., 2001). Wild-type (autophagy competent) or Atg5$^{-/-}$ (autophagy deficient) MEFs were infected at MOI 0.1 and virus replication was monitored over a 72 hour period by virus titration.

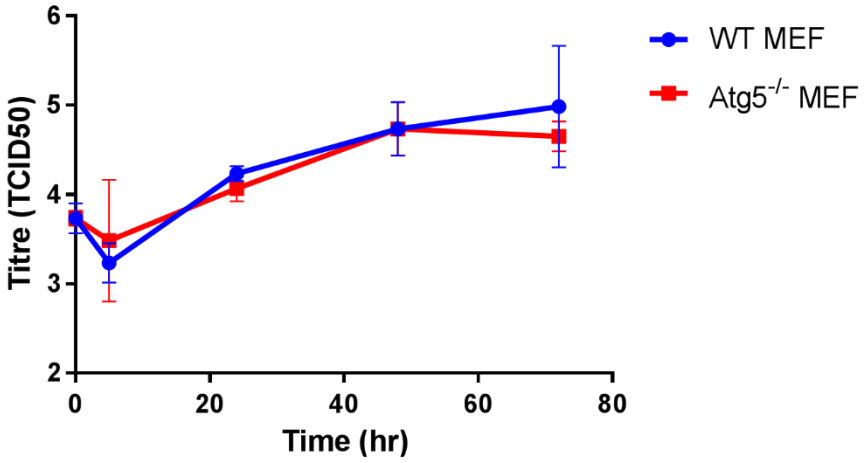

Figure 3.6 ASFV replication does not require the autophagy pathway

Wild-type (blue line) or autophagy deficient Atg5$^{-/-}$ (red line) mouse embryo fibroblasts were infected with tissue culture adapted ASFV Uganda (MOI 0.1) and incubated for the indicated time. Virus replication was assessed by virus titration calculated as TCID50. Error bars show SEM of triplicate wells. Statistical analysis was carried out in Minitab using analysis of variance with Tukey multiple comparisons test. No statistical differences in the virus titres were observed between wild- type and Atg5$^{-/-}$ cells.

No differences in virus titre at each of the five measured time points were observed between virus grown in wild-type or Atg5$^{-/-}$ MEFs showing that the attenuated Uganda strain could replicate equally in both cell lines. This experiment was conducted over a 72 hour period which provided sufficient time for the virus to progress through all stages of the virus life cycle including virus entry, replication and egress from the cell in the Atg5$^{-/-}$ MEFs. Collectively, this data therefore suggests that autophagy is not required by ASFV.

3.2.7 LC3 puncta and WIPI puncta are observed at the viral factory during late ASFV infection

In their study describing the interaction of A179L with Beclin 1, Hernaez and colleagues also investigated the distribution of LC3 puncta in ASFV infected Vero cells (Hernaez et al., 2013). They reported that structures resembling autophagosomes were detected within and around the

viral factory at 16 hpi under nutrient replete conditions although no newly formed virions were found to be colocalised with these structures. These results raise a number of questions; firstly, at what stage of infection do the LC3 puncta first appear? Secondly, does the appearance of the LC3 puncta rely on the overexpression of LC3 as the LC3 puncta were previously reported using transfected cells overexpressing GFP-LC3? Finally, does the appearance of LC3 puncta coincide with the appearance of WIPI puncta? To address these questions, infected Vero cells were analysed by confocal microscopy during late infection. Cells were infected with Ba71V (MOI 5) and harvested every 2 hours from 10 hpi to 16 hpi. Following fixation, cells were probed with anti-LC3 or anti-WIPI primary antibodies. In addition, cells were probed with an anti-p30 antibody to identify infected cells.

Visual inspection of the cells at 16 hpi showed the appearance of perinuclear DAPI stain in some cells which represents the accumulation of viral DNA and essentially demarcates the boundary of the viral factory (Figure 3.7). Labelling of p30 (Figure 3.7B and D) demonstrated ASFV infection of the aforementioned cells. The appearance of WIPI puncta could clearly be seen in close proximity to and sometimes within the viral factory (Figure 3.7A). Similarly, LC3 puncta were observed within and around the viral factory (Figure 3.7C). Examination of earlier time points indicated a small number of LC3 puncta appearing in close proximity to the viral factory from 12 hpi. WIPI puncta started to appear near the viral factory from 14 hpi. LC3 and WIPI puncta became more numerous during subsequent time points and were most evident at 16 hpi. These results indicate that LC3 puncta can be detected by labelling endogenous LC3 without the requirement for over-expression and that the appearance of LC3 puncta is loosely correlated with the appearance of WIPI puncta at the viral factory.

3.2.8 Accumulation of LC3-II is observed during late ASFV infection

Coronaviruses such as mouse hepatitis virus (MHV) also induce the appearance of LC3 puncta, however these double-membrane vesicles were shown to be coated in LC3-I and not LC3-II (Reggiori et al., 2010). To investigate whether the LC3 puncta observed in ASFV infected cells could be linked to an accumulation of LC3-II, Vero cells were either mock infected or infected with Ba71V (MOI 5) and Western blot analysis was carried out to assess LC3-II levels at 12 hpi which coincides with the appearance of LC3 puncta at the viral factory. A 4 hour time point was also included for comparison as previously it was shown that ASFV did not induce an accumulation of LC3-II at 4 hpi (3.2.2). Additionally, control cells were either incubated under nutrient replete conditions or starved for 2 hours to demonstrate conventional autophagy-dependent accumulation of LC3-II. Lastly, samples were probed with anti-LC3, anti-p30 and anti-γ tubulin primary antibodies.

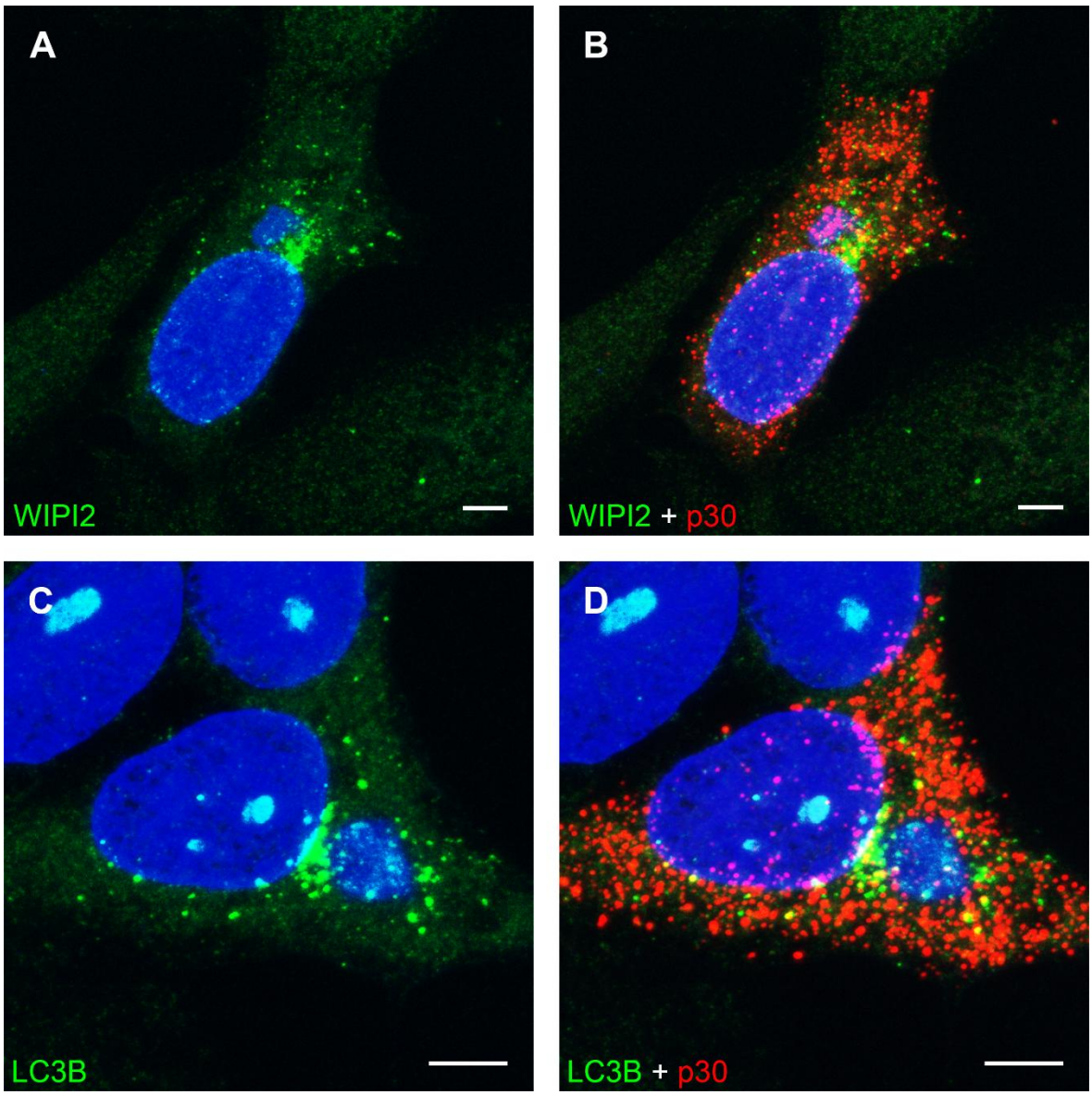

Figure 3.7 LC3 puncta and WIPI puncta are observed at the viral factory at 16 hpi

Vero cells were infected with Ba71V (MOI 5) for 16 hours. Cells were fixed and permeabilised in methanol before labelling WIPI and p30 (Panels A and B) or LC3 and p30 (Panels C and D). WIPI and LC3 are shown in green, viral protein p30 is shown in red and nuclei and viral factories are shown in blue. Panels A and C show the same infected cells as Panels B and D respectively but with the red channel removed to allow for clearer observation of WIPI and LC3 staining. Images represent a stack of ten overlaid cell section images. Scale bars represent 5 µM.

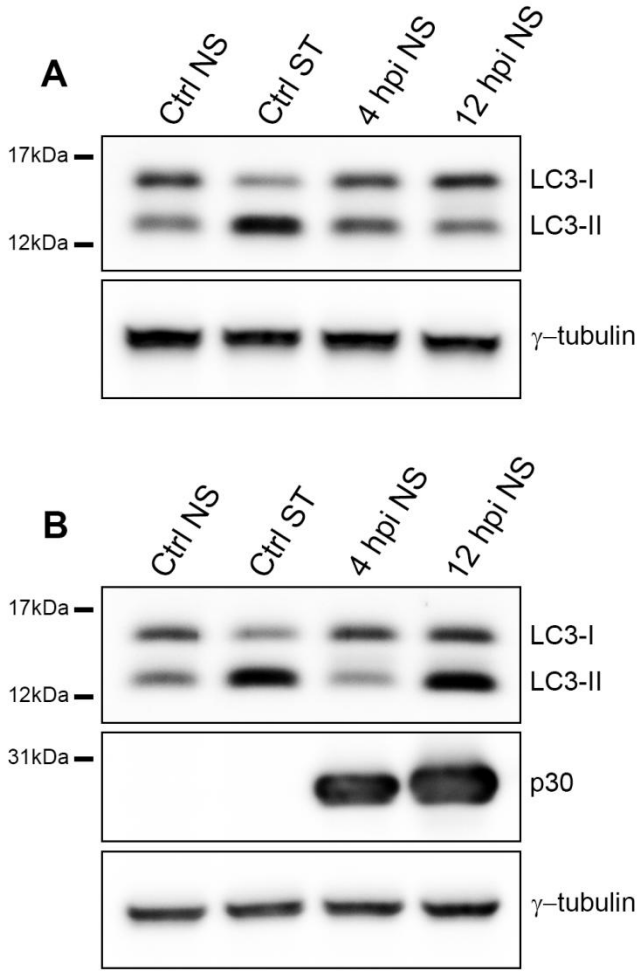

Figure 3.8.1 Accumulation of LC3-II is observed at 12 hpi in ASFV infected cells

Vero cells were either mock infected (panel A) or infected with Ba71V (MOI 5) (panel B) for a total of 4 hours or 12 hours during which cells were non-starved (NS) in complete cell media for the final 2 hours. Separately, control cells (Ctrl) were either non-starved in complete cell media or starved (ST) in EBSS for 2 hours to induce autophagy and LC3-II accumulation. Cells were lysed and samples were prepared for resolution by bis-Tris PAGE before transfer to PVDF membrane. Finally, samples were probed with anti-LC3, anti-p30 and γ-tubulin antibodies followed by appropriate HRP-conjugated secondary antibodies. The positions of molecular mass markers are indicated to the left of the gels.

A greater amount of LC3-II was observed in control cells that were starved compared to control cells that were incubated in complete cell media indicating induction of autophagy (Figure 3.8.1A and B). The intensity of LC3-II bands were comparable in mock infected cells at 4 hpi and 12 hpi suggesting that levels of LC3-II had not increased between these time points (Figure 3.8.1A). In contrast, an increase in LC3-II was observed in ASFV infected cells at 12 hpi when compared to 4 hpi showing that LC3-II accumulation was induced (Figure 3.8.1B). Comparison of the 12 hour mock infected and ASFV infected samples to the non-starved control cell sample in each respective

blot suggested that the levels of LC3-II in ASFV infected cells at this time point were greater than the mock infected cells. Anti-p30 labelling indicated successful ASFV infection.

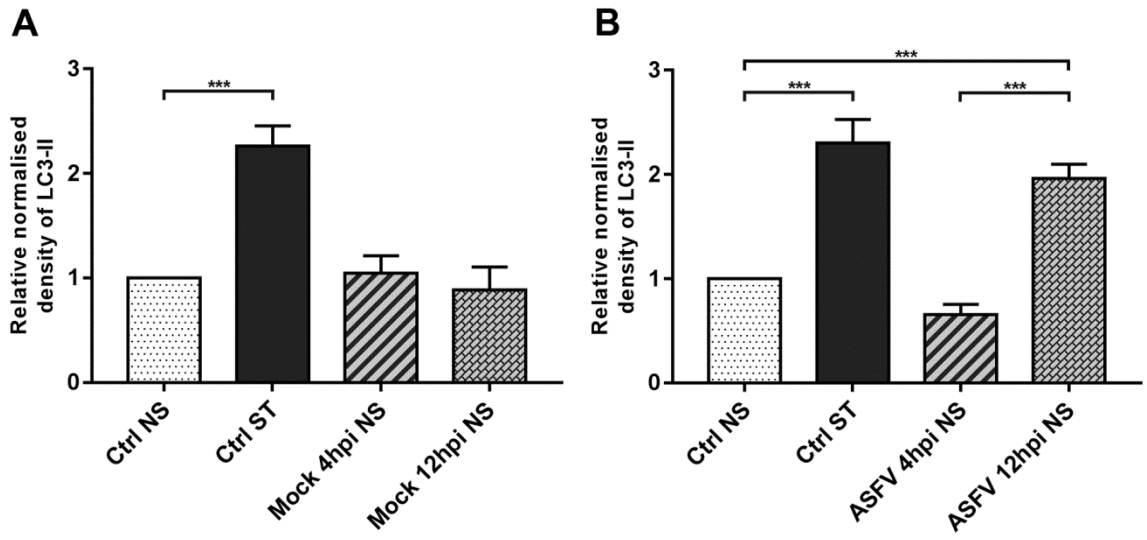

Figure 3.8.2 Densitometry analysis confirms that ASFV induces an accumulation of LC3-II at 12 hpi

Densitometry analysis was conducted using ImageJ to determine the relative densities of the LC3-II bands from Western blot data shown in Figure 3.8.1. The relative densities of the LC3-II bands were calculated by comparison to those of the non-starved control sample before normalising the values to those of γ-tubulin. This was carried out separately on the mock infected (graph A) and ASFV infected samples (graph B). Data shown is the mean of three experiments and error bars indicate SD. NS = non-starved cells. ST = starved cells. Statistical analysis was carried out in Minitab using analysis of variance with Tukey multiple comparisons test. Asterisks represent a significant difference in value between the indicated cell treatments (*** = P value of <0.001).

Densitometry analysis confirmed a statistically significant difference between the starved and non-starved control cell samples and is shown in Figure 3.8.2A ($P < 0.001$) and in Figure 3.8.2B ($P < 0.001$) consistent with a successful induction of autophagy in these cells. No statistically significant difference was observed between the mock infected cells at 4 hpi and 12 hpi ($P > 0.05$) (Figure 3.8.2A) showing that mock infection did not induce an accumulation of LC3-II. Additionally, no statistically significant difference was apparent between the 12 hour mock infected sample and the non-starved control cell sample ($P > 0.05$) (Figure 3.8.2A), however a statistically significant difference between the non-starved control cell sample and the 12 hour ASFV infected sample was apparent ($P < 0.001$) (Figure 3.8.2B). A statistically significant increase in LC3-II was seen in the ASFV infected cells at 12 hpi when compared to 4 hpi ($P < 0.001$) (Figure 3.8.2B). Collectively, these results show that ASFV causes an increase in LC3-II accumulation between 4 and 12 hpi that is not observed in mock infected cells. Furthermore, this increase coincides with the appearance of LC3 puncta at the viral factory at 12 hpi as described in section 3.2.7.

3.3 Discussion

Manipulation of cellular processes to facilitate replication and avoid innate and adaptive immune response are a crucial part of the virus life cycle. ASFV encodes for a number of proteins that modulate a variety of different pathways including A179L. The A179L gene encodes for a Bcl-2 homologue that has been shown to interact with the key autophagy protein Beclin 1 (Hernaez et al., 2013), therefore it is likely that ASFV may also modulate autophagy considering the central importance of this pathway to so many cellular processes. The aim of this investigation was to assess the effect of ASFV on autophagy, and specifically whether ASFV promotes or inhibits the pathway.

Initial analysis was conducted using confocal microscopy. Vero cells were used in this experiment as they exhibit clear autophagosome staining without the interference of autofluorescence that is often observed in primary macrophage cells and support the growth of the Vero cell adapted isolate of ASFV, Ba71V. Confocal analysis revealed that few LC3 puncta were observed in uninfected, mock infected and ASFV infected Vero cells incubated under nutrient replete conditions suggesting that ASFV infection did not promote formation of autophagosomes during early stages of the replication cycle (Figure 3.1.1). However, quantitative analysis of the number of autophagosomes per cell showed that under nutrient replete conditions ASFV infected cells had significantly less autophagosomes than uninfected and mock infected cells (Figure 3.1.3), raising the possibility that ASFV may inhibit the formation of autophagosomes. This result is at odds with results reported by Hernaez *et al* (2013) that describe similar amounts of GFP-LC3 puncta between ASFV infected and uninfected Vero cells at 12 hpi. This difference may be due to the different time points tested or the use of an overexpression model of GFP-LC3 by Hernaez and colleagues. Transient overexpression of LC3 can lead to LC3 aggregation in an autophagy-independent manner leading to a false representation of autophagosomes within the cytoplasm (Kuma et al., 2007).

To test for inhibition of autophagy, cells were starved to induce the formation of autophagosomes and then labelled for LC3. In uninfected and mock infected cells, a much higher number of autophagosomes was observed after starvation (Figure 3.1.2). However, no LC3 puncta were seen in infected cells in response to starvation suggesting that ASFV inhibits starvation-induced formation of autophagosomes in Vero cells during the early stages of the replication cycle.

Autophagosome formation is linked to the conversion of LC3-I to LC3-II and therefore to confirm the results obtained by confocal microscopy, levels of LC3-II were analysed by Western blot (Figure 3.2). Due to a difference in immunoreactivity of LC3-I and LC3-II, in most cases the sensitivity of detection of LC3‑II by anti‑LC3 antibodies is much higher (Mizushima and Yoshimori, 2007). For this reason, appropriate interpretation of LC3 blots was carried out by comparison of LC3-II between samples rather than comparisons between LC3-I and LC3-II. Under nutrient replete conditions, comparable levels of LC3-II were detected in uninfected, mock infected

and ASFV infected Vero cells at 4 hpi. In both uninfected and mock infected cells that had been starved, the intensity of the LC3-II bands were greater than the bands seen in samples taken from cells under nutrient replete conditions. However in ASFV infected cells this was not apparent as the intensity of the bands were comparable between the starved and non-starved samples. The levels of LC3-II in all of the samples tested corresponded to the number of LC3 puncta seen by confocal microscopy and taken together confirmed that ASFV inhibits autophagosome formation in Vero cells early during the replication cycle.

ASFV naturally targets cells of the monocyte-macrophage lineage, and hence the ability of a field strain of the virus to inhibit autophagy in macrophages was tested. Similar levels of LC3-II were observed in infected blood derived macrophages at 6 hpi as were seen in equivalent mock infected cells suggesting that the virus does not induce autophagosome formation in macrophages. Additionally, LC3-II did not accumulate in infected macrophages after stimulation with Torin2. In macrophages, LC3-II accumulation was stimulated by pharmacological inhibition of mTORC1 using Torin2 whereas previously in Vero cells, LC3-II accumulation was stimulated by starvation as macrophages did not tolerate incubation in EBSS well. This demonstrates that the inhibitory effect on LC3-II accumulation is independent of the method of autophagy induction. The experiment carried out in macrophages was repeated three times to account for potential variability between cells harvested from individual animals and densitometry analysis confirmed a consistent outcome between replicates (Figure 3.3.2). Taken together this showed that ASFV inhibits LC3-II accumulation in a biologically relevant system and that the effect of ASFV on the autophagy pathway is independent of both the virus strain and cell type studied.

As described in the introduction, autophagosome formation is a carefully controlled multi-step process. Recruitment of LC3-II to autophagosomes is dependent on WIPI and upon induction of autophagy, WIPI forms punctate structures that can be observed by confocal microscopy. In stark contrast to LC3 there were many more WIPI puncta in ASFV infected cells compared to mock infected cells under both nutrient replete conditions and starvation conditions (Figures 3.4.1 and 3.4.2). This suggested that ASFV promotes the formation of WIPI complexes at 4 hpi in a manner unaffected by nutrient availability.

The assembly of WIPI complexes is an integral step in the generation of autophagosomes and therefore their appearance in ASFV infected cells is interesting considering that the formation of autophagosomes is blocked by the virus. To provide clarity on autophagy status in infected cells, a p62 degradation assay was used to assess if autophagic flux is blocked by ASFV. Figure 3.5.1 demonstrates the correlation between starvation-induced activation of autophagy and a reduced level of p62. Figure 3.5.2 shows that in mock infected cells, a reduction in p62 levels was observed at 4 hpi and 12 hpi following a 2 hour starvation period as would be expected. In contrast, ASFV infected cells did not show significantly less p62 under starvation conditions as demonstrated by the densitometry analysis of three replicate experiments shown in Figure 3.5.3. It was therefore

concluded that ASFV is able to block autophagic flux during early and late infection which suggests that ASFV does not use autophagy at any stage of its replication.

To further substantiate the aforementioned conclusion, virus replication was compared by titration of virus grown in $Atg5^{-/-}$ autophagy deficient and autophagy competent MEF cell lines using the attenuated Uganda strain. Despite the virus reaching a respectable titre in both cell lines after 72 hours, the increase in titre from the start of the experiment only represented an approximate 10-fold increase. This may suggest that viral growth is in some way limited in the MEF cells. Nevertheless, the results shown in Figure 3.6 demonstrate that no statistically significant decrease in replication was observed in the autophagy deficient cells which indicates that ASFV does not require the autophagy pathway for its replication. This is in agreement with a previous study that tested the effect of 3-methyladenine (3-MA) on the replication capacity of ASFV in macrophages and found that 3-MA had relatively little influence (Basta et al., 2010). 3-MA is a transient inhibitor of class III PI3K which forms part of the vital Vps34 autophagy complex (Wu et al., 2010).

The results described in section 3.2.7 reported the appearance of viral factories that were observed in close proximity to the nucleus in ASFV infected cells. LC3 puncta were seen forming at the viral factory from 12 hpi, becoming more numerous until 16 hpi. Western blot analysis in Figure 3.8.1 demonstrated that an accumulation of LC3-II is detected in infected cells at 12 hpi which coincides precisely with the first appearance of LC3 puncta at the viral factory. Hernaez *et al* (2013) reported the appearance of LC3 puncta at the viral factory at 16 hpi but at 12 hpi described similar amounts of LC3 puncta between uninfected and infected cells. The detection of GFP-LC3 as opposed to endogenous LC3 could explain the difference in results at 12 hpi as a low transfection efficiency of GFP-LC3 may have limited the detection of LC3 puncta.

Confocal analysis of infected cells also revealed the appearance of WIPI puncta that formed in close proximity to and sometimes within the viral factory from 14 hpi becoming more evident at 16 hpi (Figure 3.7). The close association of WIPI puncta with viral factories is interesting as the WIPI puncta that were previously observed at 4 hpi were observed in a perinuclear location which clearly contrasted with the diffusely located WIPI complexes in mock infected cells (Figure 3.4.2). This could suggest that sub-cellular location of the WIPI complexes at 4 hpi is linked to the requirements of virus replication and could be important in the formation of the viral factory. The appearance of WIPI puncta at the viral factory may also suggest that the observed LC3 lipidation in infected cells is dependent on the formation of WIPI complexes. In the future, conducting an experiment to determine whether the observed LC3 and WIPI puncta colocalise around the viral factory may point to a link in their formation.

The previously described block in starvation-induced p62 degradation is evidence of the fact that autophagic flux is restricted at 12 hpi. This could mean that formation of autophagosomes is induced during late infection, hence the appearance of LC3 puncta at the viral factory, but that they

subsequently do not undergo breakdown via lysosome fusion potentially due to a mechanism of viral inhibition. A similar effect is seen in cells infected with infectious bronchitis virus (IBV) in which the virus promotes the formation of small size-restricted autophagosomes that do not undergo autophagosome-lysosome expansion (Cottam et al., 2014). In the case of IBV infection, the purpose of this is unknown but it may serve to contribute membranes to sites of virus replication.

Studies on the potential role that autophagy plays during virus infection have revealed other viruses such as poliovirus (PV) that also subvert the autophagy pathway to promote their own replication (Jackson et al., 2005). Specifically, PV induces formation of LC3 staining double-membrane vesicles resembling autophagosomes that are thought to be required for non-lytic virus release from cells (Bird et al., 2014). However, formation of these vesicles has been shown to be independent of the canonical ULK1 autophagy signalling complex (Corona Velazquez et al., 2018). It has also been shown that the formation of LC3-staining double-membrane vesicles in MHV infected cells does not rely on autophagy and that MHV replication was shown to be unaffected in Atg5 knock-out cells (Reggiori et al., 2010, Zhao et al., 2007). Collectively, these examples reveal potential autophagy-independent functions of proteins such as LC3 that are vital for successful virus infection. The accumulation of LC3-II during late ASFV infection may therefore be a pro-viral mechanism that uses lipidated LC3 independently of the canonical autophagy pathway. In support of this, ultrastructural studies have not reported the association of double-membrane vesicles with ASFV factories (Brookes et al., 1996, Nunes et al., 1975). The study by Hernaez *et al* (2013) reported that no examples of colocalisation between mature virions labelled against p72 and LC3 puncta were evident.

Infection with influenza A virus (IAV) causes the accumulation of LC3-II in perinuclear regions and at the plasma membrane (Beale et al., 2014). Further research has revealed that IAV-induced LC3 lipidation is driven predominantly by non-canonical autophagy (Fletcher et al., 2018). It may be possible that the appearance of LC3 puncta during late ASFV infection is a non-canonical autophagy response to membrane re-arrangements around the viral factory rather than a pro-viral mechanism. Crucially however, lipidation of LC3 during non-canonical autophagy is not dependent on recruitment of WIPI (Fletcher et al., 2018). If the observed LC3 lipidation in ASFV infection is WIPI dependent, this would more likely point to a canonical pathway. In this regard, infecting WIPI knock-out cells with ASFV and monitoring for the appearance of LC3 puncta would provide valuable insight into their provenance.

Another possibility is that the appearance of LC3 puncta at the viral factory is entirely non-specific. During ASFV infection, other membrane markers such as endosomal markers like Rab7 and lysosomal markers like Lamp1 are recruited to the periphery of the viral factory (Cuesta-Geijo et al., 2017). Interestingly, addition of the microtubule-depolymerizing drug nocodazole abolished this recruitment and also impaired formation of viral factories pointing to a requirement of the

microtubule network. In support of this, research has shown that ASFV infection leads to disruption of centrosome assembly and function which could mediate the observed re-organisation of microtubules (Jouvenet and Wileman, 2005).

In summary this work has showed that ASFV negatively modulates the formation of autophagosomes in Vero cells and primary macrophage cells. In addition, it shows that ASFV is able to block autophagic flux and that canonical autophagy is dispensable for virus replication. The appearance of LC3 and WIPI puncta at the viral factory has also been described. The fact that ASFV modulates autophagy, a pathway that performs such an integral function in host defence, could provide new opportunities for disease intervention. It may be possible to exploit the anti-microbial nature of autophagy by suppressing or entirely abrogating the ability of vaccine strain viruses to control it. However this approach would be reliant on a firm understanding of the mechanisms of modulation which could guide the selection of viral genes for a targeted mutation strategy. In this regard, the chapter presented next was aimed at examining the mechanisms of autophagy modulation by ASFV.

4 Investigation of the mechanisms of autophagy modulation by ASFV

4.1 Introduction

Autophagy can act either at a basal level that functions to maintain cellular homeostasis or can be dramatically stimulated in response to externally derived stresses such as starvation, radiation and pathogen invasion. In many cases, selective forms of autophagy that rely on an array of autophagy receptors which target specific cargo for lysosomal degradation are induced. Selective autophagy includes mitophagy and pexophagy to name a few which is the selective degradation of mitochondria and peroxisomes respectively. In addition, a targeted anti-microbial form of autophagy called xenophagy is an important intrinsic cell defence mechanism and can be induced in response to immune-sensing signalling via the action of pattern recognition receptors (PRR) such as Toll-like receptors (TLRs) (Deretic, 2011, Gomes and Dikic, 2014). Moreover, autophagy can promote MHC class II presentation and generation of antigen-specific CD4+ T cell responses (Deretic et al., 2013). With such a multifaceted and potent threat to virus infection, it becomes unsurprising that viruses have developed very specialised ways to negatively modulate autophagy.

Some viruses have evolved a capacity to modulate the signalling pathways that regulate autophagy whereas others directly target the host autophagy machinery. Interestingly, HSV-1 conducts both of these activities via ICP34.5 which is able to antagonize protein kinase R (PKR)-mediated autophagy induction and also inhibit autophagy via its interaction with Beclin 1 (Orvedahl et al., 2007, Talloczy et al., 2006). Indeed, Beclin 1 seems to be a common target for viral manipulation, perhaps due to its integral role as part of the autophagy core machinery or perhaps due to the direct involvement of Beclin 1 in autophagy induction in response to TLR signalling (Shi and Kehrl, 2010). Exogenous expression of the ASFV Beclin 1-interacting protein A179L not only protects cells against induced cell death but also inhibits the induction of autophagy in response to starvation (Hernaez et al., 2013, Revilla et al., 1997). It is therefore tempting to speculate that A179L may play a role in the inhibition of autophagy by ASFV.

The PI3K-Akt-mTOR axis is a major regulatory pathway. The activation of Akt effects multiple cell functions such as cell growth, proliferation and protein translation (Manning and Toker, 2017). Signalling via Akt can also suppress apoptosis and modulate the induction of autophagy (Cooray, 2004, Sengupta et al., 2010). In the case of the latter, Akt is able to phosphorylate and inhibit the mTORC1 inhibitor TSC2, leading to the activation of mTORC1 and the inhibition of the autophagy pathway. This mechanism can be exploited by viruses, for example HSV-1 encodes the Us3 kinase protein that acts in an identical manner to Akt by activating mTORC1 via phosphorylation of TSC2 leading to stimulation of mRNA translation and viral replication (Chuluunbaatar et al., 2010).

The aim of this study was to identify potential mechanisms that are responsible for the previously described inhibition of autophagosome formation (see Chapter 3). These investigations initially looked at the role that A179L might play in blocking starvation-induced autophagosomes. Whereas

Hernaez *et al* (2013) conducted their studies using a model of A179L over-expression which may not accurately reflect the level of A179L expression during infection, the study conducted here was carried out using a mutant strain of ASFV that lacks A179L. In this way, the effect that the absence of A179L has on the induction of autophagy could be examined in the context of infection and any potential artefacts of transfection and over-expression could be excluded.

The vast body of literature reporting the interaction of numerous viruses with the PI3K-Akt-mTOR pathway and its vital role in the induction of autophagy pointed to the potential that the block in autophagy induction in ASFV infected cells may be mediated via the PI3K-Akt-mTOR pathway. The activation status of mTORC1 and Akt was therefore analysed by Western blot over a time course of ASFV infection. This also included an experiment to determine if mTORC1 activity was likely the result of a viral mechanism of action rather than constitutive activity. Following this, a purified virus was used in experiments to analyse mTORC1 and Akt activity to rule out possible variations of the results resulting from the method of virus preparation. Finally, investigations were carried out using pharmacological inhibitors of Akt and mTOR to determine if ASFV is able to use Akt-mTORC1 signalling as a mechanism to negatively modulate autophagy.

Gaining further insight into how ASFV is able to regulate autophagy could provide opportunity to partially disrupt the system of viral control of the host immune response. For example, a strategy of targeted viral gene deletion may help to engineer a situation in which the cell is able to counter infection via the activation of autophagy. Considering the well-established links between autophagy and innate and adaptive immunity, this could lead to viral vaccine strains with improved immunogenicity.

4.2 Results

4.2.1 A mutant virus lacking A179L inhibits formation of starvation-induced autophagosomes

A179L, a viral Bcl2 homolog encoded by ASFV has been shown to interact with Beclin 1 via its BH3 homology domain (Hernaez et al., 2013). Furthermore, it was shown that overexpression of A179L in HeLa cells caused a reduction in the number of starvation-induced autophagosomes when compared to control cells. This suggests that ASFV could potentially modulate the autophagy response through a mechanism involving the interaction between A179L and Beclin 1. In other studies, it was shown that A179L is able to protect cells against induced cell death (Revilla et al., 1997) and also inhibit the activation of CHOP during the UPR response (Barber, 2015). As part of the work conducted by Barber, a deletion mutant of Ba71V was engineered in which the A179L gene was removed and replaced with a reporter gene using homologous recombination.

To address the question of whether an A179L knock-out virus (A179L KO) is able to inhibit the formation of starvation-induced autophagosomes, an experiment was carried out essentially in the same way as described in section 3.2.1. Using the A179L KO virus described above, the number of autophagosomes in ASFV infected Vero cells (MOI 5) was visualised by confocal microscopy and compared to mock infected cells in either nutrient replete conditions (Figure 4.1.1) or starved (Figure 4.1.2) conditions. In this way, any modulation of autophagy by the virus could be analysed. Cells were infected for a total period of 4 hours during which cells were incubated for the last 2 hours in either complete cell media (non-starved) or EBSS (starved) prior to being fixed and labelled for immunofluorescence.

LC3 labelling in mock infected cells (Figure 4.1.1A) showed a mostly diffuse cytoplasmic pattern with a small number of sporadic puncta that would be expected under nutrient replete conditions. A similar pattern of LC3 staining was observed in ASFV infected cells (Figure 4.1.1B). Labelling of viral protein p30 (Figure 4.1.1C) identified cells expressing ASFV genes and interestingly, very few puncta were apparent in these cells. This demonstrates that the A179L KO virus does not induce the formation of autophagosomes under nutrient replete conditions.

Mock infected cells under starvation conditions (Figure 4.1.2A) showed a comparably higher number of LC3 puncta when compared to mock infected cells under non-starved conditions (Figure 4.1.1A) indicating that autophagy had been induced in these cells. In contrast, cells that had been infected with the A179L KO virus (Figure 4.1.2B) demonstrated a predominantly diffuse pattern of LC3 staining with very few puncta under starvation conditions. Labelling of viral protein p30 (Figure 4.1.2C) showed that LC3 puncta were mainly observed in cells that were not expressing ASFV genes. Collectively these results reveal that the A179L KO virus is able to inhibit starvation-induced formation of autophagosomes.

Imaris analysis was used to enumerate the total number of autophagosomes per cell in 30 cells for each experimental condition (Figure 4.1.3). The number of autophagosomes per cell increased in mock infected cells following starvation ($P < 0.001$). There was no difference in the number of autophagosomes between non-starved and starved cells that had been infected with A179L KO ($P > 0.05$). Similar to what was observed with wild-type virus there were less autophagosomes in resting cells infected with A179L KO when compared to mock infected cells ($P < 0.05$) and also significantly less autophagosomes in cells infected with A179L KO under starvation conditions when compared to starved mock infected cells ($P < 0.001$). This confirms the inhibitory effect of the A179L KO virus on the formation of starvation-induced autophagosomes.

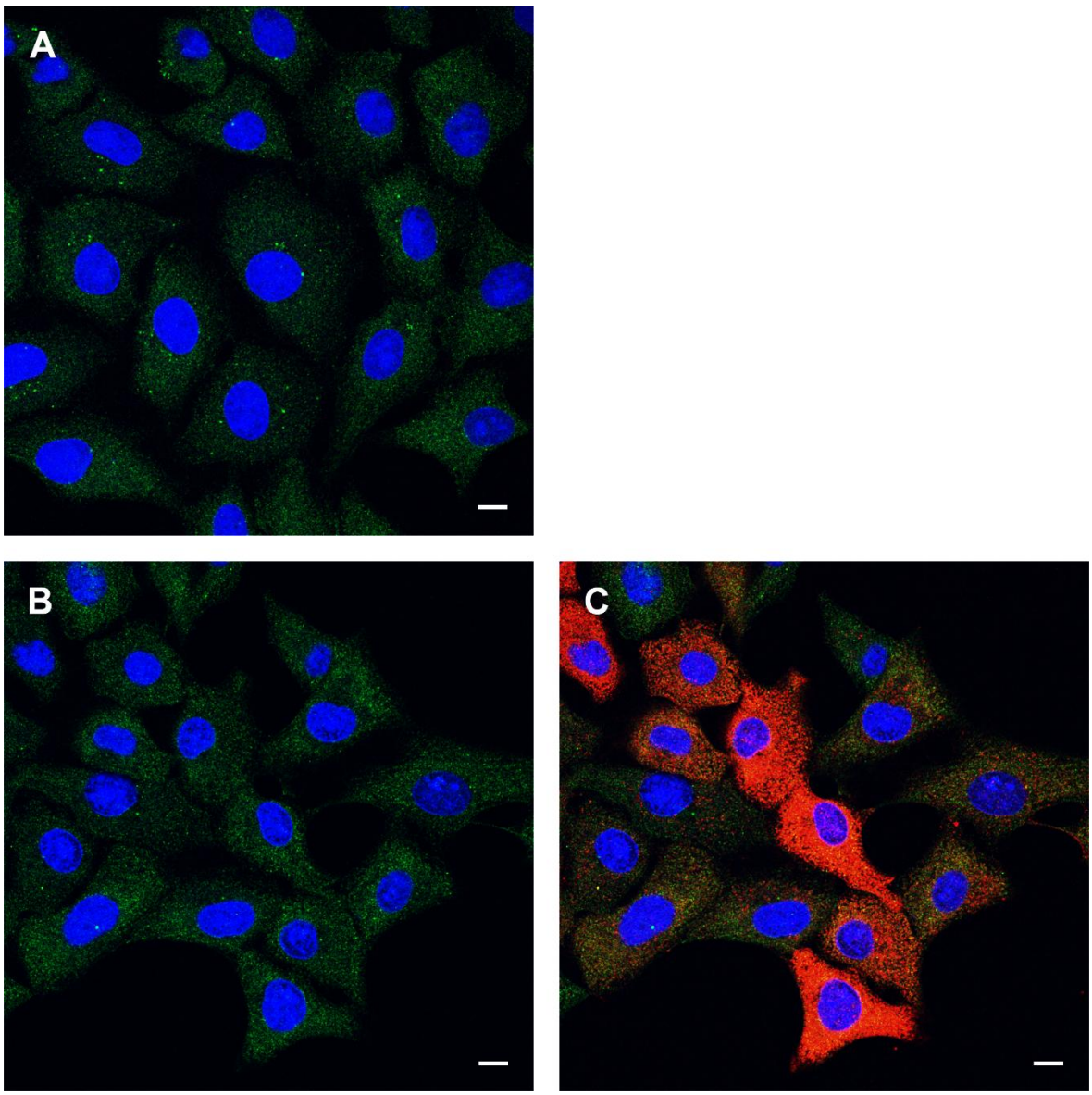

Figure 4.1.1 A179L KO virus does not induce the formation of autophagosomes at 4 hpi

Vero cells were mock infected (Panel A) or infected with A179L KO virus (MOI 5) (Panels B and C) for a total of 4 hours during which cells were non-starved in complete Vero cell media for the last 2 hours. Cells were then fixed and permeabilised in methanol before labelling LC3 shown in green, viral protein p30 shown in red and nuclei shown in blue. Panels A and C were stained with anti-p30 antibody and Panel B shows the same infected cells as Panel C but with the red channel removed to allow for clearer observation of LC3 staining. Scale bars represent 10 µM.

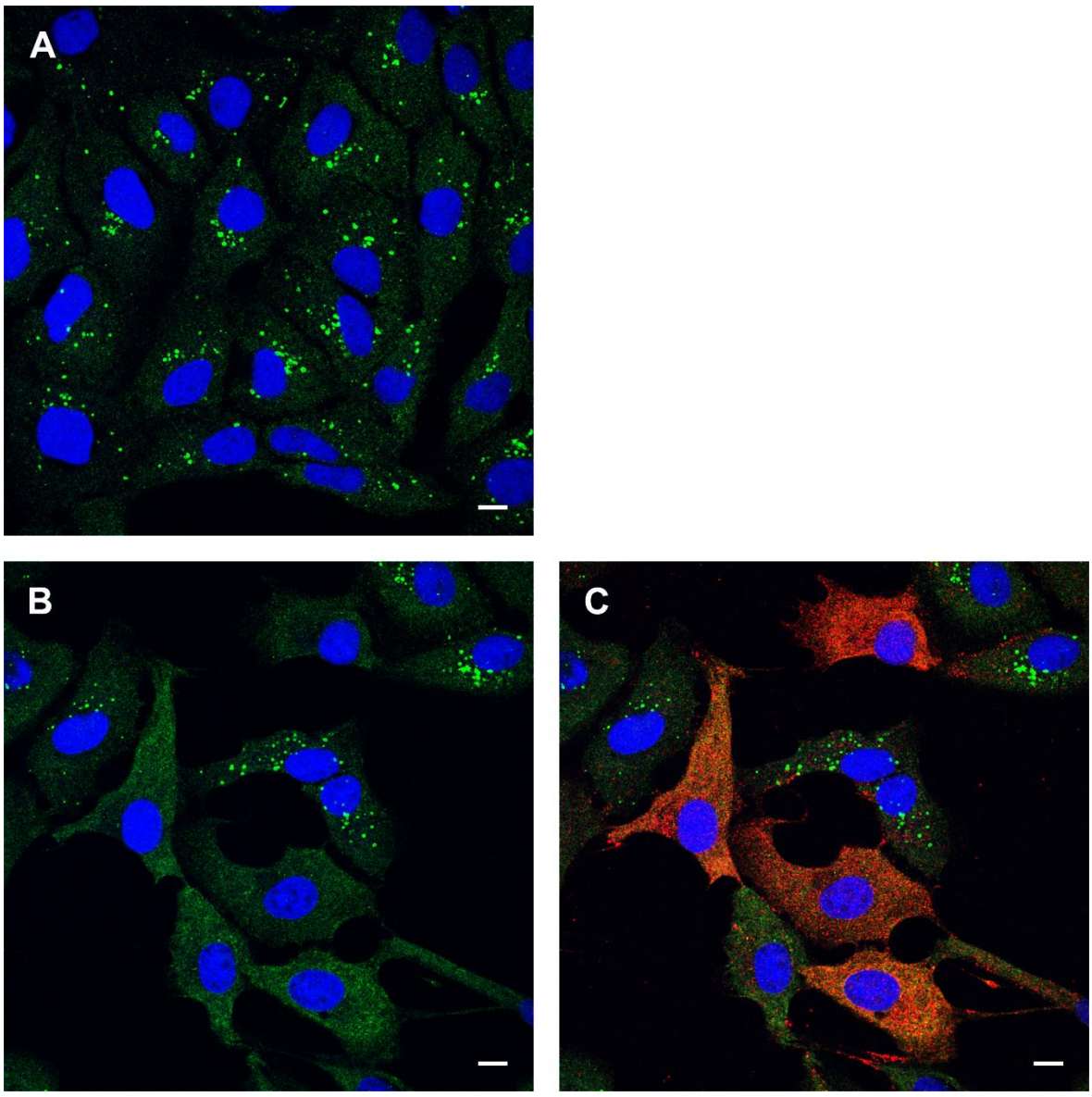

Figure 4.1.2 A179L KO virus has an inhibitory effect on the formation of starvation-induced autophagosomes at 4 hpi

Vero cells were mock infected (Panel A) or infected with A179L KO virus (MOI 5) (Panels B and C) for a total of 4 hours during which cells were starved in EBSS to induce autophagy for the last 2 hours. Cells were then fixed and permeabilised in methanol before labelling LC3 shown in green, viral protein p30 shown in red and nuclei shown in blue. Panel B shows the same infected cells as Panel C but with the red channel removed to allow for clearer observation of LC3 staining. Scale bars represent 10 µM.

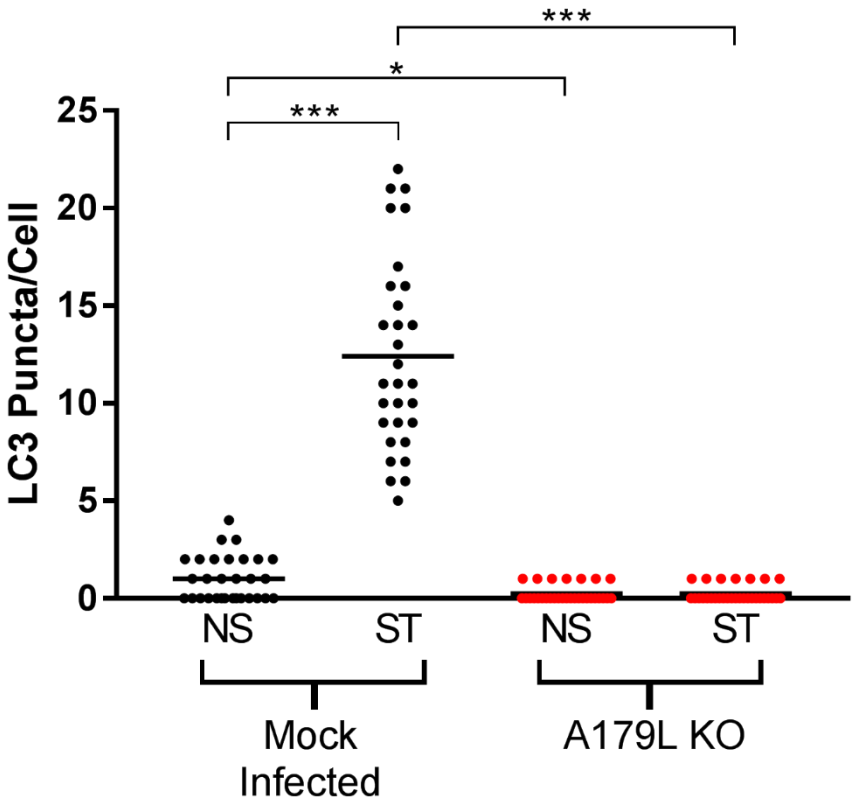

Figure 4.1.3 Imaris analysis confirms that an A179L KO virus inhibits induction of autophagosomes in response to starvation

Imaris analysis was carried out on confocal images to quantify the number of LC3 puncta per cell for 30 individual cells per indicated experimental condition. Vero cells were either mock infected or infected with the A179L KO virus for a total of 4 hours. Prior to fixation, cells were either non-starved in complete cell media or starved in EBSS for 2 hours to induce autophagy. Centre lines show the medians. NS = Non-starved cells. ST = Starved cells. Statistical analysis was carried out in Minitab using analysis of variance with Tukey multiple comparisons test. Asterisks represent significant differences in value between NS and ST conditions and between the indicated infection status of the cells (* = P value of <0.05, *** = P value of <0.001).

4.2.2 mTORC1 remains active during ASFV infection

Deleting A179L, the only identified ASFV autophagy-interacting protein, did not abrogate the ability of the virus to block starvation-induced formation of autophagosomes. Targeting host pathways could involve several viral encoded modulators and thus exhibit some redundancy. For example, at least four apoptosis modulators have been described (Dixon et al., 2017). One could therefore predict that autophagy is also likely to be modulated by ASFV in a number of ways.

mTORC1 is a master nutrient sensing kinase that is activated in nutrient rich conditions which serves to halt the downstream initiation of autophagy (Yang and Klionsky, 2009). This is mediated by mTORC1-dependent phosphorylation of ULK1 which supresses the kinase activity of the ULK1

complex. In this way, phosphorylation of ULK1 can be used as a read-out for mTORC1 activity. Similarly, mTORC1-dependent phosphorylation of p70-S6K and 4E-BP1 can be used as further evidence to demonstrate the activation status of mTORC1. To gain insight into whether mTORC1 might be involved in the inhibition of autophagosome formation by ASFV, analysis was carried out to determine its activation status in infected cells.

Vero cells were either mock infected or infected with the Ba71V strain of ASFV (MOI 5). Virus was added to cells and incubated for 1 hour to allow virus entry. Cells were washed to remove residual virus at which stage cells were harvested for the first time point (0 hour time point). Remaining cells were incubated in nutrient replete conditions and harvested at multiple time points over a 16 hour course of infection. In addition, control cells were incubated in complete cell media or starved in EBSS for 3 hours to demonstrate starvation-induced reduction in phosphorylation of mTORC1 substrate proteins. Samples were prepared from cells for analysis by immunoblotting and probed using anti-ULK1, anti-p70-S6K, anti-4E-BP1, anti-p30 viral protein and anti-γ tubulin antibodies. Total protein levels and the phosphorylation status of ULK1, p70-S6K and 4E-BP1 were analysed.

Western blot analysis in Figure 4.2 showed that p30 expression was apparent in ASFV infected cells from 4 hpi, increasing as infection progressed towards 16 hpi as would be expected. A lower level of phosphorylation of ULK1 (P-ULK1), p70-S6K (P-p70-S6K) and 4E-BP1 (P-4E-BP1) was seen in the starved control cells when compared to control cells incubated in complete cell media. This demonstrates that starvation induced inactivation of mTORC1 leads to reduced phosphorylation of mTORC1 target proteins. No major difference in P-ULK1 was observed between mock infected cells and ASFV infected cells until 4 hpi at which stage phosphorylation in virus infected cells became marginally elevated until 16 hpi. Initially, a greater amount of P-p70-S6K was seen in virus infected cells at 0 hpi when compared to mock infected cells but this was no longer apparent at 1 hpi. From 4 to 16 hpi, P-p70-S6K was dramatically increased above the level of mock infected cells. Levels of P-4E-BP1 were unchanged between mock infected and ASFV infected cells up to 4 hpi, after which phosphorylation increased in infected cells. Analysis of total protein levels of ULK1, p70-S6K and 4E-BP1 consistently demonstrated equivalent levels between mock infected and ASFV infected cells for the duration of the time course.

Phosphorylation of ULK1, p70-S6K and 4E-BP1 was therefore evident throughout a 16 hour time course of ASFV infection and was at certain times elevated above the background levels seen in mock infected cells. This analysis presents a clear indication that mTORC1 remains active during ASFV infection.

Figure 4.2 mTORC1 remains active during ASFV infection

Vero cells were either mock infected or infected with Ba71V (MOI 5) for 1 hr before residual virus was washed off and the 0 hr time point was harvested. The remaining cells were incubated in 2% media and harvested at multiple time points over a 16 hour time course of infection. Control cells were either incubated in complete cell media (NS) or starved (ST) in EBSS for 3 hours to induce inactivation of mTORC1. Cells were lysed and samples prepared for resolution by bis-Tris PAGE before transfer to PVDF membrane. Finally, samples were probed with ULK1, p70-S6K, 4E-BP1, p30 viral protein and anti-γ tubulin antibodies followed by appropriate HRP-conjugated secondary antibodies. The positions of molecular mass markers are indicated to the left of the gels.

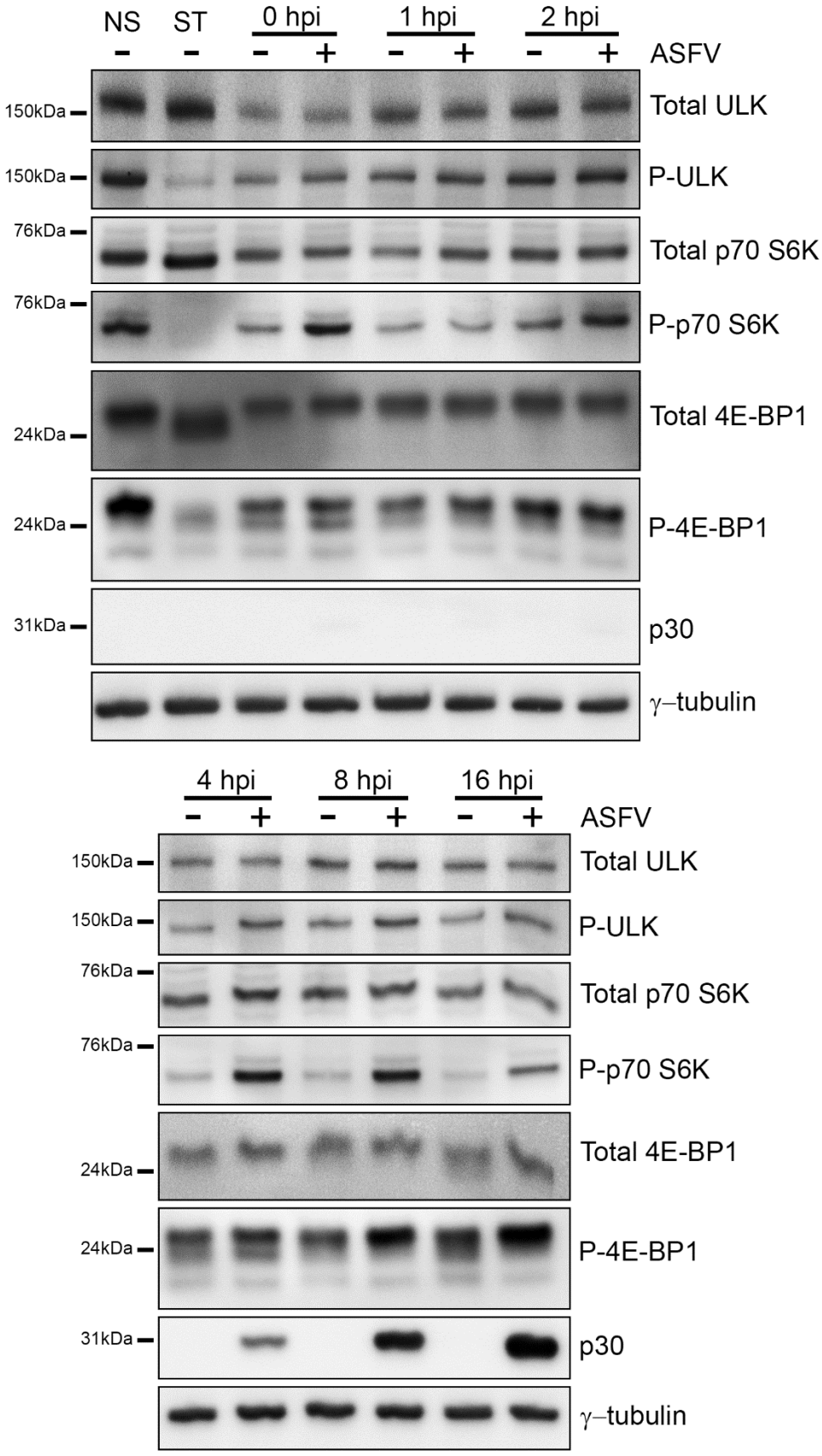

Figure 4.2 mTORC1 remains active during ASFV infection

4.2.3 Starvation-induced inactivation of mTORC1 is inhibited by ASFV

The serine/threonine kinase p70-S6K that targets the S6 ribosomal protein is important in the control of translation initiation and one of the most well characterised mTORC1 substrates along with 4E-BP1 (Ma and Blenis, 2009). Under nutrient replete conditions, phosphorylation of p70-S6K by active mTORC1 results in the promotion of protein translation. However, under starvation conditions, multiple signals are relayed to mTORC1 in response to nutrient and energy sensing, ultimately resulting in its inactivation and the decrease in cell translation via rapid dephosphorylation of p70-S6K.

The results in Figure 4.2 show that p70-S6K phosphorylation levels are not only maintained but actually increase during the 16 hour period of infection, indicating the maintenance or possible elevation of the active state of mTORC1. This experiment was conducted under nutrient replete conditions such that even in the absence of infection, mTORC1 would be expected to be active. In this way the aforementioned experiment was more suited to testing for potential inactivation of mTORC1 by ASFV. This raises the possibility that the observed active state of mTORC1 in infected cells is simply the result of its resting state remaining unchanged although this would seem unlikely because mTORC1 would usually be inactivated in response to cell stress resulting from infection. Alternatively, the active state of mTORC1 may be the result of a targeted mechanism by the virus. To investigate this further, phosphorylation of p70-S6K was analysed in infected cells that were placed under starvation conditions to inactivate mTORC1. Vero cells were infected with the Ba71V strain of ASFV (MOI 5) and harvested at multiple time points over a 16 hour time course of infection. Prior to harvest, cells were starved for 1 hour in EBSS to induce inactivation of mTORC1 and the dephosphorylation of p70-S6K. In addition, cells were mock infected and harvested at a single 16 hour time point, prior to which cells were either incubated in complete cell media or starved in EBSS for 1 hour to demonstrate a reduction in p70-S6K phosphorylation. Samples were prepared from cells for analysis by immunoblotting and probed using anti-p70-S6K, anti-p30 viral protein and anti-γ tubulin antibodies. Total protein levels for p70-S6K were analysed in addition to analysis of phosphorylation levels.

Samples from mock infected cells that were analysed by Western blot analysis demonstrated dramatically less phosphorylated p70-S6K (P-p70-S6K) after 1 hour starvation when compared to non-starved conditions at 16 hpi (Figure 4.3). This indicates that 1 hour of starvation is sufficient to reduce mTORC1-dependent phosphorylation of its substrate proteins. Slightly greater levels of P-p70-S6K were apparent in ASFV infected cells at 1 hpi and 2 hpi relative to mock infected cells that were incubated under starvation conditions. The P-p70-S6K levels increased in ASFV infected cells over time, peaking at 4 hpi and 8 hpi before decreasing again at 16 hpi. Levels of total p70-S6K were similar between mock infected and ASFV infected cells and also remained unchanged throughout the time course of ASFV infection. Labelling of viral protein p30 showed increasing

levels of protein expression in ASFV infected cells from 4 hpi indicating that replication proceeded as expected during the experiment.

This data demonstrates that ASFV is able to circumvent starvation-dependent signals that lead to mTORC1 inactivation. However, this effect is observed in a time-dependent manner, becoming more evident as infection progresses.

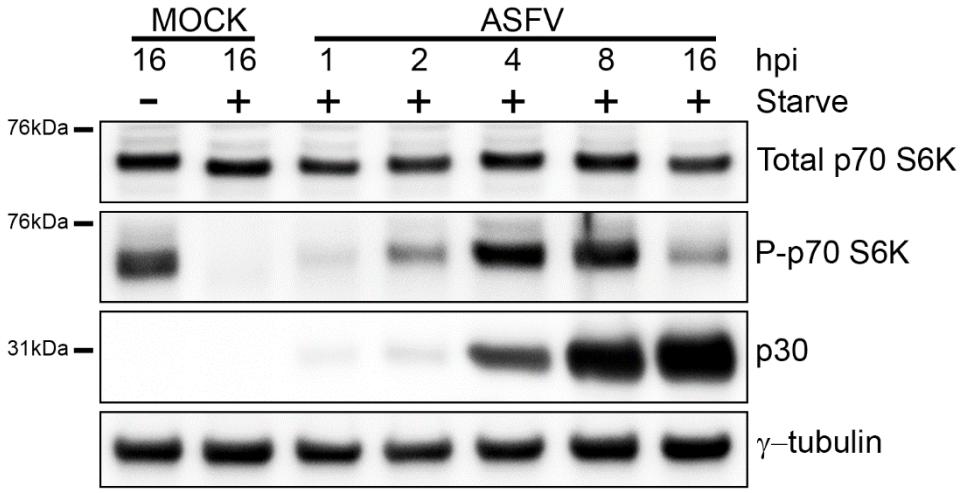

Figure 4.3 Starvation-induced inactivation of mTORC1 is inhibited by ASFV

Vero cells were infected with Ba71V (MOI 5) and harvested at multiple time points over a 16 hour time course of infection. Prior to harvest, cells were starved for 1 hour in EBSS. Separately, cells were mock infected for a total of 16 hours and either incubated in complete cell media or starved for 1 hour in EBSS prior to harvest. Cells were lysed and samples prepared for resolution by bis-Tris PAGE before transfer to PVDF membrane. Finally, samples were probed with p70-S6K, p30 viral protein and anti-γ tubulin antibodies followed by appropriate HRP-conjugated secondary antibodies. Hours post infection (hpi) are indicated at the top of the gel. The positions of molecular mass markers are indicated to the left of the gels.

4.2.4 Akt remains active during ASFV infection

Akt is a critical upstream mediator of mTORC1. The activation of Akt leads to the activation of mTORC1, a mechanism that occurs either directly via the Akt-mediated phosphorylation and suppression of the mTORC1 negative regulator, TSC2 or via the negative regulation of AMPK which is an activator of the TSC complex (Hahn-Windgassen et al., 2005). The complete activation of Akt is accompanied by its phosphorylation on residues T308 and S473 (Alessi et al., 1996). This is triggered following the binding of Akt to phospholipids produced by class I PI3K at the plasma membrane, a process that can be blocked using the PI3K inhibitor LY294002 (Franke et al., 1995, Klippel et al., 1996, Vlahos et al., 1994). Class I PI3K is activated following growth factor and insulin stimulation and conversely, the absence of growth factor stimulation can lead to the downstream inactivation of Akt (Liao and Hung, 2010).

The previous results described in sections 4.2.2 and 4.2.3 revealed that mTORC1 was active in ASFV infected cells. To investigate if mTORC1 activity could be linked to that of Akt, an investigation was conducted to determine if Akt is also active during infection. Vero cells were either mock infected or infected with the Ba71V strain of ASFV (MOI 5). Virus was added to cells and incubated for 1 hour to allow virus entry. Cells were washed to remove residual virus at which stage cells were harvested for the first time point (0 hour time point). Remaining cells were incubated in nutrient replete conditions and harvested at multiple time points over a 16 hour course of infection. In addition, control cells were either incubated in complete cell media or starved in EBSS for 3 hours to demonstrate the reduced phosphorylation of Akt following removal of growth factors. Another set of control cells were incubated in media containing DMSO (solvent control) or 50 nM LY294002 for 3 hours to demonstrate an additional means of Akt dephosphorylation. Samples were prepared from cells for analysis by immunoblotting and probed using anti-Akt, anti-p30 viral protein and anti-γ tubulin antibodies. Total protein levels for Akt were analysed in addition to analysis of phosphorylation at the T308 and S473 sites.

Western blot analysis in Figure 4.4 showed a substantial reduction of phosphorylated Akt at T308 and S473 in starved control cells when compared to cells incubated under nutrient replete conditions. Control cells that were treated with DMSO showed similar levels of phosphorylated Akt to non-starved cells indicating that DMSO alone had no effect on Akt phosphorylation. Comparison of the non-starved cells to the cells treated with LY294002 demonstrated a dramatic reduction in phosphorylation at T308 and S473 in the latter. Phosphorylated Akt bands under LY294002 treatment were also less intense when compared with cells that were starved. Collectively, these results indicate that while starvation leads to a moderate reduction in Akt phosphorylation, using the PI3K inhibitor LY294002 induces greater levels of dephosphorylation.

Phosphorylation of Akt at S473 in ASFV infected cells was at an equivalent level to mock infected cells up to 1 hpi but from 2 to 8 hpi, an increase above mock was observed. This increase was however no longer apparent at 16 hpi when instead similar levels of S473 phosphorylation were seen between mock infected and ASFV infected cells. Phosphorylation at T308 remained comparable between ASFV and mock infected cells throughout the time course of infection. Additionally, no differences in total Akt levels between mock and ASFV infected cells were apparent over the duration of the time course. Taken together these results indicate that Akt remains active throughout the ASFV replication cycle. Since AKT is upstream of mTORC1, the maintenance of the active state of AKT is consistent with the maintenance of active mTORC1 and the downstream inactivation of autophagy.

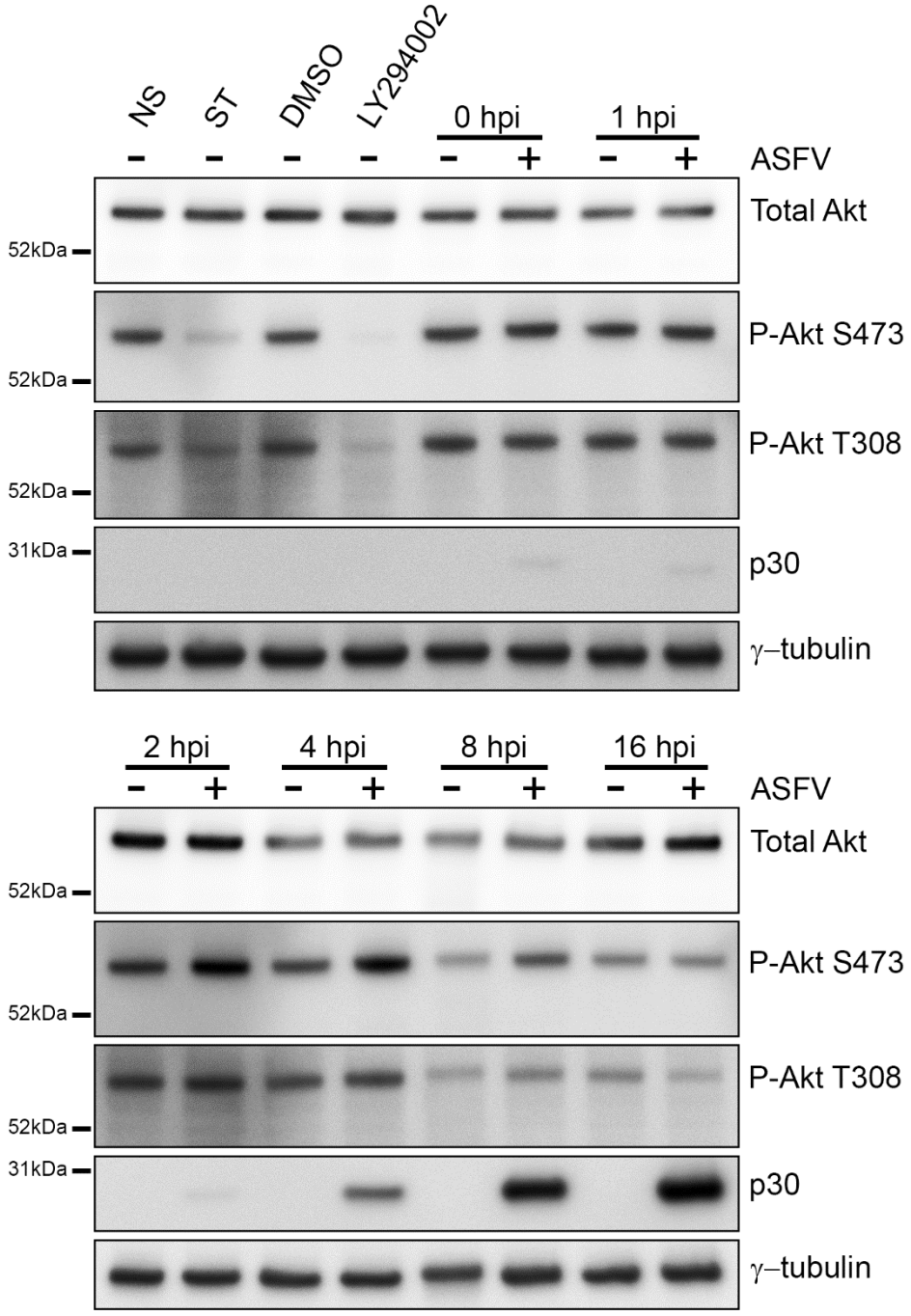

Figure 4.4 Akt remains active during ASFV infection

Vero cells were either mock infected or infected with Ba71V (MOI 5) for 1 hr before residual virus was washed off and the 0 hr time point was harvested. The remaining infected cells were incubated in 2% media and harvested at multiple time points over a 16 hour time course of infection. Control cells were either non-starved (NS) in complete cell media, starved (ST) in EBSS, incubated in media containing DMSO or incubated in media containing 50 nM LY294002 for 3 hours. Cells were lysed and samples prepared for resolution by bis-Tris PAGE before transfer to PVDF membrane. Finally, samples were probed with Akt, p30 viral protein and anti-γ tubulin antibodies followed by appropriate HRP-conjugated secondary antibodies. The positions of molecular mass markers are indicated to the left of the gels.

4.2.5 Purification and electron microscopy analysis of ASFV

The results described in sections 4.2.2 to 4.2.4 revealed that mTORC1 and Akt remain active during ASFV infection, however the mechanism by which this occurs is unknown. Vaccinia virus (VACV) has also been shown to activate the PI3K-Akt pathway at early and late times of the infection cycle (Soares et al., 2009). Further research showed that this was important for endocytosis-dependent virus entry but more specifically that PI3K-Akt activation was linked to β1 integrin mediated entry (Izmailyan et al., 2012). ASFV has also been shown to use the endocytosis pathway for virus entry, however the cell receptor is currently unknown (Cuesta-Geijo et al., 2012). Interestingly, a separate study implicated macropinocytosis in virus entry (Sanchez et al., 2012) and it was later described that ASFV is internalized into macrophages by both clathrin-mediated endocytosis and macropinocytosis (Hernaez et al., 2016). However, it was found that in the case of the latter, macropinocytosis was not specifically stimulated by ASFV but rather that the internalisation of virions in macropinosomes was the result of constitutive macropinocytosis for example via natural sampling of the cells microenvironment (Hernaez et al., 2016). In the aforementioned study, the authors hypothesised that the use of a clarified virus inoculum as opposed to a purified virus inoculum may influence the stimulation of macropinocytosis due to the presence of significant amounts of contaminant cell and viral debris in non-purified virus stocks.

The previous experiments in sections 4.2.2 to 4.2.4 were conducted using clarified Ba71V virus inoculum. As the activation of Akt in VACV models has been shown to be affected by the virus entry mechanism, purification of ASFV was undertaken here with the intention of re-examining the activity of Akt and mTORC1. Clarified cell supernatant containing Ba71V was either concentrated by ultra-centrifugation or concentrated and then purified in a double round of Percoll purification. A detailed method of virus purification is described in section 2.2.5. The concentrated non-purified and concentrated purified virus stocks were then fixed using glutaraldehyde and examined by negative stain electron microscopy. Electron microscopy methods are described in section 2.9.

Figure 4.5 Electron microscopy analysis of non-purified and purified virus inocula

Vero cells were infected with Ba71V (MOI 1) and incubated until complete cell detachment. Cell supernatants were harvested and clarified by low-speed centrifugation. Supernatants were either concentrated using ultra-centrifugation or concentrated and purified using a double round of Percoll purification. Concentrated non-purified (Panel A) and concentrated purified stocks (Panel B) were then fixed using glutaraldehyde and analysed by negative stain electron microscopy. Arrows point to ASFV virus particles. Scale bars are represented below each panel.

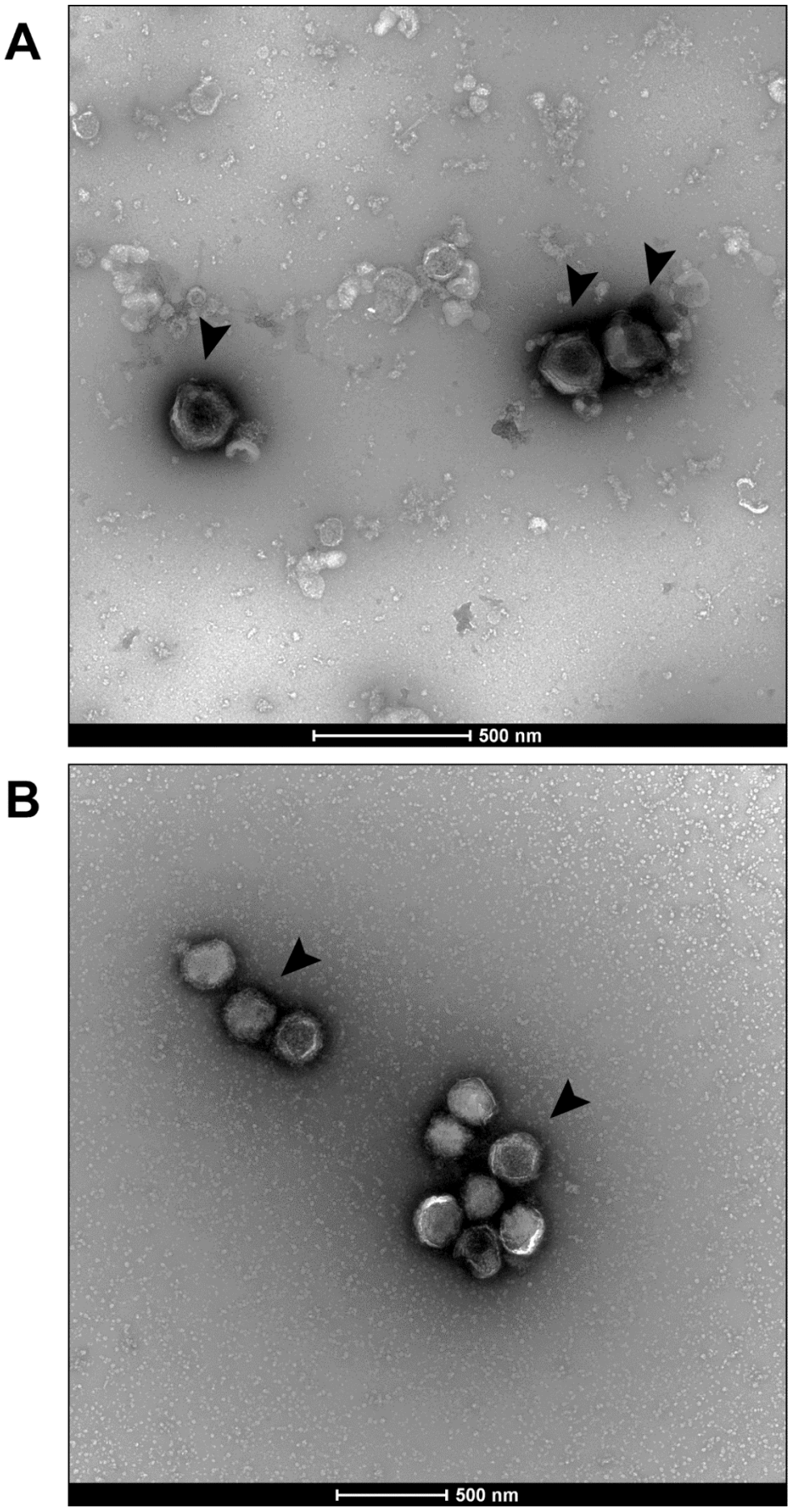

Figure 4.5 **Electron microscopy analysis of non-purified and purified virus inocula**

EM analysis of concentrated non-purified Vero cell supernatant containing Ba71V (Figure 4.5A) revealed the presence of dark staining geometrically-shaped particles that were either grouped together or in isolation. Particle size was estimated by visual inspection to be approximately 200 nM across. The shape and size of these particles was therefore consistent with ASFV virus particles. Large amounts of lighter staining material was dispersed throughout the image. This material was of varying size and shape and was therefore inconsistent with virus particles and more likely consisted of cell and viral debris. Identical analysis of purified cell supernatant containing Ba71V shown in Figure 4.5B also indicated clusters of particles that were consistent in both shape and size of ASFV virions. However, evidence of cell and viral debris was no longer apparent suggesting that purification of the supernatant successfully removed this material. These results therefore revealed that the purified virus was suitable for use in downstream experiments in which the potential influence on Akt and mTORC1 activity by the presence of cell debris could be excluded.

4.2.6 Purified ASFV inhibits starvation-induced accumulation of LC3-II

The investigation carried out in section 3.2.2 showed that at 4 hpi, starvation of mock infected Vero cells induced an increase in LC3-II when compared to cells under nutrient rich conditions and that the same effect was observed in uninfected cells. In contrast, starvation did not induce any increase in LC3-II relative to non-starved conditions in cells infected with a clarified stock of cell supernatant containing Ba71V suggesting that the induction of autophagy by starvation is inhibited by ASFV. Part of the same experiment but not previously described were cells that were infected with purified Ba71V virus (MOI 5). This was aimed at facilitating side-by-side comparison of the effects of infection on LC3-II levels between using non-purified and purified virus inocula and results from this analysis are described below. Cells were either incubated in complete cell media or starved in EBSS for 2 hours prior to harvest at 4 hpi and samples were then prepared from cells for analysis by immunoblotting. Finally, samples were probed using anti-LC3, anti-p30 viral protein and anti-γ tubulin antibodies.

Figure 4.6 shows the same Western blot analysis that was previously carried out on uninfected, mock infected and non-purified ASFV infected cells in Figure 3.2 but with additional analysis indicated of cells infected with purified ASFV. Labelling of p30 revealed comparable levels of virus protein expression between non-purified and purified viruses. In similarity to what was previously seen using non-purified virus, comparable amounts of LC3-II were also observed between starved and non-starved conditions using purified virus. These results therefore demonstrate that purified virus acts in the same way as non-purified virus by inhibiting starvation-induced accumulation of LC3-II. Consequently, the presence of cell and viral debris in non-purified virus does not seem to be responsible for the block in autophagy induction but rather points to a virus specific mechanism.

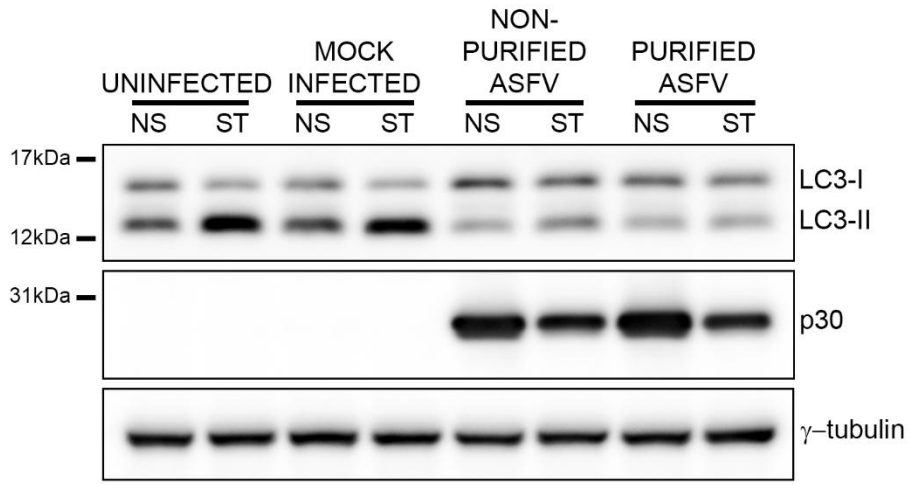

Figure 4.6 Purified ASFV inhibits starvation-induced accumulation of LC3-II in Vero cells

Vero cells were incubated with media alone (uninfected), mock inoculum (mock infected), non-purified Ba71V (MOI 5) or purified Ba71V (MOI 5) for 1 hour. Inocula were removed and cells were incubated for a total of 4 hours during which cells were either non-starved (NS) in complete cell media or starved (ST) in EBSS for the final 2 hours. Cells were then lysed and samples prepared for resolution by bis-Tris PAGE before transfer to PVDF membrane. Finally, samples were probed with anti-LC3, anti-p30 and γ-tubulin antibodies followed by appropriate HRP-conjugated secondary antibodies. The positions of molecular mass markers are indicated to the left of the gels.

4.2.7 Akt and mTORC1 are active in cells infected with purified ASFV

In section 4.2.2 it was hypothesised that the observed active state of mTORC1 in infected cells could be a means by which ASFV negatively modulates the autophagy pathway. The results in section 4.2.4 further established that Akt remains active over a time course of infection which may lead to downstream mTORC1 activation. The aforementioned experiments were carried out using non-purified Ba71V and in section 4.2.6, Western blot analysis revealed that purified virus acted in the same way as non-purified virus with regard to inhibition of starvation-induced LC3-II accumulation. It could therefore be expected that Akt and mTORC1 are likely be active in cells infected with purified ASFV as was demonstrated using non-purified virus. To test this, Vero cells were either mock infected or infected with purified cell supernatant containing Ba71V (MOI 5) and incubated under nutrient replete conditions for a total of 4 hours. Samples were prepared from cells for analysis by immunoblotting. Finally, samples were probed using anti-Akt, anti-p70-S6K, anti-p30 viral protein and anti-γ tubulin antibodies. Total protein levels for Akt and p70-S6K were analysed in addition to analysis of phosphorylation of these proteins.

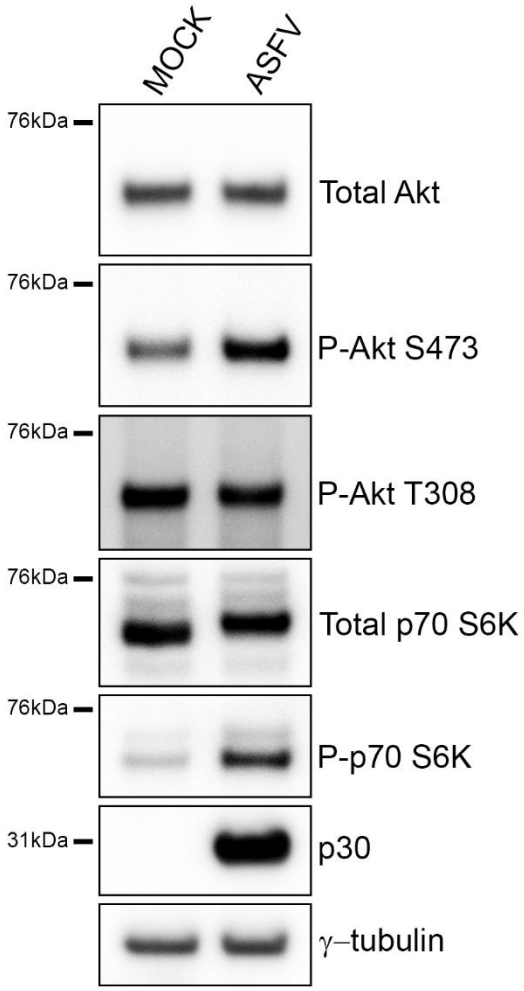

Figure 4.7 Akt and mTORC1 are active in cells infected with purified ASFV

Vero cells were incubated with mock inoculum (mock infected) or purified Ba71V (MOI 5) for 1 hour. Inocula were removed and cells were incubated for a total of 4 hours. Cells were then lysed and samples prepared for resolution by bis-Tris PAGE before transfer to PVDF membrane. Finally, samples were probed with anti-Akt, anti-p70-S6K, anti-p30 and γ-tubulin antibodies followed by appropriate HRP-conjugated secondary antibodies. The positions of molecular mass markers are indicated to the left of the gels.

Western blot analysis of viral protein p30 in Figure 4.7 showed the presence of ASFV gene expression in cells infected with purified Ba71V but not in cells that were mock infected. Greater amounts of phosphorylated p70-S6K and phosphorylated Akt at S473 were evident in ASFV infected cells when compared to mock infected cells, however a similar level of phosphorylated Akt at T308 was observed between mock infected and ASFV infected cells. Analysis of total Akt and total p70-S6K did not reveal any differences between mock infected and ASFV infected cells. Taken together these results demonstrate that Akt and mTORC1 are active following infection with purified ASFV which corresponds to the previous result using the non-purified virus. It can

therefore be concluded that the presence of cell and viral debris in the non-purified virus does not induce the activation of Akt and mTORC1 and that this is more likely a virus specific effect.

4.2.8 Analysis of the effects of MK-2206 and Torin1 on Akt and mTORC1 substrate phosphorylation

The investigation in section 4.2.2 revealed that an active state of mTORC1 was maintained during ASFV infection. Additionally, it was shown in section 4.2.3 that mTORC1 was activated in infected cells despite attempting to inactivate it under starvation conditions. Taken together, these results suggest that ASFV exerts a modulatory effect on mTORC1. Following the results in section 4.2.4 that demonstrated the active state of Akt over a time course of ASFV infection, it was hypothesised that perhaps the virus drives the activation of mTORC1 via the activity of Akt. This model is based on the fact that Akt mediates the activity of mTORC1 via the phosphorylation of TSC2, an inhibitor of mTORC1. However, mTORC1 can also be regulated independently of Akt via AMPK, a TSC complex activator.

To provide a potential means of inactivating mTORC1 and Akt, the phosphorylation of Akt and mTORC1 substrate protein p70-S6K was analysed in the presence of pharmacological inhibitors, Torin1 and MK-2206. Research on Torin1 has revealed that it offers a more potent inhibition of mTORC1 when compared to rapamycin treatment and that it also inhibits mTORC2 (Thoreen et al., 2009). In similarity to mTORC1, mTORC2 is a large protein kinase comprising the catalytic subunit mTOR. However, some of the protein partners of mTORC2 and mTORC1 are different (Jhanwar-Uniyal et al., 2019). Whereas mTORC1 acts on the ULK1 autophagy complex and the translation factors p70-S6K and 4E-BP1, mTORC2 directly phosphorylates Akt on S473 facilitating phosphorylation on T308 by PDK1 and the eventual activation of Akt (Sarbassov et al., 2005). MK-2206 is a highly potent and selective allosteric Akt inhibitor that blocks its activation and kinase activity preventing the downstream phosphorylation and inactivation of TSC2 (Yan, 2009).

In this experiment, Vero cells were either mock infected or infected with Ba71V (MOI 5) for a total of 4 hours. During the final 2 hours of infection cells were incubated in conventional 2% media or in 2% media containing either 200 nM Torin1 or 5 µM MK-2206 or a combination of both drugs. Separately, cells were also incubated in EBSS containing both drugs to test whether starvation alters the effects of the drugs. A 4 hour period of infection was chosen as previously it was at this stage of the replication cycle that Akt and mTORC1 demonstrated obvious activity in ASFV infected cells. Samples were prepared from cells for analysis by immunoblotting. Finally, samples were probed using anti-Akt, anti-p70-S6K, anti-p30 viral protein and anti-γ tubulin antibodies. Total protein levels and the phosphorylation status of Akt and p70-S6K were analysed.

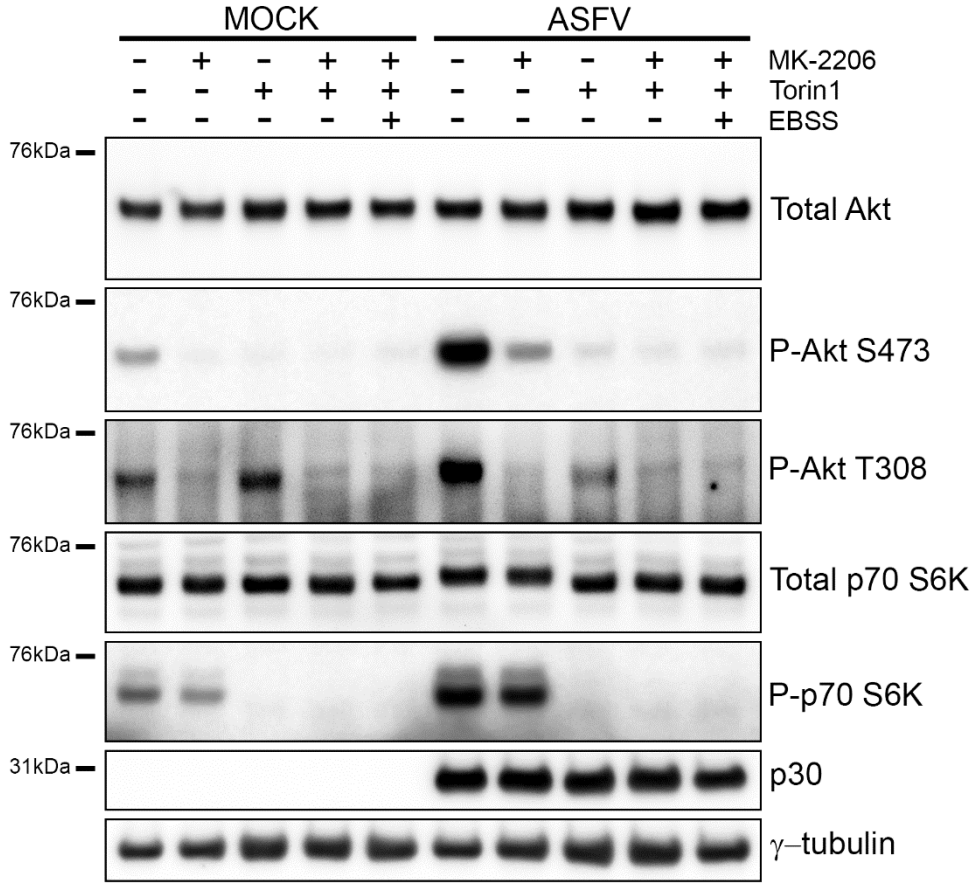

Figure 4.8 Analysis of the effects of MK-2206 and Torin1 on Akt and mTORC1 substrate phosphorylation

Vero cells were incubated with mock inoculum (mock infected) or Ba71V (MOI 5) for 1 hour. Inocula were removed and cells were incubated for a total of 4 hours. During the last 2 hours, cells were incubated in regular 2% media or in 2% media containing 200 nM Torin1 or 5 µM MK-2206 or a combination of both drugs. Separately, cells were starved in EBSS in the presence of both drugs. Cells were then lysed and samples prepared for resolution by bis-Tris PAGE before transfer to PVDF membrane. Finally, samples were probed with anti-Akt, anti-p70-S6K, anti-p30 and γ-tubulin antibodies followed by appropriate HRP-conjugated secondary antibodies. The positions of molecular mass markers are indicated to the left of the gels.

Western blot analysis in Figure 4.8 showed the expression of viral protein p30 in ASFV infected cells only. In conventional 2% media, a greater amount of phosphorylated p70-S6K (P-p70-S6K) and phosphorylated Akt on S473 (P-Akt S473) and T308 (P-Akt T308) was evident in ASFV infected cells compared to mock infected cells. This shows that Akt and mTORC1 were active in ASFV infected cells as previously reported. Almost a complete loss of P-Akt S473 and P-Akt T308 was observed in mock infected cells in the presence of MK-2206. Interestingly, under the same conditions only a moderate loss of P-Akt S473 was observed in ASFV infected cells and a near complete loss of P-Akt T308. This could suggest that while MK-2206 alone is sufficient to inactivate Akt in mock infected cells, it is only able to partially inactivate Akt in ASFV infected cells at the concentration used. Mock infected cells incubated in the presence of Torin1

demonstrated a loss of P-p70-S6K and a loss of P-Akt S473 but phosphorylation on Akt T308 was still apparent. This shows that Torin1 is able to inactivate mTORC1 preventing the downstream phosphorylation of p70-S6K and is also able to inhibit the activity of mTORC2 which phosphorylates Akt on S473. Torin1 treatment of ASFV infected cells led to dramatic reductions of P-p70-S6K, P-Akt S473 and P-Akt T308 compared to untreated cells however some P-Akt S473 and P-Akt T308 was still apparent. Treatment of mock infected or ASFV infected cells with both MK-2206 and Torin1 facilitated the greatest loss of P-p70-S6K, P-Akt S473 and P-Akt T308 compared to untreated cells or cells treated with drugs in isolation. Incubating the cells in EBSS rather than 2% media did not make any difference to phosphorylation levels. Additionally, analysis of total p70-S6K and total Akt did not indicate any differences between mock infected and ASFV infected cells or between cell treatments.

Collectively these results suggest that using MK-2206 and Torin1 in combination provides the most effective means of reducing the activity of Akt and mTORC1 in mock infected and ASFV infected cells.

4.2.9 Low numbers of autophagosomes are evident at 4 hpi in ASFV infected cells in the presence of Torin1 and MK-2206

Both Ba71V and Ba71V A179L KO virus were able to inhibit starvation induced formation of autophagosomes at 4 hpi (see sections 3.2.1 and 4.2.1). Adding to this, the results in section 4.2.8 demonstrated that Akt and mTORC1 can be sufficiently inactivated in ASFV infected cells at 4 hpi using a combination of Torin1 and MK-2206. This provides an opportunity to explore whether Akt-mTORC1 activity is a means by which ASFV negatively modulates the induction of autophagy. In this respect, a confocal microscopy experiment was conducted using starvation conditions as described in sections 3.2.1 and 4.2.1 but with Torin1 and MK-2206 included. Vero cells were mock infected or infected with either Ba71V (MOI 5) or the Ba71V A179L KO virus (MOI 5) for a total period of 4 hours during which cells were incubated for the final 2 hours in EBSS alone or EBSS containing 200 nM Torin1 and 5 μM MK-2206. Cells were then fixed and labelled for LC3 to detect autophagosomes and viral protein p30 to detect infected cells.

Figure 4.9.1 Starvation-induced formation of autophagosomes is inhibited in ASFV infected cells at 4 hpi

Vero cells were incubated with mock inoculum (Panel A) or Ba71V (MOI 5) (Panels B and C) or Ba71V A179L KO (MOI 5) (Panels D and E) for 1 hour. Inocula were removed and cells were incubated for a total of 4 hours during which cells were starved in EBSS media for the final 2 hours. Cells were then fixed and permeabilised in methanol before labelling LC3 shown in green, viral protein p30 shown in red and nuclei shown in blue. Panels C and E are stained with p30. Panels B and D show the same infected cells as Panels C and E respectively but with the red channel removed to allow for clearer observation of LC3 staining. Scale bars represent 10 µM.

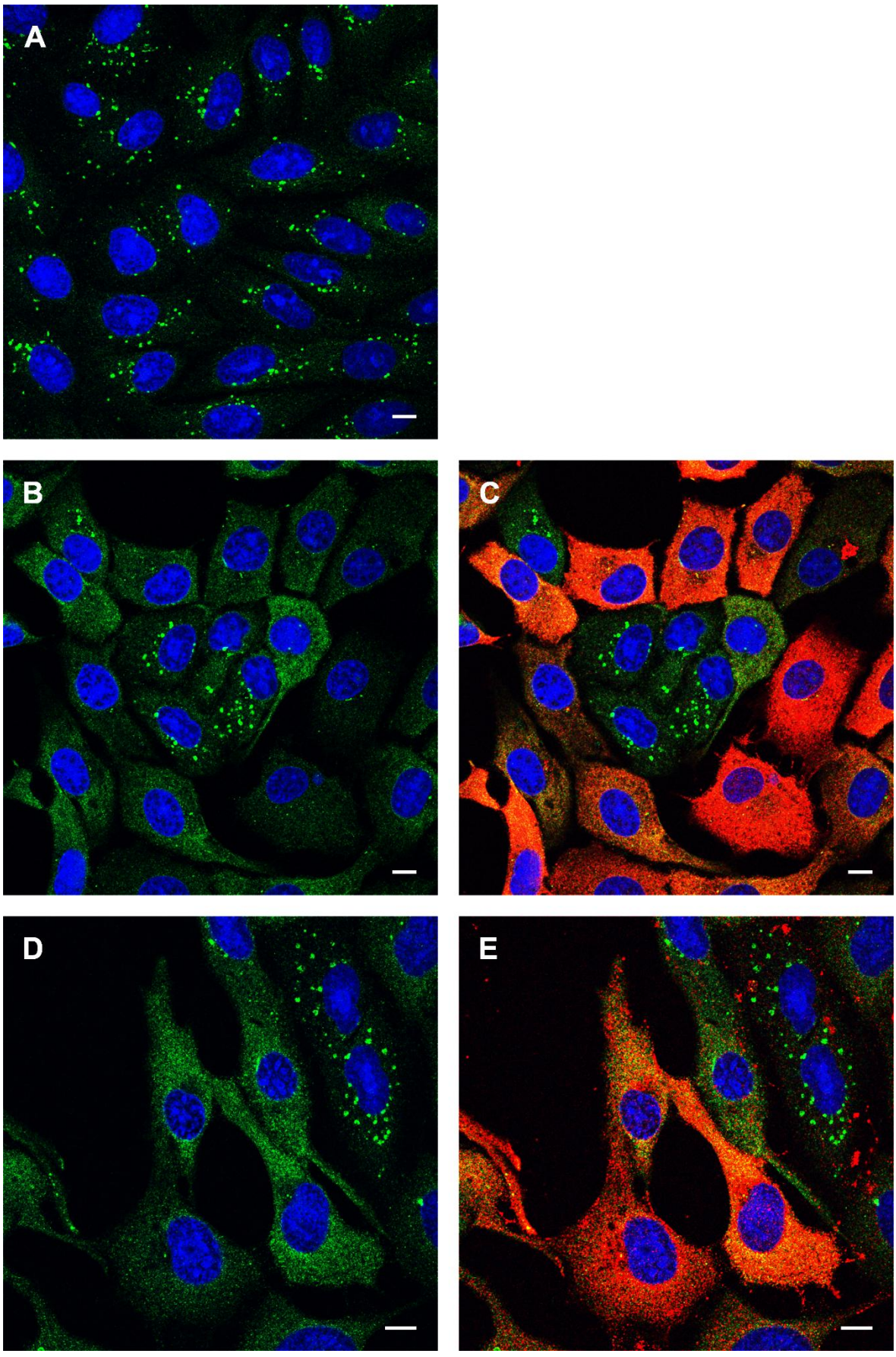

Figure 4.9.1 Starvation-induced formation of autophagosomes is inhibited in ASFV infected cells at 4 hpi

Figure 4.9.2 Low numbers of autophagosomes are evident at 4 hpi in ASFV infected cells in the presence of Torin1 and MK-2206

Vero cells were incubated with mock inoculum (Panel A) or Ba71V (MOI 5) (Panels B and C) or Ba71V A179L KO (MOI 5) (Panels D and E) for 1 hour. Inocula were removed and cells were incubated for a total of 4 hours during which cells were starved in EBSS media containing 200 nM Torin1 and 5μM MK-2206 for the final 2 hours. Cells were then fixed and permeabilised in methanol before labelling LC3 shown in green, viral protein p30 shown in red and nuclei shown in blue. Panels C and E are stained with p30. Panels B and D show the same infected cells as Panels C and E respectively but with the red channel removed to allow for clearer observation of LC3 staining. Scale bars represent 10 μM.

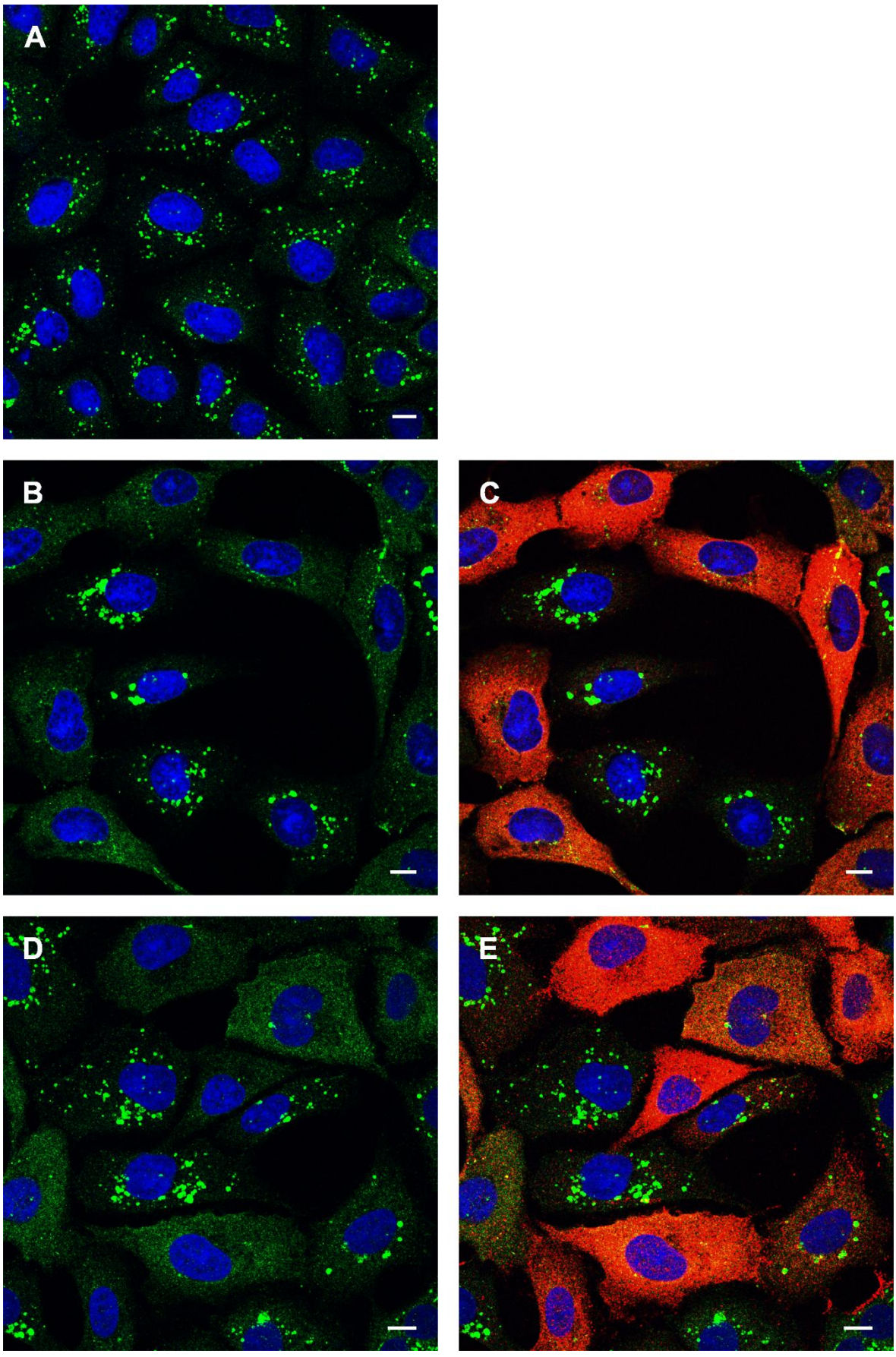

Figure 4.9.2 Low numbers of autophagosomes are evident at 4 hpi in ASFV infected cells in the presence of Torin1 and MK-2206

The immunofluorescence results shown in Figure 4.9.1A demonstrated high numbers of LC3 puncta in mock infected cells as would be expected under starvation conditions. In contrast, cells that had been infected with Ba71V (Figure 4.9.1B) and the A179L KO virus (Figure 4.9.1D) showed some cells that contained comparable numbers of LC3 puncta to mock infected cells and other cells that showed a near complete absence of LC3 puncta. Labelling of p30 (Figure 4.9.1C and E) revealed that cells that demonstrated almost no LC3 puncta were expressing ASFV proteins whereas cells with a high number of LC3 puncta were not. Taken together, this data confirms the results that were described in sections 3.2.1 and 4.2.1 that indicate that ASFV inhibits the induction of autophagy at 4 hpi.

In cells that were incubated in EBSS in the presence of Torin1 and MK-2206, LC3 labelling revealed a high number of autophagosomes in mock infected cells as one would expect under starvation conditions (Figure 4.9.2A). LC3 and p30 labelling of cells that had been infected with Ba71V (Figure 4.9.2B and C) or the Ba71V A179L KO virus (Figure 4.9.2D and E) indicated that cells demonstrating high numbers of LC3 puncta were not expressing ASFV proteins and that cells in which low numbers of LC3 puncta were observed labelled positively for p30. Visual inspection of the number of LC3 puncta in ASFV infected cells in the presence of Torin1 and MK-2206 (Figure 4.9.2B and D) seemed to indicate a slightly greater number of puncta compared to cells infected with ASFV in the absence of drugs (Figure 4.9.1B and D). Collectively, these results suggest that ASFV was perhaps unable to entirely block the formation of autophagosomes in the presence of Torin1 and MK-2206 although it was able to still restrict the number of observed autophagosomes.

4.2.10 Autophagosome formation can be stimulated in ASFV infected cells at 2 hpi in the presence of Torin1 and MK-2206

Overall the results in section 4.2.9 indicated that ASFV is able to restrict the formation of autophagosomes at 4 hpi in the presence of Akt and mTORC1 inhibitors although perhaps not completely. To investigate if this restriction was related to the timing at which the analysis was conducted with regard to the stage of virus replication, the same experiment was conducted but analysis was carried out at 2 hpi rather than 4 hpi. A 2 hour time point was used as this marks the early stages of viral protein translation and therefore influence from additional viral virulence factors could be kept to a minimum. Vero cells were mock infected or infected with Ba71V (MOI 5) or the Ba71V A179L KO virus (MOI 5) and analysis was carried out under starvation conditions whereby cells were starved for 2 hours in EBSS alone or in EBSS containing 200 nM Torin1 and 5 µM MK-2206 prior to fixing and labelling the cells for immunofluorescence. Cells were labelled for LC3 to detect autophagosomes and viral protein p30 to detect infected cells.

LC3 labelling of mock infected cells under starvation conditions predictably revealed an extensive amount of LC3 puncta (Figure 4.10.1A). Cells that had been infected with Ba71V (Figure 4.10.1B

and C) showed almost no detectable puncta in p30 expressing cells and in cells not expressing p30, similar amounts of LC3 puncta to the mock infected cells were observed. Cells that were infected with the A179L KO virus demonstrated a high number of LC3 puncta in cells that were not expressing p30 and an absence of puncta in cells expressing p30 (Figure 4.10.1D and E). Collectively, these results suggest that the Ba71V strain of ASFV is able to inhibit the induction of autophagosomes at 2 hpi as was previously demonstrated at 4 hpi and that the mutant A179L KO virus acts in the same way.

Mock infected cells that had been starved in the presence of Torin1 and MK-2206 (Figure 4.10.2A) showed similar amounts of LC3 puncta at 2 hpi compared to mock infected cells that were starved in the absence of drugs (Figure 4.10.1A). This shows that Torin1 and MK-2206 had no effect on the starvation-induced formation of autophagosomes. LC3 labelling of cells that had been infected with Ba71V and starved in the presence of Torin1 and MK-2206 (Figure 4.10.2B) demonstrated a substantial number of LC3 puncta at 2 hpi and labelling of p30 indicated that LC3 puncta were evident in ASFV infected cells (Figure 4.10.2C). A considerable number of LC3 puncta were also observed at 2 hpi in cells that had been infected with the A179L KO virus and starved in the presence of Torin1 and MK-2206 (Figure 4.10.2D). Labelling of p30 shown in Figure 4.10.2E indicated that LC3 puncta were evident in cells expressing ASFV proteins. Taken together the results show that inhibitors of Akt and mTORC1 can effectively induce autophagy, that ASFV infection blocks starvation induced or inhibitor induced autophagy, but that this block takes several hours to become effective in infected cells.

Figure 4.10.1 ASFV inhibits the formation of autophagosomes at 2 hpi

Vero cells were incubated with mock inoculum (Panel A) or Ba71V (MOI 5) (Panels B and C) or Ba71V A179L KO (MOI 5) (Panels D and E) for 1 hour. Inocula were removed and cells were incubated for a total of 2 hours during which cells were starved in EBSS media. Cells were then fixed and permeabilised in methanol before labelling LC3 shown in green, viral protein p30 shown in red and nuclei shown in blue. Panels C and E are stained with p30. Panels B and D show the same infected cells as Panels C and E respectively but with the red channel removed to allow for clearer observation of LC3 staining. Scale bars represent 10 μM.

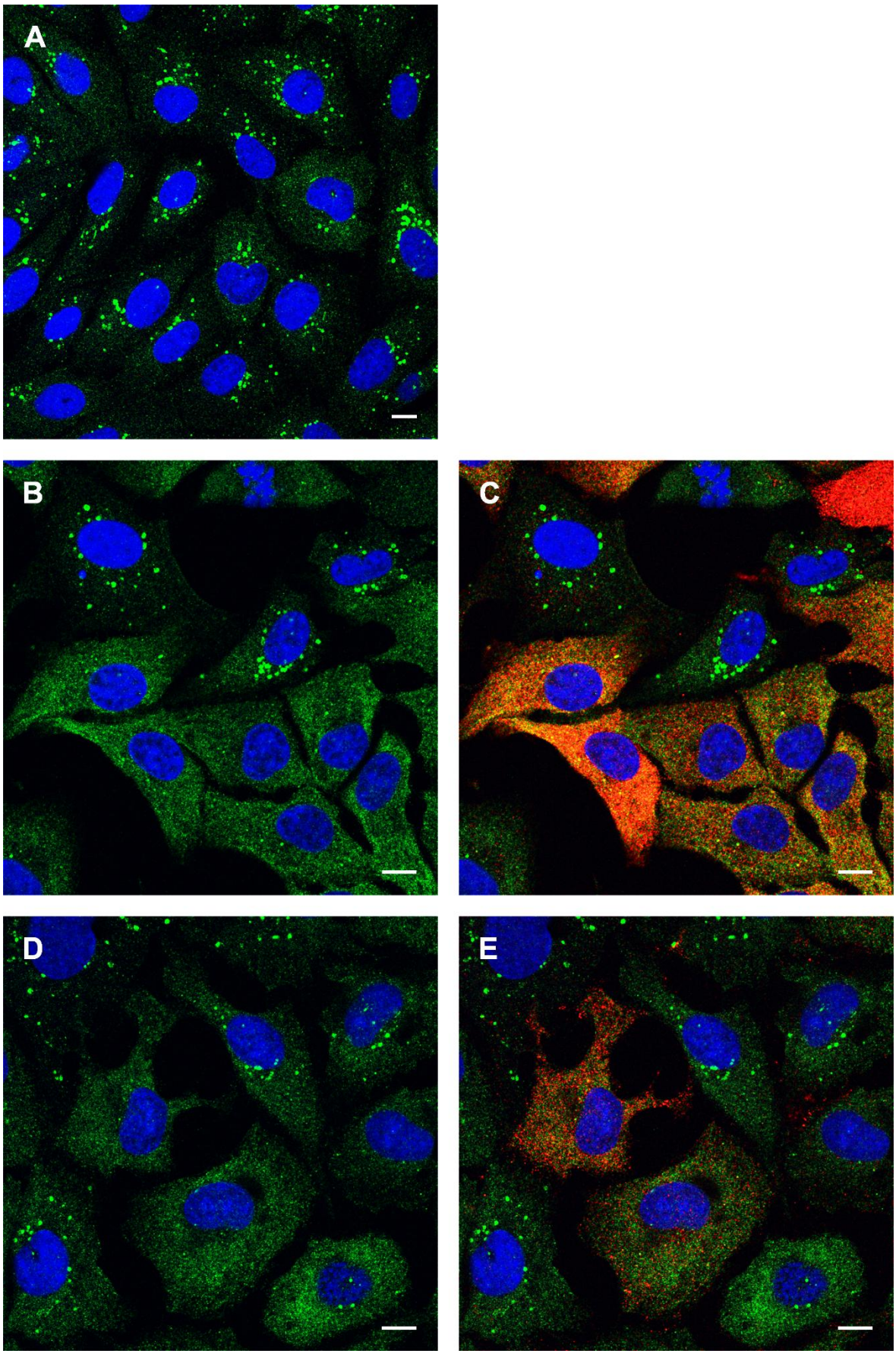

Figure 4.10.1 ASFV inhibits the formation of autophagosomes at 2 hpi

Figure 4.10.2 Autophagosomes can be induced in ASFV infected cells at very early stages of the replication cycle in the presence of Akt and mTORC1 inhibitors

Vero cells were incubated with mock inoculum (Panel A) or Ba71V (MOI 5) (Panels B and C) or Ba71V A179L KO (MOI 5) (Panels D and E) for 1 hour. Inocula were removed and cells were incubated for a total of 2 hours during which cells were starved in EBSS media containing 200 nM Torin1 and 5μM MK-2206. Cells were then fixed and permeabilised in methanol before labelling LC3 shown in green, viral protein p30 shown in red and nuclei shown in blue. Panels C and E are stained with p30. Panels B and D show the same infected cells as Panels C and E respectively but with the red channel removed to allow for clearer observation of LC3 staining. Scale bars represent 10 μM.

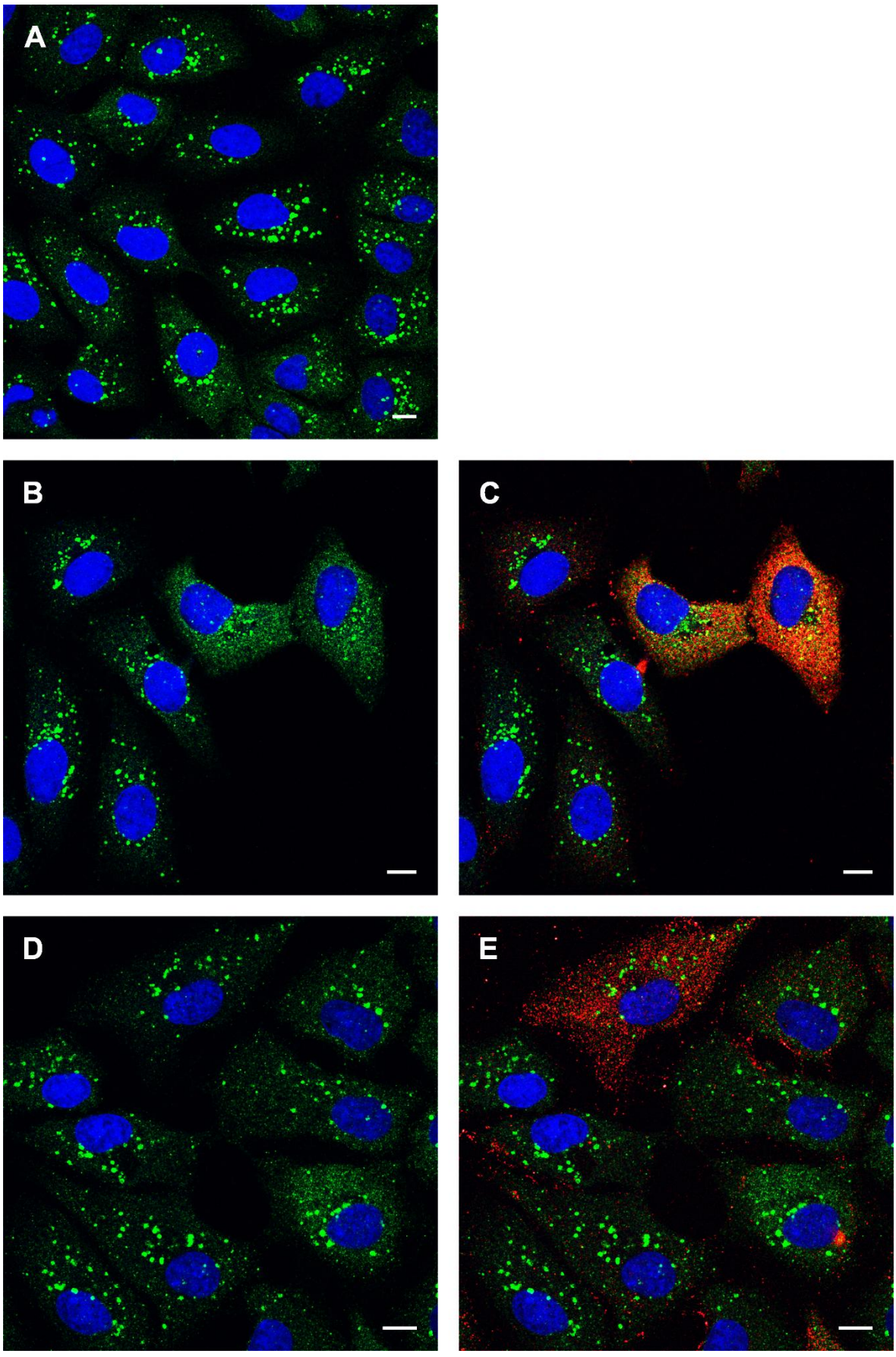

Figure 4.10.2 Autophagosomes can be induced in ASFV infected cells at very early stages of the replication cycle in the presence of Akt and mTORC1 inhibitors

4.3 Discussion

In the previous chapter the inhibition of autophagosome formation by ASFV at an early stage of the virus replication cycle was described. The absence of autophagic flux measured by p62 degradation was also demonstrated providing confirmation that ASFV blocks autophagy. Experiments were then conducted to try to elucidate the potential mechanisms employed by the virus to restrict the induction of autophagy. These mechanisms may be centred on the interaction of viral proteins with the autophagy machinery or could take the form of a more complex strategy in which signalling used by the cell to switch autophagy off is exploited by the virus. Alternatively, ASFV may rely on a combination of these mechanisms to ensure that the threat imposed by autophagy is disrupted.

The A179L gene was considered a likely modulator of autophagy due to its reported interaction with the key autophagy protein Beclin 1 (Hernaez et al., 2013) but also because its early expression during viral replication coincides with the observed inhibition of autophagy during early virus infection. Vero cells were mock infected or infected for 4 hours with the Vero adapted strain Ba71V in which A179L had been knocked out by homologous recombination. No difference in the number of autophagosomes between mock infected and A179L KO infected cells was apparent suggesting that the A179L KO virus did not induce autophagy (Figure 4.1.1). To test whether the A179L KO virus could inhibit autophagy, cells were incubated in starvation media to induce the appearance of autophagosomes. The results in Figure 4.1.2 revealed that while an extensive number of autophagosomes could be observed in mock infected cells, a near complete absence of autophagosomes was observed in cells expressing viral protein p30 showing that the A179L KO virus is able to inhibit starvation-induced autophagy.

Quantification of the number of autophagosomes per individual cell demonstrated a statistically significant difference between mock infected and ASFV infected cells when separately comparing cells under non-starved and starved conditions (Figure 4.1.3). In terms of blocking the formation of autophagosomes, the outcome of using the A179L KO virus therefore mirrors what was previously observed using the non-mutated Ba71V virus (see section 3.2.1). Consequently, it can be concluded that knocking out A179L from ASFV does not abolish its ability to inhibit autophagy. This could mean that the previously described inhibition of starvation-induced autophagosomes by A179L is an artefact of its overexpression. Indeed, A179L has been shown to have a much greater affinity for other Bcl2 proteins when compared to Beclin 1 (Banjara et al., 2017). Alternatively, these results could point to a redundancy in the ASFV genome whereby additional genes are encoded that are able to replicate the effects of A179L or perhaps the influence of A179L represents just a single layer of a multi-layered strategy to perturb the autophagy response in ASFV infected cells.

The nutrient sensor mTORC1 is a master regulator of autophagy that when activated, inhibits the induction of autophagy primarily via phosphorylation of the ULK1 complex. Active mTORC1 also leads to the downstream phosphorylation of two key proteins involved in translation, p70-S6K and

4E-BP1. The phosphorylation of mTORC1 substrate proteins can be readily detected by Western blot analysis providing an effective means of determining the activation status of mTORC1. To try to identify additional means by which ASFV could inhibit the induction of autophagy, the activation status of mTORC1 was determined in infected cells.

This experiment was carried out by harvesting cells at multiple time points over a 16 hour time course of infection by which time at least one round of virus replication would be complete. At each time point the phosphorylation level of ULK1, p70-S6K and 4E-BP1 was analysed and the results in Figure 4.2 showed that phosphorylation of all of these proteins could be detected over the entire time course of infection indicating the active state of mTORC1. Accordingly, the active state of mTORC1 and the downstream phosphorylation of ULK1 during ASFV infection could be a mechanism by which starvation-induced formation of autophagosomes is inhibited by the virus. Comparing the level of phosphorylation between mock infected and ASFV infected cells revealed a reasonably consistent pattern of greater phosphorylation in ASFV infected cells from 4 hpi. This suggests that ASFV is able to induce a degree of mTORC1 activity that is greater than the level of constitutive activity perhaps indicating that mTORC1 is purposefully targeted by the virus for activation. The fact that this effect was seen from 4 hpi could mean that viral proteins expressed during early replication are responsible. Physiological changes in the cell during viral infection such as energy and nutrient depletion would usually result in a cell stress response that leads to the inactivation of mTORC1 and the activation of autophagy, however in ASFV infected cells mTORC1 activity is maintained most likely to also benefit from host cell translation.

To provide confirmation that the observed activity of mTORC1 is the result of infection rather than constitutive activity, a 16 hour time course of ASFV infection was carried out in Vero cells during which cells were starved to inactivate mTORC1 (see Figure 4.3). Cells were harvested at multiple time points for analysis by Western blot and phosphorylated p70-S6K (P-p70-S6K) was used as a readout for mTORC1 activity. Mock infected cells that were subjected to 1 hour of starvation demonstrated a near complete loss of P-p70-S6K. In contrast, under the same starvation conditions P-p70-S6K was evident in ASFV infected cells and was particularly elevated at 4 and 8 hpi while a subsequent reduction at 16 hpi was apparent. It was therefore concluded that ASFV is able to block starvation-induced inactivation of mTORC1. The fact that levels of P-p70-S6K in ASFV infected cells at 4 hpi, when viral translation has commenced, were at least equivalent to or slightly greater than constitutive levels observed in non-starved mock infected cells may indicate that this mechanism is dependent on virally encoded factors. The decreased activation of mTORC1 at 16 hpi could suggest that the aforementioned viral mechanism is no longer required at such late stages of infection. Previously in Figure 4.2, it was demonstrated that P-p70-S6K was still evident at 16 hpi under nutrient replete conditions albeit slightly decreased from 4 and 8 hpi indicating that the virus does not inactivate mTORC1 at 16 hpi. Collectively, the results from Figures 4.2 and 4.3

provide compelling evidence that mTORC1 is specifically activated during ASFV infection and that viral mechanisms are in place to maintain this activity in the face of cell stress responses.

When considering the mechanisms that ASFV might use to activate mTORC1, numerous studies on virus-cell interactions have reported the activation of Akt in infected cells (Benetti and Roizman, 2006, Dawson et al., 2003, Esfandiarei et al., 2004, Lee et al., 2005, Thomas et al., 2002). The activation of Akt can lead to the downstream activation of mTORC1 by directly phosphorylating and inactivating TSC2, a negative regulator of mTORC1. Human cytomegalovirus (HCMV) which in similarity to ASFV is also a large double-stranded DNA virus was shown to maintain mTORC1 activity under amino acid deprivation and that Akt was also activated by HCMV encoded proteins in a PI3K-dependent manner (Clippinger et al., 2011, Yu and Alwine, 2002). Complete activation of Akt is characterised by phosphorylation on residues S473 and T308 (Alessi et al., 1996). To investigate whether Akt is active in ASFV infected cells, a 16 hour time course of infection was carried out in Vero cells during which cells were harvested at multiple time points for Western blot analysis. The results presented in Figure 4.4 showed that Akt was phosphorylated on both S473 at T308 residues throughout the time course of ASFV infection demonstrating its active status. Between 2 and 8 hpi a greater level of phosphorylation on S473 was observed in ASFV infected cells when compared to mock infected cells. Phosphorylation on S473 is carried out by mTORC2 (Sarbassov et al., 2005) which could suggest that mTORC2 activity is specifically stimulated by ASFV. Nevertheless, this result provides clear evidence that Akt is activated during ASFV infection which could be a mechanism used by the virus to activate mTORC1.

Regulation of mTORC1 can also be achieved through Akt-independent mechanisms. For example, low intracellular energy stores can lead to the activation of AMPK which is able to phosphorylate and activate the TSC complex leading to the downstream inactivation of mTORC1 (Kimball, 2006). This response is aimed at stimulating autophagy to raise energy availability to maintain vital cell functions. The targeting of AMPK by viruses has been reported. For example HCMV is able to circumvent AMPK-mediated inhibition of mTORC1 (Kudchodkar et al., 2007). Another possibility is that mTORC1 could be acted upon directly via virally encoded virulence factors. During HSV-1 infection, mTORC1 signalling was maintained in the presence of Akt inhibitors (Chuluunbaatar et al., 2010). An Akt mimic encoded by the virus called Us3 was later shown to be responsible for this effect (Chuluunbaatar and Mohr, 2011). One could therefore speculate that ASFV might encode a protein with similar function.

The method of cell entry for ASFV has been the subject of keen debate. Examples of virus entry via clathrin-mediated endocytosis and macropinocytosis have been separately reported in the past (Cuesta-Geijo et al., 2012, Sanchez et al., 2012). More recently, a study described the internalisation of virus particles via clathrin-mediated endocytosis and macropinocytosis into macrophages, the natural host cell of ASFV (Hernaez et al., 2016). Using purified virus inoculum,

entry via macropinocytosis was found to be non-specific and more likely the result of the cells constitutively sampling their environment. The authors speculated that the presence of cell and viral debris in non-purified virus inoculum could potentially affect the route of virus entry by specifically stimulating macropinocytosis. With this in mind, and following a report describing how the activation of Akt during VACV infection was dependent on the viral entry mechanism (Izmailyan et al., 2012), it was decided to re-examine the effects of ASFV infection on autophagy using a purified virus.

Purification was carried out using density-gradient separation in a Percoll suspension. Clarified virus stocks that had either been concentrated only or concentrated and then purified were visually assessed by negative stain electron microscopy. Images of this analysis presented in Figure 4.5 showed the presence of particles that were consistent in shape and size with ASFV virions in both non-purified and purified virus samples. Analysis also demonstrated the presence of substantial amounts of cell and viral debris in the non-purified virus sample but that this debris was entirely absent in the purified virus sample. Using the Percoll method of purification has the potential to lead to samples containing residual amounts of Percoll and it was previously reported that macrophages were able to ingest Percoll (Wakefield et al., 1982). However, using a Percoll purified virus to infect Vero cells, Hernaez *et al* (2016) found no evidence of significant induction of membrane protrusions at the cell surface demonstrating that the potential presence of Percoll was not a factor in stimulating macropinocytosis.

The purified virus described above was used to infect Vero cells and analysis by Western blot showed that at 4 hpi, the starvation-induced accumulation of LC3-II was inhibited in ASFV infected cells (see Figure 4.6). Under nutrient replete conditions, a lower amount of LC3-II was seen when compared to mock infected cells demonstrating that the purified virus did not induce an autophagy response. These results were consistent with what was previously reported using a non-purified virus (see section 3.2.2). In Figure 4.7, Western blot analysis of Vero cells that had been infected with the purified virus for 4 hours showed greater levels of phosphorylated p70-S6K and phosphorylated Akt on residue S473 when compared to mock infected cells. A comparable level of phosphorylation of Akt on residue T308 was observed between mock infected and ASFV infected cells. Once again, these results were consistent with the results reported from experiments using a non-purified virus (see sections 4.2.2 and 4.2.4) and demonstrate that mTORC1 and Akt are active in cells infected with purified ASFV. It was therefore concluded that the presence of viral and cell debris in the non-purified virus was not responsible for the observed block of autophagy induction and that similarly these debris were also not responsible for the observed activation of Akt and mTORC1 in ASFV infected cells.

To provide a means to study the capacity of ASFV to inhibit autophagy induction in the absence of Akt-mTORC1 activity, an investigation was carried out to characterise the effects of pharmacological inhibitors on Akt-mTORC1 signalling. Vero cells were either mock infected or

infected with ASFV and then incubated in the presence of a combination of the Akt inhibitor MK-2206 and the mTOR inhibitor Torin1 or in the presence of these drugs in isolation. Torin1 is able to block the activity of both mTORC1 and mTORC2. Analysis was carried out by Western blot whereby the phosphorylation of Akt on residues S473 and T308 was used to evaluate Akt activity and the phosphorylation of p70-S6K was used as a readout for mTORC1 activity. Overall, the results in Figure 4.8 showed that Torin1 is an effective inhibitor of mTORC1 activity in both mock infected and ASFV infected cells evidenced by a lack of phosphorylated p70-S6K. Additionally, using MK-2206 in isolation is an effective means of inhibiting Akt activity in mock infected cells but this is not the case in ASFV infected cells when in contrast, using MK-2206 and Torin1 in combination was far more effective. The fact that less P-Akt S473 was observed in ASFV infected cells treated with Torin1 compared to cells treated with MK-2206 may indicate that ASFV is able to drive phosphorylation on S473 via mTORC2 in a manner that overcomes the inhibitory effects of MK-2206 at the concentration used. In addition, the clear presence of P-p70-S6K following treatment of mock infected and ASFV infected cells with MK-2206 shows that reducing the activity of Akt alone is not sufficient to inactivate mTORC1 which could be due to mTORC1 receiving signals from AMPK independently of Akt.

The fact that Akt and mTORC1 can be effectively switched off in ASFV infected cells using a combination of pharmacological inhibitors provided an opportunity to test whether the activation of Akt and mTORC1 constitutes a mechanism by which ASFV inhibits the induction of autophagy. To carry out this investigation, Vero cells were either mock infected or infected with Ba71V or the A179L KO virus and analysed by confocal microscopy for the appearance of autophagosomes. Cells were infected for a total of 4 hours and were starved in either the presence or absence of a combination of Torin1 and MK-2206. Cells that had been infected with either wild-type ASFV or the A179L KO virus in the absence of the drugs showed a block in the induction of autophagosomes (see Figure 4.9.1). This was in contrast to mock infected cells that showed a substantial number of autophagosomes that were formed in response to starvation. These results confirmed previous observations that ASFV, including the A179L KO mutant virus, is able to inhibit autophagy induction at 4 hpi. Interestingly, ASFV infected cells that were starved in the presence of Torin1 and MK-2206 seemed to show a slightly elevated level of autophagosome formation when compared to infected cells in the absence of the drugs (see Figure 4.9.2). However, the number of autophagosomes in these cells appeared to be less than in mock infected cells under the same conditions. This suggested that in the presence of Akt and mTOR inhibitors, ASFV was unable to restrict the formation of autophagosomes to the same degree as when Akt and mTOR are completely active.

In order to gain further clarity on the effects of MK-2206 and Torin1 during ASFV infection, an additional experiment was carried out at 2 hpi rather than at 4 hpi. A 2 hour period of infection was chosen in an attempt to limit the effects of potential virally encoded factors that are expressed

during early replication while providing sufficient time of exposure to the Akt-mTOR inhibitors. Under starvation conditions and in the absence of the drugs, cells that had been infected with the wild-type virus or the A179L KO virus (see Figure 4.10.1) showed a similar level of autophagosome inhibition that was seen in ASFV infected cells at 4 hpi. Under starvation conditions and in the presence of the drugs, autophagosomes were clearly present in cells that had been infected with wild-type ASFV or the A179L KO virus (see Figure 4.10.2). Visually comparing the number of autophagosomes between infected cells in the presence or absence of the drugs revealed a much higher number of autophagosomes in the drug treated cells. This is therefore a clear indication that the activity of Akt and mTOR are able to negatively modulate the induction of autophagy in ASFV infected cells. Additionally, a comparison between ASFV infected cells at 2 hpi and at 4 hpi in the presence of the drugs showed substantially more autophagosomes at 2 hpi. This could suggest that viral virulence factors that are expressed between 2 and 4 hpi are also implicated in the inhibition of autophagy. However, evidence that the same effect was observed using the A179L KO virus, strongly indicates that additional genes are involved.

In section 4.2.8, Western blot analysis of the effects of MK-2206 and Torin1 revealed that a combination of both drugs was required to provide the maximum inhibition of Akt and mTORC1 activity. This result was also confirmed using confocal microscopy in which autophagosomes were most apparent in ASFV infected cells at 2 hpi using a combination of the drugs rather than using the drugs in isolation (data not shown). This suggests that the activity of mTORC1 is not solely responsible for the inhibition of autophagy induction and that Akt activity is also required for this effect. These results potentially highlight a mechanism by which Akt-mediated inhibition of autophagy is not only directed via the activation of mTORC1 but also via alternative pathways. Indeed, the direct phosphorylation of Beclin 1 by Akt resulting in autophagy inhibition has been reported and may offer an explanation (Wang et al., 2012).

The investigations that were carried out here were aimed at identifying ways in which ASFV exerts a block on the induction of autophagy. This strategy was implemented to provide the potential for downstream intervention in the interaction between ASFV and autophagy with the hope that having the ability to induce an autophagy response to infection could stimulate a potent immune response. In summary, the results of this work showed that the combined activity of Akt and mTORC1 in ASFV infected cells is sufficient to inhibit autophagy during the early stages of virus replication. This means that any attempts to induce autophagy in ASFV infected cells would need to include measures to inactivate Akt-mTORC1 signalling or bypass its effects. By 4 hpi additional mechanisms of control are implemented by the virus, presumably through the use of virally encoded modulators. Using a recombinant virus showed that A179L is not the only protein that potentially regulates autophagy and that additional viral proteins must be involved. In order to identify these modulators of autophagy, the study that followed this work consisted of screening multiple ASFV genes for the inhibition of starvation-induced autophagy.

5 Screening an ASFV gene library for potential autophagy modulators

5.1 Introduction

The observation that formation of autophagosomes could be induced in ASFV infected cells in the presence of pharmacological inhibitors of Akt and mTOR at 2 hpi, but not at 4 hpi, pointed to an Akt/mTOR independent mechanism of autophagy inhibition. The timing of this inhibition coincides with early viral protein expression and therefore strongly suggests the involvement of ASFV encoded protein modulators.

ASFV encodes a protein called A179L that can block drug-induced cell death (Revilla et al., 1997). A179L is a viral Bcl-2 homolog that was shown to be functionally similar to cellular Bcl-2 through its capacity to interact with BH3-only pro-apoptotic proteins as well the key autophagy protein Beclin1 (Banjara et al., 2017, Galindo et al., 2008, Hernaez et al., 2013). In addition, exogenous expression of A179L was shown to inhibit the formation of autophagosomes under starvation conditions (Hernaez et al., 2013). However, the results in the previous chapter showed that starvation-induced autophagosome formation was still inhibited after infection with an A179L deletion mutant indicating that additional viral modulators of autophagy are involved. Further evidence to support this theory is the fact that redundancies in gene function are known to occur in the ASFV genome as for example multiple apoptosis modulators (Dixon et al., 2017) and interferon response modulators (Reis et al., 2017b) have been described.

To identify additional viral inhibitors of autophagy, a screen was carried out in which individual ASFV genes were expressed in Vero cells and tested for their ability to block the formation of autophagosomes under starvation conditions. Common methods of monitoring autophagy are indirect immunofluorescent labelling of LC3 or the use of GFP-LC3 in direct fluorescence microscopy. Using these techniques, the induction of autophagy can be visualised by an increase in the number of LC3 puncta (Klionsky et al., 2016). The use of Vero cells in the screen was advantageous as starvation leads to very clear redistribution of endogenous LC3 into punctate structures representative of autophagosomes. This negated the requirement to use an exogenous source of LC3 such as GFP-LC3 which can potentially lead to artefacts as a consequence of over-expression (Kuma et al., 2007).

The basis for the selection of ASFV genes that were screened was predominantly centred on two criteria. Firstly, Akt/mTOR independent inhibition of autophagy was seen from 4 hpi and therefore genes were chosen that are expressed during the early stages of the viral replication cycle. Secondly, the inhibition of autophagy by ASFV has been observed across multiple virus strains indicating that this ability is highly conserved, perhaps unsurprisingly given the importance of autophagy in the immune response. Genes that are highly conserved between ASFV isolates were therefore also included in the screen. Previously it was shown that both the Vero adapted strain Ba71V (Figure 3.1.2) and the field strain OURT88/1 (Figure 3.3.1) were able to inhibit starvation-

induced autophagy. The genomes of these ASFV isolates primarily differ in the number of genes encoded in the multigene families (MGFs), with Ba71V lacking multiple copies of some MGF genes (Chapman et al., 2008). Considerable variation in the number of MGF genes has also been reported among other isolates (de la Vega et al., 1990, Portugal et al., 2015) and for this reason, MGF genes were mostly excluded from the screen.

The ASFV gene library was comprised of 76 genes that were cloned into plasmid constructs or into adenovirus vectors with an HA tag at either the N or C terminus to facilitate detection of protein expression. The majority of the gene sequences were taken from the OURT88/3 strain with the remainder from the Georgia and Benin 1997/1 strains. Plasmid constructs were delivered into Vero cells using transient transfection and adenovirus vectors were used to transduce the cells, following which cells were starved and visually inspected for the inhibition of autophagosome formation. To validate this assay, A179L was used as a control gene to demonstrate the detection of autophagosome inhibition. Any proteins that altered the typical starvation-induced redistribution of LC3 into round punctate structures were subjected to further investigation by confocal microscopy.

The results from the ASFV gene library screen were aimed at identifying additional ASFV encoded autophagy modulators that could be targeted in downstream mutation experiments. For example, the previous mutation of Ba71V in which the A179L gene was deleted from the genome was well tolerated by the virus and demonstrates the potential to engineer a mutant virus that lacks the ability to inhibit the autophagy response. A virus with this characteristic could prove to be a powerful tool in the development of a vaccine against ASFV.

5.2 Results

5.2.1 Plasmid screen optimisation to limit the appearance of transfection-induced autophagosomes

The majority of the ASFV gene library consisted of plasmid constructs that were delivered into Vero cells by transient transfection. This was carried out using the lipopolyplex transfection reagent TransIT-LT1 (see methods section 2.6 for detailed transfection method). Recently, the induction of autophagy in response to gene delivery by lipoplex and polyplex reagents was reported (Roberts et al., 2013). The authors found that a lipoplex transfection reagent similar to TransIT-LT1 activated autophagy and generated autophagosomes following entry to cells by endocytosis. Endosomes then became fused with autophagosomes to form large tubulovesicular autophagosomes (TVAs) that were positively labelled for LC3 and located close to the nucleus.

Screening of the ASFV gene library was conducted using a confocal microscopy assay based on visually assessing potential inhibition of starvation-induced autophagy by expression of individual ASFV genes. In this regard, background levels of autophagy induced by transfection including the

formation of TVAs could potentially interfere with the results by masking changes in starvation-induced levels of autophagy. To address this, an assay was carried out to determine whether passaging the cells after transfection would reduce the appearance of autophagosomes resulting from the transfection process. Vero cells were mock transfected with TransIT-LT1 using the manufacturer's recommended protocol with the exception that no DNA was included. Cells were either incubated for a total of 48 hours or were passaged after 24 hours before incubating the cells for a further 24 hours. For 3 hours prior to fixing, cells were incubated in complete cell media to minimise potential induction of autophagy through reduced nutrient availability. Cells were then labelled for immunofluorescence using an antibody against LC3 and the nuclear marker DAPI.

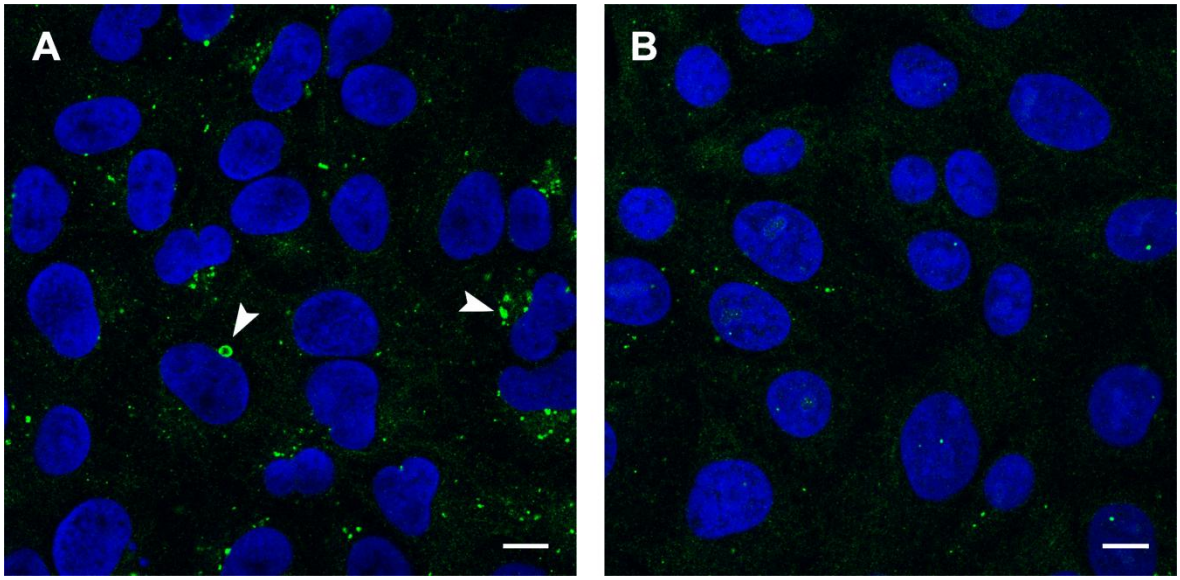

Figure 5.1 Passaging cells after transfection reduces the appearance of transfection-induced autophagosomes and TVAs

Vero cells were mock transfected with TransIT-LT1 in the absence of DNA using the manufacturer's protocol and incubated for a total of 48 hours (Panel A) or passaged 24 hours after transfection before incubating for a further 24 hours (Panel B). Cells were incubated in complete Vero cell media for the final 3 hours prior to being fixed and permeabilised in methanol. Cells were then labelled for LC3 shown in green and nuclei shown in blue. White arrows in Panel A indicate TVAs. Scale bars represent 10 µM.

Cells that were mock transfected with TransIT-LT1 and incubated for 48 hours without cell passaging demonstrated a substantial number of LC3 puncta in the cytoplasm indicating the induction of autophagy (Figure 5.1A). Additionally, some very large puncta were apparent in close proximity to the cell nuclei and were consistent in appearance with TVAs that were described by Roberts *et al* (2013). In contrast, much fewer puncta were observed in cells that had been mock transfected with TransIT-LT1 and passaged after 24 hours (Figure 5.1B) indicating a reduced level of autophagy in these cells compared to cells in Figure 5.1A. Additionally, no TVAs were apparent

in cells in Figure 5.1B evidenced by a lack of the large LC3-puncta that were seen in cells in Figure 5.1A. Collectively, these results show that passaging cells following transfection is a suitable method to reduce the appearance of autophagosomes that result from the transfection process.

5.2.2 Characterising the effects of transduction on autophagy using an adenovirus vector

The use of viral vectors such as adenovirus offers a highly efficient means of gene delivery and a proportion of the ASFV gene library that was screened included human adenovirus type 5 (AdH5) vectors. The AdH5 vector has been highly modified and adapted for the purpose of gene delivery and is replication deficient outside of specific cell lines used for its propagation. Nevertheless, reports of the modulation of mTOR activity and the induction of autophagy by adenoviruses have been published (O'Shea et al., 2005, Rodriguez-Rocha et al., 2011). Screening of the ASFV gene library was based on evaluating the effects of gene expression on levels of starvation-induced autophagy and consequently, the induction or inhibition of autophagy by the viral vector itself would be problematic as it could mask changes induced by the ASFV gene being investigated. The effects of transduction on autophagy using the AdH5 vector was therefore assessed by confocal microscopy using a control vector expressing GFP only.

Vero cells were transduced with AdH5 encoding GFP (see methods section 2.6 for details of the transduction method) then incubated for a total of 24 hours to allow time for gene expression. During the final 3 hours, cells were either incubated in complete cell media or starved in EBSS to induce autophagy. In this way it could be investigated whether the AdH5 vector was able to induce or inhibit autophagy. Separately, a set of control cells that had not been transduced were either incubated in complete cell media or starved in EBSS. Cells were then fixed in PFA and permeabilised in methanol. Finally, cells were labelled for immunofluorescence using an antibody against LC3 and the nuclear marker DAPI.

A very low amount of LC3 puncta representative of autophagosomes were observed in cells that had been transduced and incubated in complete cell media (Figure 5.2A). A pattern of diffuse green fluorescence was observed in some cells indicating the expression of GFP (Figure 5.2B). Cells expressing GFP did not exhibit a greater amount of LC3 puncta compared to cells that were not expressing GFP demonstrating that the AdH5 vector alone does not induce the appearance of autophagosomes. Cells that had been transduced and starved in EBSS media contained a large amount of LC3 puncta (Figure 5.2C), typical of what is usually observed in cells under starvation conditions. Analysis of cells expressing GFP showed that comparable amounts of LC3 puncta were observed between these cells and cells that were not expressing GFP (Figure 5.2D) demonstrating that the AdH5 vector alone does not inhibit the appearance of autophagosomes. Control cells that had not been transduced showed a low number of LC3 puncta under nutrient replete conditions and a much greater amount of LC3 puncta under starvation conditions as would be expected (data not shown).

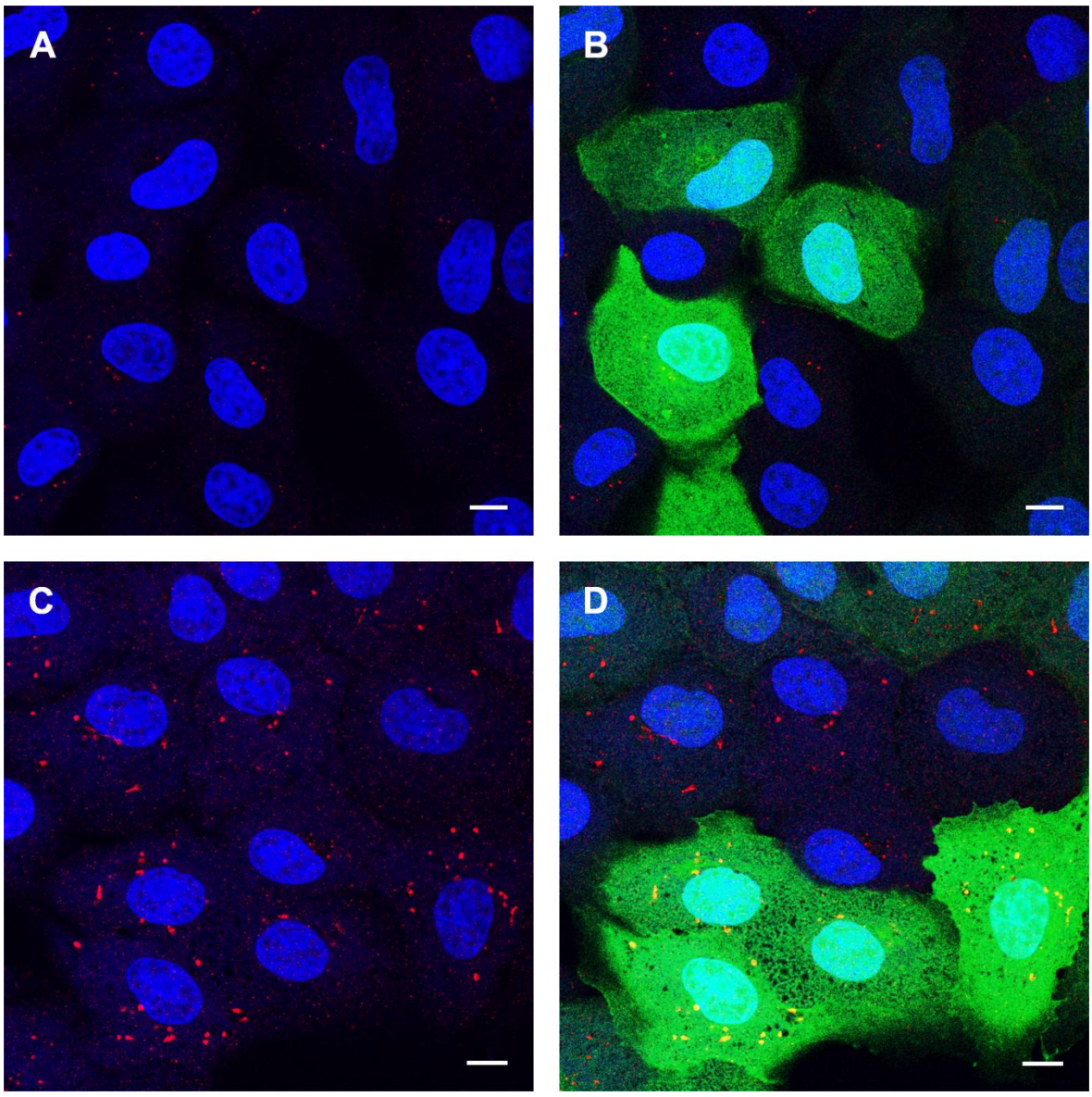

Figure 5.2 An AdH5 vector expressing GFP does not induce or inhibit autophagy

Vero cells were transduced using an AdH5 vector expressing GFP only and were incubated for a total of 24 hours to allow time for gene expression. During the final 3 hours, cells were either incubated in complete cell media (Panels A and B) or starved in EBSS media (Panels C and D) prior to being fixed in PFA and permeabilised in methanol. Cells were then labelled for LC3 shown in red and nuclei shown in blue. GFP expression was visualised in the green channel. Panels A and C show the same cells as Panels B and D respectively but with the green channel removed to allow for clearer observation of LC3 staining. Scale bars represent 10 μM.

5.2.3 Generation of A179L constructs and mutagenesis of the A179L ligand binding groove

To provide confirmation that the confocal microscopy based screening method of the ASFV gene library was suitable for the detection of autophagosome inhibition, A179L was used as a control gene. A179L is well conserved among ASFV isolates and was previously reported to inhibit the induction of starvation-induced autophagosomes in HeLa cells, presumably via an interaction with Beclin1 (Hernaez et al., 2013). The A179L sequence taken from the OURT88/3 strain was cloned into pcDNA3.1 with an N-terminus HA-tag (cloning methods are described in section 2.3). The C-terminus of A179L was not considered to be appropriate for insertion of a tag due to the presence of a hydrophobic domain that is predicted to be a membrane anchorage region and could be critical to protein function.

Recent investigation of the ability of A179L to inhibit apoptosis revealed that A179L is able to bind to all major pro-apoptotic mammalian Bcl-2 proteins (Banjara et al., 2017). Analysis of crystal structures of the A179L ligand binding groove suggested a high degree of binding flexibility providing an explanation for its promiscuity. To act as a negative control for the screen, a mutant version of A179L with a reduced ability to suppress the formation of autophagosomes was engineered by mutating two residues that are key to forming the ligand binding groove. Residues valine-73 and glycine-89 were mutated to tyrosine residues as it was predicted that the relatively greater size of the tyrosine residues would reduce the ligand binding capacity of the protein (mutagenesis methods are described in section 2.3.5).

The position of the binding groove mutations were mapped onto a structural image of A179L (Figure 5.3A). One of the Bcl-2 proteins that A179L is able to bind to called Bid is shown in the ligand binding groove alongside the residues that were targeted for mutation where residue I is glycine-89 and residue II is valine-73. Sequencing of the wild-type and mutant constructs was carried out to confirm that cloning and mutagenesis had been carried out correctly. Inspection of the sequence traces confirmed that the valine residue encoded at position 73 (Figure 5.3B) and glycine residue at position 89 (Figure 5.3D) of the wild-type protein had been correctly mutated to tyrosine residues in the mutant protein (Figure 5.3C and E).

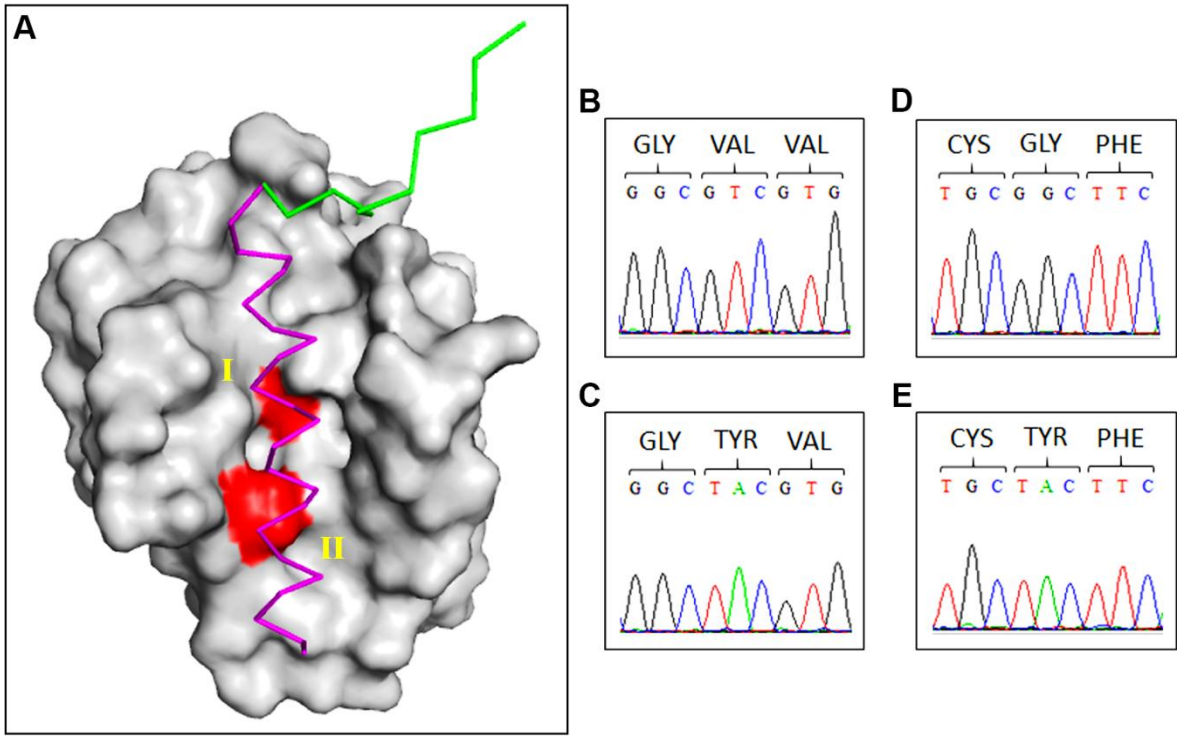

Figure 5.3 Mutagenesis of the A179L ligand binding groove

A) Structural image of A179L (grey) with Bid (magenta and green) positioned in the ligand binding groove. Residues targeted for mutation are indicated in red where residue I is glycine-89 and residue II is valine-73. B to E) Sequence traces confirming the mutations of residue 73 from valine (B) to tyrosine (C) and residue 89 from glycine (D) to tyrosine (E).

5.2.4 Wild-type A179L suppresses the formation of starvation-induced autophagosomes in Vero cells but mutant A179L does not

To test the effects of A179L expression on starvation-induced autophagy, Vero cells were transfected with plasmids encoding either wild-type (WT) A179L or mutant (YY) A179L. Following transfection, cells were incubated for 24 hours before passaging the cells and incubating them for a further 24 hours. During the final 3 hours, cells were incubated in complete cell media or were starved in EBSS media to induce autophagy. Separately, control cells that had not been transfected were starved in EBSS or incubated under nutrient replete conditions. Cells were fixed and labelled for immunofluorescence using anti-LC3 and anti-HA tag antibodies and the nuclear marker DAPI.

Cells expressing HA-tagged WT A179L (Figure 5.4.1B) showed significantly fewer puncta when compared to cells in the same field with no detectable A179L (Figure 5.4.1A). Cells that had been transfected with the YY A179L plasmids and incubated under starvation conditions showed a high number of LC3 puncta in all of the cells (Figure 5.4.1C) and examination of HA-tagged protein expression revealed no difference in the number of LC3 puncta between cells expressing YY A179L and cells that were not (Figure 5.4.1D). Collectively these results show that WT A179L is

able to suppress starvation-induced autophagosome formation while YY A179L is not. Additionally, cells that had been transfected with either the WT or YY A179L constructs and incubated under nutrient replete conditions demonstrated no increase in LC3 puncta in cells expressing A179L compared to cells that were not showing that expression of these proteins did not induce autophagy (data not shown). Finally, control cells that had not been transfected showed a low number of LC3 puncta under nutrient replete conditions and a much greater amount of LC3 puncta under starvation conditions as would be expected (data not shown).

Transient transfection led to relatively low numbers of cells expressing A179L, therefore in order to increase the number of expressing cells, WT A179L and YY A179L sequences were cloned into separate AdH5 vectors (see methods section 2.3.6 for generation of adenovirus vectors). The adenoviruses were used individually to transduce Vero cells which were then incubated for 24 hours during which cells were either incubated in nutrient replete conditions or were starved in EBSS for the final 3 hours. Separately, control cells that had not been transduced were incubated in either complete cell media or were starved in EBSS media for 3 hours to induce autophagy. Cells were fixed and labelled for immunofluorescence using anti-LC3 and anti-HA tag antibodies and the nuclear marker DAPI.

Control cells that had been incubated in complete cell media showed mostly cytoplasmic LC3 staining with the occasional LC3 puncta (Figure 5.4.2A). The low number of autophagosomes in these cells is typical of what would be expected under nutrient replete conditions and similar results were observed in cells that had been transduced with both WT A179L (Figure 5.4.2B) or YY A179L (Figure 5.4.2D). Labelling of HA-tagged protein showed a high number of cells expressing either WT A179L (Figure 5.4.2C) or YY A179L (Figure 5.4.2E) and inspection of the number of LC3 puncta in these cells revealed similar numbers when compared to the control cells. These results demonstrate that transduction of the cells with either WT or YY A179L did not induce the formation of autophagosomes.

A much higher number of LC3 puncta were observed in control cells that had been starved in EBSS (Figure 5.4.3A) when compared to the control cells that had been incubated in complete cell media (Figure 5.4.2A). This increase in LC3 puncta is indicative of the induction of autophagy. In cells that had been transduced with WT A179L, some cells showed high numbers of LC3 puncta whereas other cells seemed to demonstrate a reduction in the number of LC3 puncta (Figure 5.4.3B). Labelling of HA-tagged protein showed that cells demonstrating lower numbers of LC3 puncta were expressing WT A179L (Figure 5.4.3C). Inspection of cells that had been transduced with YY A179L revealed a high number of LC3 puncta in nearly all of the cells (Figure 5.4.3D) and labelling of HA-tagged protein indicated cells that were expressing YY A179L (Figure 5.4.3E). Assessing the number of LC3 puncta in these cells showed that there were similar numbers of LC3 puncta in cells that were expressing YY A179L and cells that were not. Collectively, these results

indicate that WT A179L is able to suppress the formation of starvation-induced autophagosomes but YY A179L is not.

The number of LC3 puncta per cell was enumerated using Imaris software in 30 cells per experimental condition (Figure 5.4.4). This analysis revealed a statistically significant increase in the number of LC3 puncta per cell under starvation conditions when compared to non-starved conditions in the control cells ($P < 0.001$) and cells expressing WT A179L ($P < 0.05$) or YY A179L ($P < 0.001$). This demonstrates that autophagy was induced in the control cells as well as cells expressing each of the A179L proteins. However, whereas a comparison between starved control cells and starved cells expressing YY A179L did not reveal any statistically significant difference ($P > 0.05$), there was a statistically significant reduction in the number of LC3 puncta in starved cells expressing WT A179L when compared to starved control cells ($P < 0.001$). Collectively, these results confirm that expression of WT A179L is able to suppress but not entirely inhibit the formation of starvation-induced autophagosomes in Vero cells but that expression of YY A179L has no effect.

In summary, analysis of the effects of A179L expression on starvation-induced autophagy by either transfection or transduction methods showed that the confocal microscopy assay can be used to screen the ASFV gene library for the detection of changes in the number of LC3 puncta.

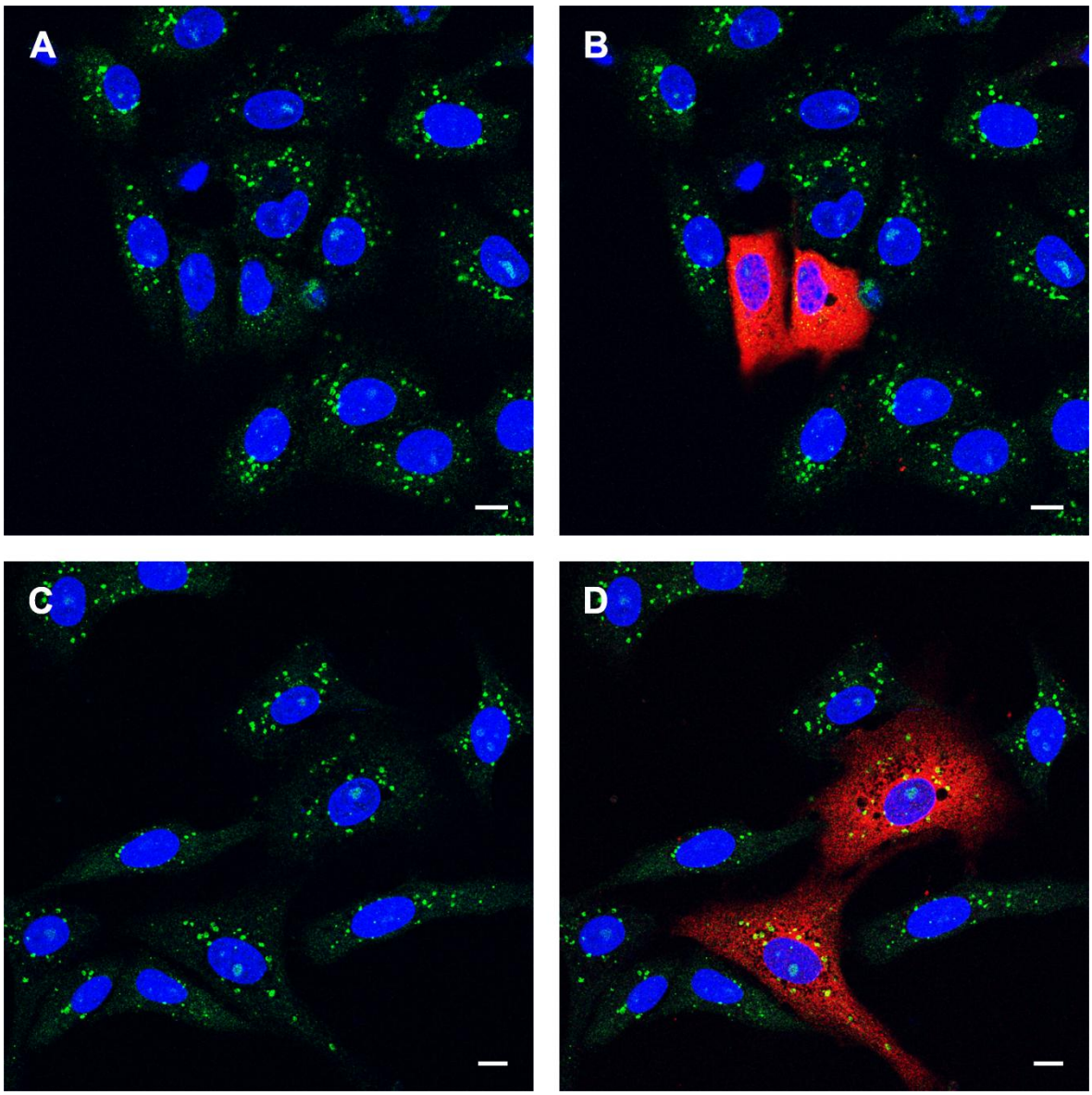

Figure 5.4.1 Expression of WT A179L suppresses starvation-induced autophagosome formation but expression of YY A179L does not

Vero cells were transfected with plasmids encoding either WT A179L (Panels A and B) or YY A179L (Panels C and D) and were incubated for 24 hours before passaging the cells and incubating them for a further 24 hours. During the final 3 hours, cells were starved in EBSS media prior to being fixed and permeabilised in methanol. Cells were then labelled for LC3 shown in green, HA-tagged protein shown in red and nuclei shown in blue. Panels A and C show the same cells as Panels B and D respectively but with the red channel removed to allow for clearer observation of LC3 staining. Scale bars represent 10 µM.

Figure 5.4.2 Transduction of Vero cells with either WT or YY A179L does not induce autophagy

Vero cells were transduced with adenoviruses encoding either WT A179L (Panels B and C) or YY A179L (Panels D and E) and were incubated for 24 hours during which cells were incubated in complete Vero cell media for the final 3 hours. Additionally, control cells that had not been transduced were incubated in complete Vero cell media for 3 hours (Panel A). Cells were fixed and permeabilised in methanol and then labelled for LC3 shown in green, HA-tagged protein shown in red and nuclei shown in blue. Panels B and D show the same cells as Panels C and E respectively but with the red channel removed to allow for clearer observation of LC3 staining. Scale bars represent 10 µM.

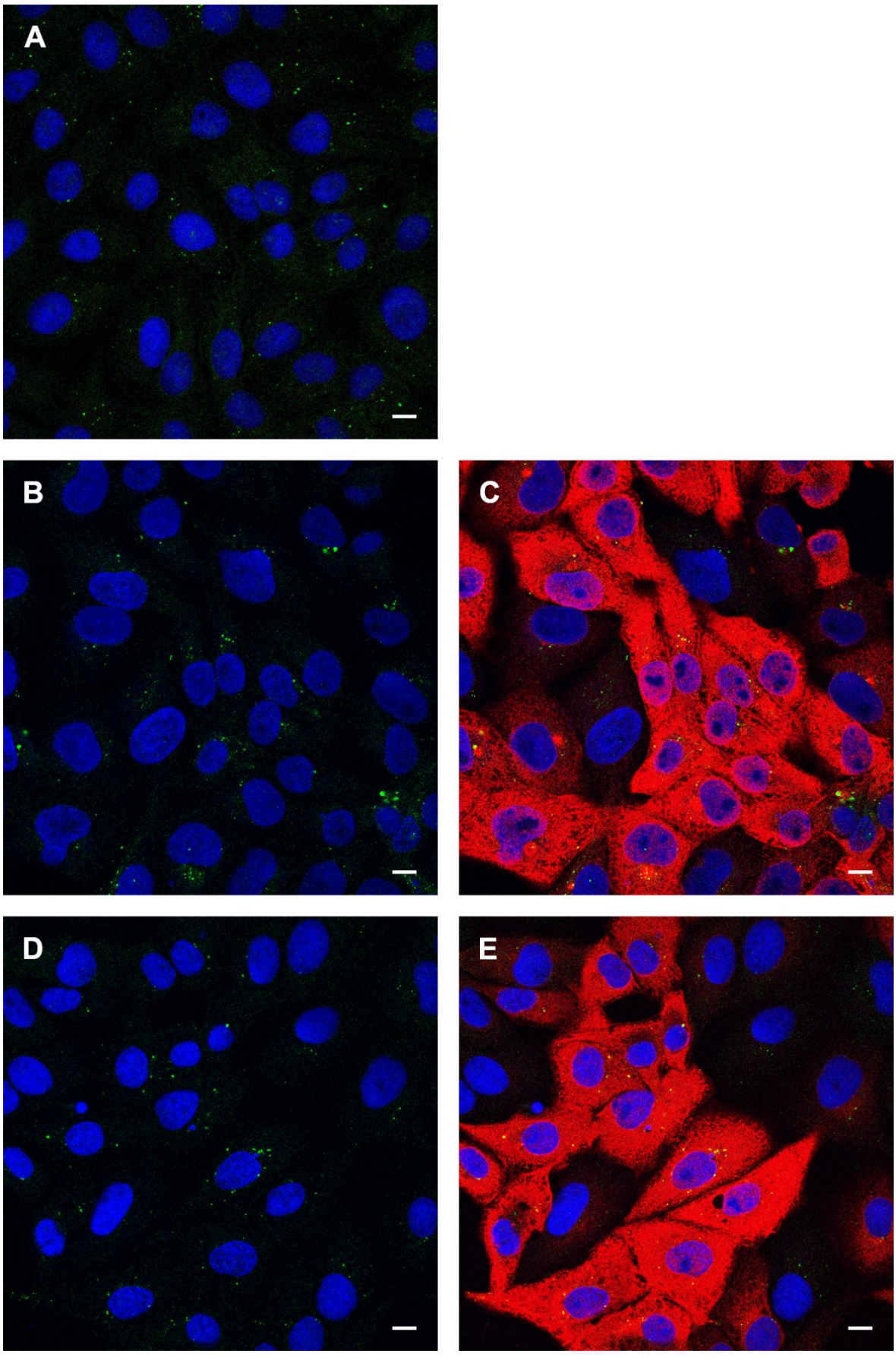

Figure 5.4.2 Transduction of Vero cells with either WT or YY A179L does not induce autophagy

Figure 5.4.3 WT A179L suppresses the formation of starvation-induced autophagosomes but YY A179L does not

Vero cells were transduced with adenoviruses encoding either WT A179L (Panels B and C) or YY A179L (Panels D and E) and were incubated for 24 hours during which cells were starved in EBSS media for the final 3 hours. Additionally, control cells that had not been transduced were incubated in EBSS media for 3 hours (Panel A). Cells were fixed and permeabilised in methanol and then labelled for LC3 shown in green, HA-tagged protein shown in red and nuclei shown in blue. Panels B and D show the same cells as Panels C and E respectively but with the red channel removed to allow for clearer observation of LC3 staining. Scale bars represent 10 μM.

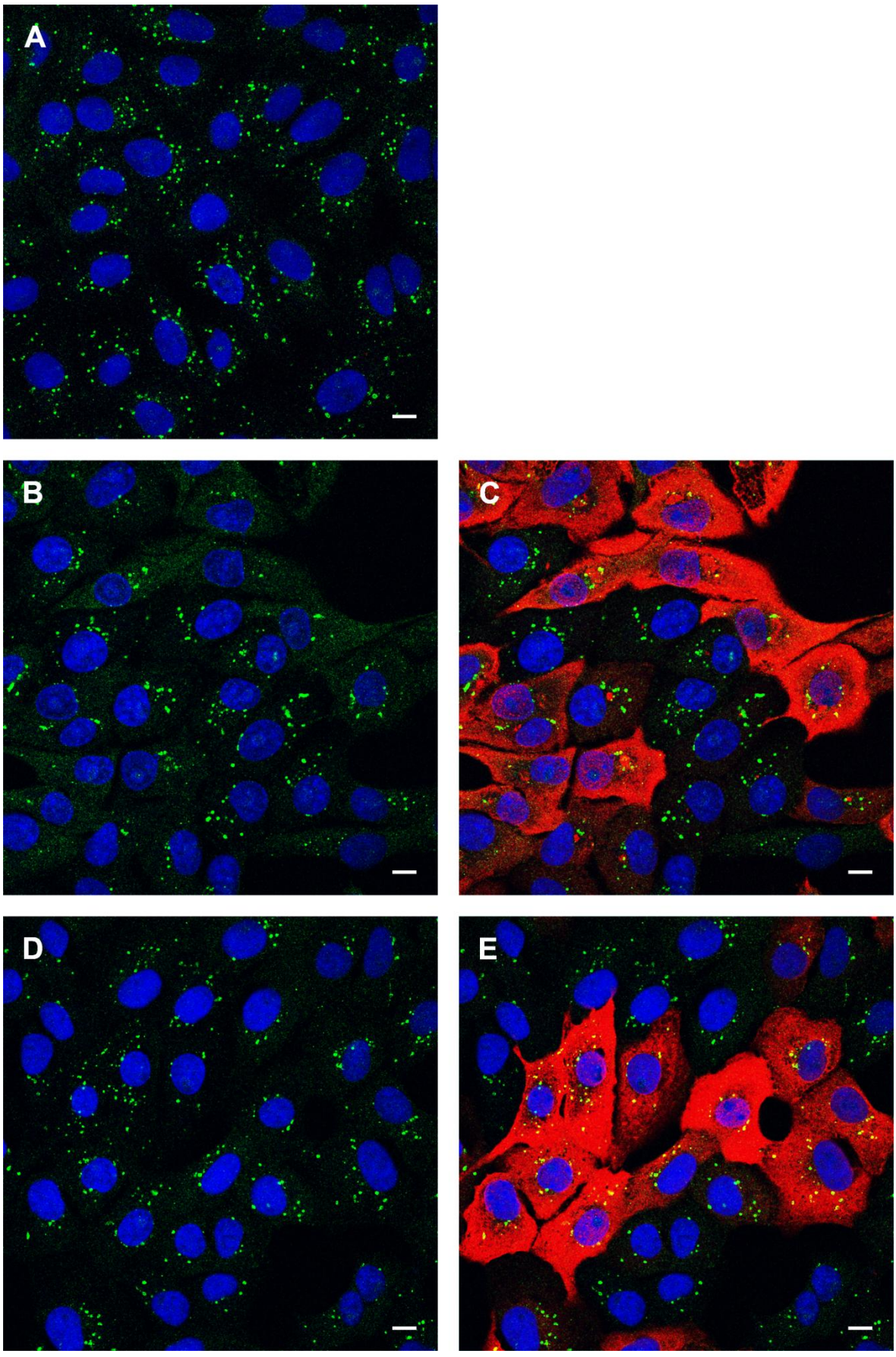

Figure 5.4.3 WT A179L suppresses the formation of starvation-induced autophagosomes but YY A179L does not

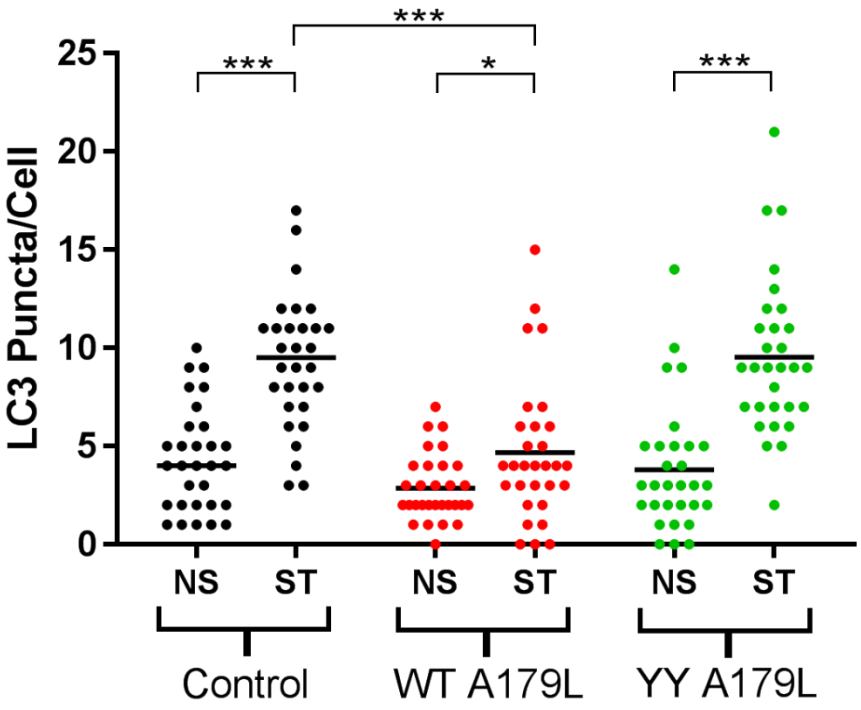

Figure 5.4.4 Imaris analysis confirms that WT A179L suppresses the formation of starvation-induced autophagosomes but YY A179L does not

The number of LC3 puncta per cell for 30 individual cells per indicated experimental condition was quantified by Imaris analysis of confocal images. Vero cells were transduced with AdH5 vectors encoding either WT A179L or YY A179L and were incubated for a total of 24 hours. Prior to fixation, cells were either non-starved in complete cell media (NS) or starved in EBSS (ST) for 3 hours to induce autophagy. Separately, control cells that had not been transduced were also either non-starved in complete cell media (NS) or starved in EBSS (ST) for 3 hours. Centre lines show the medians. Statistical analysis was carried out in Minitab using analysis of variance with Tukey multiple comparisons test. Asterisks represent significant differences in value between NS and ST conditions and between the indicated transduction status of the cells (* = P value of <0.05, *** = P value of <0.001).

5.2.5 Screening of the ASFV gene library

The ASFV gene library was comprised of a combination of plasmid and adenovirus vectors (see methods section 2.5 for details) and was therefore screened for the inhibition of starvation-induced autophagy using two different methods. Plasmid screening was carried out as described in section 5.2.1 and adenovirus screening as per section 5.2.2. Both methods included a period of starvation in EBSS media for the final 3 hours of incubation to induce autophagy. Cells were labelled for immunofluorescence using anti-LC3 and anti-HA tag antibodies and the nuclear marker DAPI, except in the case of CP196L, MGF110-4L and MGF110-5L that were labelled using protein-specific antibodies instead of an anti-HA tag antibody.

Table 5.1 Summary of ASFV gene library screening results

Gene	Virus strain	Function	Plasmid/ AdH5	HA Tag	Screening result
A104R	Georgia	Histone-like structural protein	pCMV	N	No detectable inhibition
A118R	OURT88/3	Unknown	pcDNA3.1	C	No detectable inhibition
A151R	OURT88/3	Disulphide bond formation	AdH5	C	No detectable inhibition
A179L	OURT88/3	Bcl2 apoptosis inhibitor	AdH5	N	No detectable inhibition
A224L	Georgia	Apoptosis inhibitor	pCMV	N	No detectable inhibition
B66L	OURT88/3	Unknown	pcDNA3.1	C	No detectable inhibition
B117L	Georgia	Unknown	pCMV	N	No detectable inhibition
B125R	Georgia	Unknown	pCMV	N	No detectable inhibition
B175L	Georgia	A1-like late transcription factor	pCMV	N	No detectable inhibition
B263R	OURT88/3	Unknown	pcDNA3.1	C	No detectable inhibition
B318L	Georgia	Prenyltransferase	pCMV	N	No detectable inhibition
B385R	Georgia	A2-like late transcription factor	pCMV	N	No detectable inhibition
B407L	OURT88/3	Unknown	pcDNA3.1	C	No detectable inhibition
B475L	OURT88/3	Unknown	pcDNA3.1	C	No detectable inhibition
B602L	OURT88/3	Chaperone protein	AdH5	C	No detectable inhibition
B646L	OURT88/3	p72 structural protein	AdH5/ pcDNA3.1	C	Inconsistent inhibition. See Fig 5.5.1
C62L	OURT88/3	Unknown	pcDNA3.1	C	No detectable inhibition
C84L	OURT88/3	Unknown	pcDNA3.1	C	No detectable inhibition
C122R	Georgia	Unknown	pCMV	N	No detectable inhibition
C129R	OURT88/3	Unknown	AdH5	C	No detectable inhibition
C147L	Georgia	RNA polymerase subunit	pCMV	N	Inconsistent inhibition See Fig 5.5.2
C257L	Georgia	Unknown	pCMV	N	No detectable inhibition
C315R	OURT88/3	RNA polymerase subunit	pcDNA3.1	C	No detectable inhibition
C475L	Georgia	Poly(A) polymerase	pCMV	N	No detectable inhibition
C717R	OURT88/3	Unknown	pcDNA3.1	C	No detectable inhibition
CP123L	OURT88/3	Unknown	pcDNA3.1	C	No detectable inhibition
CP196L	OURT88/3	p30 structural protein	AdH5	No tag	No detectable inhibition
CP312R	OURT88/3	Known antigen	AdH5	C	No detectable inhibition
CP530R	OURT88/3	Polyprotein precursor	AdH5	C	No detectable inhibition
D345L	OURT88/3	Unknown	pcDNA3.1	C	No detectable inhibition

Gene	Virus strain	Function	Plasmid/ AdH5	HA Tag	Screening result
DP71L	Georgia	EIF2α phosphorylation modulator	pCMV	N	No detectable inhibition
DP79L	Georgia	Unknown	pCMV	N	No detectable inhibition
DP96R	Georgia	Virulence determinant	pCMV	N	No detectable inhibition
DP148R	Benin 1997/1	Virulence determinant	pcDNA3.1	C	Tiny LC3 puncta. See Fig 5.5.5
DP238L	OURT88/3	Unknown	pcDNA3.1	C	No detectable inhibition
E146L	OURT88/3	Unknown	AdH5	C	No detectable inhibition
E165R	OURT88/3	dUTPase	AdH5	C	No detectable inhibition
E183L	OURT88/3	p54 structural protein	AdH5	C	Induces LC3 aggregates. See Fig 5.5.3
E184L	OURT88/3	Unknown	AdH5	C	No detectable inhibition
E199L	OURT88/3	Structural protein	AdH5	C	Induces LC3 aggregates. See Fig 5.5.4
E248R	Georgia	Essential for early post-entry stage	pCMV	N	No detectable inhibition
E301R	Georgia	Proliferating cell nuclear antigen	pCMV	N	No detectable inhibition
E423R	OURT88/3	Unknown	pcDNA3.1	C	No detectable inhibition
EP84R	Georgia	Unknown	pCMV	N	No detectable inhibition
EP152R	OURT88/3	Interacts with BAG-6	pcDNA3.1	C	No detectable inhibition
EP153R	Benin 1997/1	Apoptosis inhibitor. Haemadsorption enhancer	AdH5	C	No detectable inhibition
EP364R	OURT88/3	Unknown	AdH5	C	No detectable inhibition
F317L	OURT88/3	Unknown	AdH5	C	No detectable inhibition
H108R	Georgia	Unknown	pCMV	N	No detectable inhibition
H124R	Georgia	Unknown	pCMV	N	No detectable inhibition
H233R	Georgia	Unknown	pCMV	N	No detectable inhibition
H339R	Georgia	Unknown	pCMV	N	No detectable inhibition
I73R	OURT88/3	Unknown	pcDNA3.1	C	No detectable inhibition
I177L	Georgia	Unknown	pCMV	N	No detectable inhibition
I196L	Georgia	Unknown	pCMV	N	No detectable inhibition
I215L	OURT88/3	Ubiquitin conjugation enzyme	AdH5	C	No detectable inhibition
I267L	OURT88/3	Unknown	pcDNA3.1	C	No detectable inhibition
I329L	OURT88/3	Inhibitor of TLR3 signalling	AdH5	C	No detectable inhibition

Gene	Virus strain	Function	Plasmid/ AdH5	HA Tag	Screening result
K78R	OURT88/3	DNA-binding structural protein	pcDNA3.1	C	No detectable inhibition
KP177R	OURT88/3	p22 structural protein	pcDNA3.1	C	No detectable inhibition
L7L	Georgia	Unknown	pCMV	N	No detectable inhibition
L8L	OURT88/3	Unknown	AdH5	C	No detectable inhibition
L9R	Georgia	Unknown	pCMV	N	No detectable inhibition
L10L	OURT88/3	p22 family	AdH5	C	No detectable inhibition
L60L	OURT88/3	Unknown	pcDNA3.1	C	No detectable inhibition
M448R	OURT88/3	RNA ligase	AdH5	C	Inconsistent inhibition
MGF110-1L	OURT88/3	Unknown	AdH5	C	No detectable inhibition
MGF110-4L	OURT88/3	Unknown	pcDNA3.1	No tag	No detectable inhibition
MGF110-5L	OURT88/3	Unknown	pcDNA3.1	No tag	No detectable inhibition
MGF360-11L	Benin 1997/1	Unknown	AdH5	C	Inconsistent inhibition
MGF505-4R	OURT88/3	Unknown	AdH5	C	Cell toxicity
MGF505-5R	OURT88/3	Unknown	AdH5	C	Inconsistent inhibition
QP383R	OURT88/3	Unknown	pcDNA3.1	C	No detectable inhibition
R298L	OURT88/3	Serine protein kinase	pcDNA3.1	N	Inconsistent inhibition
S183L	OURT88/3	Unknown	pcDNA3.1	C	No detectable inhibition
X69R	OURT88/3	Unknown	pcDNA3.1	C	No detectable inhibition

The majority of the ASFV genes that were screened showed no detectable inhibition of starvation-induced autophagosomes. Expression of MGF505-4R led to cell toxicity and therefore the detection of LC3 puncta was not possible. Expression of B646L resulted in some cells that demonstrated low numbers of autophagosomes while in other cells this was not apparent. To investigate this further, Vero cells were transduced with an AdH5 vector encoding B646L and were incubated for 24 hours during which cells were either incubated under nutrient replete conditions or starvation conditions for the final 3 hours. Cells were fixed and labelled for immunofluorescence using anti-LC3 and anti-HA tag antibodies and the nuclear marker DAPI.

Under nutrient replete conditions, cells showed typically low numbers of LC3 puncta (Figure 5.5.1A) suggesting that B646L expression did not induce the formation of autophagosomes. Labelling of HA-tagged protein did not reveal any difference in protein expression between the non-starved (Figure 5.5.1B) and starved cells (Figure 5.5.1D). Protein expression in some cells was evident as a diffuse cytoplasmic pattern whereas in others, protein expression was concentrated around the nucleus. In some cells, a combination of these patterns was observed. Analysing the number of LC3 puncta in the starved cells (Figure 5.5.1C) revealed that cells with protein expression concentrated around the nucleus contained almost no LC3 puncta whereas high numbers of LC3 puncta were observed in cells with a diffuse pattern of protein expression. Similar results

were obtained using plasmid expression (data not shown) demonstrating that these effects were not specific to the method of gene delivery. Taken together these results show that B646L expression leads to inconsistent inhibition of starvation-induced autophagy that may be linked to protein localisation.

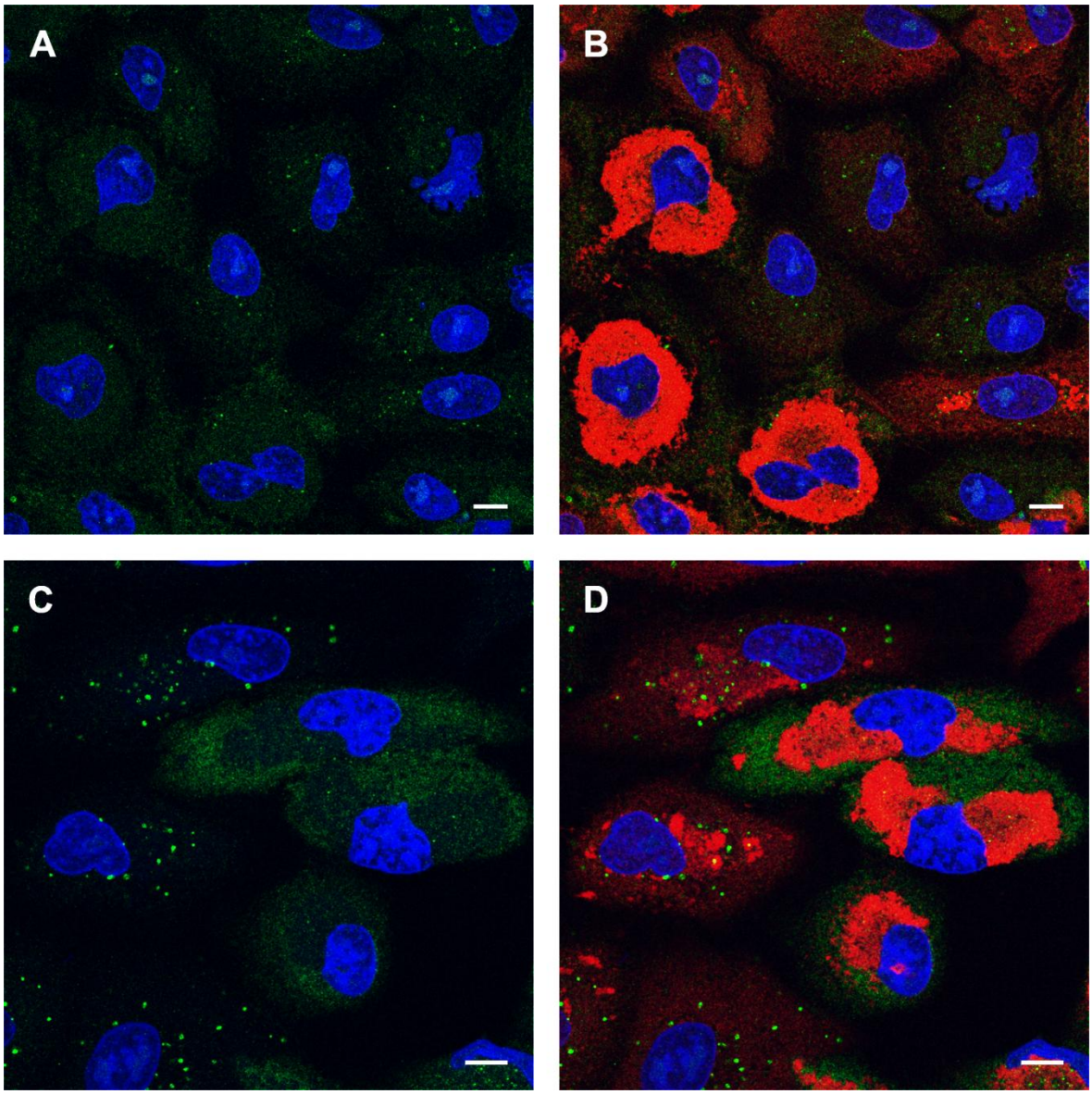

Figure 5.5.1 B646L expression leads to inconsistent inhibition of starvation-induced autophagy

Vero cells were transduced with adenovirus encoding B646L and were incubated for 24 hours during which cells were incubated in complete Vero cell media (Panels A and B) or were starved in EBSS media (Panels C and D) for the final 3 hours. Cells were fixed and permeabilised in methanol and then labelled for LC3 shown in green, HA-tagged protein shown in red and nuclei shown in blue. Panels A and C show the same cells as Panels B and D respectively but with the red channel removed to allow for clearer observation of LC3 staining. Scale bars represent 10 µM.

Inconsistent inhibition of autophagosomes was also seen in cells expressing MGF360-11L, MGF505-5R and R298L (data not shown). In these cases, cells that showed a reduction in the number of autophagosomes often demonstrated very high levels of protein expression which may point to a non-specific mechanism of autophagosome inhibition. Expression of C147L also demonstrated an inconsistent inhibition of LC3 puncta under starvation conditions and in some cases, inhibition was accompanied by an unusual pattern of DAPI staining. In place of normal diffuse staining, the nucleus instead showed a segmented pattern of staining (Figure 5.5.2). There was no difference in the localisation of C147L when comparing cells with altered patterns of DAPI staining and those with no changes in the nucleus.

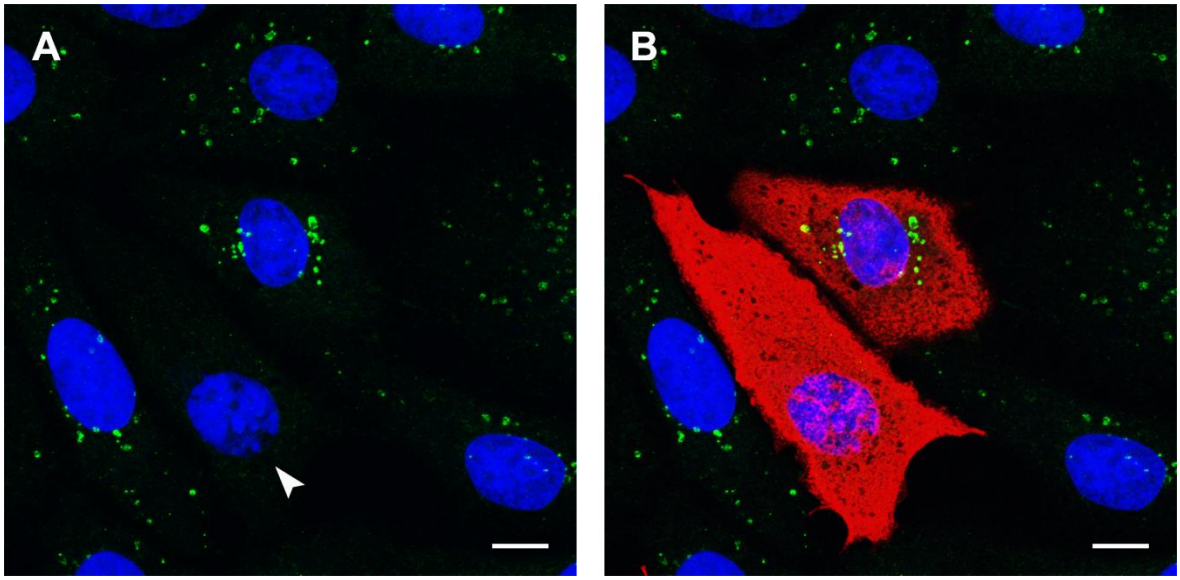

Figure 5.5.2 C147L expression inhibits starvation induced autophagy in cells that demonstrate changes in the nucleus

Vero cells were transfected with plasmids encoding C147L and were incubated for 24 hours before passaging the cells and incubating them for a further 24 hours. During the final 3 hours, cells were starved in EBSS media prior to being fixed and permeabilised in methanol. Cells were then labelled for LC3 shown in green, HA-tagged protein shown in red and nuclei shown in blue. Panel A shows the same cells as Panel B but with the red channel removed to allow for clearer observation of LC3 staining. The arrow in Panel A indicates unusual pattern of DAPI staining. Scale bars represent 10 µM.

The screening results of E183L and E199L revealed a pattern of LC3 labelling that was atypical of the pattern usually associated with the induction of autophagy. To investigate this further, Vero cells were transduced with AdH5 vectors encoding either E183L or E199L and cells were incubated for 24 hours during which cells were either incubated in nutrient replete conditions or starvation conditions for the final 3 hours. Cells were fixed and labelled for immunofluorescence using anti-LC3 and anti-HA tag antibodies and the nuclear marker DAPI.

Under nutrient replete conditions, a very low number of LC3 puncta are usually observed in cells due to the absence of autophagy induction. However, in cells transduced with E183L (Figure 5.5.3A), numerous LC3 labelled structures were evident. These were not only present as the round punctate structures usually representative of autophagosomes but also as structures in which LC3 seemed to be aggregated into slightly larger structures. A similar pattern of LC3 labelling was observed in cells incubated under starvation conditions (Figure 5.5.3C) and labelling of HA-tagged protein revealed that the aforementioned LC3 labelled structures were evident in cells expressing E183L (Figure 5.5.3B and D). In cells that were transduced with E199L, much larger LC3 aggregates were observed when compared to E183L. These were evident in cells that were incubated under nutrient replete conditions (Figure 5.5.4A) and starvation conditions (Figure 5.5.4C). Analysis of cells that were labelled with HA tag antibodies revealed that these large LC3 aggregates were only evident in cells expressing E199L (Figure 5.5.4B and D). Taken together, these results show that expression of E183L and E199L induces the appearance of LC3 labelled structures that are not representative of autophagosomes and in a manner that is unaffected by nutrient availability.

The screening results of DP148R revealed an unusual pattern of LC3 labelling which was investigated further. Vero cells were transfected with plasmids encoding DP148R and cells were incubated for 24 hours before they were passaged. Cells were then incubated for a further 24 hours during which cells were either incubated under nutrient replete conditions or starvation conditions for the final 3 hours. Finally, cells were fixed and labelled for immunofluorescence using anti-LC3 and anti-HA tag antibodies and the nuclear marker DAPI.

Under nutrient replete conditions, some cells demonstrated low levels of autophagosomes as would be expected however, in other cells numerous tiny LC3 puncta were observed in the cell cytoplasm (Figure 5.5.5A). Labelling of HA-tagged protein revealed that these were predominantly evident in cells expressing DP148R (Figure 5.5.5B). Cells that were incubated under starvation conditions mostly showed a high number of autophagosomes as would be expected after the induction of autophagy although some cells demonstrated LC3 puncta that were much smaller in size (Figure 5.5.5C). These tiny puncta were comparable to the size of puncta observed under nutrient replete conditions. Labelling of HA-tagged protein showed that the tiny LC3 puncta were only present in DP148R expressing cells (Figure 5.5.5D) and that cells that were not expressing DP148R demonstrated LC3 puncta that were of a size usually representative of autophagosomes. Collectively, these results suggest that under nutrient replete conditions DP148R is able to induce the formation of LC3 puncta that are smaller in size to autophagosomes and that DP148R is also able to inhibit or restrict the formation of autophagosomes under starvation conditions.

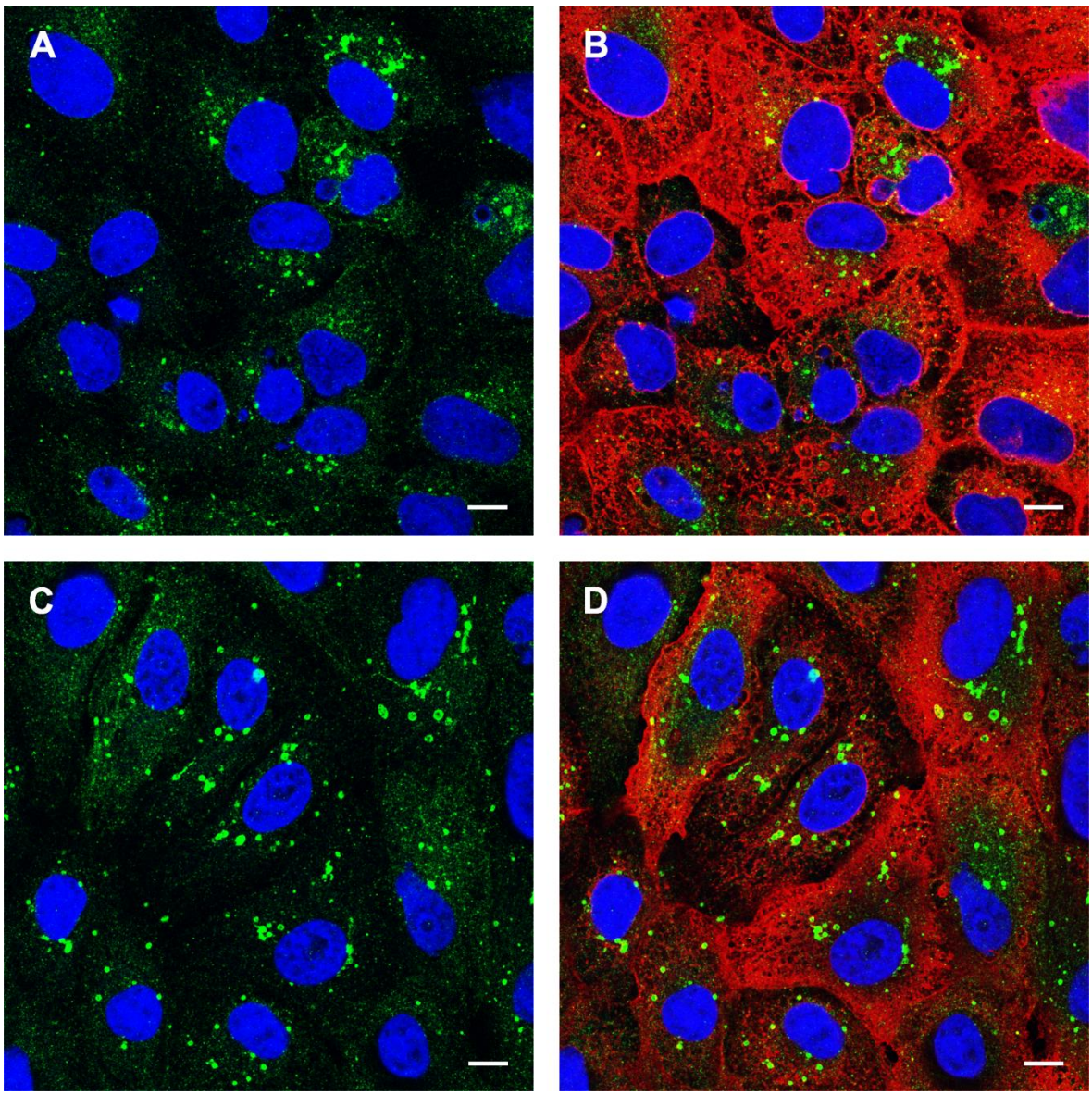

Figure 5.5.3 E183L expression induces the appearance of LC3 labelled structures

Vero cells were transduced with adenovirus encoding E183L and were incubated for 24 hours during which cells were incubated in complete Vero cell media (Panels A and B) or were starved in EBSS media (Panels C and D) for the final 3 hours. Cells were fixed and permeabilised in methanol and then labelled for LC3 shown in green, HA-tagged protein shown in red and nuclei shown in blue. Panels A and C show the same cells as Panels B and D respectively but with the red channel removed to allow for clearer observation of LC3 staining. Scale bars represent 10 µM.

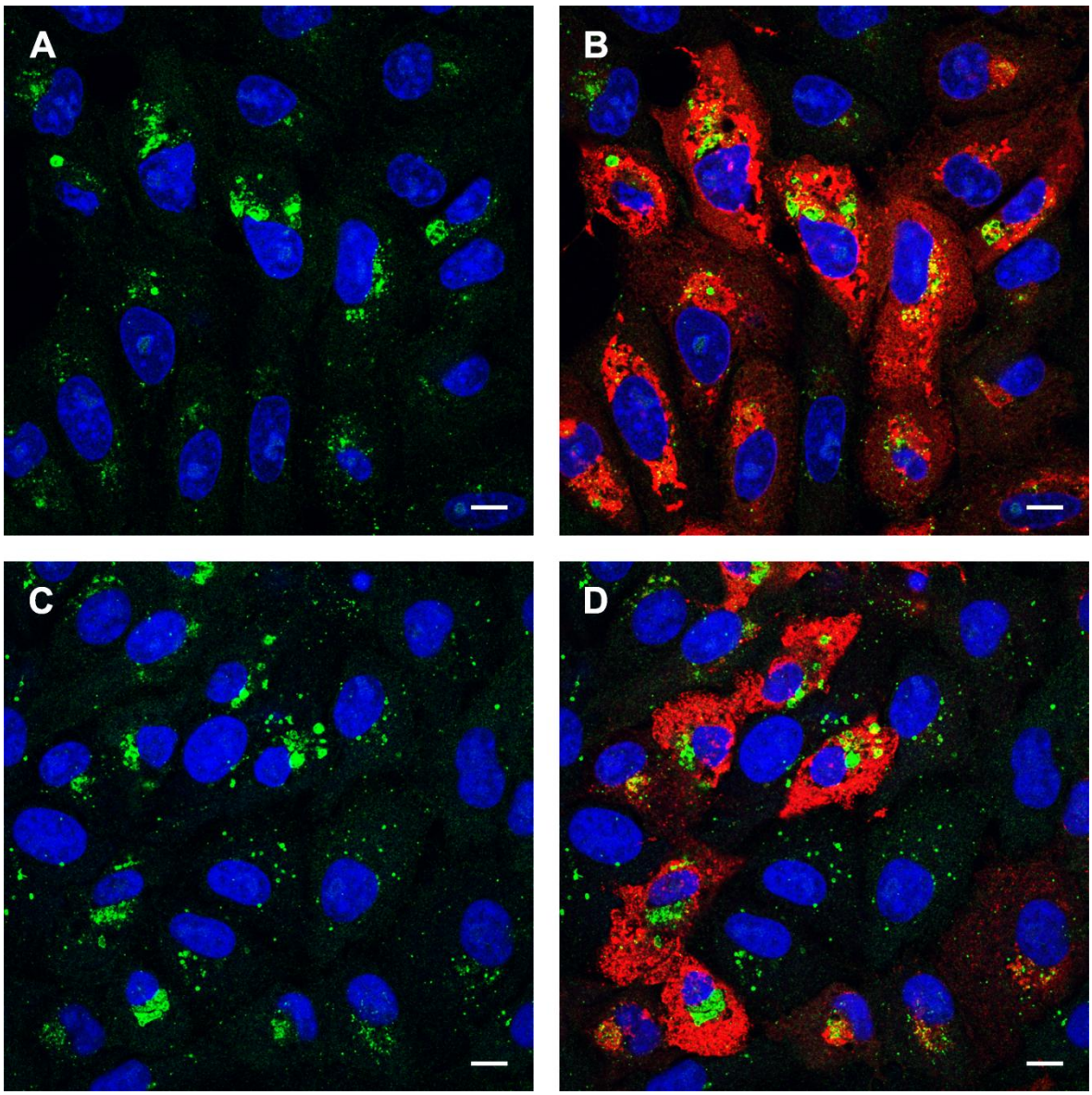

Figure 5.5.4 E199L expression induces the appearance of LC3 labelled structures

Vero cells were transduced with adenovirus encoding E199L and were incubated for 24 hours during which cells were incubated in complete Vero cell media (Panels A and B) or were starved in EBSS media (Panels C and D) for the final 3 hours. Cells were fixed and permeabilised in methanol and then labelled for LC3 shown in green, HA-tagged protein shown in red and nuclei shown in blue. Panels A and C show the same cells as Panels B and D respectively but with the red channel removed to allow for clearer observation of LC3 staining. Scale bars represent 10 µM.

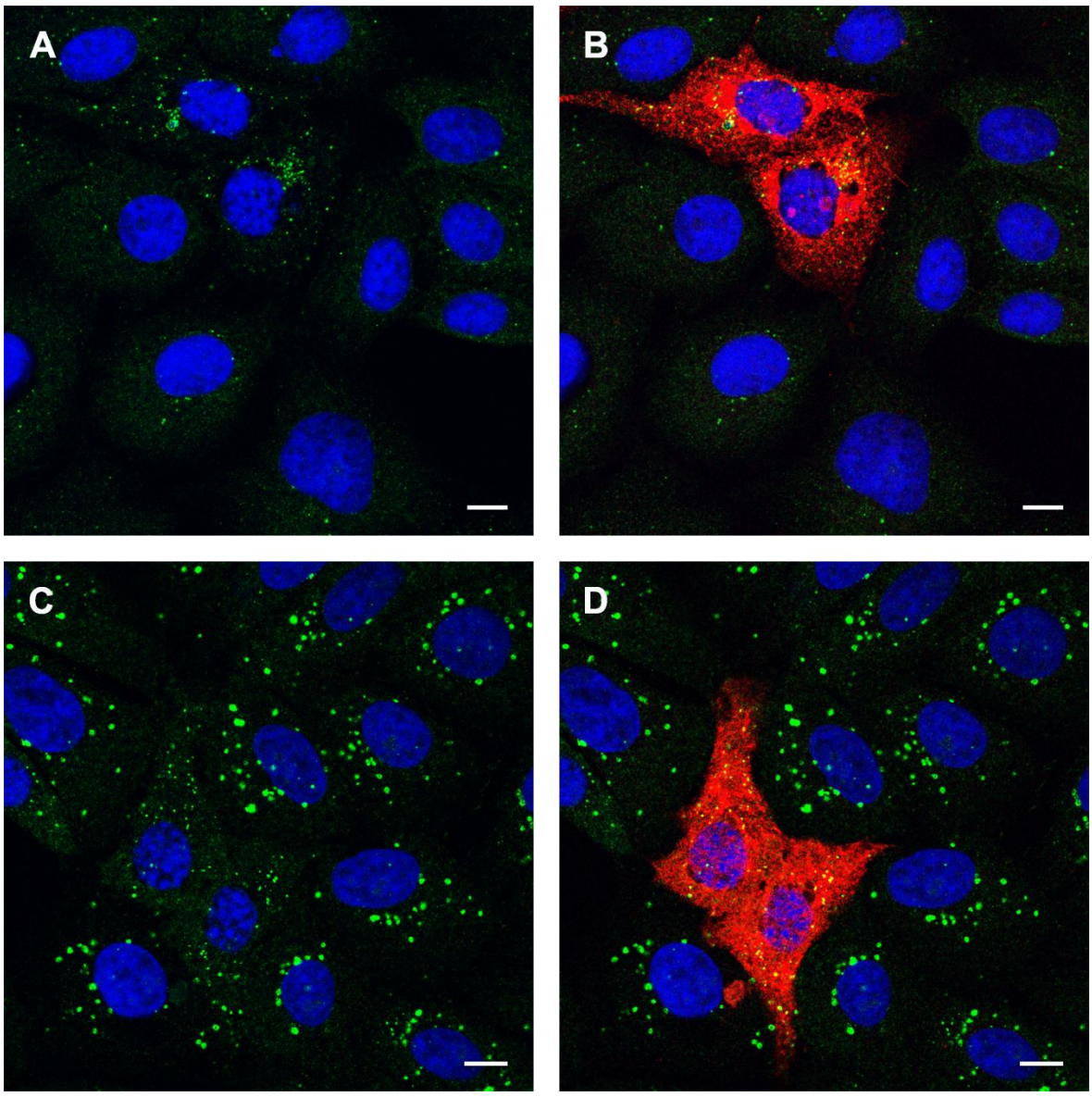

Figure 5.5.5 DP148R expression induces tiny LC3 puncta in Vero cells and restricts the formation of starvation-induced autophagosomes

Vero cells were transfected with plasmids encoding DP148R and were incubated for 24 hours before passaging the cells and incubating them for a further 24 hours. During the final 3 hours, cells were incubated in complete Vero cell media (Panels A and B) or were starved in EBSS media (Panels C and D) prior to being fixed and permeabilised in methanol. Cells were then labelled for LC3 shown in green, HA-tagged protein shown in red and nuclei shown in blue. Panels A and C show the same cells as Panels B and D but with the red channel removed to allow for clearer observation of LC3 staining. Scale bars represent 10 μM.

5.2.6 Characterising the effects of the N-terminus and C-terminus of DP148R on LC3 recruitment

The DP148R plasmid that was used in the gene library screen was constructed using the sequence from the Benin 1997/1 strain of ASFV. This sequence encodes a protein of 254 amino acids. In comparison, the equivalent sequence in the OURT88/3 strain encodes a frame shift which

introduces a stop codon essentially dividing the protein into an N and C terminus known as MGF360-17R and DP148R respectively. MGF360-17R is 72 amino acids long and DP148R is 148 amino acids long. An amino acid sequence alignment was carried out to illustrate this (Figure 5.6.1) and shows MGF360-17R and DP148R of the OURT88/3 strain aligned against DP148R of the Benin 1997/1 strain.

Figure 5.6.1 Amino acid sequence alignment of DP148R in Benin 1997/1 and OURT88/3

The amino acid sequences of MGF360-17R (top) and DP148R (bottom) of the OURT88/3 strain of ASFV were aligned to the DP148R sequence of the Benin 1997/1 strain (middle).

Plasmids encoding MGF360-17R or DP148R from the OURT88/3 strain (provided by Dr Ana Reis) were used to test for similar effects on LC3 recruitment that were described using full length DP148R from the Benin 1997/1 strain. Vero cells were transfected with the aforementioned plasmids and cells were incubated for 24 hours before they were passaged. Cells were then incubated for a further 24 hours during which cells were either incubated under nutrient replete conditions or starvation conditions for the final 3 hours. Finally, cells were fixed and labelled for immunofluorescence using anti-LC3 and anti-HA tag antibodies and the nuclear marker DAPI.

Under nutrient replete conditions, cells that were transfected with MGF360-17R showed typically low levels of autophagosomes (Figure 5.6.2A) and labelling of HA-tagged protein revealed that cells expressing MGF360-17R displayed similar levels of LC3 puncta compared to cells that were not expressing MGF360-17R (Figure 5.6.2B). In cells incubated under starvation conditions, a high number of autophagosomes were observed as would be expected (Figure 5.6.2C) and labelling of HA-tagged protein revealed that similar numbers of LC3 puncta were evident between cells expressing MGF360-17R and cells that were not (Figure 5.6.2D). Collectively these results show

that MGF360-17R does not induce LC3 puncta under nutrient replete conditions and does not restrict the formation of starvation-induced autophagosomes as was previously seen in cells expressing Benin 1997/1-DP148R.

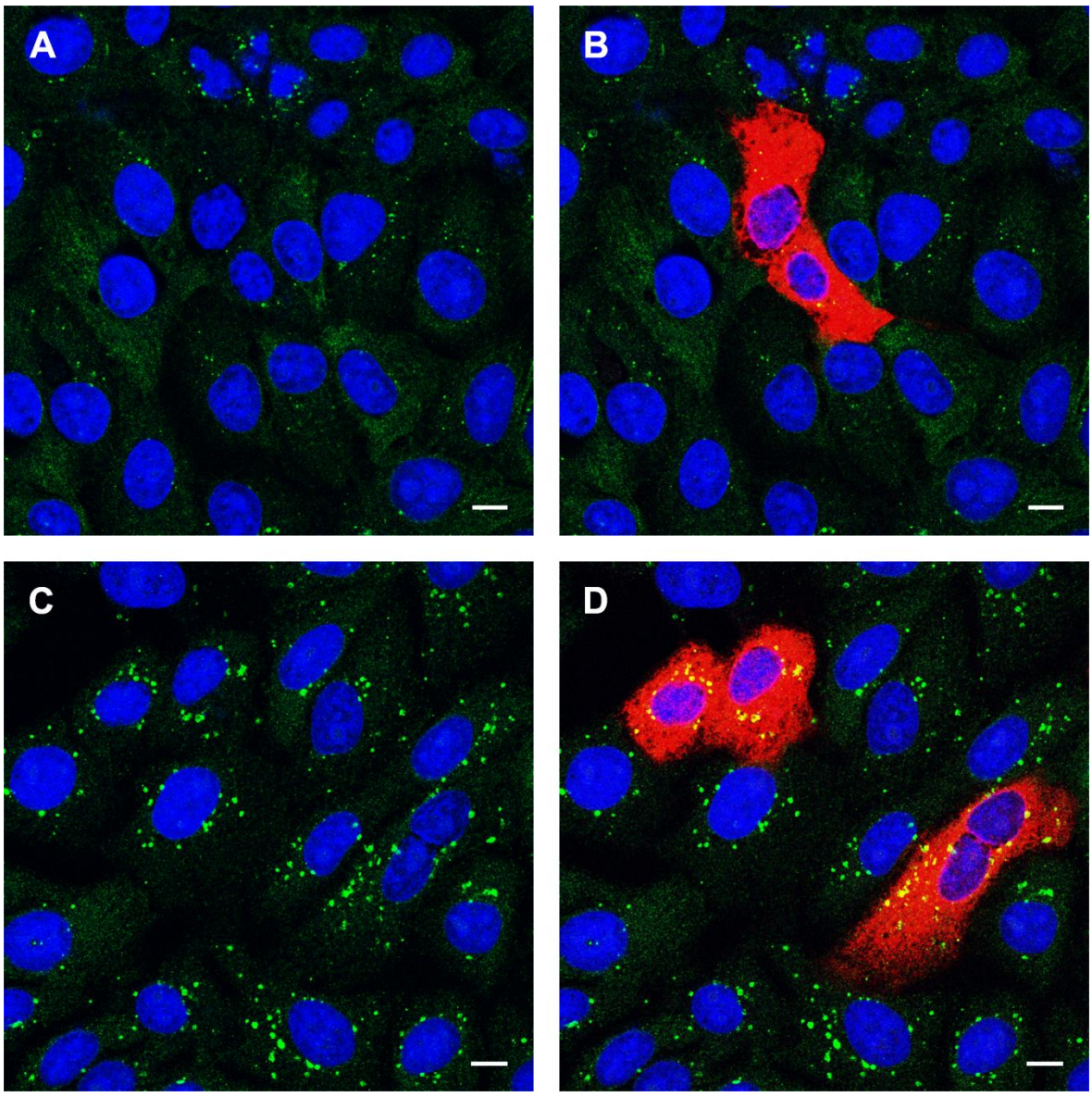

Figure 5.6.2 OURT88/3-MGF360-17R expression does not induce LC3 puncta or restrict starvation-induced autophagosome formation

Vero cells were transfected with plasmids encoding OURT88/3-MGF360-17R and were incubated for 24 hours before passaging the cells and incubating them for a further 24 hours. During the final 3 hours, cells were incubated in complete Vero cell media (Panels A and B) or were starved in EBSS media (Panels C and D) prior to being fixed and permeabilised in methanol. Cells were then labelled for LC3 shown in green, HA-tagged protein shown in red and nuclei shown in blue. Panels A and C show the same cells as Panels B and D but with the red channel removed to allow for clearer observation of LC3 staining. Scale bars represent 10 μM.

In cells that were transfected with OURT88/3-DP148R under nutrient replete conditions, low numbers of LC3 puncta were observed in most cells although a few tiny LC3 puncta were also apparent in some of the cells (Figure 5.6.3A). Labelling of HA-tagged protein revealed that some of the tiny LC3 puncta were evident in cells expressing DP148R (Figure 5.6.3B). Under starvation conditions, a high number of autophagosomes was observed in the cells as would be expected (Figure 5.6.3C) and labelling of HA-tagged protein revealed that similar numbers of LC3 puncta were evident between cells expressing DP148R and cells that were not (Figure 5.6.3D). Taken together, these results suggest that OURT88/3-DP148R may be able to act in a similar way to Benin 1997/1-DP148R by inducing tiny LC3 puncta in non-starved cells. However, the number of LC3 puncta induced by OURT88/3-DP148R seemed to be less when compared to the amount of LC3 puncta that were previously seen in cells expressing Benin 1997/1-DP148R (Figure 5.5.5). In addition, the results indicate that OURT88/3-DP148R was not able to restrict the formation of starvation-induced autophagosomes as was previously seen in cells expressing Benin 1997/1-DP148R (Figure 5.5.5).

5.2.7 DP148R is unlikely to be expressed by the Ba71V strain of ASFV

To investigate whether DP148R could be acting as a viral modulator of autophagy, analysis of the DP148R promotor region and potential translation start sites in Ba71V was carried out and compared to the Benin 1997/1 and OURT88/3 strains by DNA sequence alignment (Figure 5.7).

The ATG start codon at the beginning of Benin 1997/1-DP148R and OURT88/3-MGF360-17R (labelled as start codon X) was identified, however the corresponding sequence at this site in Ba71V was ATA and therefore did not represent a start codon. Upstream of this start codon, AT rich regions consistent with promotor sequences were apparent in Benin 1997/1 and OURT88/3 but were absent in Ba71V. Downstream of start codon X, another potential ATG start codon (codon Y) was identified in Benin 1997/1 and OURT88/3 however the corresponding sequence in Ba71V was TTA. An ATG start codon (codon Z) was identified in the Ba71V strain that aligns with the start codon of OURT88/3-DP148R, however no promotor sequence was evident upstream of this location indicating that this region is not transcribed in Ba71V. Collectively, these results suggest that DP148R is unlikely to be expressed during Ba71V infection.

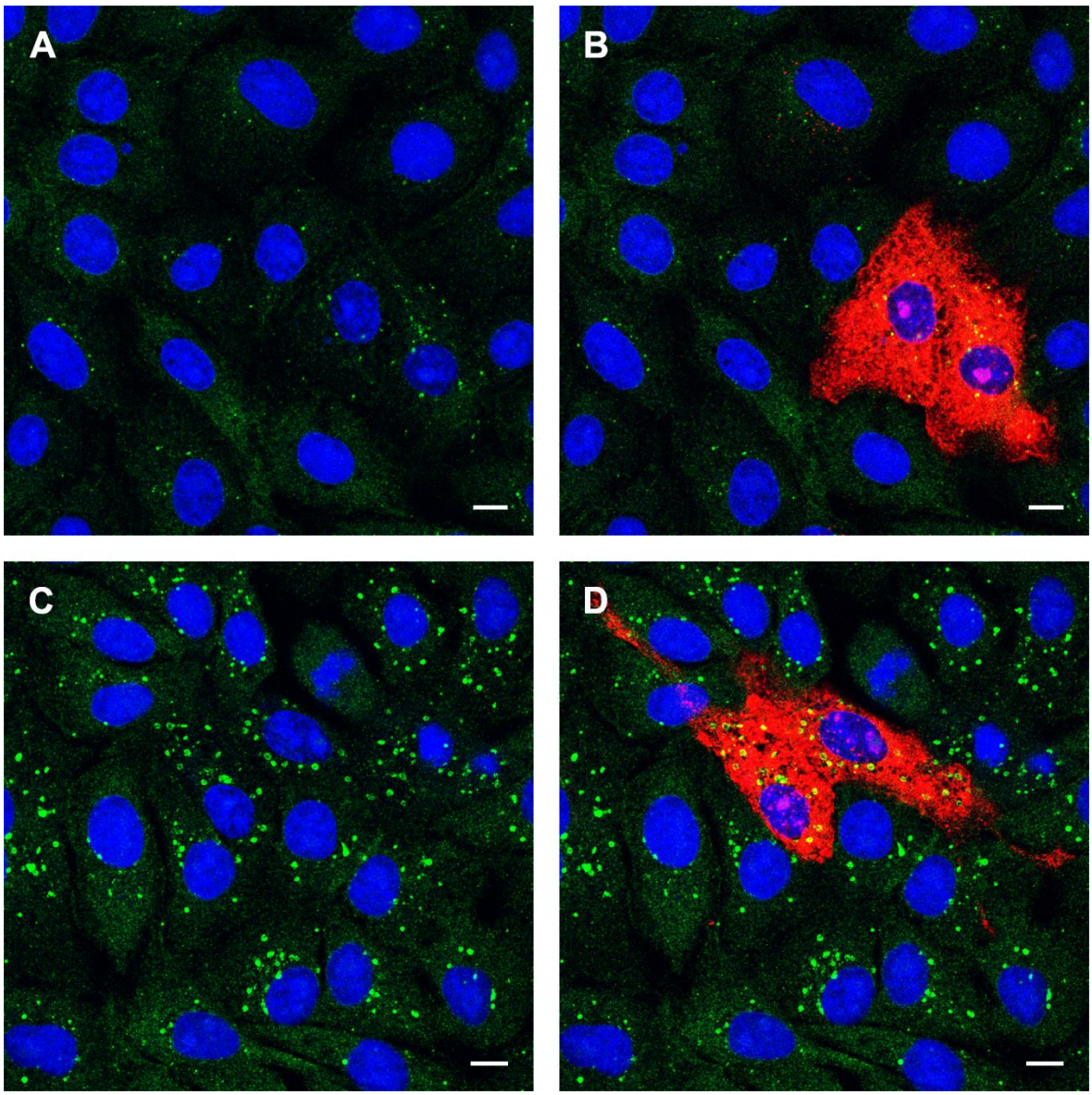

Figure 5.6.3 OURT88/3-DP148R expression induces low numbers of LC3 puncta and does not restrict starvation-induced autophagosome formation

Vero cells were transfected with plasmids encoding OURT88/3-DP148R and were incubated for 24 hours before passaging the cells and incubating them for a further 24 hours. During the final 3 hours, cells were incubated in complete Vero cell media (Panels A and B) or were starved in EBSS media (Panels C and D) prior to being fixed and permeabilised in methanol. Cells were then labelled for LC3 shown in green, HA-tagged protein shown in red and nuclei shown in blue. Panels A and C show the same cells as Panels B and D but with the red channel removed to allow for clearer observation of LC3 staining. Scale bars represent 10 μM.

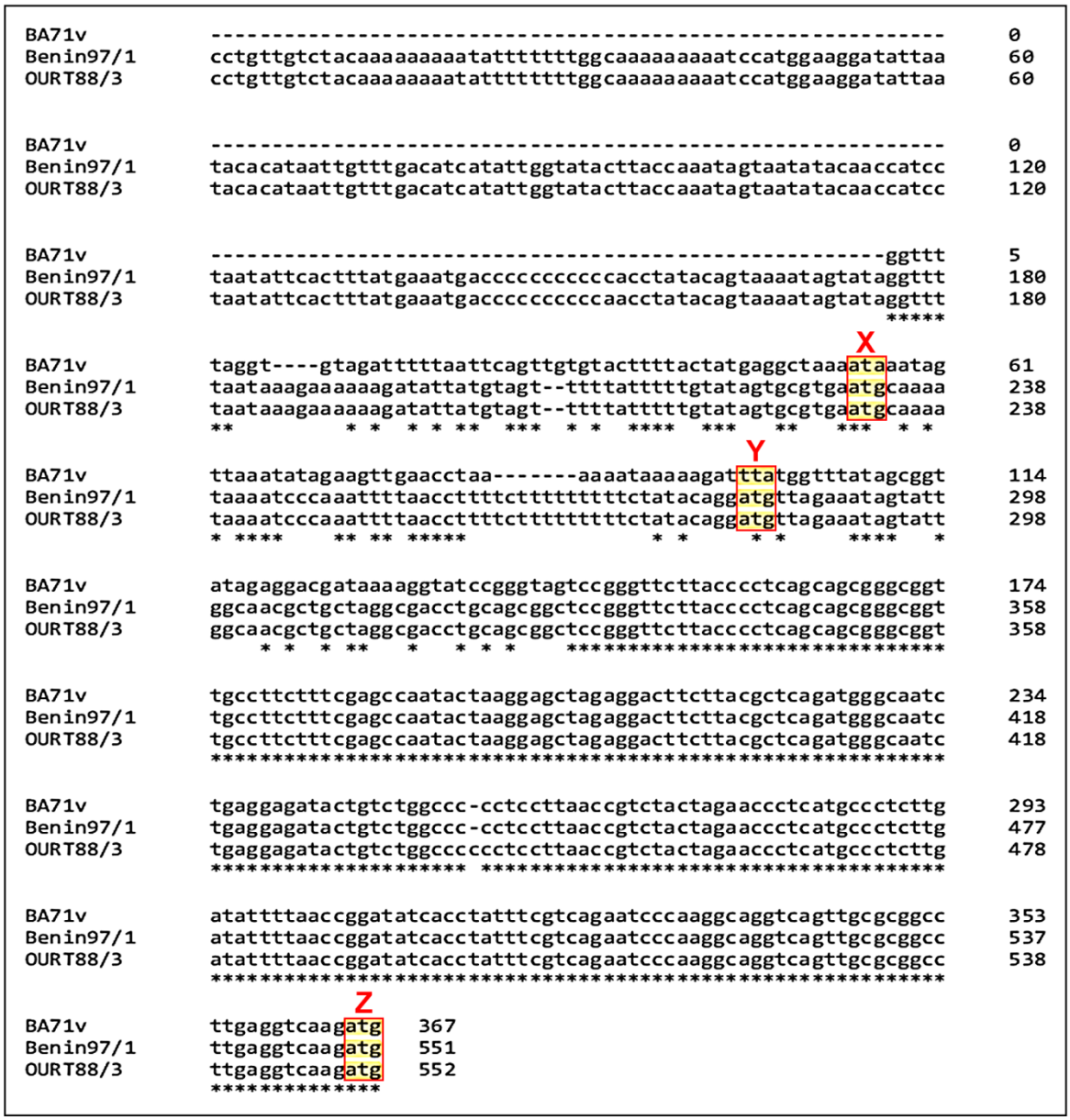

Figure 5.7 DNA sequence alignment of the DP148R region in Ba71V, Benin 1997/1 and OURT88/3 strains

The DNA sequences of the DP148R region in the Ba71V (top), Benin 1997/1 (middle) and OURT88/3 (bottom) strains were aligned. Potential start codons are indicated (X; Y and Z). Asterisks indicate the position of identical bases between all three strains. Accumulative number of bases for each strain is indicated to the right.

5.3 Discussion

ASFV inhibits autophagy during the very early stages of infection and it is likely that Akt/mTOR activity is responsible for this. By 4 hpi an additional mechanism of inhibition is employed by the virus, presumably through the action of viral proteins that are expressed during early replication. One of these proteins is possibly the Beclin1 interacting protein A179L, but experiments with an A179L KO virus showed that additional proteins must be involved. To attempt to identify these

additional modulators of autophagy, a library of ASFV genes was screened for their ability to inhibit starvation-induced autophagosomes.

Optimisation of the plasmid screening process revealed that passaging the cells 24 hours post-transfection considerably reduced the amount of autophagosomes and TVAs when compared to cells that had not been passaged (Figure 5.1). This method of plasmid screening was therefore adopted in downstream experiments. Likewise an experiment showed that an AdH5 vector expressing GFP alone does not induce autophagy or inhibit starvation-induced autophagosomes (Figure 5.2). A179L was chosen to test whether the confocal microscopy based screening method was suitable for identifying genes that could inhibit the formation of autophagosomes. In addition to wild-type A179L, a mutant version of A179L was engineered that swapped in two tyrosine residues within the ligand binding groove in order to provide a negative control (Figure 5.3).

Wild-type (WT) and mutant (YY) A179L were each cloned into plasmid and AdH5 vectors and tested for their ability to suppress the formation of starvation-induced autophagosomes. Under starvation conditions, plasmid expression of WT A179L resulted in fewer autophagosomes when compared to cells that did not express WT A179L whereas expression of YY A179L had no effect (Figure 5.4.1). Similar results were obtained under starvation conditions in cells that were transduced using an AdH5 vector encoding either WT A179L or YY A179L (Figure 5.4.3) and these results were confirmed by Imaris quantification (Figure 5.4.4). Interestingly, there was still a significant increase in the number of LC3 puncta in WT A179L expressing cells under starvation conditions when compared to cells incubated under nutrient replete conditions indicating that autophagy had not been entirely inhibited by WT A179L. Taken together, these results showed that WT A179L was able to suppress the formation of starvation-induced autophagosomes but YY A179L was not. More importantly, the results showed that using the confocal microscopy based assay to detect the inhibition of autophagy was a suitable method to screen both the plasmid based and adenovirus ASFV gene libraries.

In total, 76 ASFV genes were screened for which the majority did not exhibit any detectable inhibition of autophagy. Expression of MGF505-4R resulted in cell toxicity. The reason for this is currently unknown and the function of this protein has not been studied in detail although it may play a role in the regulation of the interferon response (Reis et al., 2016). Screening of B646L initially showed inhibition in some cells and upon further investigation, it was revealed that cells with protein expression concentrated around the nucleus contained almost no LC3 puncta whereas typical numbers of LC3 puncta were observed in cells with a diffuse pattern of protein expression (Figure 5.5.1). This could suggest that the inhibition seen in some cells may be linked to protein localisation or levels of protein expression.

The B646L gene encodes the major capsid protein of ASFV called p72 and repression of this protein severely hinders viral morphogenesis (Garcia-Escudero et al., 1998). A study of the sub-

cellular localisation of p72 in infected cells revealed that approximately 50% of the intracellular pool of p72 was associated with membranes and membrane fractionation showed that newly synthesized p72 molecules co-sedimented with ER membranes (Cobbold et al., 1996). Furthermore, using immunofluorescence microscopy in the aforementioned study, p72 was shown to be colocalised with the ER marker PDI and therefore suggests that the protein which was observed around the nucleus in Figure 5.5.1 could also be localised at the ER. The ER is important during the biogenesis of autophagosomes, as membrane structures known as omegasomes form on the ER surface and provide a compartment in which autophagosomal proteins accumulate (Axe et al., 2008). Additionally, evidence suggests that the ER contributes membrane to the forming phagophore (Ge et al., 2013). This could explain why inhibition is only seen in cells in which p72 was observed around the nucleus, as ER-bound protein could interfere with autophagosome biogenesis. In the context of autophagosome inhibition in infected cells, B646L was not favoured as a candidate to pursue for knock-out studies. This was firstly due to the fact that B646L is an essential gene and secondly because B646L is expressed during late stages of the replication cycle whereas the inhibition of autophagy was previously observed during the early stages of replication.

Screening of MGF360-11L, MGF505-5R and R298L resulted in the inhibition of autophagy in only some of the cells and in most cases these were cells that demonstrated very high levels of protein expression which may point to a non-specific mechanism of autophagosome inhibition. It could be possible that high levels of exogenous protein expression alter the internal cell environment to an extent where normal cell processes including the autophagy pathway are hindered. Nevertheless, the inhibition by R298L is interesting as this gene encodes a serine/threonine-protein kinase 1 enzyme (Baylis et al., 1993). The phosphorylation of Akt and the downstream activation of mTORC1 in ASFV infected cells was previously demonstrated to be a mechanism used by the virus to inhibit autophagy during early stages of the replication cycle. R298L is incorporated into the mature virion and could therefore be immediately available to influence cell signalling at the start of infection (Alejo et al., 2018). Consequently, it may play a role in the observed inhibition of autophagy by phosphorylating proteins involved in the signalling cascades that are crucial to the induction of autophagy.

C147L, an RNA polymerase subunit (Lu et al., 1993) also showed inhibition of starvation-induced autophagosomes in some cells. Interestingly, inhibition was sometimes evident in cells that demonstrated atypical DAPI staining which could indicate morphological changes in the nucleus (Figure 5.5.2). The segmented appearance of the nucleus may point to nuclear fragmentation that is associated with the onset of apoptosis. Apoptosis has been shown to inhibit autophagy via caspase-mediated cleavage of Beclin1 (Luo and Rubinsztein, 2010) and may explain the lack of LC3 puncta in these cells. In this regard, carrying out an apoptosis detection assay in the future may provide clarity as to whether the over-expression of C147L induces this pathway. As is the case for R298L, C147L is incorporated into the virus particle which suggests an essential function in the virus life

cycle. For this reason, R298L and C147L were not considered favourable targets for downstream knock-out experiments.

The screening results and subsequent investigation of E183L and E199L revealed that these proteins are able to induce structures that label positively for LC3 but that are relatively larger when compared to typical autophagosomes. This was observed under nutrient replete and starvation conditions indicating that this effect is unaffected by nutrient availability. In E199L expressing cells (Figure 5.5.4), much larger structures were apparent when compared to cells expressing E183L (Figure 5.5.3). The basis for these effects is currently unknown. In the case of E199L, this was investigated in detail and results are described in Chapter 6.

E183L encodes a major structural protein called p54 that has been shown to be essential for the recruitment and transformation of ER membranes into the precursors of the viral envelope (Rodriguez et al., 2004). In the study by Rodriguez and colleagues, p54 was targeted to the ER membrane following transient expression and repression of p54 in infected cells led to the arrest of viral morphogenesis. A separate study revealed that transient expression of E183L led to significant modifications of the ER including the collapse of ER cisternae (Windsor et al., 2012). It may be possible that these extensive changes to the ER are responsible for activating the autophagy pathway. Indeed, this has been described in a study that demonstrated the induction of autophagy as a countermeasure to ER stress (Ogata et al., 2006). This however does not explain why relatively larger aggregated LC3 structures were observed in place of the round punctate structures usually associated with autophagosomes. In their study on the effects of E183L expression on the ER, Windsor *et al* (2012) described whorls of ER membrane appearing as disks in the cytoplasm. With the ER acting as the site of early autophagosome biogenesis, it may be possible that the induction of autophagy in response to ER stress leads to LC3 recruitment to these ER discs which could in turn give the appearance of aggregations of LC3.

Initial screening of DP148R resulted in an unusual pattern of LC3 labelling and further investigation revealed the appearance of tiny LC3 puncta under nutrient replete conditions (Figure 5.5.5). Under starvation conditions, the same tiny LC3 puncta were observed in addition to an absence of the relatively larger LC3 puncta that are representative of autophagosomes (Figure 5.5.5) suggesting that this protein may be able to inhibit the induction of autophagy. DP148R has no known function, however research has shown that it is expressed at early times post-infection which could indicate a role in the evasion of host cell defence (Reis et al., 2017a).

The initial investigations of DP148R were conducted using the sequence from the virulent ASFV strain Benin 1997/1 which encodes a protein of 254 amino acids. When this was compared to the equivalent sequence in the attenuated strain OURT88/3, it was discovered that the latter encoded two proteins instead which were separated by a frame-shift mutation (Figure 5.6.1). Expression of MGF360-17R, which corresponds to the N-terminus of the Benin DP148R protein, did not result in

the same effects on LC3 that were previously observed using the Benin 1997/1 construct under nutrient replete or starvation conditions (Figure 5.6.2). However, expression of the OURT88/3 homologue of DP148R, which corresponds to the C-terminus of the Benin homologue resulted in the induction of low numbers of the tiny LC3 puncta that were previously described (Figure 5.6.3). Expression of the C-terminus protein did not lead to any change in the number of starvation induced autophagosomes suggesting that the full length protein is required for this effect.

To determine whether DP148R could play a role in the inhibition of autophagy that was observed at early times post-infection, the DP148R coding region of the Ba71V genome was compared to the Benin 1997/1 and OURT88/3 strains (Figure 5.7). Analysis of a DNA sequence alignment revealed that the start codon present in Benin 1997/1 did not correspond to a start codon in Ba71V. This was also the case for another potential start codon situated just downstream in the Benin 1997/1 sequence. Despite the presence of a start codon in Ba71V that corresponded to the start codon of DP148R in the OURT88/3 strain, no promotor sequence upstream of this was evident. Research carried out by Gwenny Cackett (UCL – data unpublished) showed that RNA sequence analysis of the Ba71V transcriptome did not reveal the presence of transcripts encoding DP148R. In conjunction with the genome analysis described above, it seems highly unlikely that DP148R is expressed in the Ba71V strain.

With the exception of DP148R, screening of the ASFV gene library did not identify any inhibitors of autophagy that could be easily deleted from the virus. DP148R has been successfully knocked out of the Benin 1997/1 strain without adversely affecting virus growth in macrophages (Reis et al., 2017a), indicating that DP148R is not an essential protein. However, the lack of evidence for expression of DP148R in Ba71V infected cells argues against a critical role for this protein in modulating autophagy. For this reason DP148R was not pursued as a candidate for downstream knock-out studies.

In summary, the results of the gene library screen did not reveal any obvious inhibitors of autophagy. In addition to MGF genes that were largely excluded from the screen due to variation between isolates, some plasmids were excluded due to a lack of gene expression. It may be possible that this group of genes included one or more autophagy inhibitors. In the future, codon optimising genes could improve gene expression levels and screening of MGF genes could uncover potential inhibitors. The results also highlight a potential barrier to the design of a mutant virus that lacks the capacity to modulate autophagy. This is due to the possibility that autophagy is regulated by essential virus proteins that cannot be removed from the virus without severely impeding its ability to replicate. In this regard, an alternative strategy may need to be adopted and could include mutation of protein domains specifically responsible for the modulation of autophagy.

6 Investigation of the redistribution of LC3 by E199L

6.1 Introduction

The interaction between viruses and autophagy is often very complex and in many cases cannot be simply defined as the global inhibition or promotion of the autophagy pathway. For example, autophagy is upregulated during human immunodeficiency virus (HIV) infection and some autophagy proteins have been shown to act in a pro-viral manner (Brass et al., 2008) raising the possibility that autophagosomes could provide a source of membrane for viral replication (Nardacci et al., 2017). However, HIV has also been shown to block autophagosome maturation (Kyei et al., 2009). ASFV has been shown to inhibit the formation of autophagosomes but the appearance of WIPI and LC3 puncta at the viral factory suggests that elements of the autophagy machinery may be required for virus replication. The results described in section 5.2.5 showed that E199L expression in Vero cells induced a redistribution of LC3 into structures that were inconsistent with the shape and size typically associated with autophagosomes. These results indicate that E199L may interact with or disrupt certain aspects of the autophagy pathway.

The function of E199L is currently unknown although it shares sequence similarity with protein members of the poxvirus entry/fusion complex which suggests that it may be involved in ASFV fusion. Initial characterisation of E199L was carried out by Sun and colleagues and showed that E199L is well conserved amongst ASFV isolates (Sun et al., 1996). In the Vero adapted strain Ba71V, the E199L ORF encodes a protein of 199 amino acids although variation in the length of the protein has been observed for example the Malawi LIL20/1 field isolate encodes a protein of 195 amino acids. E199L is detected from 10 hpi in infected cell lysates and its expression is sensitive to the DNA synthesis inhibitor cytosine arabinoside demonstrating that E199L is a late protein. Furthermore, E199L was detected by immunofluorescence at perinuclear locations from 10 hpi (Sun et al., 1996).

E199L contains a hydrophobic domain near the C-terminus which may anchor the protein in membranes. Proteins containing putative transmembrane regions might be incorporated in internal or external virion membranes or expressed on the cell surface, all of which are of particular interest in the search for immunogenic antigens. Indeed, proteomics analysis confirmed that E199L is present in ASFV virions (Alejo et al., 2018) and the possible role that E199L plays in the ASFV fusion machinery suggests that it is likely located in the inner viral membrane. E199L can be detected using antisera from infected pigs demonstrating that host antibodies are induced against E199L (Sun et al., 1996).

The lipidation of LC3 and assembly of WIPI complexes are both hallmarks of the induction of autophagy. To investigate if E199L may be inducing an autophagy response, Western blot analysis was carried out to determine if E199L induces the lipidation of LC3 and confocal analysis was used to determine whether E199L promotes the formation of WIPI complexes. To assess if there may be

a link between E199L expression and the appearance of WIPI and LC3 puncta at the viral factory, immunofluorescent labelling of infected cells over a time course of infection was used to examine the timing and location of E199L expression. To further investigate the nature of the LC3 labelled structures in E199L expressing cells, electron microscopy of transduced cells was conducted. In addition, samples were prepared from E199L transduced cells for analysis by mass spectrometry to determine if any proteins interacting with E199L belonged to the autophagy pathway. Finally, the potential that E199L expression is localised to the ER and causes an ER stress response was explored.

In the pursuit of novel therapeutics against viral infections, uncovering host proteins that play essential roles in viral replication can provide key opportunities for intervention. For example, rotavirus infection has been shown to induce LC3 lipidation independently of autophagosome formation and silencing of Atg7, a protein involved in LC3 lipidation, results in significant reduction of viral titres (Arnoldi et al., 2014). If autophagy associated processes such as LC3 lipidation are required for ASFV replication and furthermore are stimulated via the action of viral proteins, a layered strategy of intervention could be implemented in which the functions of either host proteins, viral proteins or both are disrupted.

6.2 Results

6.2.1 E199L expression induces an accumulation of LC3-II in Vero cells

Previously it was shown that transduced cells expressing E199L demonstrated a redistribution of LC3 (See Figure 5.5.4). The aforementioned assay was conducted by confocal microscopy using an antibody against LC3 which labels both LC3-I and LC3-II. To investigate whether the observed LC3-labelled structures were formed from the redistribution of LC3-I or LC3-II, further analysis was carried out by Western blot. Vero cells were transduced with adenovirus encoding either GFP or E199L and incubated for 24 hours to allow gene expression. During the final 3 hours of incubation, cells were either incubated in complete cell media, were starved in EBSS media or were starved in EBSS media in the presence of 100 nM Bafilomycin A1. Control cells that had not been transduced were treated under the same set of conditions. Samples were prepared from cells for analysis by immunoblotting and probed using anti-LC3 and anti-γ tubulin antibodies.

The intensity of the band corresponding to LC3-II in the lane containing sample from the control cells under starvation conditions was greater than that from non-starved cells demonstrating the induction of autophagy (Figure 6.1). Control cells that had been starved in the presence of Bafilomycin A1 showed a greater amount of LC3-II when compared to cells that were starved in EBSS only indicating that lysosome fusion had been blocked which leads to the accumulation of autophagosomes. Comparing LC3-II levels between the control cells and cells that had been

transduced with the GFP adenovirus did not show a substantial difference under any of the treatment conditions demonstrating that transduction with the AdH5 vector did not have any effects on LC3-II. In cells that had been transduced with the E199L adenovirus, LC3-II levels were substantially greater when compared to the control cells under non-starved and starved conditions indicating that E199L expression induces the accumulation of LC3-II to a greater extent than starvation and in a manner that is unaffected by nutrient availability. Interestingly, the amount of LC3-II in E199L transduced cells that had been starved in the presence of Bafilomycin A1 was comparable to LC3-II levels under non-starved and starved conditions indicating that a block in autophagosome-lysosome fusion had no effect on the accumulation of LC3-II. Collectively, these results show that the redistribution of LC3 in cells expressing E199L is likely to be associated with an accumulation of LC3-II but that these effects are unlikely to be linked to a canonical autophagy response.

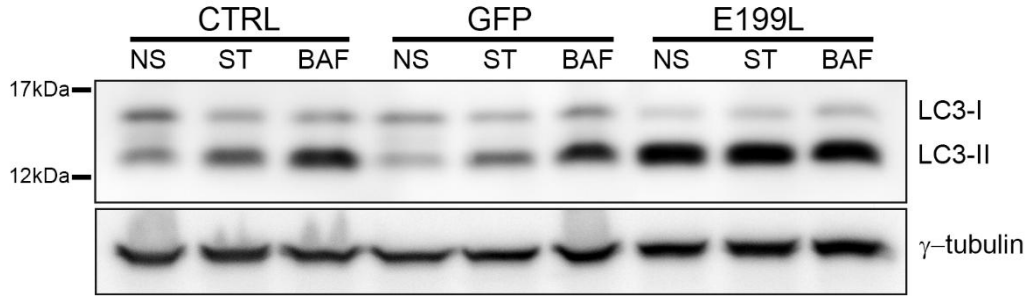

Figure 6.1 E199L expression induces an accumulation of LC3-II in Vero cells

Vero cells were transduced with adenovirus encoding GFP or E199L and incubated for 24 hours during which cells were either non-starved (NS) in complete cell media, starved (ST) in EBSS or starved in the presence of Bafilomycin A1 (BAF) for the final 3 hours. Control cells (CTRL) that had not been transduced were incubated under the same set of conditions. Cells were then lysed and samples prepared for resolution by bis-Tris PAGE before transfer to PVDF membrane. Finally, samples were probed with anti-LC3 and γ-tubulin antibodies followed by appropriate HRP-conjugated secondary antibodies. The positions of molecular mass markers are indicated to the left of the gels.

6.2.2 E199L expression promotes the formation of WIPI complexes

The formation of WIPI complexes is essential to the process of LC3 lipidation and the downstream assembly of autophagosomes (Proikas-Cezanne et al., 2015). To investigate whether E199L expression induces the appearance of WIPI puncta, Vero cells that had been transduced with E199L were analysed by confocal microscopy. Previously, the redistribution of LC3 by E183L was described (see section 5.2.5) and therefore cells that had been transduced with E183L were also analysed for the appearance of WIPI puncta in addition to analysis of control cells that had not been transduced. Cells were incubated for a total period of 24 hours during which cells were incubated for the last 3 hours in either complete cell media (non-starved) or EBSS (starved) prior to

being fixed and labelled for immunofluorescence. Cells were labelled using anti-WIPI and anti-HA tag antibodies to detect transduced cells.

Control cells that had not been transduced showed typically low numbers of WIPI puncta under nutrient replete conditions (Figure 6.2.1A) and similar to this, cells that had been transduced with E183L also showed low numbers of WIPI puncta (Figure 6.2.1B). Labelling of HA-tag protein revealed that cells expressing E183L did not exhibit an increase in WIPI puncta when compared to non-expressing cells (Figure 6.2.1C) demonstrating that E183L does not induce the appearance of WIPI puncta. In contrast, labelling of WIPI in cells that had been transduced with E199L showed some cells with a very high number of WIPI puncta and other cells with a comparable number of WIPI puncta to the control cells (Figure 6.2.1D). Labelling of HA-tag protein revealed that cells containing an elevated number of WIPI puncta were also expressing E199L (Figure 6.2.1E) suggesting that E199L is able to induce the assembly of WIPI complexes.

Control cells that had been incubated in EBSS showed a high number of WIPI puncta as would be expected under starvation conditions (Figure 6.2.2A). Cells that had been transduced with E183L (Figure 6.2.2B) demonstrated similar numbers of WIPI puncta to the control cells and visual inspection of cells expressing E183L did not show any difference to non-expressing cells (Figure 6.2.2C) indicating that E183L does not inhibit the assembly of WIPI complexes. The majority of cells that had been transduced with E199L (Figure 6.2.2D) showed a much greater number of WIPI puncta when compared to the control cells suggesting that the WIPI puncta were not formed exclusively in response to starvation. Visual inspection of cells expressing E199L (Figure 6.2.2E) revealed a higher number of WIPI puncta when compared to non-expressing cells. Interestingly, the WIPI puncta in some of the E199L expressing cells appeared to be concentrated in perinuclear locations rather than in the diffuse cytoplasmic pattern that was observed in the control cells and the E183L transduced cells. Collectively, these results indicate that E199L does not inhibit the formation of starvation-induced WIPI puncta but may be able to induce the formation of WIPI puncta in a way that is unaffected by the starvation status of the cells.

Figure 6.2.1 Transduction of Vero cells with E199L but not E183L induces the appearance of WIPI puncta

Vero cells were transduced with adenoviruses encoding either E183L (Panels B and C) or E199L (Panels D and E) and were incubated for 24 hours during which cells were incubated in complete Vero cell media for the final 3 hours. Additionally, control cells that had not been transduced were incubated in complete Vero cell media for 3 hours (Panel A). Cells were fixed and permeabilised in methanol and then labelled for WIPI shown in green, HA-tagged protein shown in red and nuclei shown in blue. Panels B and D show the same cells as Panels C and E respectively but with the red channel removed to allow for clearer observation of WIPI staining. Scale bars represent 10 μM.

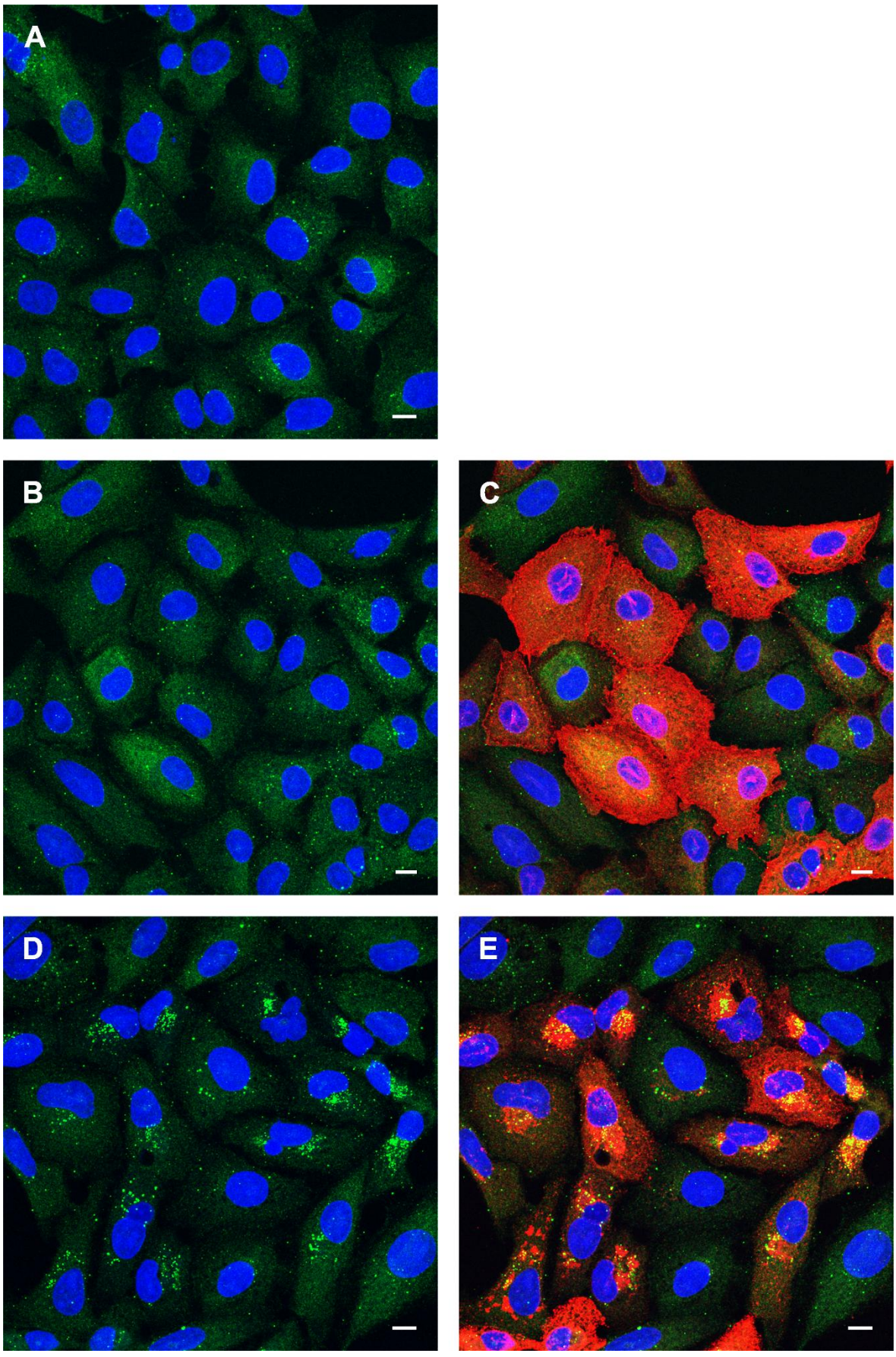

Figure 6.2.1 Transduction of Vero cells with E199L but not E183L induces the appearance of WIPI puncta

Figure 6.2.2 Transduction of Vero cells with E199L or E183L does not inhibit the formation of starvation-induced WIPI puncta

Vero cells were transduced with adenoviruses encoding either E183L (Panels B and C) or E199L (Panels D and E) and were incubated for 24 hours during which cells were incubated in EBSS starvation media for the final 3 hours. Additionally, control cells that had not been transduced were incubated in EBSS starvation media for 3 hours (Panel A). Cells were fixed and permeabilised in methanol and then labelled for WIPI shown in green, HA-tagged protein shown in red and nuclei shown in blue. Panels B and D show the same cells as Panels C and E respectively but with the red channel removed to allow for clearer observation of WIPI staining. Scale bars represent 10 μM.

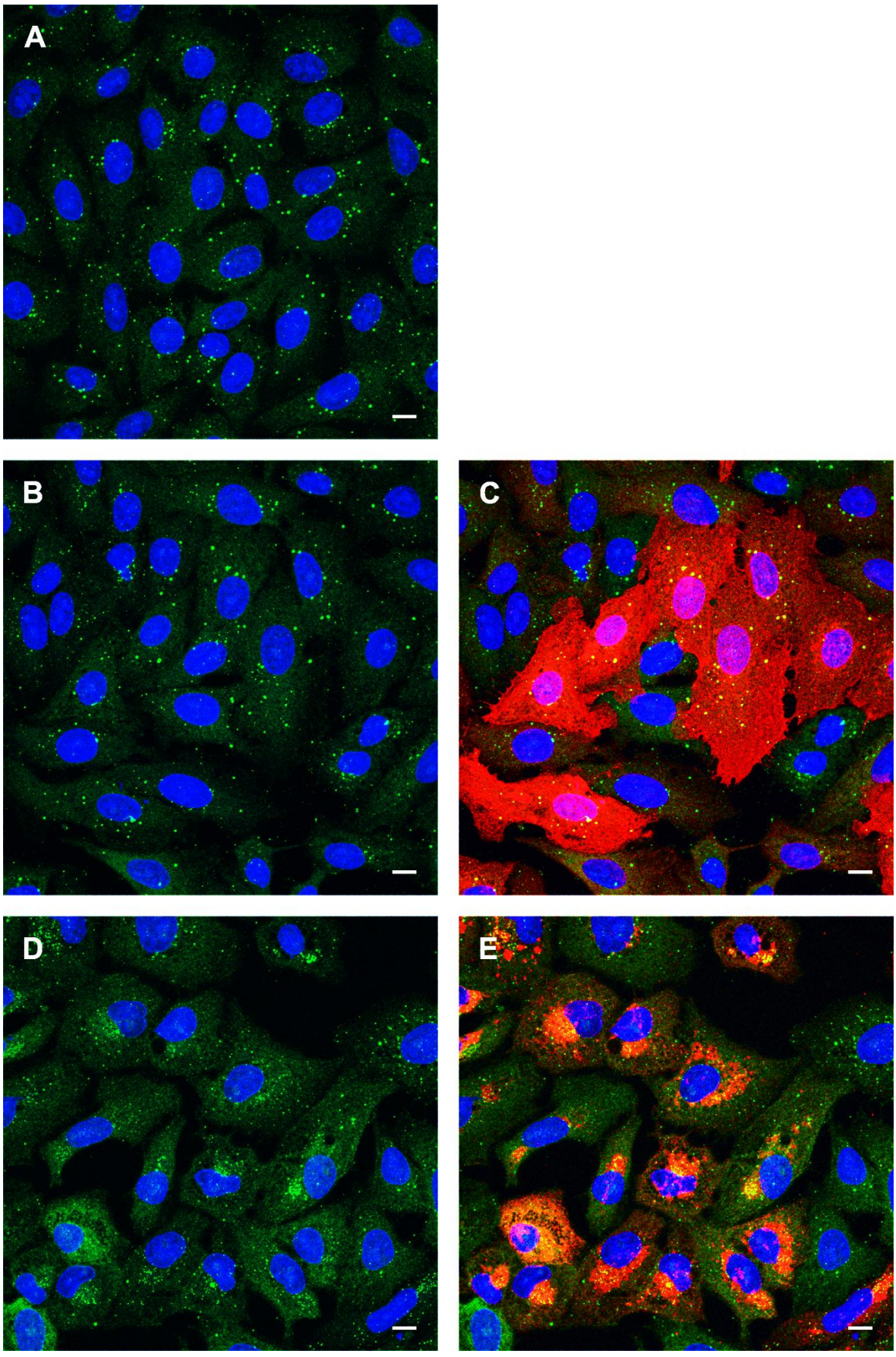

Figure 6.2.2 Transduction of Vero cells with E199L or E183L does not inhibit the formation of starvation-induced WIPI puncta

The number of WIPI puncta per cell was enumerated using Imaris software in 30 cells per experimental condition (Figure 6.2.3). This analysis revealed an increase in the number of WIPI puncta per cell under starvation when compared to non-starved conditions in the control cells ($P < 0.001$) demonstrating that autophagy was induced. Whereas a comparison between non-starved control cells and cells expressing E183L did not reveal any difference ($P > 0.05$), there was an increase in the number of WIPI puncta in non-starved cells expressing E199L when compared to non-starved control cells ($P < 0.001$) or E183L expressing cells ($P < 0.001$). A comparison of the starved cells revealed no difference ($P > 0.05$) between the control cells and cells expressing E183L but did reveal an increase in WIPI puncta in E199L expressing cells when compared to the control cells ($P < 0.001$). Collectively, these results confirm that expression of E183L does not induce or inhibit the formation of WIPI puncta but that expression of E199L is able to induce the formation of WIPI complexes in a manner that is unaffected by nutrient availability.

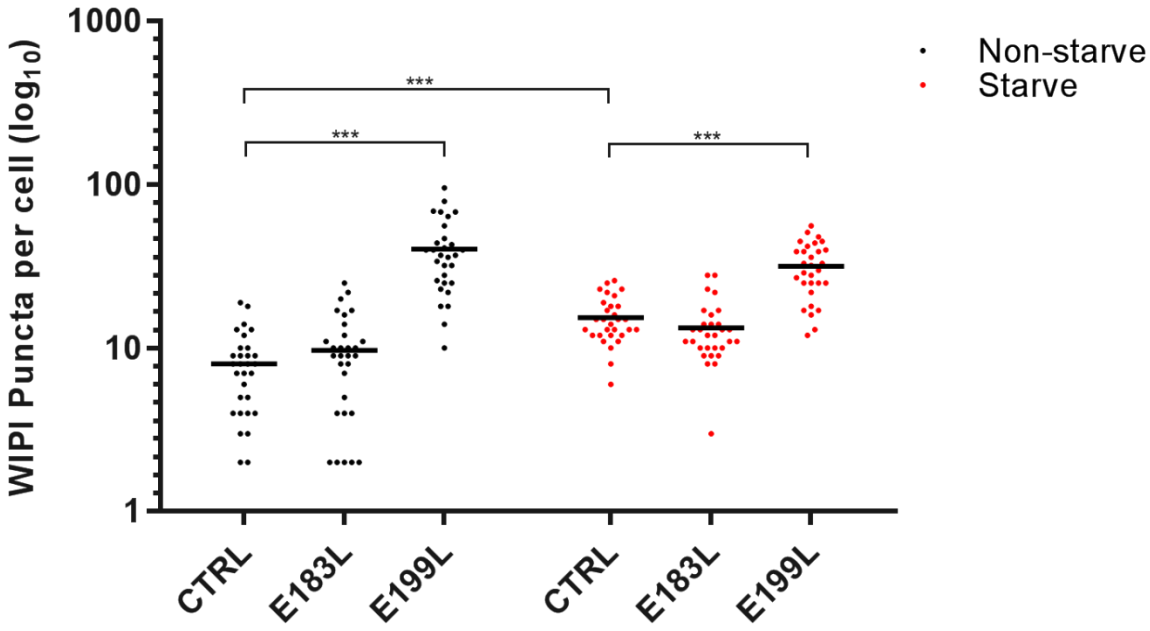

Figure 6.2.3 Imaris analysis confirms that E199L induces the formation of WIPI puncta but E183L does not

The number of WIPI puncta per cell for 30 individual cells per indicated experimental condition was quantified by Imaris analysis of confocal images. Vero cells were transduced with AdH5 vectors encoding either E183L or E199L and were incubated for a total of 24 hours. Prior to fixation, cells were either non-starved in complete cell media or starved in EBSS for 3 hours to induce autophagy. Separately, control cells (CTRL) that had not been transduced were also either non-starved or starved for 3 hours. Centre lines show the means. Statistical analysis was carried out in Minitab using analysis of variance with Tukey multiple comparisons test. Asterisks represent significant differences in value between indicated experimental conditions (*** = P value of <0.001).

6.2.3 E199L can be detected at the viral factory during late stages of replication

Previous results showed that ASFV promotes the formation of WIPI complexes at 4 hpi independently of nutrient availability (see section 3.2.4). In addition, WIPI and LC3 puncta were evident at the viral factory during the late stages of replication (see section 3.2.7). Whether WIPI and LC3 are vital proteins for virus replication is currently unknown as is the mechanism underlying their redistribution into punctate structures during infection. Following the results describing the appearance of WIPI puncta (see section 6.2.2) and LC3 labelled structures (see section 5.2.5) in cells expressing E199L, it is possible that E199L plays a role in inducing the appearance of WIPI and LC3 puncta in infected cells.

In their study on the characterisation of E199L, Sun and colleagues generated polyclonal antiserum against purified E199L protein in rabbits (Sun et al., 1996). To test whether the antiserum could be used to accurately label expression of E199L in transduced Vero cells, a confocal assay was carried out to detect colocalisation with anti-HA tag labelling. Cells were transduced with adenovirus encoding E199L-HA and incubated for 24 hours to allow protein expression. Separately, control cells that had not been transduced were maintained under the same conditions. Cells were then fixed and labelled for immunofluorescence using anti-HA tag antibodies and anti-E199L polyclonal antiserum.

In the control cells, no fluorescent signal was detected using either the anti-serum or the anti-HA tag antibody (Figure 6.3.1A) demonstrating the absence of any non-specific binding. Labelling of E199L transduced cells using rabbit antiserum (Figure 6.3.1B) revealed that protein was predominantly concentrated in discreet locations in the cell cytoplasm. A similar pattern was observed using the anti-HA tag antibody (Figure 6.3.1C) but this was in combination with a diffuse pattern of cytoplasmic protein expression that was not evident using rabbit antiserum. Viewed simultaneously, signal colocalisation from antiserum and anti-HA tag labelling was evident at sites of concentrated protein expression (Figure 6.3.1D) demonstrating the detection of E199L by the rabbit antiserum.

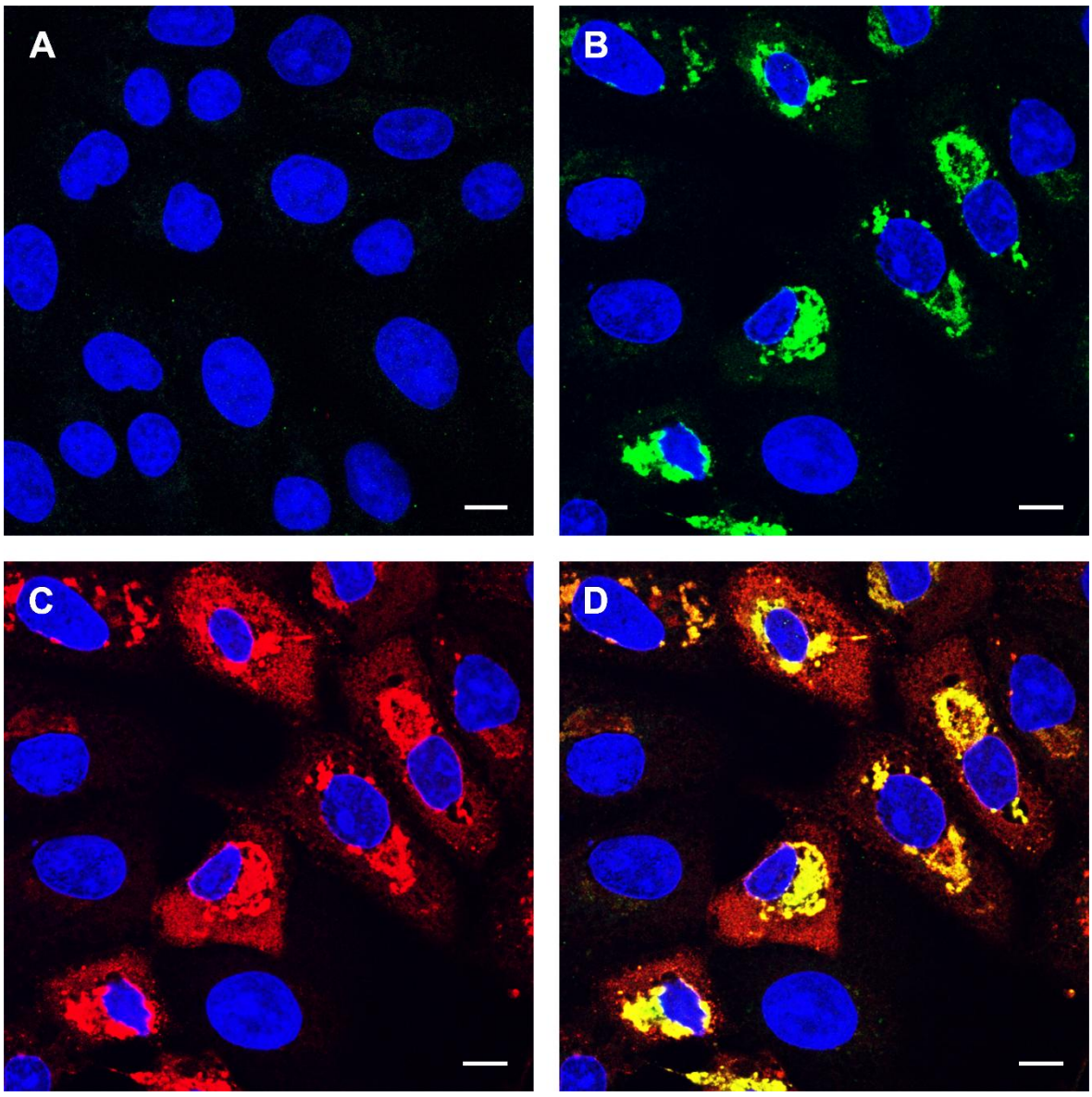

Figure 6.3.1 Rabbit antiserum detects E199L expression in transduced Vero cells

Vero cells were transduced with adenovirus encoding E199L (Panels B - D) and were incubated for 24 hours. Additionally, control cells that had not been transduced were incubated under the same conditions (Panel A). Cells were fixed and permeabilised and then labelled for E199L expression using rabbit antiserum shown in green (panel B), HA-tagged protein shown in red (Panel C) and nuclei shown in blue. Panel D shows the same cells as Panels B and C but with the red and green channels viewed simultaneously to show colocalisation (yellow). To detect non-specific antibody binding, control cells in panel A were imaged with both the red and green channels visible. Scale bars represent 10 µM.

To investigate if E199L may be involved in the appearance of LC3 and WIPI puncta, the timing of E199L expression and sub-cellular location of the protein was analysed by confocal microscopy in infected cells. Vero cells were infected with Ba71V (MOI 5) and harvested at 2 hour intervals over a 16 hour time course of infection. Following fixation, cells were probed with polyclonal rabbit antiserum against E199L and anti-p30 antibody to identify infected cells.

From 8 hpi, DAPI staining revealed the appearance of viral factories at the nuclear periphery of infected cells as would be expected. Inspection of cells labelled for E199L expression showed the appearance of protein from 10 hpi. This was predominantly located at the viral factory although some diffuse cytoplasmic labelling was also visible (Figure 6.3.2A). Labelling of viral protein p30 confirmed that E199L was only detected in cells expressing ASFV proteins (Figure 6.3.2B). The presence of E199L at the viral factory was also evident from 12 to 16 hpi (data not shown). Collectively, these results show that the timing and location of E199L expression coincides with the appearance of WIPI and LC3 puncta at the viral factory.

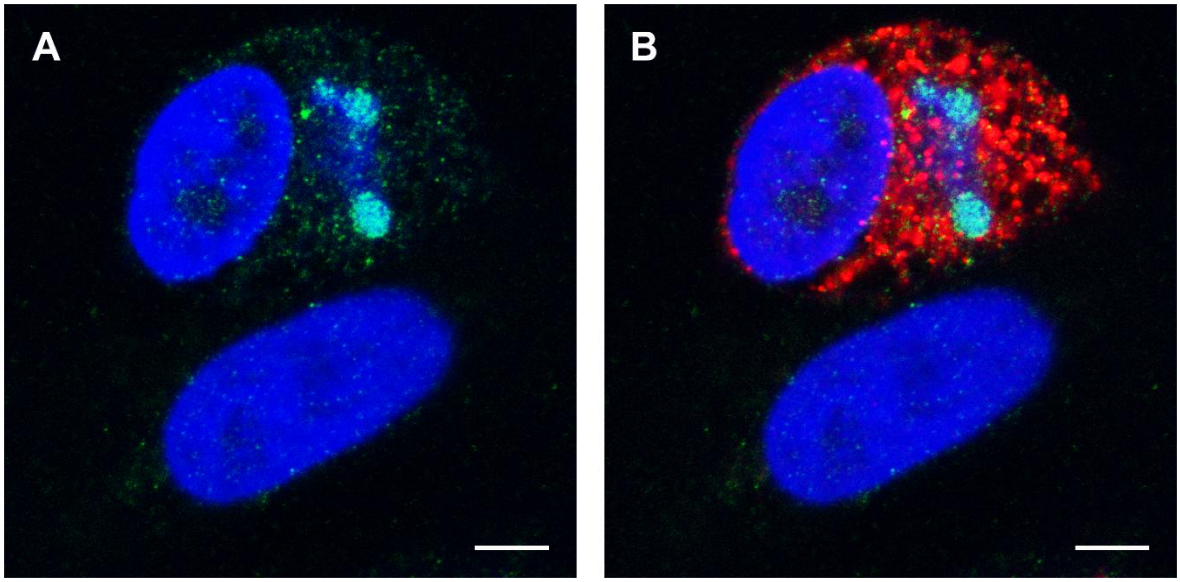

Figure 6.3.2 E199L is located at the viral factory at 10 hpi

Vero cells were infected with Ba71V (MOI 5) for 10 hours. Cells were fixed and permeabilised before labelling E199L and p30. E199L is shown in green, viral protein p30 is shown in red and nuclei and viral factories are shown in blue. Panel A shows the same infected cells as Panel B but with the red channel removed to allow for clearer observation of E199L staining. Scale bars represent 5 µM.

6.2.4 Electron microscopy analysis of cells transduced with AdH5 E199L

Visualised by confocal microscopy, the LC3-labelled structures induced by E199L expression did not resemble the typical rounded punctate structures that are representative of autophagosomes (see Figure 5.5.4). LC3-labelling was clumped together into much larger structures and was not observed as the dispersed cytoplasmic puncta that are usually associated with the induction of autophagy. This suggests that the redistribution of LC3 by E199L is not indicative of an autophagy response. However, evidence of WIPI complex assembly as well as LC3 lipidation in E199L expressing cells are both hallmarks of the early stages of autophagosome formation. To gain further clarity into whether E199L is able to induce the appearance of autophagosomes, transduced cells were examined by electron microscopy (EM). Expression of E183L was previously shown to also

induce the redistribution of LC3 (see Figure 5.5.3) and was therefore used as a control in this experiment. Vero cells were transduced with adenovirus encoding either E199L or E183L and were incubated for 24 hours to allow protein expression. Additionally, control cells that had not been transduced were incubated under the same conditions. Cells were fixed and processed for EM analysis according to the methods described in section 2.9.

Visual inspection of the control cells revealed a typically normal cell environment with an intact nuclear membrane with cell organelles including mitochondria located at the nuclear periphery (Figure 6.4A). In contrast, cells that had been transduced with E183L demonstrated large arrays of membrane extending from and located in proximity to the nucleus (Figure 6.4B). Evidence of double-membrane vesicles consistent with the size of autophagosomes (0.5 to 1.5 μM in mammalian cells) were not apparent in these cells suggesting that the redistribution of LC3 is not linked to the induction of autophagy in E183L expressing cells. In cells that had been transduced with E199L, changes to the ER were apparent (Figure 6.4C). Dark patches of staining, believed to be locations of condensed protein were observed amongst ER membrane. Also observed in and around the ER were membrane-bound vesicles, however these were much smaller than the size typically associated with autophagosomes. These results therefore suggest that the large LC3 labelled structures induced by E199L do not correspond to mature autophagosomes.

Figure 6.4 Electron microscopy analysis of cells transduced with E183L and E199L

Vero cells were transduced with adenovirus encoding either E183L (Panel B) or E199L (Panel C) and incubated for 24 hours to allow protein expression. Control cells (Panel A) that had not been transduced were incubated under the same conditions. Cells were fixed and processed for EM analysis. Arrows in Panel B indicate whorls of ER. Arrows in Panel C indicate patches of condensed protein. N = nucleus. Scale bars are represented below each panel.

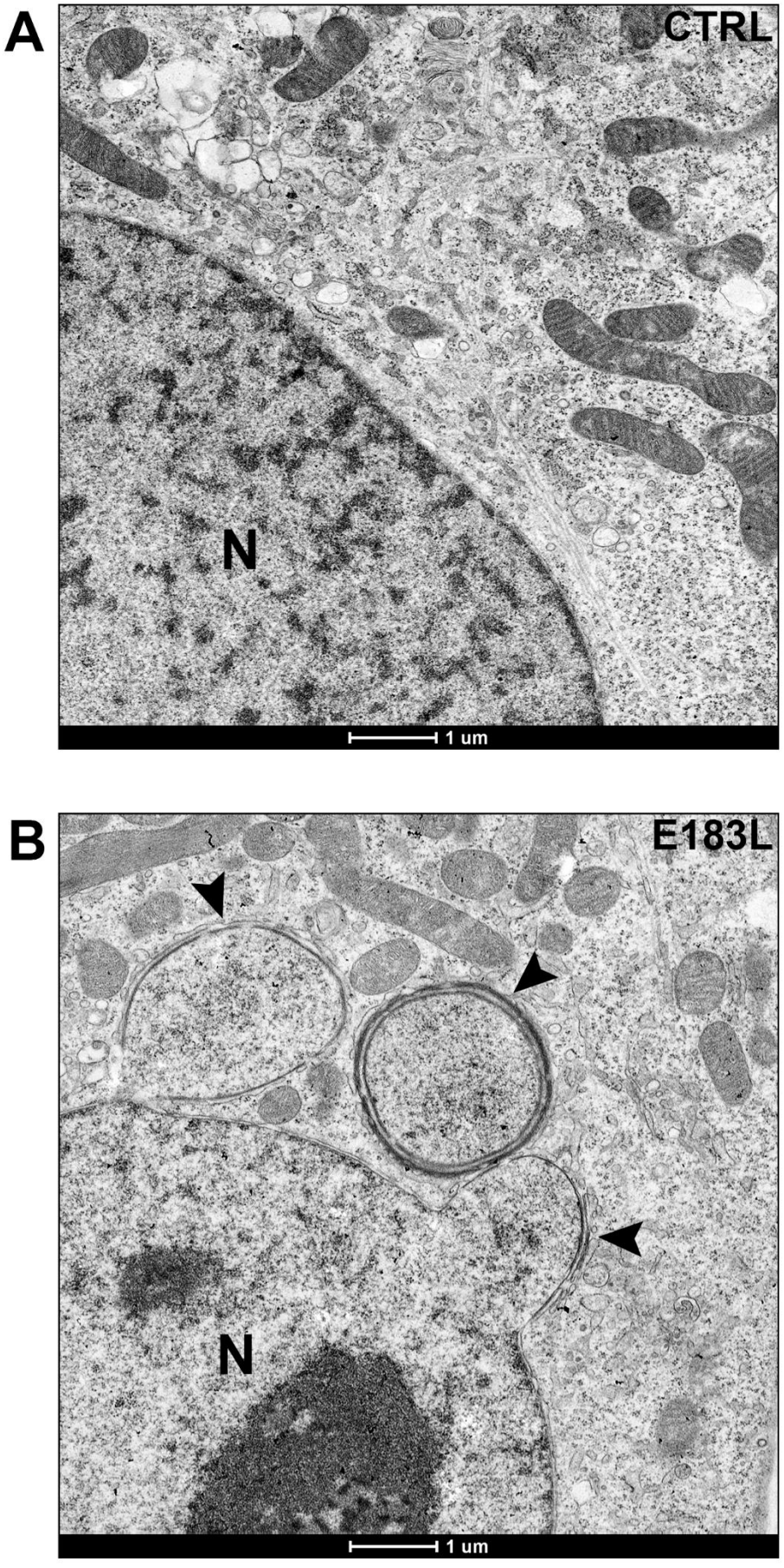

Figure 6.4 Electron microscopy analysis of cells transduced with E183L and E199L

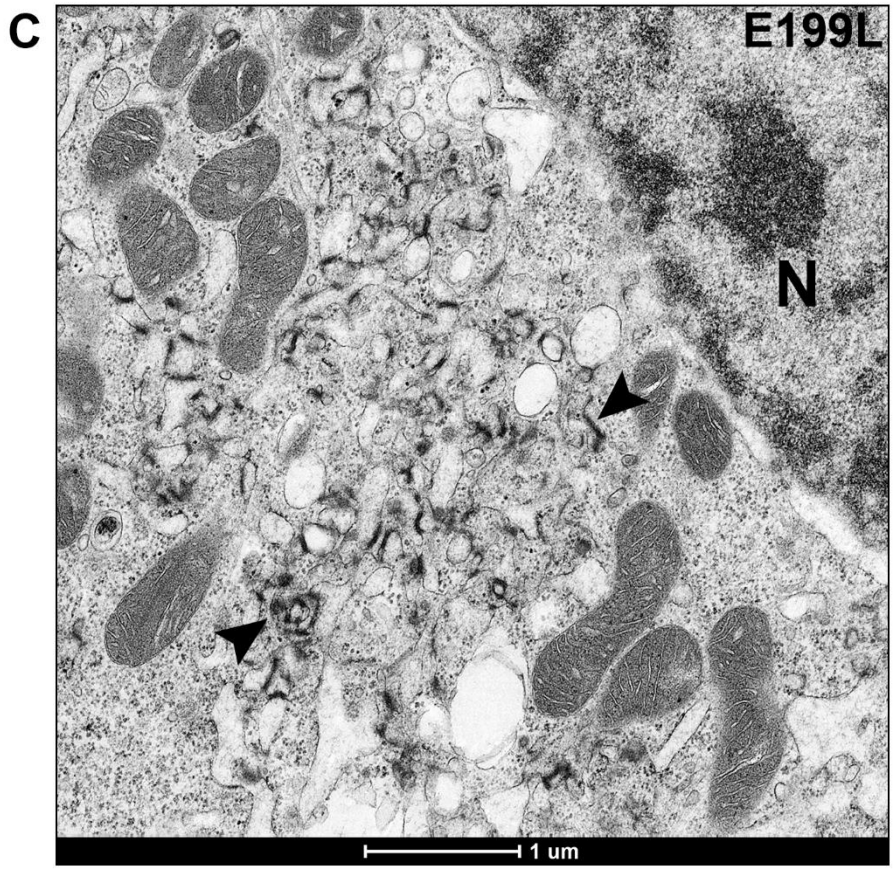

Figure 6.4 Electron microscopy analysis of cells transduced with E183L and E199L

Vero cells were transduced with adenovirus encoding either E183L (Panel B) or E199L (Panel C) and incubated for 24 hours to allow protein expression. Control cells (Panel A) that had not been transduced were incubated under the same conditions. Cells were fixed and processed for EM analysis. Arrows in Panel B indicate whorls of ER. Arrows in Panel C indicate patches of condensed protein. N = nucleus. Scale bars are represented below each panel.

6.2.5 Mass spectrometry analysis of E199L interacting proteins

To gain further insight into whether E199L could be involved in the regulation of autophagy, mass spectrometry (MS) analysis was used to detect potential E199L interacting proteins (mass spectrometry methods are described in section 2.10). Vero cells were transduced with AdH5 E199L-HA and were incubated for 24 hours to allow protein expression. In addition, control cells that had not been transduced were incubated under the same conditions. Three replicates of each of the transduced and control cells were included in the experiment. Cells were lysed and following centrifugation, cell supernatants were incubated with anti-HA affinity matrix. Captured protein was eluted from the matrix and samples were prepared for analysis by Western blot and were probed using anti-HA tag antibody.

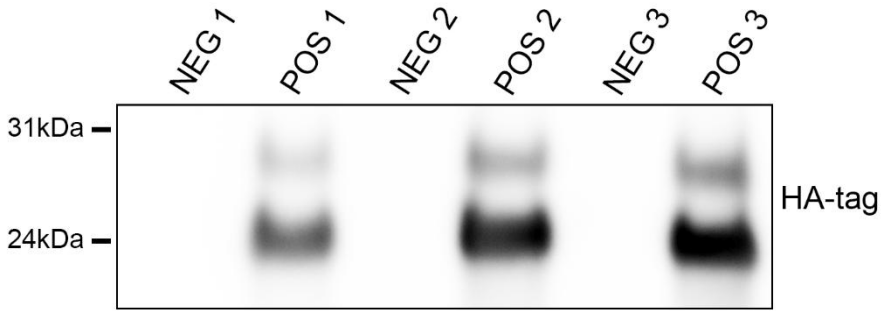

Figure 6.5.1 Analysis of E199L expression and capture using anti-HA affinity matrix

Vero cells were transduced with adenovirus encoding E199L-HA and were incubated for 24 hours. Control cells that had not been transduced were incubated under the same conditions. Three replicates of each of the transduced (POS 1-3) and control cells (NEG 1-3) were analysed. Cell lysates were incubated with anti-HA affinity matrix and samples were generated from eluted supernatant before preparation for resolution by bis-Tris PAGE and transfer to PVDF membrane. Finally, samples were probed using an anti-HA tag + HRP-conjugated antibody. The positions of molecular mass markers are indicated to the left of the gel.

In each of the samples prepared from E199L transduced cells (POS 1-3) two protein bands were detected and no bands were detected in the samples prepared from the control cells (NEG 1-3) (Figure 6.5.1). Inspection of the protein bands in each sample from the transduced cells revealed that the lower band had an apparent molecular weight of approximately 24kDa and the upper band had an apparent molecular weight of approximately 30kDa. In each sample, the lower band indicated a much greater amount of protein when compared to the upper band. The molecular weight of E199L is approximately 22kDa (Sun et al., 1996) and would therefore roughly correspond to the lower band. The small difference in size could be due to the addition of an HA tag or alternatively the high level of protein expression may give the appearance of a greater molecular weight. The identity of the upper band is unknown but could be a protein with altered levels of glycosylation or myristoylation. E199L contains two potential glycosylation sites and five potential myristoylation sites (Sun et al., 1996).

MS analysis was conducted on the eluted samples as well as samples prepared by treatment of the affinity matrix with reducing buffer to remove remaining proteins. A substantially greater amount of data was generated from analysis of the samples prepared from the affinity matrix when compared to samples prepared from the initial elution. For this reason, descriptions of the results pertain to data generated from the affinity matrix samples. MS spectra data was searched against either a human protein database or *Chlorocebus sabaeus* (African green monkey) protein database. The highly characterised human proteome was used to provide a comprehensive list of E199L interacting proteins and the less characterised monkey proteome was used to avoid potential loss of statistically significant proteins that may have occurred by conducting the experiment in Vero cells.

Significant proteins were determined by statistical comparison of intensity values between transduced and non-transduced cells where a p-value <0.05 and a fold change >2 were considered statistically significant.

A total of 49 significant proteins were generated from the human data in comparison to 35 from the monkey data. In both cases, the large majority of proteins were identified from the proteasome (31 from human and 23 from monkey) which may be due to mis-folding or ubiquitination of E199L. The remaining significant proteins are presented in Appendix I and inspection of these did not reveal any belonging to the autophagy pathway. Strikingly, examination of the human data revealed 10 proteins that are involved in ER function. Calreticulin, an ER chaperone protein was identified as the most significant E199L interacting protein. The human data is presented as a volcano plot in Figure 6.5.2. Significant proteins related to ER function have been highlighted and are also listed in Table 6.1.

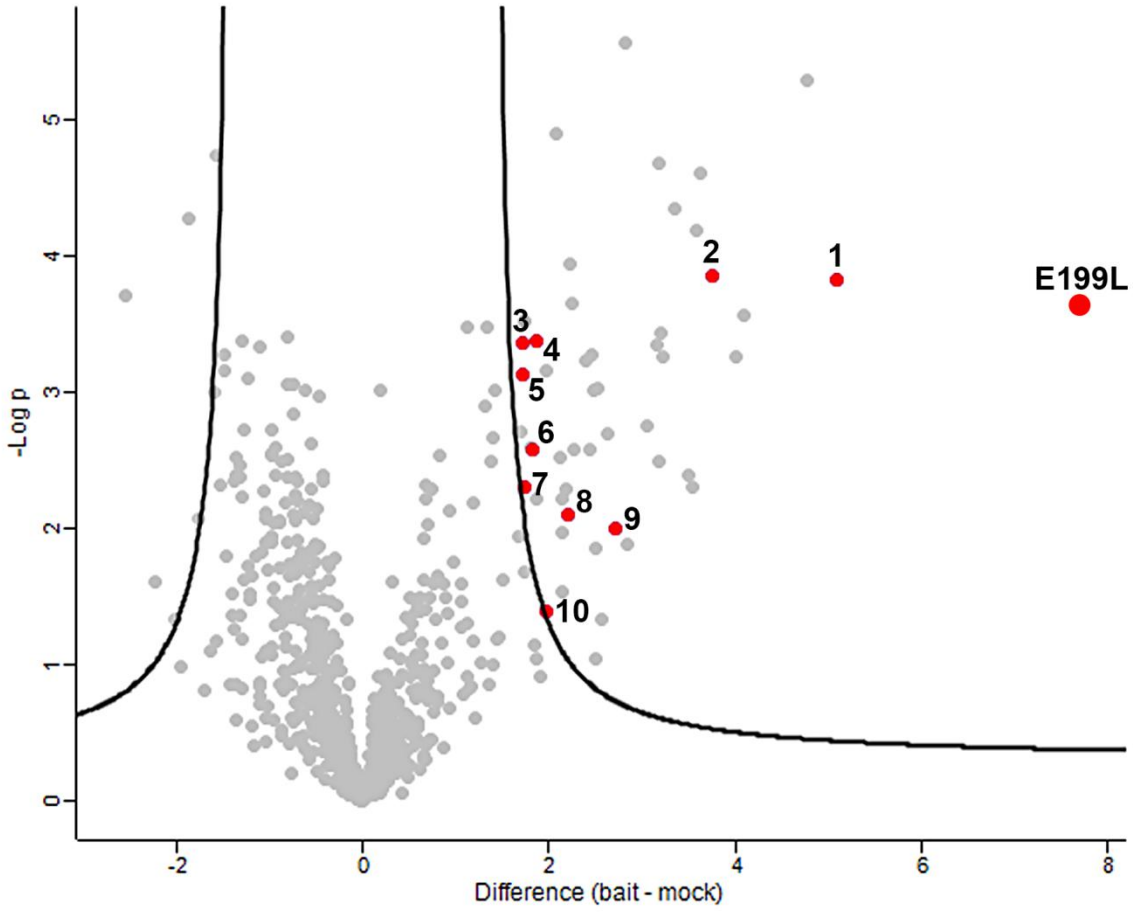

Figure 6.5.2 Analysis of E199L interacting proteins

Analysis of E199L interacting proteins identified by mass spectrometry where each dot represents a unique protein. Statistically significant proteins are positioned to the right of and above the significance curve signifying a p-value <0.05 and a fold change >2. Significant proteins related to ER function are highlighted in red in addition to the E199L bait protein. Numbered dots correspond to the proteins presented in Table 6.1

Table 6.1 Significant E199L interacting proteins related to ER function

#	Protein name	Function
1	Calreticulin	Calcium-binding chaperone that promotes folding, oligomeric assembly and quality control in the ER
2	Glucosidase 2 subunit beta	Subunit of glucosidase II that cleaves glucose residues from the oligosaccharide precursor of immature glycoproteins
3	Calnexin	Calcium-binding protein that interacts with newly synthesized glycoproteins in the ER
4	Prolyl 4-hydroxylase subunit alpha-1	Catalyses the post-translational modification of collagens and other proteins
5	Prolyl 4-hydroxylase subunit alpha-2	Catalyses the post-translational modification of collagens and other proteins
6	Endoplasmin	Molecular chaperone that functions in the processing and transport of secreted proteins
7	Vesicular integral-membrane protein VIP36	Plays a role as an intracellular lectin in the early secretory pathway
8	Large proline-rich protein BAG6	Molecular chaperone preventing the aggregation of misfolded and hydrophobic patches-containing proteins
9	Protein ERGIC-53	Mannose-specific lectin that may be involved in the sorting or recycling of proteins, lipids, or both
10	Peptidyl-prolyl cis-trans isomerase FKBP10	Accelerates the folding of proteins during protein synthesis

In summary, MS analysis did not uncover any direct links between E199L and the autophagy machinery. However the data did reveal a potential link to the ER which would be in agreement with EM analysis that showed changes to the ER in cells transduced with E199L.

6.2.6 E199L colocalises with the ER chaperone calnexin

Calnexin (Cnx) is an integral ER membrane protein that functions in the retention of glycoproteins within the ER until they are correctly folded or targeted for degradation (Williams, 2006). Along with calreticulin, Cnx is one of the most well characterised molecular ER chaperones and can act as a useful ER marker in immunofluorescent studies. MS analysis of E199L interacting proteins revealed a significant interaction with Cnx (see section 6.2.5). To further examine the link between E199L and the ER, including the interaction with Cnx, Vero cells were transduced with AdH5 E199L-HA and were incubated for 24 hours to allow protein expression. Control cells that had not been transduced were incubated under the same conditions. Cells were fixed and labelled for immunofluorescence using anti-Cnx antibodies as well as anti-HA tag antibodies to identify cells expressing E199L. In addition, cells were labelled with anti-WIPI antibodies to identify whether WIPI complexes induced by E199L expression are located at the ER.

Control cells that were labelled with anti-Cnx antibodies demonstrated a typical ER pattern that is predominantly concentrated around the periphery of the nucleus and radiates outwards into the cell

cytoplasm (Figure 6.6A). Labelling of the control cells with WIPI antibodies revealed a very low number of WIPI puncta as would be expected in cells incubated under nutrient replete conditions (Figure 6.6A). In contrast, cells that were transduced with E199L showed a much greater number of WIPI puncta and these were observed in close proximity to areas of abundant E199L expression (Figure 6.6B). This confirms the previous result describing the induction of WIPI complex formation in E199L expressing cells (see section 6.2.2). When compared to the network-like pattern of Cnx observed in the control cells, cells expressing E199L showed an altered pattern of labelling in which Cnx seemed to be concentrated in defined areas of the cell cytoplasm (Figure 6.6C). WIPI labelling showed that WIPI puncta were clustered together in close proximity to the labelled areas of Cnx (Figure 6.6C). Viewed simultaneously, signal colocalisation from Cnx and anti-HA tag labelling was evident at sites of extensive E199L expression (Figure 6.6D) demonstrating that E199L was located at the ER. Collectively, these results support previous observations that E199L is evident in the ER where it likely interacts with Cnx.

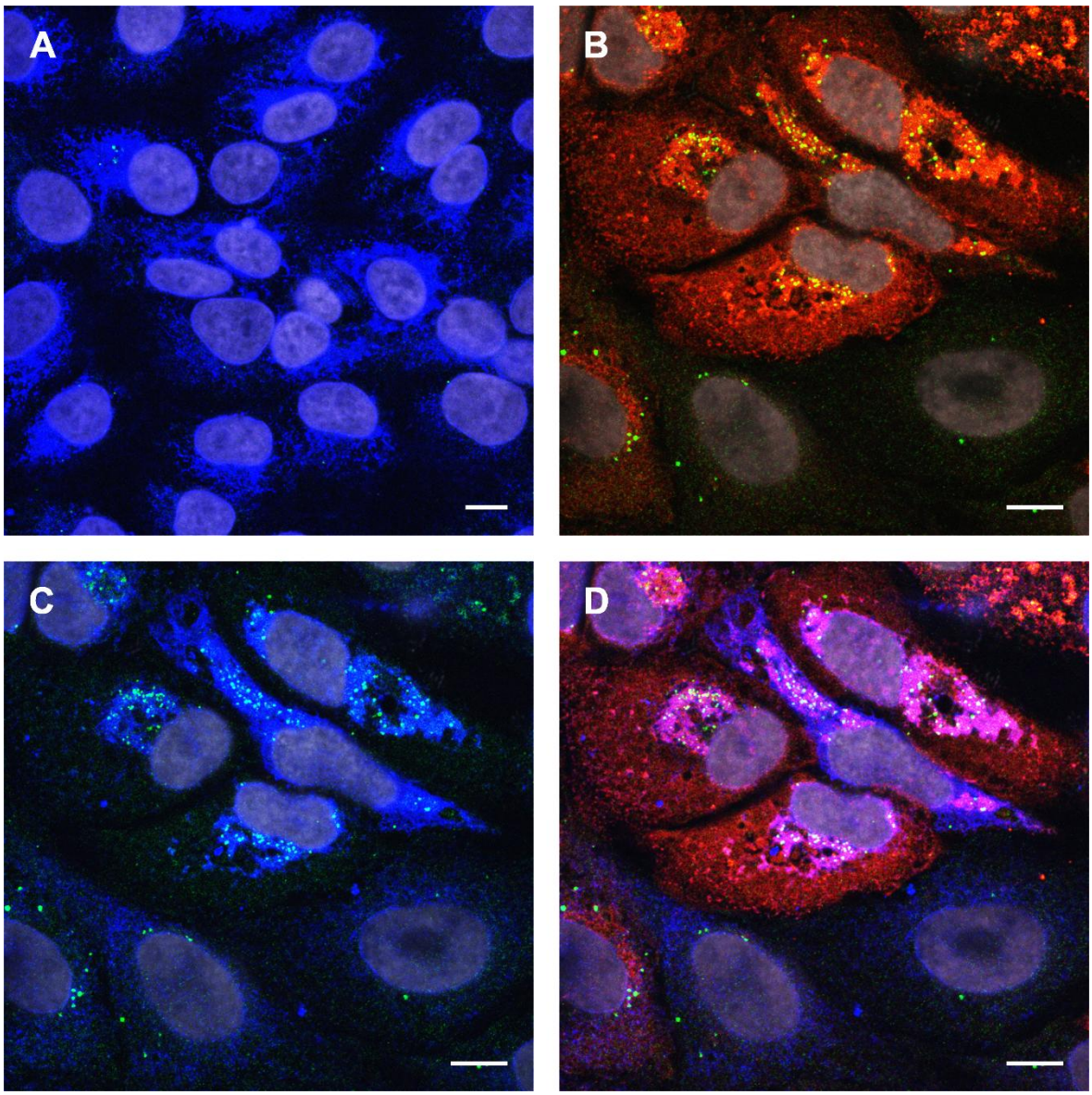

Figure 6.6 E199L colocalises with the ER chaperone calnexin

Vero cells were transduced with adenovirus encoding E199L (Panels B - D) and were incubated for 24 hours. Additionally, control cells that had not been transduced were incubated under the same conditions (Panel A). Cells were fixed and permeabilised and then labelled for calnexin shown in blue (Panels A; C and D), WIPI shown in green (Panels A - D), HA-tagged protein shown in red (Panels B and D) and nuclei shown in grey. Panel D shows the same cells as Panels B and C but with the red and blue channels viewed simultaneously to show colocalisation (pink). Scale bars represent 10 µM.

6.2.7 E199L expression induces ER stress

The ER is the site where proteins are processed, modified and folded prior to being transported to other locations in the cell. Various stresses such as hypoxia, calcium dysregulation and viral infection can alter the balance of protein folding within the ER, leading to the accumulation of unfolded proteins. If this accumulation continues, the unfolded protein response (UPR) is triggered (Chakrabarti et al., 2011). Activation of the UPR can lead to upregulated expression of the pro-

apoptotic transcription factor C/EBP homologous protein (CHOP). Elevated levels of CHOP can therefore be used as an indication of ER stress. Prolonged activation of the UPR has been shown to induce autophagy (Bernales et al., 2006) and could potentially explain the LC3 lipidation and formation of WIPI complexes in E199L expressing cells.

To investigate if E199L expression induces ER stress, Western blot analysis was carried out to determine the levels of CHOP in transduced cells. LC3 lipidation and Cnx levels were also analysed. Vero cells were transduced with adenovirus encoding either E199L, E183L or GFP and were incubated for 24 hours to allow protein expression. Control cells that had not been transduced were incubated under the same conditions. Separately, cells were treated for 16 hours with 20 µg/ml of the N-glycosylation inhibitor tunicamycin. Treatment with tunicamycin has been shown to induce the UPR and trigger an increase in the expression of CHOP (Okada et al., 2002). Samples were prepared from cells for analysis by immunoblotting and probed using anti-CHOP, anti-calnexin, anti-LC3, anti-GFP, anti-HA tag and anti-γ tubulin antibodies.

Expression of GFP was only detected in cells transduced with AdH5 GFP as expected which demonstrates the successful transduction of the cells (Figure 6.7). Similarly, expression of HA-tagged protein was only detected in cells that were transduced with E183L or E199L. Labelling for CHOP revealed an elevated amount in cells that were treated with tunicamycin when compared to the control cells demonstrating the induction of the UPR in response to ER stress. When compared to the control cells, greater amounts of CHOP were detected in E199L and E183L transduced cells but not GFP transduced cells suggesting that E199L and E183L expression trigger the UPR response. Interestingly, transduction with E183L led to a much greater amount of CHOP compared to cells transduced with E199L which may reflect a difference in the degree of induced ER stress or a difference in protein expression levels.

Analysis of LC3-II levels revealed a much greater amount in cells that were treated with tunicamycin when compared to the control cells indicating that LC3 was lipidated in response to ER stress. Cells that were transduced with E183L or E199L also showed greater amounts of LC3-II when compared to the control cells which confirms the previous result that described the lipidation of LC3 by E199L (see Figure 6.1) and further reveals that E183L has the same effect. As seen previously in Figure 6.1, cells transduced with GFP showed a similar amount of LC3-II to the control cells demonstrating that transduction with AdH5 alone does not lead to LC3 lipidation. A comparison of Cnx levels revealed a similar amount between the control cells and all of the transduced cells, however in the tunicamycin treated cells, a slightly increased level of Cnx was detected. Taken together these results indicate that the lipidation of LC3 in response to E199L expression could be the consequence of an ER stress response.

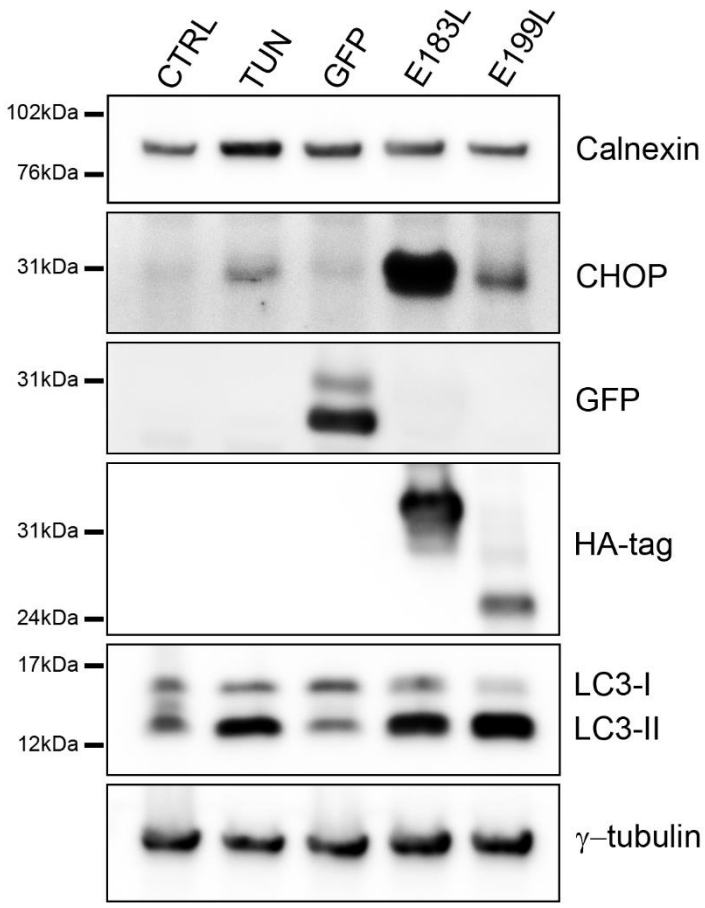

Figure 6.7 E199L expression induces ER stress

Vero cells were transduced with adenovirus encoding GFP, E183L or E199L and were incubated for 24 hours to allow protein expression. Control cells (CTRL) that had not been transduced were incubated under the same set of conditions. Separately, cells were treated for 16 hours with 20 µg/ml tunicamycin (TUN) to induce ER stress. Cells were then lysed and samples prepared for resolution by bis-Tris PAGE before transfer to PVDF membrane. Finally, samples were probed with anti-calnexin, anti-CHOP, anti-GFP, anti-HA tag, anti-LC3 and anti-γ tubulin antibodies followed by appropriate HRP-conjugated secondary antibodies. The positions of molecular mass markers are indicated to the left of the gels.

6.3 Discussion

ASFV infection induces the appearance of WIPI and LC3 puncta at the viral factory during the late stages of viral replication. The appearance of the puncta coincides with the lipidation of LC3 but the function of these events in the context of viral replication is currently unknown as is the mechanisms underlying their occurrence. E199L is expressed as a late protein and transducing cells with E199L leads to the redistribution of LC3. The experiments that were described in this chapter were aimed at exploring the potential link between E199L and the puncta that are observed at the viral factory.

Vero cells that were transduced with E199L and analysed by Western blot showed elevated levels of LC3-II when compared to control cells or cells transduced with GFP (Figure 6.1) demonstrating that E199L expression causes the lipidation of LC3. The accumulation of LC3-II was evident under nutrient replete and starvation conditions indicating that this effect was not dependent on nutrient availability. Similarly, imposing a block on lysosome fusion using Bafilomycin A1 did not alter the levels of LC3-II. These results therefore suggest that the redistribution and lipidation of LC3 by E199L are likely linked but that these effects are probably not associated with a canonical autophagy response.

Confocal analysis was carried out on cells that had been transduced with E183L or E199L to determine if expression of these proteins induces the formation of WIPI complexes which are critical to the assembly of autophagosomes. The results showed that under nutrient replete conditions, E199L stimulated the formation of WIPI complexes whereas E183L did not (Figure 6.2.1). Under starvation conditions, similar numbers of WIPI puncta were observed between E183L expressing cells and non-transduced control cells, however in cells expressing E199L a much greater number of WIPI puncta were evident (Figure 6.2.2). These results were confirmed using Imaris analysis (Figure 6.2.3) and demonstrated that E199L stimulates the formation of WIPI complexes independently of nutrient availability, once again suggesting that these effects do not occur via the canonical autophagy pathway. In support of this, the WIPI puncta in E199L expressing cells were predominantly located in perinuclear regions which was in stark contrast to the diffusely located WIPI puncta in the control cells possibly suggesting an autophagy-independent function. Interestingly, WIPI puncta were observed in perinuclear locations in infected cells at 4 hpi (see section 3.2.4), however it is unlikely that this is linked to E199L expression which occurs during the late stages of viral replication. The fact that E183L expression does not induce the appearance of WIPI puncta is also interesting as previously it was shown that E183L causes the redistribution of LC3 (see section 5.2.5). This could therefore suggest that the redistribution of LC3 in these cells is not indicative of the autophagosome assembly process.

To investigate a possible link between E199L and the appearance of WIPI and LC3 puncta at the viral factory, infected Vero cells were monitored for E199L expression by confocal microscopy over a time course of infection. Testing of polyclonal antiserum showed that it accurately detected E199L in transduced cells and was therefore suitable for the labelling of infected cells (Figure 6.3.1). From 10 hpi infection, E199L was detected at the viral factory (Figure 6.3.2) and was also evident at the viral factory between 12 and 16 hpi confirming that E199L was expressed as a late protein. LC3 and WIPI puncta were shown to appear at the viral factory from 12 hpi and 14 hpi respectively (see section 3.2.7), indicating that the timing of E199L expression coincides with these events. E199L therefore may play a role in stimulating the formation of WIPI and LC3 puncta late in infected cells.

Electron microscopy analysis was used to analyse cells that had been transduced with E183L or E199L to determine whether the redistribution of LC3 that was observed by confocal microscopy was potentially linked to the formation of autophagosomes. Images of cells transduced with E183L revealed striking changes to the ER which was arranged in large arrays of membrane at the nuclear periphery (Figure 6.4B). These were consistent with the disc-shaped whorls of ER that were previously described (Windsor et al., 2012) and demonstrate the extensive reorganisation of the ER by E183L. An abnormal appearance of the ER was also observed in E199L transduced cells in which the ER exhibited numerous patches of dark staining material believed to be condensed protein (Figure 6.4C). These results may point to the ER as the site of WIPI complex assembly and LC3 redistribution in cells expressing E199L. In this regard, conducting correlative light electron microscopy (CLEM) analysis would provide clarity. Double membrane vesicles consistent with the size of autophagosomes were not observed in either E183L or E199L transduced cells indicating that the redistribution of LC3 is not the result of a canonical autophagy response.

To investigate whether E199L interacts with any proteins belonging to the autophagy pathway, E199L was affinity purified from transduced cell lysates and samples were analysed by mass spectrometry. Prior to this, Western blot analysis showed that E199L had been successfully expressed, captured and eluted from the affinity matrix (Figure 6.5.1). Analysis of the mass spectrometry data did not uncover any significant proteins that are involved in the autophagy pathway (Figure 6.5.2), however ten proteins related to ER function were revealed as having a significant interaction with E199L (Figure 6.5.2 and Table 6.1). In similarity to the electron microscopy analysis, this data therefore suggests a link between E199L expression and the ER which could indicate that the redistribution of LC3 in E199L transduced cells occurs at the ER. This may be interesting as the autophagy pathway is intimately associated with the ER which acts as the site of early autophagosome assembly and also contributes membrane to the expanding autophagosome (Axe et al., 2008, Ge et al., 2013). In addition, studies have shown that the ER is directly involved in the assembly of virus particles at the periphery of viral factories (Andres et al., 1998, Rouiller et al., 1998) and therefore the location of E199L at the viral factory may suggest a functional role linked to the ER and virus morphogenesis.

To confirm if E199L expression is located at the ER, an immunofluorescence experiment was carried out in which transduced cells were labelled for the detection of E199L and the ER. In addition, WIPI complexes were labelled to assess if they were located near the ER. Figure 6.6 shows that E199L expression colocalised with the ER chaperone protein calnexin which mass spectrometry analysis had shown was a significant E199L interacting protein (see section 6.2.5). This confirms the link between E199L and the ER which could point to an ER-related function. Interestingly, WIPI puncta were seen clustered together in close proximity to the ER which may suggest that the stimulation of WIPI complex formation and the redistribution of LC3 by E199L is linked to ER disruption.

Studies of ER stress and the UPR have uncovered important connections with the autophagy pathway. In yeast cells, the UPR stimulates significant ER proliferation and autophagy provides a means to limit this expansion by degrading ER-derived membrane stacks to maintain homeostasis (Bernales et al., 2006). Similar links between the ER and autophagy have been described in mammalian cells in which autophagy acts to degrade unfolded proteins accumulated in the ER (Ogata et al., 2006) and is also involved in ER turnover (Khaminets et al., 2015). Although there are mechanistic differences between yeast and mammalian cells, collectively these events are termed ER-phagy (Lipatova and Segev, 2017).

To investigate whether E199L may be inducing the UPR and stimulating ER-phagy, transduced cells were analysed by Western blot to detect changes in CHOP expression (Figure 6.7). The analysis showed that cells that were treated with the ER stress inducer, tunicamycin, demonstrated a substantially greater level of CHOP expression compared to control cells and that CHOP expression was also upregulated in E199L transduced cells. These results suggest that E199L expression is able to induce an ER stress response. An elevated level of CHOP was also observed in cells transduced with E183L but not in cells transduced with GFP. Examination of LC3-II levels showed that tunicamycin treatment had led to an increase in the amount of LC3-II demonstrating that LC3 was lipidated in response to ER stress most likely due to the stimulation of ER-phagy. Similar levels of LC3 lipidation were evident in cells transduced with E199L and E183L which may suggest that expression of these proteins had caused the induction of ER-phagy. Interestingly, labelling of calnexin revealed that upregulation of expression had only occurred in the tunicamycin treated cells which could reflect the difference in how ER stress had been induced compared to the transduced cells.

Newly synthesised polypeptides are targeted to the ER as they emerge from the ribosome. Proteins that contain a signal sequence or hydrophobic domain are bound by the signal recognition particle which prevents inappropriate targeting of peptides to the ER (Keenan et al., 2001). The C-terminal hydrophobic domain of E199L is likely to play a part in directing it to the ER and it may be possible that the level of expression exceeds the capacity of the ER to maintain correct protein folding. Alternatively, the correct folding of E199L could be reliant on a virally-encoded chaperone as is the case with the specialised folding of the major capsid protein p72 by B602L (Cobbold et al., 2001). Finally, the addition of an HA-tag at the C-terminus of E199L may in some way disrupt its folding ability. The high number of E199L-interacting proteasomal proteins detected by mass spectrometry suggests that E199L is degraded by the proteasome and is a further indication of protein mis-folding. In all of these scenarios, activation of the UPR which was demonstrated by the induction of CHOP expression, could lead to an autophagy response which may explain the redistribution of LC3 and appearance of WIPI puncta in E199L transduced cells. However, the absence of autophagosomes as shown by electron microscopy analysis (Figure 6.4C) is at odds with this hypothesis. The reason for this discrepancy is unknown but it may be possible that such a

high level of protein expression alters the internal cell environment to the extent of disrupting normal cell function. Indeed, tiny vesicles were observed in the vicinity of the ER but it is not known whether these consisted of single or double membranes. Evidence of double membrane vesicles could raise the possibility that these are early autophagosomes that have failed to mature.

To provide greater insight into the link between the UPR and ER-phagy, future immunofluorescence experiments could be aimed at detecting similarities in the pattern of LC3 redistribution between Vero cells treated with tunicamycin and cells transduced with E199L. Analysing whether WIPI complexes are assembled in response to tunicamycin treatment may also help to understand why WIPI puncta appear in cells transduced with E199L but not in cells transduced with E183L. E183L has been shown to cause the collapse of ER cisternae (Windsor et al., 2012) and therefore may induce a different ER stress pathway.

In summary, these experiments did not establish any firm link between E199L expression and the appearance of WIPI and LC3 puncta at the viral factory. The observed effect of E199L on WIPI and LC3 has been shown to be more likely connected to an ER stress response. In the future, studies using E199L deletion mutants would be unlikely to succeed as E199L is almost certainly an essential virus protein evidenced by its incorporation into the virus particle and its putative role in virus fusion. Nevertheless, engineering a truncated version of E199L in which the hydrophobic domain has been deleted and monitoring for the potential abrogation of WIPI puncta and LC3 redistribution could help to establish a link between ER stress and an autophagy response.

7 Final discussion

African swine fever is a highly transmissible disease of domestic pigs that can inflict devastating socio-economic consequences on affected countries. The inter-continental spread of ASF following the 2007 outbreak in the Caucasus region has highlighted the urgent requirement for effective vaccines. The prospects for vaccine development are promising as low virulent strains can offer protection against high virulent strains, however, using this as a vaccine model has been limited by safety concerns. To address these concerns, a rational design approach incorporating genetic modifications of vaccine strain viruses may prove useful. This could be aimed at promoting viral attenuation or enhancing immunogenicity, however a significant barrier to this approach is the lack of knowledge surrounding the function of ASFV encoded proteins and the mechanisms by which the virus controls and subverts host cell pathways.

To initiate and sustain a productive infection, viruses require a tremendous amount of cell resources which inevitably activates stress response pathways such as the unfolded protein response (UPR) and apoptosis. Viruses are thus required to overcome or limit the effects of these pathways and research has showed that ASFV encodes multiple modulators for this purpose (Dixon et al., 2019). Autophagy is a highly conserved process that is not only vital to the host cell stress response but also plays an integral role in both innate and adaptive immunity. Presenting such a potent threat, autophagy is specifically targeted for inhibition by numerous viruses and even harnessed by some to act in a pro-viral manner. ASFV encodes a protein, A179L that was shown to specifically bind to the key autophagy protein Beclin 1 which forms part of the Vps34 lipid kinase complex (Hernaez et al., 2013). The Vps34 complex is essential during the very early stages of the autophagy pathway and over-expression of A179L inhibits the formation of starvation-induced autophagosomes. Research has showed however that viruses often modulate autophagy at multiple steps in the pathway. For example, HSV-1 inhibits Beclin 1 function but can also inhibit stimulatory signals that are situated higher up in the pathway (Lussignol et al., 2013, Orvedahl et al., 2007). With this in mind, it may be possible that ASFV employs multiple strategies to modulate autophagy.

Research conducted by Hernaez and colleagues demonstrated that autophagy is not induced during ASFV infection (Hernaez et al., 2013) and Basta *et al* reported that blocking autophagy had no effect on viral replication (Basta et al., 2010). These experiments do not however provide any clear evidence as to whether ASFV actively modulates the autophagy pathway. The aim of this project was therefore to characterise the modulation of autophagy by ASFV, principally to determine whether autophagy is specifically inhibited during infection. In addition, work was carried out to investigate if viral replication may require distinct elements of the autophagy machinery. Following this, experiments were conducted to try to elucidate the mechanisms of viral modulation including whether ASFV is able to activate the PI3K/Akt signalling pathway. Finally, a library of ASFV genes were screened for their potential to modify the autophagy response to starvation and some of

these were subjected to further investigation. Collectively, the goal of this work was to improve our understanding of the modulation of the host cell stress response by ASFV with the aim of providing potentially novel opportunities for therapeutic intervention including anti-viral and vaccine development.

7.1 Characterisation of the modulation of autophagy by ASFV

Initial characterisation of the effects of ASFV infection on autophagy was conducted by immunofluorescent detection of LC3-labelled autophagosomes using the Vero cell adapted strain Ba71V. This analysis revealed that ASFV infected cells demonstrated a reduced number of autophagosomes at 4 hpi when compared to control cells under nutrient replete conditions indicating that ASFV does not promote autophagy during the early stages of viral replication. This is consistent with previous results shown at later time points of viral replication (Hernaez et al., 2013). To test if autophagy is inhibited by ASFV, cells were starved to induce autophagy and in comparison to the high number of autophagosomes detected in control cells, a significantly lower number were detected in cells infected with ASFV, suggesting that the virus actively inhibits autophagy. To confirm these results, Western blot analysis of LC3-II levels demonstrated that ASFV was able to block starvation-induced accumulation of LC3-II at 4 hpi.

In the mammalian host, ASFV naturally targets cells of the monocyte/macrophage lineage. To ensure that the above results were not cell type specific or specific to the virus strain, Western blot analysis of LC3-II was carried out on porcine macrophages that had been infected with the field isolate OUR T88/1. In this experiment, autophagy was stimulated pharmacologically as opposed to using starvation. Consistent with the Vero cell results, ASFV was able to inhibit accumulation of LC3-II demonstrating that autophagy is also inhibited in macrophages and that this effect is not specific to cell type, virus strain or method of autophagy induction.

Analysis of WIPI puncta was conducted to determine if ASFV targets the autophagy pathway during the very early stages of autophagosome formation. Unexpectedly, the results revealed that ASFV infection promotes the assembly of WIPI complexes at 4 hpi. This is despite the fact that ASFV was shown to inhibit the formation of autophagosomes. To provide clarity on the autophagy status of infected cells, an investigation into p62 levels in ASFV infected cells was carried out and showed that p62 is not degraded during the early or late stages of infection. A block in the degradation of p62 suggests that the breakdown of cargo via autophagosome-lysosome fusion, known as autophagic flux, is inhibited by ASFV. The observed block in autophagosome formation and autophagic flux provides compelling evidence that autophagy is not required by ASFV. This was confirmed by infecting an autophagy deficient cell line and demonstrating that a similar level of virus replication was achieved when compared to an autophagy competent cell line.

The inhibition of autophagy by ASFV raises the question of the role of WIPI complexes during infection. It may be possible that WIPI puncta are formed due to the host response to infection and

that ASFV inhibits the autophagy pathway between the stages of WIPI complex assembly and autophagosome formation. Alternatively, WIPI complex assembly may be unrelated to the autophagy response and instead be required for viral replication. Indeed, their appearance at the nuclear periphery is in contrast to the diffusely located puncta observed in uninfected cells. WIPI and LC3 puncta were also observed at the viral factory during the late stages of infection which was accompanied by an accumulation of LC3-II in infected cell lysates. The structural nature of these puncta is currently unknown. In the future, correlative light electron microscopy (CLEM) to visualise membrane structure may help determine if the LC3 puncta are representative of autophagosomes. If autophagosomes are present at this stage of infection, they are unlikely to undergo lysosome fusion due to the observed block in autophagic flux.

In summary, the results described in chapter 3 demonstrate that ASFV inhibits autophagy and that autophagy is not required for viral replication. However, the potential that parts of the autophagy machinery may be required at specific times during the virus life cycle requires further investigation. Using a panel of Atg knock-out cells may be useful in determining which elements of the autophagy pathway are required. Utilising this method, a recent publication described the use of distinct sets of autophagy initiation components by positive-strand RNA viruses (Abernathy et al., 2019).

In the context of macrophages, autophagy has been shown to be a fundamental regulator of inflammasomes (Germic et al., 2019). Inflammasomes are protein complexes that are activated upon cellular infection or stress that initiate the maturation of pro-inflammatory cytokines to engage innate immune defences (Schroder and Tschopp, 2010). In order to regulate the levels of inflammasomes, cells target them for degradation by autophagy (Shi et al., 2012). The inhibition of autophagy by ASFV may therefore be a significant contributor to the potent inflammatory responses that are observed in the infected host.

7.2 Investigation of the mechanisms of autophagy modulation by ASFV

When considering the mechanisms by which ASFV may modulate the autophagy pathway, the Beclin 1 binding capacity of A179L was regarded as a potential route of autophagy inhibition. The research conducted by Hernaez *et al* (2013) that showed the ability of A179L to inhibit autophagosome formation was based on an over-expression model but it is yet to be determined whether A179L is involved in the modulation of autophagy during infection. In analysing the capacity of recombinant A179L to bind to Bcl-2 proteins, Banjara and colleagues found that A179L possessed a relatively weaker affinity for Beclin 1 compared to other pro-apoptotic Bcl-2 members (Banjara et al., 2017) which could suggest a reduced role in modulating autophagy compared to apoptosis. In chapter 4, an A179L KO virus was tested for its ability to inhibit starvation-induced autophagosome assembly. The results showed that infected cells demonstrated significantly less autophagosomes when compared to control cells indicating that the A179L KO

virus was also able to inhibit autophagy. This suggests that if A179L does play a role in inhibiting autophagy in infected cells, it is not the only means of inhibition employed by ASFV.

To try to identify additional mechanisms by which ASFV could inhibit the induction of autophagy, the activation status of mTORC1 was determined in infected cells. The activation of mTORC1 is often required by viruses to maintain protein translation and its activation also inhibits autophagy via the ULK1 complex. In ASFV infected Vero cells, mTORC1 was shown to be active throughout a 16 hour time course of infection. Starvation of cells is an effective method of inactivating mTORC1 and the attempted inactivation of mTORC1 by starvation of infected cells was blocked by ASFV demonstrating that mTORC1 is specifically targeted by the virus. The activation of mTORC1 was observed in a time-dependent manner, becoming increasingly apparent as infection progressed which may suggest that the expression of virally encoded proteins are required for this effect. This has been reported for HSV-1, whereby expression of the Us3 kinase protein is directly linked to mTORC1 activation (Chuluunbaatar et al., 2010). Irrespective of the underlying mechanism, the ability of ASFV to activate mTORC1 represents a clear means by which autophagy may be inhibited.

Akt activity can lead to the activation of mTORC1 via the inactivation of the mTORC1 repressor, TSC2. To investigate if mTORC1 activity in ASFV infected cells could be linked to Akt, Western blot analysis was conducted to determine if Akt is active during infection of Vero cells. A 16 hour time course showed that Akt remained active throughout infection signifying a potential route of mTORC1 activation that is exploited by the virus. Akt and mTORC1 were also shown to be active following infection with a highly purified virus, suggesting that Akt/mTORC1 activity is not affected by the presence of cell debris in the virus stock which has previously been hypothesised to potentially influence the method of virus entry (Hernaez et al., 2016). Preliminary studies have indicated that Akt and mTORC1 are also activated during infection of macrophages (data not shown) which may contribute to the previously observed inhibition of autophagy in these cells.

Akt is predominantly activated via the action of class I PI3K at the cell surface in response to hormones or growth factors and this can be blocked by small molecule PI3K inhibitors such as LY294002. Akt can also be activated by I-kappa-B kinase epsilon (IKKε), a Ser/Thr kinase that plays a vital role in interferon mediated antiviral immunity (Guo et al., 2011). TANK-binding kinase 1 (TBK1) which is critical for the phosphorylation and activation of interferon response factors has also been shown to interact with and phosphorylate Akt following activation of Toll-like receptors (TLR) in macrophages (Joung et al., 2011). Both IKKε and TBK1 activate Akt independently of PI3K as treatment of cells with LY294002 does not abrogate Akt activity. It would be interesting to test whether PI3K is involved in Akt activation during ASFV infection by treating infected cells with LY294002 and analysing Akt phosphorylation. However, LY294002 would likely also inhibit the class III PI3K Vps34 autophagy complex and therefore conclusions regarding any direct links between PI3K activation at the cell surface and autophagy would not be

possible. It is worth highlighting that class I PI3K activity can act to suppress IL-12 production triggered by TLR signalling (Fukao et al., 2002) and therefore the potential activity of PI3K in ASFV infected cells could primarily be used to negatively regulate the innate immune response and the activation of Akt is a side-effect of this rather than by design. Finally, it would be interesting to determine if viral protein expression is essential for Akt/mTORC1 activation or if the PI3K/Akt signalling cascade is triggered in response to virus entry as has been reported for vaccinia virus (Soares et al., 2009). Infecting cells with UV or chemically inactivated virus may be useful in this respect.

The capacity of ASFV to inhibit autophagy induction in the absence of Akt/mTORC1 activity was investigated using pharmacological inhibitors. Efficacy testing was conducted by Western blot analysis of Akt and mTORC1 substrate phosphorylation. The results showed that using a combination of Torin1 (mTOR inhibitor) and MK-2206 (Akt inhibitor) was an effective means of substantially reducing Akt/mTORC1 function. Interestingly, the use of both MK-2206 and Torin1 was required to completely block phosphorylation of Akt at S473. This suggests that mTORC2, which phosphorylates Akt at S473 and is inhibited by Torin1, is likely targeted by ASFV and used to drive Akt activation. Techniques for the specific inhibition of mTORC2 are beginning to emerge (Murray and Cameron, 2017) which could be useful in determining the precise role of mTORC2 in ASFV infection. In the future it may be useful to test higher concentrations of MK-2206 to determine if Akt could be completely inactivated without the requirement for Torin1. Under complete Akt inactivation, testing for mTORC1 activity may help to determine if Akt is exclusively responsible for the activation of mTORC1 or if ASFV may be activating mTORC1 via alternative means such as virally encoded proteins.

ASFV infected cells were analysed by immunofluorescence for the inhibition of autophagy at 2 and 4 hpi in the presence or absence of Torin1 and MK-2206. Inhibition of starvation-induced autophagosomes was observed at both time points in the absence of the drugs. The inhibition at 2 hpi is particularly interesting as at this stage of the replication cycle, the influence of viral protein expression would be minimal, suggesting that the activity of Akt and mTORC1 is sufficient to inhibit autophagy. Additional evidence to support this conclusion is the fact that at 2 hpi, the formation of autophagosomes could be induced in the presence of pharmacological inhibition of Akt and mTORC1 indicating that no other factors are involved. Testing the inhibition of Akt and mTORC1 in isolation rather than in combination showed that autophagy could not be induced and that both inhibitors were required to stimulate autophagosome formation. This demonstrates that the activity of mTORC1 is not exclusively responsible for the inhibition of autophagy and that Akt is also likely contributing to this effect. Future studies could examine the potential role that Akt plays in inhibiting Beclin 1 function which has previously been reported (Wang et al., 2012). By 4 hpi, early viral protein expression is well established and despite the inhibition of Akt and mTORC1, ASFV is able to substantially reduce the number of starvation-induced autophagosomes

pointing to the involvement of virally encoded factors. These results were consistent between cells infected with wild-type virus and cells infected with the A179L KO virus suggesting that either A179L does not play a role in the inhibition of autophagy or that additional viral proteins are involved.

The studies in chapter 4 reveal that the inhibition of autophagy by ASFV is multi-layered and linked to diverse elements of the autophagy pathway. The involvement of the Akt/mTORC1 signalling cascade in addition to virally encoded modulators could point to a model of phased control. The PI3K/Akt pathway may be activated first at the point of virus entry to provide a preliminary defence mechanism against autophagy but as the viral replication cycle progresses and host cell stress responses are activated, an additional level of control is implemented by expression of viral factors. In this scenario, an attempt to limit the ability of the virus to inhibit autophagy would need to address both phases of modulation.

7.3 Screening an ASFV gene library for potential autophagy modulators

A library of 76 ASFV genes that predominantly consisted of highly conserved genes that are expressed during early virus replication was screened using an immunofluorescence assay to detect inhibition of starvation-induced autophagosomes. Tagged genes were delivered into Vero cells either by transient transfection of plasmids or by transduction using an adenovirus vector. A179L was used as a positive control and showed that the inhibition of autophagosome formation could be easily detected. A double mutation of the A179L Bcl-2 ligand binding groove was engineered to provide a negative control.

The majority of genes demonstrated no detectable inhibition of autophagy. MGF360-11L, MGF505-5R and R298L showed inconsistent inhibition of autophagy that was predominantly seen in cells with extremely high levels of protein expression. It was therefore concluded that this effect may be the result of an artefact and could potentially represent a limitation of this assay. Having said that, further investigation of R298L may be warranted as this gene encodes a protein kinase that might play a role in the phosphorylation of proteins involved in the Akt/mTORC1 signalling cascade. Expression of C147L, an RNA polymerase subunit, resulted in the inhibition of autophagy in some cells that demonstrated potential morphological changes in the nucleus. This may be of interest in the future as ASFV replication includes an early nuclear phase that includes morphological modifications, the timing of which might coincide with the inhibition of autophagy. The major structural protein encoded by B646L was shown to inhibit autophagosome formation in some cells but not others. Further investigation revealed that this was likely linked to the level of protein expression or a difference in protein localisation. Nevertheless, this raises the possibility that structural proteins may be involved in inhibiting autophagy. A recent proteomics study revealed that the ASFV virion is comprised of 68 proteins (Alejo et al., 2018). In the future, screening of these genes may be beneficial in uncovering autophagy modulators although knocking

these proteins out does not seem feasible. Further testing could be conducted by using gene silencing such as RNAi in place of knock-out studies or by identifying specific autophagy regulating domains which can be targeted for modification.

Unexpectedly, screening of E183L and E199L revealed a redistribution of LC3 into structures that were inconsistent with the pattern and size of LC3 puncta that are usually associated with autophagosomes. Further investigation in chapter 6 uncovered the potential mechanisms underlying these effects and this is discussed in detail below. Interestingly, expression of DP148R under nutrient replete conditions induced LC3 puncta that were much smaller than the size usually representative of autophagosomes. Under starvation conditions, similar sized LC3 puncta were observed and autophagosome-sized puncta were notably absent suggesting that this protein may be involved in the inhibition of autophagy. A comparison of the amino acid sequence of DP148R between the Benin 1997/1 and OURT88/3 strains showed that the latter encodes two separate proteins that are separated by a frameshift mutation. Testing of each of the aforementioned proteins individually did not reveal the same restriction of autophagosome formation as previously seen, demonstrating that the full length protein is required for this effect. Additionally, analysis of the DP148R coding sequence in the Ba71V strain showed that in comparison to the Benin 1997/1 and OURT88/3 strains, multiple start codons and putative promotor regions for this gene were absent. Together with transcriptome data generated in a separate study (Unpublished - Gwenny Cackett, UCL), this suggests that DP148R is not expressed during infection with Ba71V and therefore is not a factor in the inhibition of autophagy by this particular strain of ASFV.

DP148R was shown to be expressed during early times post-infection using a Benin 1997/1 isolate (Reis et al., 2017a) which coincides with the timing of autophagy inhibition. In the study by Reis and colleagues, infection of pigs with a DP148R knock-out virus led to a dramatic reduction in pathogenesis when compared to the parental virus. Furthermore, immunization of pigs with the mutant virus provided near complete protection against challenge however the precise mechanism of protection could not be determined. In the future, it would be useful to determine if DP148R expression can restrict autophagosome formation in macrophages as previously observed in Vero cells. Additionally, it would be interesting to ascertain if the DP148R knock-out virus is unable to inhibit the induction of autophagy. In this scenario, it would be tempting to speculate whether an altered ability of the DP148R knock-out virus to modulate autophagy could be involved in generating a protective host immune response. Indeed, a mutant HSV-1 virus lacking the ability to control autophagy was shown to induce significantly greater interferon gamma production which is an important correlate of protection against ASFV (King et al., 2011, Leib et al., 2009).

In summary, the gene library screen did not uncover any obvious autophagy modulators that were suitable for knock-out studies which raises the possibility that some of the ASFV genes that were excluded from the screen are involved in the inhibition of autophagy. Additionally, it may be possible that multiple proteins act on different parts of the process that when combined show the

dramatic inhibitory effect seen in infected cells. Alternatively, some genes may require virally encoded binding partners to exert their function or perhaps the combination of protein modulators and Akt/mTORC1 activation is required to inhibit autophagy.

Screening was carried out using an immunofluorescence assay and it may be possible that an alternative approach could provide greater sensitivity. For example, a panel of Atg genes could be cloned and used as bait proteins in yeast two hybrid or mass spectrometry screening. A yeast two hybrid assay was previously used to identify the interaction between Beclin 1 and A179L (Hernaez et al., 2013). A potential limitation of the immunofluorescence assay is that it relied on visual inspection of the cells to detect inhibition which might be susceptible to relatively higher levels of subjectivity compared to other assays. An alternative method could be the use of flow cytometry. Commercial kits are available that permit the detection of changes in total cellular fluorescence which can be precisely quantified in large numbers of cells to obtain robust data (Eng et al., 2010). This method is however more suited to cells that grow in suspension rather than adherent cell lines and it has been reported that preparation of cell suspensions can lead to cell damage which may activate autophagy (Klionsky et al., 2016). In addition, plasmid transfection can sometimes lead to low levels of expression which imposes a limitation on the number of cells that can be analysed by high throughput methods.

7.4 Investigation of the redistribution of LC3 by E199L

Screening of E199L showed that protein expression induces a redistribution of LC3 and further investigation revealed that this effect is unaffected by nutrient availability. To explore the possibility that E199L may be inducing an autophagy response, Western blot analysis showed that E199L expression causes an accumulation of lipidated LC3 (LC3-II) and confocal analysis showed that E199L induces the appearance of WIPI puncta. The lipidation of LC3 and assembly of WIPI complexes are both hallmarks of the induction of autophagy, however the accumulation of LC3-II was unaffected by the addition of Bafilomycin A1 and the assembly of WIPI complexes was unaffected by the starvation status of the cells suggesting that a canonical autophagy response may not be involved. Nevertheless, it was hypothesised that E199L could be implicated in the appearance of WIPI and LC3 puncta at the viral factory during the late stages of infection. Indeed, immunofluorescent labelling of infected cells over a time course of infection showed that E199L expression at the viral factory roughly coincides with the appearance of the aforementioned puncta.

To provide clarity on whether E199L is able to induce an autophagy response, transduced cells were analysed by electron microscopy. Interestingly, control cells that had been transduced with E183L, which had previously been shown to induce the redistribution of LC3, demonstrated substantial modifications to the ER which was arranged in large whorls. An altered ER morphology was also apparent in cells transduced with E199L in which numerous patches of dark staining material believed to be protein aggregates were observed. Membrane vesicles that were consistent

with the size of autophagosomes were not apparent in either E183L or E199L transduced cells suggesting that a canonical autophagy response had not been stimulated.

Mass spectrometry was used to determine whether E199L interacts with components of the autophagy machinery. Cells were transduced with E199L which acted as a bait protein and was captured using affinity purification. Analysis of the captured samples revealed a number of proteins with a significant interaction with E199L, the most prevalent of which were proteins belonging to the proteasome. This indicates that E199L expression likely results in protein mis-folding leading to proteasomal degradation. No interactions with the autophagy pathway were identified, however the analysis uncovered multiple interactions with proteins belonging to the ER which supports the EM data. Immunofluorescent labelling of the ER chaperone protein Calnexin demonstrated colocalisation with E199L expression providing further evidence of a link to the ER.

Accumulation of mis-folded proteins can lead to ER stress which can result in the activation of the unfolded protein response (UPR). Prolonged activation of the UPR has been shown to induce autophagy (Bernales et al., 2006) and could explain the LC3 lipidation and formation of WIPI complexes in E199L expressing cells. Indeed, E199L was shown to upregulate expression of the pro-apoptotic transcription factor, CHOP which is a hallmark of the activation of the UPR.

Collectively, the evidence thus points to a non-specific induction of autophagy whereby the redistribution of LC3 is stimulated via an ER stress response as opposed to a specific function of E199L. The over-expression of E199L may be exceeding the capacity of the ER to maintain correct protein folding. In this regard, a time course of E199L expression could be conducted to determine if LC3 lipidation only occurs after large amounts of protein are expressed. Additionally, future investigations could include the removal of the hydrophobic domain at the C-terminus of E199L to determine if this alleviates induction of the UPR. E199L is purported to localise to the inner membrane of the ASFV virion which is derived from the ER during viral morphogenesis and thus conversely, it cannot be excluded that E199L could play a role in morphogenesis. In this regard, E199L may be vital to successful completion of the virus lifecycle by serving to alter ER structure or function.

7.5 Concluding remarks

As ASF is fast becoming a threat to major pork-producing countries in Europe, the necessity for protective vaccines is approaching a critical level. A rational design approach could prove to be a key factor in engineering a safe commercial vaccine. The research conducted here was aimed at characterising the modulation of autophagy by ASFV and investigating the viral mechanisms of modulation. It was envisaged that this may provide an opportunity to harness the important function that autophagy plays in host immunity which could be used to enhance vaccine strain immunogenicity. However, the emerging model indicates that ASFV employs an intricate strategy of autophagy control, targeting key cell signalling cascades such as the PI3K/Akt pathway as well

as components of the autophagy machinery. Consequently, it may prove challenging to overcome this. Nevertheless, this work has provided further insight into the complex interaction between ASFV and the host cell. As well as implementing an immune evasion strategy, ASFV is required to prolong cell survival in order to complete its replication cycle. The observation that two proteins, E183L and E199L are capable of inducing a host cell stress response highlights the importance of the ability of the virus to regulate cellular homeostasis.

8 References

ABERNATHY, E., MATEO, R., MAJZOUB, K., VAN BUUREN, N., BIRD, S. W., CARETTE, J. E. & KIRKEGAARD, K. 2019. Differential and convergent utilization of autophagy components by positive-strand RNA viruses. *PLoS Biol,* 17**,** e2006926.

ALCAMI, A., CARRASCOSA, A. L. & VINUELA, E. 1989. The entry of African swine fever virus into Vero cells. *Virology,* 171**,** 68-75.

ALEJO, A., MATAMOROS, T., GUERRA, M. & ANDRES, G. 2018. A Proteomic Atlas of the African Swine Fever Virus Particle. *J Virol,* 92.

ALESSI, D. R., ANDJELKOVIC, M., CAUDWELL, B., CRON, P., MORRICE, N., COHEN, P. & HEMMINGS, B. A. 1996. Mechanism of activation of protein kinase B by insulin and IGF-1. *EMBO J,* 15**,** 6541-51.

ALONSO, C., MISKIN, J., HERNAEZ, B., FERNANDEZ-ZAPATERO, P., SOTO, L., CANTO, C., RODRIGUEZ-CRESPO, I., DIXON, L. & ESCRIBANO, J. M. 2001. African swine fever virus protein p54 interacts with the microtubular motor complex through direct binding to light-chain dynein. *J Virol,* 75**,** 9819-27.

ANDRES, G., ALEJO, A., SALAS, J. & SALAS, M. L. 2002. African swine fever virus polyproteins pp220 and pp62 assemble into the core shell. *J Virol,* 76**,** 12473-82.

ANDRES, G., ALEJO, A., SIMON-MATEO, C. & SALAS, M. L. 2001a. African swine fever virus protease, a new viral member of the SUMO-1-specific protease family. *J Biol Chem,* 276**,** 780-7.

ANDRES, G., GARCIA-ESCUDERO, R., SIMON-MATEO, C. & VINUELA, E. 1998. African swine fever virus is enveloped by a two-membraned collapsed cisterna derived from the endoplasmic reticulum. *J Virol,* 72**,** 8988-9001.

ANDRES, G., GARCIA-ESCUDERO, R., VINUELA, E., SALAS, M. L. & RODRIGUEZ, J. M. 2001b. African swine fever virus structural protein pE120R is essential for virus transport from assembly sites to plasma membrane but not for infectivity. *J Virol,* 75**,** 6758-68.

ANDRES, G., SIMON-MATEO, C. & VINUELA, E. 1997. Assembly of African swine fever virus: role of polyprotein pp220. *J Virol,* 71**,** 2331-41.

ANDREWES, C. H. 1963. Classification of Viruses of Vertebrates. *In:* KENNETH, M. S. & MAX, A. L. (eds.) *Advances in Virus Research.* Academic Press.

ARGILAGUET, J. M., PEREZ-MARTIN, E., NOFRARIAS, M., GALLARDO, C., ACCENSI, F., LACASTA, A., MORA, M., BALLESTER, M., GALINDO-CARDIEL, I., LOPEZ-SORIA, S., ESCRIBANO, J. M., RECHE, P. A. & RODRIGUEZ, F. 2012. DNA vaccination partially protects against African swine fever virus lethal challenge in the absence of antibodies. *PLoS One,* 7**,** e40942.

ARIAS, M. & SÁNCHEZ-VIZCAÍNO, J. M. 2002a. African Swine Fever. *Trends in Emerging Viral Infections of Swine***,** 119-124.

ARIAS, M. & SÁNCHEZ-VIZCAÍNO, J. M. 2002b. African Swine Fever Eradication: The Spanish Model. *Trends in Emerging Viral Infections of Swine***,** 133-139.

ARICO, S., PETIOT, A., BAUVY, C., DUBBELHUIS, P. F., MEIJER, A. J., CODOGNO, P. & OGIER-DENIS, E. 2001. The tumor suppressor PTEN positively regulates macroautophagy by inhibiting the phosphatidylinositol 3-kinase/protein kinase B pathway. *J Biol Chem,* 276**,** 35243-6.

ARNOLDI, F., DE LORENZO, G., MANO, M., SCHRANER, E. M., WILD, P., EICHWALD, C. & BURRONE, O. R. 2014. Rotavirus increases levels of lipidated LC3 supporting accumulation of infectious progeny virus without inducing autophagosome formation. *PLoS One,* 9**,** e95197.

AXE, E. L., WALKER, S. A., MANIFAVA, M., CHANDRA, P., RODERICK, H. L., HABERMANN, A., GRIFFITHS, G. & KTISTAKIS, N. T. 2008. Autophagosome formation from membrane compartments enriched in phosphatidylinositol 3-phosphate and dynamically connected to the endoplasmic reticulum. *J Cell Biol,* 182**,** 685-701.

BALLESTER, M., RODRIGUEZ-CARINO, C., PEREZ, M., GALLARDO, C., RODRIGUEZ, J. M., SALAS, M. L. & RODRIGUEZ, F. 2011. Disruption of nuclear organization during the initial phase of African swine fever virus infection. *J Virol,* 85**,** 8263-9.

BANJARA, S., CARIA, S., DIXON, L. K., HINDS, M. G. & KVANSAKUL, M. 2017. Structural Insight into African Swine Fever Virus A179L-Mediated Inhibition of Apoptosis. *J Virol,* 91.

BARBER, C. A. 2015. *Stress modulators encoded by African swine fever virus.* Doctor of Philosophy, St George's University of London.

BARDERAS, M. G., RODRIGUEZ, F., GOMEZ-PUERTAS, P., AVILES, M., BEITIA, F., ALONSO, C. & ESCRIBANO, J. M. 2001. Antigenic and immunogenic properties of a chimera of two immunodominant African swine fever virus proteins. *Arch Virol,* 146**,** 1681-91.

BASTA, S., GERBER, H., SCHAUB, A., SUMMERFIELD, A. & MCCULLOUGH, K. C. 2010. Cellular processes essential for African swine fever virus to infect and replicate in primary macrophages. *Vet Microbiol,* 140**,** 9-17.

BASTOS, A. D., PENRITH, M. L., CRUCIERE, C., EDRICH, J. L., HUTCHINGS, G., ROGER, F., COUACY-HYMANN, E. & G, R. T. 2003. Genotyping field strains of African swine fever virus by partial p72 gene characterisation. *Arch Virol,* 148**,** 693-706.

BATRA, A. 2016. *The role of the PI3K/AKT signalling pathway during infectious bronchitis virus infection.* Doctor of Philosophy, University of Liverpool.

BAYLIS, S. A., BANHAM, A. H., VYDELINGUM, S., DIXON, L. K. & SMITH, G. L. 1993. African swine fever virus encodes a serine protein kinase which is packaged into virions. *J Virol,* 67**,** 4549-56.

BEALE, R., WISE, H., STUART, A., RAVENHILL, B. J., DIGARD, P. & RANDOW, F. 2014. A LC3-interacting motif in the influenza A virus M2 protein is required to subvert autophagy and maintain virion stability. *Cell Host Microbe,* 15**,** 239-47.

BENETTI, L. & ROIZMAN, B. 2006. Protein kinase B/Akt is present in activated form throughout the entire replicative cycle of deltaU(S)3 mutant virus but only at early times after infection with wild-type herpes simplex virus 1. *J Virol,* 80**,** 3341-8.

BERNALES, S., MCDONALD, K. L. & WALTER, P. 2006. Autophagy counterbalances endoplasmic reticulum expansion during the unfolded protein response. *PLoS Biol,* 4**,** e423.

BIRD, S. W., MAYNARD, N. D., COVERT, M. W. & KIRKEGAARD, K. 2014. Nonlytic viral spread enhanced by autophagy components. *Proc Natl Acad Sci U S A,* 111**,** 13081-6.

BIRGISDOTTIR, A. B., LAMARK, T. & JOHANSEN, T. 2013. The LIR motif - crucial for selective autophagy. *J Cell Sci,* 126**,** 3237-47.

BJORKOY, G., LAMARK, T., BRECH, A., OUTZEN, H., PERANDER, M., OVERVATN, A., STENMARK, H. & JOHANSEN, T. 2005. p62/SQSTM1 forms protein aggregates degraded by autophagy and has a protective effect on huntingtin-induced cell death. *J Cell Biol,* 171**,** 603-14.

BJORKOY, G., LAMARK, T., PANKIV, S., OVERVATN, A., BRECH, A. & JOHANSEN, T. 2009. Monitoring autophagic degradation of p62/SQSTM1. *Methods Enzymol,* 452**,** 181-97.

BLASCO, R., DE LA VEGA, I., ALMAZAN, F., AGUERO, M. & VINUELA, E. 1989. Genetic variation of African swine fever virus: variable regions near the ends of the viral DNA. *Virology,* 173**,** 251-7.

BLOME, S., GABRIEL, C. & BEER, M. 2013. Pathogenesis of African swine fever in domestic pigs and European wild boar. *Virus Res,* 173**,** 122-30.

BLOME, S., GABRIEL, C. & BEER, M. 2014. Modern adjuvants do not enhance the efficacy of an inactivated African swine fever virus vaccine preparation. *Vaccine,* 32**,** 3879-82.

BOINAS, F. S., HUTCHINGS, G. H., DIXON, L. K. & WILKINSON, P. J. 2004. Characterization of pathogenic and non-pathogenic African swine fever virus isolates from Ornithodoros erraticus inhabiting pig premises in Portugal. *J Gen Virol,* 85**,** 2177-87.

BOINAS, F. S., WILSON, A. J., HUTCHINGS, G. H., MARTINS, C. & DIXON, L. J. 2011. The persistence of African swine fever virus in field-infected Ornithodoros erraticus during the ASF endemic period in Portugal. *PLoS One,* 6**,** e20383.

BORCA, M. V., CARRILLO, C., ZSAK, L., LAEGREID, W. W., KUTISH, G. F., NEILAN, J. G., BURRAGE, T. G. & ROCK, D. L. 1998. Deletion of a CD2-like gene, 8-DR, from African swine fever virus affects viral infection in domestic swine. *J Virol,* 72**,** 2881-9.

BORCA, M. V., IRUSTA, P., CARRILLO, C., AFONSO, C. L., BURRAGE, T. & ROCK, D. L. 1994. African swine fever virus structural protein p72 contains a conformational neutralizing epitope. *Virology,* 201**,** 413-8.

BOYA, P., REGGIORI, F. & CODOGNO, P. 2013. Emerging regulation and functions of autophagy. *Nat Cell Biol,* 15**,** 713-20.

BRASS, A. L., DYKXHOORN, D. M., BENITA, Y., YAN, N., ENGELMAN, A., XAVIER, R. J., LIEBERMAN, J. & ELLEDGE, S. J. 2008. Identification of host proteins required for HIV infection through a functional genomic screen. *Science,* 319**,** 921-6.

BREESE, S. S., JR. & DEBOER, C. J. 1966. Electron microscope observations of African swine fever virus in tissue culture cells. *Virology,* 28**,** 420-8.

BROOKES, S. M., DIXON, L. K. & PARKHOUSE, R. M. 1996. Assembly of African Swine fever virus: quantitative ultrastructural analysis in vitro and in vivo. *Virology,* 224**,** 84-92.

CARRASCO, L., DE LARA, F. C., MARTIN DE LAS MULAS, J., GOMEZ-VILLAMANDOS, J. C., HERVAS, J., WILKINSON, P. J. & SIERRA, M. A. 1996a. Virus association with lymphocytes in acute African swine fever. *Vet Res,* 27**,** 305-12.

CARRASCO, L., GOMEZ-VILLAMANDOS, J. C., BAUTISTA, M. J., MARTIN DE LAS MULAS, J., VILLEDA, C. J., WILKINSON, P. J. & SIERRA, M. A. 1996b. In vivo replication of African swine fever virus (Malawi '83) in neutrophils. *Vet Res,* 27**,** 55-62.

CARRASCOSA, A. L., BUSTOS, M. J., NOGAL, M. L., GONZALEZ DE BUITRAGO, G. & REVILLA, Y. 2002. Apoptosis induced in an early step of African swine fever virus entry into vero cells does not require virus replication. *Virology,* 294**,** 372-82.

CARRASCOSA, A. L., DEL VAL, M., SANTAREN, J. F. & VINUELA, E. 1985. Purification and properties of African swine fever virus. *J Virol,* 54**,** 337-44.

CARRASCOSA, J. L., CARAZO, J. M., CARRASCOSA, A. L., GARCIA, N., SANTISTEBAN, A. & VINUELA, E. 1984. General morphology and capsid fine structure of African swine fever virus particles. *Virology,* 132**,** 160-72.

CASTELLO, A., QUINTAS, A., SANCHEZ, E. G., SABINA, P., NOGAL, M., CARRASCO, L. & REVILLA, Y. 2009. Regulation of host translational machinery by African swine fever virus. *PLoS Pathog,* 5**,** e1000562.

CHAKRABARTI, A., CHEN, A. W. & VARNER, J. D. 2011. A review of the mammalian unfolded protein response. *Biotechnol Bioeng,* 108**,** 2777-93.

CHAN, E. Y., KIR, S. & TOOZE, S. A. 2007. siRNA screening of the kinome identifies ULK1 as a multidomain modulator of autophagy. *J Biol Chem,* 282**,** 25464-74.

CHAN, T. O., RITTENHOUSE, S. E. & TSICHLIS, P. N. 1999. AKT/PKB and other D3 phosphoinositide-regulated kinases: kinase activation by phosphoinositide-dependent phosphorylation. *Annu Rev Biochem,* 68**,** 965-1014.

CHAPMAN, D. A., TCHEREPANOV, V., UPTON, C. & DIXON, L. K. 2008. Comparison of the genome sequences of non-pathogenic and pathogenic African swine fever virus isolates. *J Gen Virol,* 89**,** 397-408.

CHEONG, H., NAIR, U., GENG, J. & KLIONSKY, D. J. 2008. The Atg1 kinase complex is involved in the regulation of protein recruitment to initiate sequestering vesicle formation for nonspecific autophagy in Saccharomyces cerevisiae. *Mol Biol Cell,* 19**,** 668-81.

CHULUUNBAATAR, U. & MOHR, I. 2011. A herpesvirus kinase that masquerades as Akt: you don't have to look like Akt, to act like it. *Cell Cycle,* 10**,** 2064-8.

CHULUUNBAATAR, U., ROLLER, R., FELDMAN, M. E., BROWN, S., SHOKAT, K. M. & MOHR, I. 2010. Constitutive mTORC1 activation by a herpesvirus Akt surrogate stimulates mRNA translation and viral replication. *Genes Dev,* 24**,** 2627-39.

CLARK, S. L., JR. 1957. Cellular differentiation in the kidneys of newborn mice studies with the electron microscope. *J Biophys Biochem Cytol,* 3**,** 349-62.

CLIPPINGER, A. J., MAGUIRE, T. G. & ALWINE, J. C. 2011. Human cytomegalovirus infection maintains mTOR activity and its perinuclear localization during amino acid deprivation. *J Virol,* 85**,** 9369-76.

COBBOLD, C., WHITTLE, J. T. & WILEMAN, T. 1996. Involvement of the endoplasmic reticulum in the assembly and envelopment of African swine fever virus. *J Virol,* 70**,** 8382-90.

COBBOLD, C., WINDSOR, M. & WILEMAN, T. 2001. A virally encoded chaperone specialized for folding of the major capsid protein of African swine fever virus. *J Virol,* 75**,** 7221-9.

COORAY, S. 2004. The pivotal role of phosphatidylinositol 3-kinase-Akt signal transduction in virus survival. *J Gen Virol,* 85**,** 1065-76.

CORONA VELAZQUEZ, A., CORONA, A. K., KLEIN, K. A. & JACKSON, W. T. 2018. Poliovirus induces autophagic signaling independent of the ULK1 complex. *Autophagy,* 14**,** 1201-1213.

COSTARD, S., WIELAND, B., DE GLANVILLE, W., JORI, F., ROWLANDS, R., VOSLOO, W., ROGER, F., PFEIFFER, D. U. & DIXON, L. K. 2009. African swine fever: how can global spread be prevented? *Philos Trans R Soc Lond B Biol Sci,* 364**,** 2683-96.

COTTAM, E. M., WHELBAND, M. C. & WILEMAN, T. 2014. Coronavirus NSP6 restricts autophagosome expansion. *Autophagy,* 10**,** 1426-41.

COX, J., HEIN, M. Y., LUBER, C. A., PARON, I., NAGARAJ, N. & MANN, M. 2014. Accurate proteome-wide label-free quantification by delayed normalization and maximal peptide ratio extraction, termed MaxLFQ. *Mol Cell Proteomics,* 13**,** 2513-26.

CUERVO, A. M. 2011. Chaperone-mediated autophagy: Dice's 'wild' idea about lysosomal selectivity. *Nat Rev Mol Cell Biol,* 12**,** 535-41.

CUESTA-GEIJO, M. A., BARRADO-GIL, L., GALINDO, I., MUNOZ-MORENO, R. & ALONSO, C. 2017. Redistribution of Endosomal Membranes to the African Swine Fever Virus Replication Site. *Viruses,* 9.

CUESTA-GEIJO, M. A., GALINDO, I., HERNAEZ, B., QUETGLAS, J. I., DALMAU-MENA, I. & ALONSO, C. 2012. Endosomal maturation, Rab7 GTPase and phosphoinositides in African swine fever virus entry. *PLoS One,* 7**,** e48853.

DAWSON, C. W., TRAMOUNTANIS, G., ELIOPOULOS, A. G. & YOUNG, L. S. 2003. Epstein-Barr virus latent membrane protein 1 (LMP1) activates the phosphatidylinositol 3-kinase/Akt pathway to promote cell survival and induce actin filament remodeling. *J Biol Chem,* 278**,** 3694-704.

DE DUVE, C. 1963. The lysosome. *Sci Am,* 208**,** 64-72.

DE DUVE, C. & WATTIAUX, R. 1966. Functions of lysosomes. *Annu Rev Physiol,* 28**,** 435-92.

DE LA VEGA, I., VINUELA, E. & BLASCO, R. 1990. Genetic variation and multigene families in African swine fever virus. *Virology,* 179**,** 234-46.

DE VILLIERS, E. P., GALLARDO, C., ARIAS, M., DA SILVA, M., UPTON, C., MARTIN, R. & BISHOP, R. P. 2010. Phylogenomic analysis of 11 complete African swine fever virus genome sequences. *Virology,* 400**,** 128-36.

DERETIC, V. 2011. Autophagy in immunity and cell-autonomous defense against intracellular microbes. *Immunol Rev,* 240**,** 92-104.

DERETIC, V., SAITOH, T. & AKIRA, S. 2013. Autophagy in infection, inflammation and immunity. *Nat Rev Immunol,* 13**,** 722-37.

DIXON, L. 1986. The structure and function of the African swine fever virus genome. *Rev. sci. tech. Off. int. Epiz.,,* 5**,** 469-475.

DIXON, L. K., BRISTOW, C., WILKINSON, P. J. & SUMPTION, K. J. 1990. Identification of a variable region of the African swine fever virus genome that has undergone separate DNA rearrangements leading to expansion of minisatellite-like sequences. *J Mol Biol,* 216**,** 677-88.

DIXON, L. K., CHAPMAN, D. A., NETHERTON, C. L. & UPTON, C. 2013. African swine fever virus replication and genomics. *Virus Res,* 173**,** 3-14.

DIXON, L. K., ISLAM, M., NASH, R. & REIS, A. L. 2019. African swine fever virus evasion of host defences. *Virus Res,* 266**,** 25-33.

DIXON, L. K., SANCHEZ-CORDON, P. J., GALINDO, I. & ALONSO, C. 2017. Investigations of Pro- and Anti-Apoptotic Factors Affecting African Swine Fever Virus Replication and Pathogenesis. *Viruses,* 9.

DUNN, E. F. & CONNOR, J. H. 2012. HijAkt: The PI3K/Akt pathway in virus replication and pathogenesis. *Prog Mol Biol Transl Sci,* 106**,** 223-50.

EFSA 2010. Scientific Opinion on African Swine Fever. *EFSA Journal,* 8**,** 1556.

ENG, K. E., PANAS, M. D., KARLSSON HEDESTAM, G. B. & MCINERNEY, G. M. 2010. A novel quantitative flow cytometry-based assay for autophagy. *Autophagy,* 6**,** 634-41.

ENGLISH, L., CHEMALI, M., DURON, J., RONDEAU, C., LAPLANTE, A., GINGRAS, D., ALEXANDER, D., LEIB, D., NORBURY, C., LIPPE, R. & DESJARDINS, M. 2009. Autophagy enhances the presentation of endogenous viral antigens on MHC class I molecules during HSV-1 infection. *Nat Immunol,* 10**,** 480-7.

ENJUANES, L., CARRASCOSA, A. L., MORENO, M. A. & VINUELA, E. 1976. Titration of African swine fever (ASF) virus. *J Gen Virol,* 32**,** 471-7.

EPIFANO, C., KRIJNSE-LOCKER, J., SALAS, M. L., SALAS, J. & RODRIGUEZ, J. M. 2006. Generation of filamentous instead of icosahedral particles by repression of African swine fever virus structural protein pB438L. *J Virol,* 80**,** 11456-66.

ESCRIBANO, J. M., GALINDO, I. & ALONSO, C. 2013. Antibody-mediated neutralization of African swine fever virus: myths and facts. *Virus Res,* 173**,** 101-9.

ESFANDIAREI, M., LUO, H., YANAGAWA, B., SUAREZ, A., DABIRI, D., ZHANG, J. & MCMANUS, B. M. 2004. Protein kinase B/Akt regulates coxsackievirus B3 replication through a mechanism which is not caspase dependent. *J Virol,* 78**,** 4289-98.

FAUQUET, M. C. & MAYO, A. M. 2001. The 7th ICTV Report. *Archives of Virology,* 146**,** 189-194.

FERNANDEZ, A., PEREZ, J., MARTIN DE LAS MULAS, J., CARRASCO, L., DOMINGUEZ, J. & SIERRA, M. A. 1992. Localization of African swine fever viral antigen, swine IgM, IgG and C1q in lung and liver tissues of experimentally infected pigs. *J Comp Pathol,* 107**,** 81-90.

FLETCHER, K., ULFERTS, R., JACQUIN, E., VEITH, T., GAMMOH, N., ARASTEH, J. M., MAYER, U., CARDING, S. R., WILEMAN, T., BEALE, R. & FLOREY, O. 2018. The WD40 domain of ATG16L1 is required for its non-canonical role in lipidation of LC3 at single membranes. *EMBO J,* 37.

FLOREY, O. & OVERHOLTZER, M. 2012. Autophagy proteins in macroendocytic engulfment. *Trends Cell Biol,* 22**,** 374-80.

FRANKE, T. F., YANG, S. I., CHAN, T. O., DATTA, K., KAZLAUSKAS, A., MORRISON, D. K., KAPLAN, D. R. & TSICHLIS, P. N. 1995. The protein kinase encoded by the Akt proto-oncogene is a target of the PDGF-activated phosphatidylinositol 3-kinase. *Cell,* 81**,** 727-36.

FUJITA, N., ITOH, T., OMORI, H., FUKUDA, M., NODA, T. & YOSHIMORI, T. 2008. The Atg16L complex specifies the site of LC3 lipidation for membrane biogenesis in autophagy. *Mol Biol Cell,* 19**,** 2092-100.

FUKAO, T., TANABE, M., TERAUCHI, Y., OTA, T., MATSUDA, S., ASANO, T., KADOWAKI, T., TAKEUCHI, T. & KOYASU, S. 2002. PI3K-mediated negative feedback regulation of IL-12 production in DCs. *Nat Immunol,* 3**,** 875-81.

FUNDERBURK, S. F., WANG, Q. J. & YUE, Z. 2010. The Beclin 1-VPS34 complex--at the crossroads of autophagy and beyond. *Trends Cell Biol,* 20**,** 355-62.

GALINDO, I., HERNAEZ, B., DIAZ-GIL, G., ESCRIBANO, J. M. & ALONSO, C. 2008. A179L, a viral Bcl-2 homologue, targets the core Bcl-2 apoptotic machinery and its upstream BH3 activators with selective binding restrictions for Bid and Noxa. *Virology,* 375**,** 561-72.

GALINDO, I., HERNAEZ, B., MUNOZ-MORENO, R., CUESTA-GEIJO, M. A., DALMAU-MENA, I. & ALONSO, C. 2012. The ATF6 branch of unfolded protein response and apoptosis are activated to promote African swine fever virus infection. *Cell Death Dis,* 3**,** e341.

GALINDO, I., VINUELA, E. & CARRASCOSA, A. L. 1997. Protein cell receptors mediate the saturable interaction of African swine fever virus attachment protein p12 with the surface of permissive cells. *Virus Res,* 49**,** 193-204.

GALLARDO, C., SOLER, A., NIETO, R., SANCHEZ, M. A., MARTINS, C., PELAYO, V., CARRASCOSA, A., REVILLA, Y., SIMON, A., BRIONES, V., SANCHEZ-VIZCAINO, J. M. & ARIAS, M. 2015. Experimental Transmission of African Swine Fever (ASF) Low Virulent Isolate NH/P68 by Surviving Pigs. *Transbound Emerg Dis,* 62**,** 612-22.

GARCIA-BEATO, R., SALAS, M. L., VINUELA, E. & SALAS, J. 1992. Role of the host cell nucleus in the replication of African swine fever virus DNA. *Virology,* 188**,** 637-49.

GARCIA-DORIVAL, I., WU, W., DOWALL, S., ARMSTRONG, S., TOUZELET, O., WASTLING, J., BARR, J. N., MATTHEWS, D., CARROLL, M., HEWSON, R. & HISCOX, J. A. 2014. Elucidation of the Ebola virus VP24 cellular interactome and disruption of virus biology through targeted inhibition of host-cell protein function. *J Proteome Res,* 13**,** 5120-35.

GARCIA-ESCUDERO, R., ANDRES, G., ALMAZAN, F. & VINUELA, E. 1998. Inducible gene expression from African swine fever virus recombinants: analysis of the major capsid protein p72. *J Virol,* 72**,** 3185-95.

GE, L., MELVILLE, D., ZHANG, M. & SCHEKMAN, R. 2013. The ER-Golgi intermediate compartment is a key membrane source for the LC3 lipidation step of autophagosome biogenesis. *Elife,* 2**,** e00947.

GELINO, S. & HANSEN, M. 2012. Autophagy - An Emerging Anti-Aging Mechanism. *J Clin Exp Pathol,* Suppl 4.

GENG, J. & KLIONSKY, D. J. 2010. The Golgi as a potential membrane source for autophagy. *Autophagy,* 6**,** 950-1.

GERMIC, N., FRANGEZ, Z., YOUSEFI, S. & SIMON, H. U. 2019. Regulation of the innate immune system by autophagy: monocytes, macrophages, dendritic cells and antigen presentation. *Cell Death Differ,* 26**,** 715-727.

GOATLEY, L. C., MARRON, M. B., JACOBS, S. C., HAMMOND, J. M., MISKIN, J. E., ABRAMS, C. C., SMITH, G. L. & DIXON, L. K. 1999. Nuclear and nucleolar localization of an African swine fever virus protein, I14L, that is similar to the herpes simplex virus-encoded virulence factor ICP34.5. *J Gen Virol,* 80 (Pt 3)**,** 525-35.

GOBEIL, P. A. & LEIB, D. A. 2012. Herpes simplex virus gamma34.5 interferes with autophagosome maturation and antigen presentation in dendritic cells. *MBio,* 3**,** e00267-12.

GOEBEL, S. J., JOHNSON, G. P., PERKUS, M. E., DAVIS, S. W., WINSLOW, J. P. & PAOLETTI, E. 1990. The complete DNA sequence of vaccinia virus. *Virology,* 179**,** 247-66, 517-63.

GOGIN, A., GERASIMOV, V., MALOGOLOVKIN, A. & KOLBASOV, D. 2013. African swine fever in the North Caucasus region and the Russian Federation in years 2007-2012. *Virus Res,* 173**,** 198-203.

GOMES, L. C. & DIKIC, I. 2014. Autophagy in antimicrobial immunity. *Mol Cell,* 54**,** 224-33.

GOMEZ-VILLAMANDOS, J. C., BAUTISTA, M. J., SANCHEZ-CORDON, P. J. & CARRASCO, L. 2013. Pathology of African swine fever: the role of monocyte-macrophage. *Virus Res,* 173**,** 140-9.

GONZALEZ, A., TALAVERA, A., ALMENDRAL, J. M. & VINUELA, E. 1986. Hairpin loop structure of African swine fever virus DNA. *Nucleic Acids Res,* 14**,** 6835-44.

GREIG, A. 1972. Pathogenesis of African swine fever in pigs naturally exposed to the disease. *J Comp Pathol,* 82**,** 73-9.

GUINAT, C., GOGIN, A., BLOME, S., KEIL, G., POLLIN, R., PFEIFFER, D. U. & DIXON, L. 2016. Transmission routes of African swine fever virus to domestic pigs: current knowledge and future research directions. *Vet Rec,* 178**,** 262-7.

GUO, J. P., COPPOLA, D. & CHENG, J. Q. 2011. IKBKE protein activates Akt independent of phosphatidylinositol 3-kinase/PDK1/mTORC2 and the pleckstrin homology domain to sustain malignant transformation. *J Biol Chem,* 286**,** 37389-98.

HAHN-WINDGASSEN, A., NOGUEIRA, V., CHEN, C. C., SKEEN, J. E., SONENBERG, N. & HAY, N. 2005. Akt activates the mammalian target of rapamycin by regulating cellular ATP level and AMPK activity. *J Biol Chem,* 280**,** 32081-9.

HAILEY, D. W., RAMBOLD, A. S., SATPUTE-KRISHNAN, P., MITRA, K., SOUGRAT, R., KIM, P. K. & LIPPINCOTT-SCHWARTZ, J. 2010. Mitochondria supply membranes for autophagosome biogenesis during starvation. *Cell,* 141**,** 656-67.

HAWES, P. C., NETHERTON, C. L., WILEMAN, T. E. & MONAGHAN, P. 2008. The envelope of intracellular African swine fever virus is composed of a single lipid bilayer. *J Virol,* 82**,** 7905-12.

HE, C. & KLIONSKY, D. J. 2009. Regulation mechanisms and signaling pathways of autophagy. *Annu Rev Genet,* 43**,** 67-93.

HE, H., DANG, Y., DAI, F., GUO, Z., WU, J., SHE, X., PEI, Y., CHEN, Y., LING, W., WU, C., ZHAO, S., LIU, J. O. & YU, L. 2003. Post-translational modifications of three members of the human MAP1LC3 family and detection of a novel type of modification for MAP1LC3B. *J Biol Chem,* 278**,** 29278-87.

HEMMINGS, B. A. & RESTUCCIA, D. F. 2012. PI3K-PKB/Akt pathway. *Cold Spring Harb Perspect Biol,* 4**,** a011189.

HERNAEZ, B. & ALONSO, C. 2010. Dynamin- and clathrin-dependent endocytosis in African swine fever virus entry. *J Virol,* 84**,** 2100-9.

HERNAEZ, B., CABEZAS, M., MUNOZ-MORENO, R., GALINDO, I., CUESTA-GEIJO, M. A. & ALONSO, C. 2013. A179L, a new viral Bcl2 homolog targeting Beclin 1 autophagy related protein. *Curr Mol Med,* 13**,** 305-16.

HERNAEZ, B., ESCRIBANO, J. M. & ALONSO, C. 2006. Visualization of the African swine fever virus infection in living cells by incorporation into the virus particle of green fluorescent protein-p54 membrane protein chimera. *Virology,* 350**,** 1-14.

HERNAEZ, B., GUERRA, M., SALAS, M. L. & ANDRES, G. 2016. African Swine Fever Virus Undergoes Outer Envelope Disruption, Capsid Disassembly and Inner Envelope Fusion before Core Release from Multivesicular Endosomes. *PLoS Pathog,* 12**,** e1005595.

HESS, W. R., COX, B. F., HEUSCHELE, W. P. & STONE, S. S. 1965. Propagation and Modification of African Swine Fever Virus in Cell Cultures. *Am J Vet Res,* 26**,** 141-6.

HUBALEK, Z., RUDOLF, I. & NOWOTNY, N. 2014. Arboviruses pathogenic for domestic and wild animals. *Adv Virus Res,* 89**,** 201-75.

ICHIMURA, Y., KIRISAKO, T., TAKAO, T., SATOMI, Y., SHIMONISHI, Y., ISHIHARA, N., MIZUSHIMA, N., TANIDA, I., KOMINAMI, E., OHSUMI, M., NODA, T. & OHSUMI, Y. 2000. A ubiquitin-like system mediates protein lipidation. *Nature,* 408**,** 488-92.

INOKI, K., ZHU, T. & GUAN, K. L. 2003. TSC2 mediates cellular energy response to control cell growth and survival. *Cell,* 115**,** 577-90.

IVANOV, V., EFREMOV, E. E., NOVIKOV, B. V., BALYSHEV, V. M., TSIBANOV, S., KALINOVSKY, T., KOLBASOV, D. V., NIEDZWIECKI, A. & RATH, M. 2011. Vaccination with viral protein-mimicking peptides postpones mortality in domestic pigs infected by African swine fever virus. *Mol Med Rep,* 4**,** 395-401.

IYER, L. M., BALAJI, S., KOONIN, E. V. & ARAVIND, L. 2006. Evolutionary genomics of nucleo-cytoplasmic large DNA viruses. *Virus Res,* 117**,** 156-84.

IZMAILYAN, R., HSAO, J. C., CHUNG, C. S., CHEN, C. H., HSU, P. W., LIAO, C. L. & CHANG, W. 2012. Integrin beta1 mediates vaccinia virus entry through activation of PI3K/Akt signaling. *J Virol,* 86**,** 6677-87.

JACKSON, W. T., GIDDINGS, T. H., JR., TAYLOR, M. P., MULINYAWE, S., RABINOVITCH, M., KOPITO, R. R. & KIRKEGAARD, K. 2005. Subversion of cellular autophagosomal machinery by RNA viruses. *PLoS Biol,* 3**,** e156.

JANEWAY, C. A., JR. & MEDZHITOV, R. 2002. Innate immune recognition. *Annu Rev Immunol,* 20**,** 197-216.

JHANWAR-UNIYAL, M., WAINWRIGHT, J. V., MOHAN, A. L., TOBIAS, M. E., MURALI, R., GANDHI, C. D. & SCHMIDT, M. H. 2019. Diverse signaling mechanisms of mTOR complexes: mTORC1 and mTORC2 in forming a formidable relationship. *Adv Biol Regul,* 72**,** 51-62.

JORI, F. & BASTOS, A. D. 2009. Role of wild suids in the epidemiology of African swine fever. *Ecohealth,* 6**,** 296-310.

JOUNG, S. M., PARK, Z. Y., RANI, S., TAKEUCHI, O., AKIRA, S. & LEE, J. Y. 2011. Akt contributes to activation of the TRIF-dependent signaling pathways of TLRs by interacting with TANK-binding kinase 1. *J Immunol,* 186**,** 499-507.

JOUVENET, N., MONAGHAN, P., WAY, M. & WILEMAN, T. 2004. Transport of African swine fever virus from assembly sites to the plasma membrane is dependent on microtubules and conventional kinesin. *J Virol,* 78**,** 7990-8001.

JOUVENET, N. & WILEMAN, T. 2005. African swine fever virus infection disrupts centrosome assembly and function. *J Gen Virol,* 86**,** 589-94.

KABEYA, Y., MIZUSHIMA, N., UENO, T., YAMAMOTO, A., KIRISAKO, T., NODA, T., KOMINAMI, E., OHSUMI, Y. & YOSHIMORI, T. 2000. LC3, a mammalian homologue of yeast Apg8p, is localized in autophagosome membranes after processing. *EMBO J,* 19**,** 5720-8.

KAMADA, Y., FUNAKOSHI, T., SHINTANI, T., NAGANO, K., OHSUMI, M. & OHSUMI, Y. 2000. Tor-mediated induction of autophagy via an Apg1 protein kinase complex. *J Cell Biol,* 150**,** 1507-13.

KÄRBER, G. 1931. Beitrag zur kollektiven Behandlung pharmakologischer Reihenversuche. *Naunyn-Schmiedebergs Archiv für experimentelle Pathologie und Pharmakologie,* 162**,** 480-483.

KEENAN, R. J., FREYMANN, D. M., STROUD, R. M. & WALTER, P. 2001. The signal recognition particle. *Annu Rev Biochem,* 70**,** 755-75.

KELLY, D. C. & ROBERTSON, J. S. 1973. Icosahedral cytoplasmic deoxyriboviruses. *J Gen Virol,* 20**,** Suppl:17-41.

KHAMINETS, A., HEINRICH, T., MARI, M., GRUMATI, P., HUEBNER, A. K., AKUTSU, M., LIEBMANN, L., STOLZ, A., NIETZSCHE, S., KOCH, N., MAUTHE, M., KATONA, I., QUALMANN, B., WEIS, J., REGGIORI, F., KURTH, I., HUBNER, C. A. & DIKIC, I. 2015. Regulation of endoplasmic reticulum turnover by selective autophagy. *Nature,* 522**,** 354-8.

KIM, E., GORAKSHA-HICKS, P., LI, L., NEUFELD, T. P. & GUAN, K. L. 2008. Regulation of TORC1 by Rag GTPases in nutrient response. *Nat Cell Biol,* 10**,** 935-45.

KIMBALL, S. R. 2006. Interaction between the AMP-activated protein kinase and mTOR signaling pathways. *Med Sci Sports Exerc,* 38**,** 1958-64.

KING, K., CHAPMAN, D., ARGILAGUET, J. M., FISHBOURNE, E., HUTET, E., CARIOLET, R., HUTCHINGS, G., OURA, C. A., NETHERTON, C. L., MOFFAT, K., TAYLOR, G., LE POTIER, M. F., DIXON, L. K. & TAKAMATSU, H. H. 2011. Protection of European domestic pigs from virulent African isolates of African swine fever virus by experimental immunisation. *Vaccine,* 29**,** 4593-600.

KIRIYAMA, Y. & NOCHI, H. 2015. The Function of Autophagy in Neurodegenerative Diseases. *Int J Mol Sci,* 16**,** 26797-812.

KIRKEGAARD, K. 2009. Subversion of the cellular autophagy pathway by viruses. *Curr Top Microbiol Immunol,* 335**,** 323-33.

KIRKEGAARD, K., TAYLOR, M. P. & JACKSON, W. T. 2004. Cellular autophagy: surrender, avoidance and subversion by microorganisms. *Nat Rev Microbiol,* 2**,** 301-14.

KLIONSKY, D. J., ABDELMOHSEN, K., ABE, A., ABEDIN, M. J., ABELIOVICH, H., ACEVEDO AROZENA, A., ADACHI, H., ADAMS, C. M., ADAMS, P. D., ADELI, K., ADHIHETTY, P. J., ADLER, S. G., AGAM, G., AGARWAL, R., AGHI, M. K., AGNELLO, M., AGOSTINIS, P., AGUILAR, P. V., AGUIRRE-GHISO, J., AIROLDI, E. M., AIT-SI-ALI, S., AKEMATSU, T., AKPORIAYE, E. T., AL-RUBEAI, M., ALBAICETA, G. M., ALBANESE, C., ALBANI, D., ALBERT, M. L., ALDUDO, J., ALGUL, H., ALIREZAEI, M., ALLOZA, I., ALMASAN, A., ALMONTE-BECERIL, M., ALNEMRI, E. S., ALONSO, C., ALTAN-BONNET, N., ALTIERI, D. C., ALVAREZ, S., ALVAREZ-ERVITI, L., ALVES, S., AMADORO, G., AMANO, A., AMANTINI, C., AMBROSIO, S., AMELIO, I., AMER, A. O., AMESSOU, M., AMON, A., AN, Z., ANANIA, F. A., ANDERSEN, S. U., ANDLEY, U. P., ANDREADI, C. K., ANDRIEU-ABADIE, N., ANEL, A., ANN, D. K., ANOOPKUMAR-DUKIE, S., ANTONIOLI, M., AOKI, H., APOSTOLOVA, N., AQUILA, S., AQUILANO, K., ARAKI, K., ARAMA, E., ARANDA, A., ARAYA, J., ARCARO, A., ARIAS, E., ARIMOTO, H., ARIOSA, A. R., ARMSTRONG, J. L., ARNOULD, T., ARSOV, I., ASANUMA, K., ASKANAS, V., ASSELIN, E., ATARASHI, R., ATHERTON, S. S., ATKIN, J. D., ATTARDI, L. D., AUBERGER, P., AUBURGER, G., AURELIAN, L., AUTELLI, R., AVAGLIANO, L., AVANTAGGIATI, M. L., AVRAHAMI, L., AWALE, S., AZAD, N., BACHETTI, T., BACKER, J. M., BAE, D. H., BAE, J. S., BAE, O. N., BAE, S. H., BAEHRECKE, E. H., BAEK, S. H., BAGHDIGUIAN, S., BAGNIEWSKA-ZADWORNA, A., et al. 2016. Guidelines for the use and interpretation of assays for monitoring autophagy (3rd edition). *Autophagy,* 12**,** 1-222.

KLIPPEL, A., REINHARD, C., KAVANAUGH, W. M., APELL, G., ESCOBEDO, M. A. & WILLIAMS, L. T. 1996. Membrane localization of phosphatidylinositol 3-kinase is sufficient to activate multiple signal-transducing kinase pathways. *Mol Cell Biol,* 16**,** 4117-27.

KROEMER, G. 1997. The proto-oncogene Bcl-2 and its role in regulating apoptosis. *Nat Med,* 3**,** 614-20.

KUDCHODKAR, S. B., DEL PRETE, G. Q., MAGUIRE, T. G. & ALWINE, J. C. 2007. AMPK-mediated inhibition of mTOR kinase is circumvented during immediate-early times of human cytomegalovirus infection. *J Virol,* 81**,** 3649-51.

KUMA, A., HATANO, M., MATSUI, M., YAMAMOTO, A., NAKAYA, H., YOSHIMORI, T., OHSUMI, Y., TOKUHISA, T. & MIZUSHIMA, N. 2004. The role of autophagy during the early neonatal starvation period. *Nature,* 432**,** 1032-6.

KUMA, A., MATSUI, M. & MIZUSHIMA, N. 2007. LC3, an autophagosome marker, can be incorporated into protein aggregates independent of autophagy: caution in the interpretation of LC3 localization. *Autophagy,* 3**,** 323-8.

KYEI, G. B., DINKINS, C., DAVIS, A. S., ROBERTS, E., SINGH, S. B., DONG, C., WU, L., KOMINAMI, E., UENO, T., YAMAMOTO, A., FEDERICO, M., PANGANIBAN, A., VERGNE, I. & DERETIC, V. 2009. Autophagy pathway intersects with HIV-1 biosynthesis and regulates viral yields in macrophages. *J Cell Biol,* 186**,** 255-68.

LEE, C. J., LIAO, C. L. & LIN, Y. L. 2005. Flavivirus activates phosphatidylinositol 3-kinase signaling to block caspase-dependent apoptotic cell death at the early stage of virus infection. *J Virol,* 79**,** 8388-99.

LEIB, D. A., ALEXANDER, D. E., COX, D., YIN, J. & FERGUSON, T. A. 2009. Interaction of ICP34.5 with Beclin 1 modulates herpes simplex virus type 1 pathogenesis through control of CD4+ T-cell responses. *J Virol,* 83**,** 12164-71.

LEITAO, A., CARTAXEIRO, C., COELHO, R., CRUZ, B., PARKHOUSE, R. M., PORTUGAL, F., VIGARIO, J. D. & MARTINS, C. L. 2001. The non-haemadsorbing African swine fever virus isolate ASFV/NH/P68 provides a model for defining the protective anti-virus immune response. *J Gen Virol,* 82**,** 513-23.

LEVINE, B. 2005. Eating oneself and uninvited guests: autophagy-related pathways in cellular defense. *Cell,* 120**,** 159-62.

LEVINE, B. & DERETIC, V. 2007. Unveiling the roles of autophagy in innate and adaptive immunity. *Nat Rev Immunol,* 7**,** 767-77.

LEWIS, T., ZSAK, L., BURRAGE, T. G., LU, Z., KUTISH, G. F., NEILAN, J. G. & ROCK, D. L. 2000. An African swine fever virus ERV1-ALR homologue, 9GL, affects virion maturation and viral growth in macrophages and viral virulence in swine. *J Virol,* 74**,** 1275-85.

LI, B., DUAN, P., LI, C., JING, Y., HAN, X., YAN, W. & XING, Y. 2015. Role of autophagy on bone marrow mesenchymal stemcell proliferation and differentiation into neurons. *Mol Med Rep*.

LI, W. W., LI, J. & BAO, J. K. 2012. Microautophagy: lesser-known self-eating. *Cell Mol Life Sci,* 69**,** 1125-36.

LIANG, X. H., KLEEMAN, L. K., JIANG, H. H., GORDON, G., GOLDMAN, J. E., BERRY, G., HERMAN, B. & LEVINE, B. 1998. Protection against fatal Sindbis virus encephalitis by beclin, a novel Bcl-2-interacting protein. *J Virol,* 72**,** 8586-96.

LIAO, Y. & HUNG, M. C. 2010. Physiological regulation of Akt activity and stability. *Am J Transl Res,* 2**,** 19-42.

LIPATOVA, Z. & SEGEV, N. 2017. Chapter 10 - ER-Phagy in Starvation, ER Stress, and Quality Control. *In:* HAYAT, M. A. (ed.) *Autophagy: Cancer, Other Pathologies, Inflammation, Immunity, Infection, and Aging.* Academic Press.

LITHGOW, P., TAKAMATSU, H., WERLING, D., DIXON, L. & CHAPMAN, D. 2014. Correlation of cell surface marker expression with African swine fever virus infection. *Vet Microbiol,* 168**,** 413-9.

LIU, Q., WANG, J., KANG, S. A., THOREEN, C. C., HUR, W., AHMED, T., SABATINI, D. M. & GRAY, N. S. 2011. Discovery of 9-(6-aminopyridin-3-yl)-1-(3-(trifluoromethyl)phenyl)benzo[h][1,6]naphthyridin-2(1H)-one (Torin2) as a potent, selective, and orally available mammalian target of rapamycin (mTOR) inhibitor for treatment of cancer. *J Med Chem,* 54**,** 1473-80.

LONG, X., ORTIZ-VEGA, S., LIN, Y. & AVRUCH, J. 2005. Rheb binding to mammalian target of rapamycin (mTOR) is regulated by amino acid sufficiency. *J Biol Chem,* 280**,** 23433-6.

LU, Z., KUTISH, G. F., SUSSMAN, M. D. & ROCK, D. L. 1993. An African swine fever virus gene with a similarity to eukaryotic RNA polymerase subunit 6. *Nucleic Acids Res,* 21**,** 2940.

LUO, S. & RUBINSZTEIN, D. C. 2010. Apoptosis blocks Beclin 1-dependent autophagosome synthesis: an effect rescued by Bcl-xL. *Cell Death Differ,* 17**,** 268-77.

LUSSIGNOL, M., QUEVAL, C., BERNET-CAMARD, M. F., COTTE-LAFFITTE, J., BEAU, I., CODOGNO, P. & ESCLATINE, A. 2013. The herpes simplex virus 1 Us11 protein inhibits autophagy through its interaction with the protein kinase PKR. *J Virol,* 87**,** 859-71.

MA, X. M. & BLENIS, J. 2009. Molecular mechanisms of mTOR-mediated translational control. *Nat Rev Mol Cell Biol,* 10**,** 307-18.

MADEO, F., ZIMMERMANN, A., MAIURI, M. C. & KROEMER, G. 2015. Essential role for autophagy in life span extension. *J Clin Invest,* 125**,** 85-93.

MALMQUIST, W. A. & HAY, D. 1960. Hemadsorption and cytopathic effect produced by African Swine Fever virus in swine bone marrow and buffy coat cultures. *Am J Vet Res,* 21**,** 104-8.

MANNING, B. D. & TOKER, A. 2017. AKT/PKB Signaling: Navigating the Network. *Cell,* 169**,** 381-405.

MCCULLOUGH, K. C., BASTA, S., KNOTIG, S., GERBER, H., SCHAFFNER, R., KIM, Y. B., SAALMULLER, A. & SUMMERFIELD, A. 1999. Intermediate stages in monocyte-macrophage differentiation modulate phenotype and susceptibility to virus infection. *Immunology,* 98**,** 203-12.

MCKERCHER, P. D., HESS, W. R. & HAMDY, F. 1978. Residual viruses in pork products. *Appl Environ Microbiol,* 35**,** 142-5.

MELLOR, P. S., KITCHING, R. P. & WILKINSON, P. J. 1987. Mechanical transmission of capripox virus and African swine fever virus by Stomoxys calcitrans. *Res Vet Sci,* 43**,** 109-12.

MIZUSHIMA, N., KUMA, A., KOBAYASHI, Y., YAMAMOTO, A., MATSUBAE, M., TAKAO, T., NATSUME, T., OHSUMI, Y. & YOSHIMORI, T. 2003. Mouse Apg16L, a novel WD-repeat protein, targets to the autophagic isolation membrane with the Apg12-Apg5 conjugate. *J Cell Sci,* 116**,** 1679-88.

MIZUSHIMA, N., YAMAMOTO, A., HATANO, M., KOBAYASHI, Y., KABEYA, Y., SUZUKI, K., TOKUHISA, T., OHSUMI, Y. & YOSHIMORI, T. 2001. Dissection of autophagosome formation using Apg5-deficient mouse embryonic stem cells. *J Cell Biol,* 152**,** 657-68.

MIZUSHIMA, N. & YOSHIMORI, T. 2007. How to interpret LC3 immunoblotting. *Autophagy,* 3**,** 542-5.

MIZUSHIMA, N., YOSHIMORI, T. & OHSUMI, Y. 2011. The role of Atg proteins in autophagosome formation. *Annu Rev Cell Dev Biol,* 27**,** 107-32.

MONTGOMERY, R. 1921. On A Form of Swine Fever Occurring in British East Africa (Kenya Colony). *Journal of Comparative Pathology and Therapeutics,* 34**,** 159-191.

MORTIMORE, G. E., HUTSON, N. J. & SURMACZ, C. A. 1983. Quantitative correlation between proteolysis and macro- and microautophagy in mouse hepatocytes during starvation and refeeding. *Proceedings of the National Academy of Sciences,* 80**,** 2179-2183.

MOSS, B. 2013. Poxvirus DNA replication. *Cold Spring Harb Perspect Biol,* 5.

MUKHOPADHYAY, S., PANDA, P. K., SINHA, N., DAS, D. N. & BHUTIA, S. K. 2014. Autophagy and apoptosis: where do they meet? *Apoptosis,* 19**,** 555-66.

MURRAY, E. R. & CAMERON, A. J. M. 2017. Towards specific inhibition of mTORC2. *Aging (Albany NY),* 9**,** 2461-2462.

NAKASHIMA, A., TANAKA, N., TAMAI, K., KYUUMA, M., ISHIKAWA, Y., SATO, H., YOSHIMORI, T., SAITO, S. & SUGAMURA, K. 2006. Survival of parvovirus B19-infected cells by cellular autophagy. *Virology,* 349**,** 254-63.

NARDACCI, R., CICCOSANTI, F., MARSELLA, C., IPPOLITO, G., PIACENTINI, M. & FIMIA, G. M. 2017. Role of autophagy in HIV infection and pathogenesis. *J Intern Med,* 281**,** 422-432.

NEILAN, J. G., LU, Z., AFONSO, C. L., KUTISH, G. F., SUSSMAN, M. D. & ROCK, D. L. 1993. An African swine fever virus gene with similarity to the proto-oncogene bcl-2 and the Epstein-Barr virus gene BHRF1. *J Virol,* 67**,** 4391-4.

NEILAN, J. G., ZSAK, L., LU, Z., BURRAGE, T. G., KUTISH, G. F. & ROCK, D. L. 2004. Neutralizing antibodies to African swine fever virus proteins p30, p54, and p72 are not sufficient for antibody-mediated protection. *Virology,* 319**,** 337-42.

NEILAN, J. G., ZSAK, L., LU, Z., KUTISH, G. F., AFONSO, C. L. & ROCK, D. L. 2002. Novel swine virulence determinant in the left variable region of the African swine fever virus genome. *J Virol,* 76**,** 3095-104.

NETHERTON, C. L., GOATLEY, L. C., REIS, A. L., PORTUGAL, R., NASH, R. H., MORGAN, S. B., GAULT, L., NIETO, R., NORLIN, V., GALLARDO, C., HO, C. S., SANCHEZ-CORDON, P. J., TAYLOR, G. & DIXON, L. K. 2019. Identification and Immunogenicity of African Swine Fever Virus Antigens. *Front Immunol,* 10**,** 1318.

NETHERTON, C. L. & WILEMAN, T. E. 2013. African swine fever virus organelle rearrangements. *Virus Res,* 173**,** 76-86.

NODA, T. & OHSUMI, Y. 1998. Tor, a phosphatidylinositol kinase homologue, controls autophagy in yeast. *J Biol Chem,* 273**,** 3963-6.

NORMILE, D. 2019. African swine fever marches across much of Asia. *Science,* 364**,** 617-618.

NOVIKOFF, A. B., BEAUFAY, H. & DE DUVE, C. 1956. Electron microscopy of lysosomerich fractions from rat liver. *J Biophys Biochem Cytol,* 2**,** 179-84.

NUNES, J. F., VIGARIO, J. D. & TERRINHA, A. M. 1975. Ultrastructural study of African swine fever virus replication in cultures of swine bone marrow cells. *Arch Virol,* 49**,** 59-66.

O'DONNELL, V., HOLINKA, L. G., GLADUE, D. P., SANFORD, B., KRUG, P. W., LU, X., ARZT, J., REESE, B., CARRILLO, C., RISATTI, G. R. & BORCA, M. V. 2015. African Swine Fever Virus Georgia Isolate Harboring Deletions of MGF360 and MGF505 Genes Is Attenuated in Swine and Confers Protection against Challenge with Virulent Parental Virus. *J Virol,* 89**,** 6048-56.

O'SHEA, C. C., CHOI, S., MCCORMICK, F. & STOKOE, D. 2005. Adenovirus overrides cellular checkpoints for protein translation. *Cell Cycle,* 4**,** 883-8.

OGATA, M., HINO, S., SAITO, A., MORIKAWA, K., KONDO, S., KANEMOTO, S., MURAKAMI, T., TANIGUCHI, M., TANII, I., YOSHINAGA, K., SHIOSAKA, S., HAMMARBACK, J. A., URANO, F. & IMAIZUMI, K. 2006. Autophagy is activated for cell survival after endoplasmic reticulum stress. *Mol Cell Biol,* 26**,** 9220-31.

OKADA, T., YOSHIDA, H., AKAZAWA, R., NEGISHI, M. & MORI, K. 2002. Distinct roles of activating transcription factor 6 (ATF6) and double-stranded RNA-activated protein kinase-like endoplasmic reticulum kinase (PERK) in transcription during the mammalian unfolded protein response. *Biochem J,* 366**,** 585-94.

OKAMOTO, K., KONDO-OKAMOTO, N. & OHSUMI, Y. 2009. Mitochondria-anchored receptor Atg32 mediates degradation of mitochondria via selective autophagy. *Dev Cell,* 17**,** 87-97.

ONISK, D. V., BORCA, M. V., KUTISH, G., KRAMER, E., IRUSTA, P. & ROCK, D. L. 1994. Passively transferred African swine fever virus antibodies protect swine against lethal infection. *Virology,* 198**,** 350-4.

ORVEDAHL, A., ALEXANDER, D., TALLOCZY, Z., SUN, Q., WEI, Y., ZHANG, W., BURNS, D., LEIB, D. A. & LEVINE, B. 2007. HSV-1 ICP34.5 confers neurovirulence by targeting the Beclin 1 autophagy protein. *Cell Host Microbe,* 1**,** 23-35.

OURA, C. A., DENYER, M. S., TAKAMATSU, H. & PARKHOUSE, R. M. 2005. In vivo depletion of CD8+ T lymphocytes abrogates protective immunity to African swine fever virus. *J Gen Virol,* 86**,** 2445-50.

OZPOLAT, B. & BENBROOK, D. M. 2015. Targeting autophagy in cancer management - strategies and developments. *Cancer Manag Res,* 7**,** 291-9.

PANKIV, S., CLAUSEN, T. H., LAMARK, T., BRECH, A., BRUUN, J. A., OUTZEN, H., OVERVATN, A., BJORKOY, G. & JOHANSEN, T. 2007. p62/SQSTM1 binds directly to Atg8/LC3 to facilitate degradation of ubiquitinated protein aggregates by autophagy. *J Biol Chem,* 282**,** 24131-45.

PANYASRIVANIT, M., GREENWOOD, M. P., MURPHY, D., ISIDORO, C., AUEWARAKUL, P. & SMITH, D. R. 2011. Induced autophagy reduces virus output in dengue infected monocytic cells. *Virology,* 418**,** 74-84.

PARKER, J., PLOWRIGHT, W. & PIERCE, M. A. 1969. The epizootiology of African swine fever in Africa. *Vet Rec,* 85**,** 668-74.

PENRITH, M. L. & VOSLOO, W. 2009. Review of African swine fever: transmission, spread and control. *J S Afr Vet Assoc,* 80**,** 58-62.

PETIOT, A., OGIER-DENIS, E., BLOMMAART, E. F., MEIJER, A. J. & CODOGNO, P. 2000. Distinct classes of phosphatidylinositol 3'-kinases are involved in signaling pathways that control macroautophagy in HT-29 cells. *J Biol Chem,* 275**,** 992-8.

PINI, A. & HURTER, L. R. 1975. African swine fever: an epizootiological review with special reference to the South African situation. *J S Afr Vet Assoc,* 46**,** 227-32.

PLOWRIGHT, W. 1986. African swine fever: a retrospective view. *Revue Scientifique et Technique de l'OIE,* 5**,** 455-468.

PLOWRIGHT, W., PARKER, J. & PEIRCE, M. A. 1969. African swine fever virus in ticks (Ornithodoros moubata, murray) collected from animal burrows in Tanzania. *Nature,* 221**,** 1071-3.

PLOWRIGHT, W., PERRY, C. T. & GREIG, A. 1974. Sexual transmission of African swine fever virus in the tick, Ornithodoros moubata porcinus, Walton. *Res Vet Sci,* 17**,** 106-13.

PLOWRIGHT, W., PERRY, C. T. & PEIRCE, M. A. 1970a. Transovarial infection with African swine fever virus in the argasid tick, Ornithodoros moubata porcinus, Walton. *Res Vet Sci,* 11**,** 582-4.

PLOWRIGHT, W., PERRY, C. T., PEIRCE, M. A. & PARKER, J. 1970b. Experimental infection of the argasid tick, Ornithodoros moubata porcinus, with African swine fever virus. *Arch Gesamte Virusforsch,* 31**,** 33-50.

PORTUGAL, R., COELHO, J., HOPER, D., LITTLE, N. S., SMITHSON, C., UPTON, C., MARTINS, C., LEITAO, A. & KEIL, G. M. 2015. Related strains of African swine fever virus with different virulence: genome comparison and analysis. *J Gen Virol,* 96**,** 408-19.

PRENTICE, E., JEROME, W. G., YOSHIMORI, T., MIZUSHIMA, N. & DENISON, M. R. 2004. Coronavirus replication complex formation utilizes components of cellular autophagy. *J Biol Chem,* 279**,** 10136-41.

PROIKAS-CEZANNE, T., TAKACS, Z., DONNES, P. & KOHLBACHER, O. 2015. WIPI proteins: essential PtdIns3P effectors at the nascent autophagosome. *J Cell Sci,* 128**,** 207-17.

RAOULT, D., AUDIC, S., ROBERT, C., ABERGEL, C., RENESTO, P., OGATA, H., LA SCOLA, B., SUZAN, M. & CLAVERIE, J. M. 2004. The 1.2-megabase genome sequence of Mimivirus. *Science,* 306**,** 1344-50.

REGGIORI, F., MONASTYRSKA, I., VERHEIJE, M. H., CALI, T., ULASLI, M., BIANCHI, S., BERNASCONI, R., DE HAAN, C. A. & MOLINARI, M. 2010. Coronaviruses Hijack the LC3-I-positive EDEMosomes, ER-derived vesicles exporting short-lived ERAD regulators, for replication. *Cell Host Microbe,* 7**,** 500-8.

REIS, A. L., ABRAMS, C. C., GOATLEY, L. C., NETHERTON, C., CHAPMAN, D. G., SANCHEZ-CORDON, P. & DIXON, L. K. 2016. Deletion of African swine fever virus interferon inhibitors from the genome of a virulent isolate reduces virulence in domestic pigs and induces a protective response. *Vaccine,* 34**,** 4698-4705.

REIS, A. L., GOATLEY, L. C., JABBAR, T., SANCHEZ-CORDON, P. J., NETHERTON, C. L., CHAPMAN, D. A. G. & DIXON, L. K. 2017a. Deletion of the African Swine Fever Virus Gene DP148R Does Not Reduce Virus Replication in Culture but Reduces Virus Virulence in Pigs and Induces High Levels of Protection against Challenge. *J Virol,* 91.

REIS, A. L., NETHERTON, C. & DIXON, L. K. 2017b. Unraveling the Armor of a Killer: Evasion of Host Defenses by African Swine Fever Virus. *J Virol,* 91.

REVILLA, Y., CEBRIAN, A., BAIXERAS, E., MARTINEZ, C., VINUELA, E. & SALAS, M. L. 1997. Inhibition of apoptosis by the African swine fever virus Bcl-2 homologue: role of the BH1 domain. *Virology,* 228**,** 400-4.

ROBERTS, R., AL-JAMAL, W. T., WHELBAND, M., THOMAS, P., JEFFERSON, M., VAN DEN BOSSCHE, J., POWELL, P. P., KOSTARELOS, K. & WILEMAN, T. 2013. Autophagy and formation of tubulovesicular autophagosomes provide a barrier against nonviral gene delivery. *Autophagy,* 9**,** 667-82.

RODRIGUEZ-ROCHA, H., GOMEZ-GUTIERREZ, J. G., GARCIA-GARCIA, A., RAO, X. M., CHEN, L., MCMASTERS, K. M. & ZHOU, H. S. 2011. Adenoviruses induce autophagy to promote virus replication and oncolysis. *Virology,* 416**,** 9-15.

RODRIGUEZ, F., FERNANDEZ, A., MARTIN DE LAS MULAS, J. P., SIERRA, M. A. & JOVER, A. 1996. African swine fever: morphopathology of a viral haemorrhagic disease. *Vet Rec,* 139**,** 249-54.

RODRIGUEZ, J. M., GARCIA-ESCUDERO, R., SALAS, M. L. & ANDRES, G. 2004. African swine fever virus structural protein p54 is essential for the recruitment of envelope precursors to assembly sites. *J Virol,* 78**,** 4299-1313.

RODRIGUEZ, J. M. & SALAS, M. L. 2013. African swine fever virus transcription. *Virus Res,* 173**,** 15-28.

ROJO, G., CHAMORRO, M., SALAS, M. L., VINUELA, E., CUEZVA, J. M. & SALAS, J. 1998. Migration of mitochondria to viral assembly sites in African swine fever virus-infected cells. *J Virol,* 72**,** 7583-8.

ROJO, G., GARCIA-BEATO, R., VINUELA, E., SALAS, M. L. & SALAS, J. 1999. Replication of African swine fever virus DNA in infected cells. *Virology,* 257**,** 524-36.

ROUILLER, I., BROOKES, S. M., HYATT, A. D., WINDSOR, M. & WILEMAN, T. 1998. African swine fever virus is wrapped by the endoplasmic reticulum. *J Virol,* 72**,** 2373-87.

ROWLANDS, R. J., MICHAUD, V., HEATH, L., HUTCHINGS, G., OURA, C., VOSLOO, W., DWARKA, R., ONASHVILI, T., ALBINA, E. & DIXON, L. K. 2008. African swine fever virus isolate, Georgia, 2007. *Emerg Infect Dis,* 14**,** 1870-4.

SALAS, M. L. & ANDRES, G. 2013. African swine fever virus morphogenesis. *Virus Res,* 173**,** 29-41.

SALGUERO, F. J., RUIZ-VILLAMOR, E., BAUTISTA, M. J., SANCHEZ-CORDON, P. J., CARRASCO, L. & GOMEZ-VILLAMANDOS, J. C. 2002. Changes in macrophages in spleen and lymph nodes during acute African swine fever: expression of cytokines. *Vet Immunol Immunopathol,* 90**,** 11-22.

SANCHEZ-BOTIJA, C. 1963. Reservorios del virus de la peste porcina Africana. *Bull Off Int Epizoot***,** 895–899.

SANCHEZ-TORRES, C., GOMEZ-PUERTAS, P., GOMEZ-DEL-MORAL, M., ALONSO, F., ESCRIBANO, J. M., EZQUERRA, A. & DOMINGUEZ, J. 2003. Expression of porcine CD163 on monocytes/macrophages correlates with permissiveness to African swine fever infection. *Arch Virol,* 148**,** 2307-23.

SANCHEZ-VIZCAINO, J. M., MUR, L., GOMEZ-VILLAMANDOS, J. C. & CARRASCO, L. 2015. An update on the epidemiology and pathology of African swine fever. *J Comp Pathol,* 152**,** 9-21.

SANCHEZ-VIZCAINO, J. M., MUR, L. & MARTINEZ-LOPEZ, B. 2012. African swine fever: an epidemiological update. *Transbound Emerg Dis,* 59 Suppl 1**,** 27-35.

SANCHEZ, E. G., QUINTAS, A., PEREZ-NUNEZ, D., NOGAL, M., BARROSO, S., CARRASCOSA, A. L. & REVILLA, Y. 2012. African swine fever virus uses macropinocytosis to enter host cells. *PLoS Pathog,* 8**,** e1002754.

SANJUAN, M. A., DILLON, C. P., TAIT, S. W., MOSHIACH, S., DORSEY, F., CONNELL, S., KOMATSU, M., TANAKA, K., CLEVELAND, J. L., WITHOFF, S. & GREEN, D. R. 2007. Toll-like receptor signalling in macrophages links the autophagy pathway to phagocytosis. *Nature,* 450**,** 1253-7.

SANJUAN, M. A., MILASTA, S. & GREEN, D. R. 2009. Toll-like receptor signaling in the lysosomal pathways. *Immunol Rev,* 227**,** 203-20.

SARBASSOV, D. D., GUERTIN, D. A., ALI, S. M. & SABATINI, D. M. 2005. Phosphorylation and regulation of Akt/PKB by the rictor-mTOR complex. *Science,* 307**,** 1098-101.

SCHILLE, S., CRAUWELS, P., BOHN, R., BAGOLA, K., WALTHER, P. & VAN ZANDBERGEN, G. 2018. LC3-associated phagocytosis in microbial pathogenesis. *Int J Med Microbiol,* 308**,** 228-236.

SCHMID, D., PYPAERT, M. & MUNZ, C. 2007. Antigen-loading compartments for major histocompatibility complex class II molecules continuously receive input from autophagosomes. *Immunity,* 26**,** 79-92.

SCHRODER, K. & TSCHOPP, J. 2010. The inflammasomes. *Cell,* 140**,** 821-32.

SENFT, D. & RONAI, Z. A. 2015. UPR, autophagy, and mitochondria crosstalk underlies the ER stress response. *Trends Biochem Sci,* 40**,** 141-8.

SENGUPTA, S., PETERSON, T. R. & SABATINI, D. M. 2010. Regulation of the mTOR complex 1 pathway by nutrients, growth factors, and stress. *Mol Cell,* 40**,** 310-22.

SHI, C. S. & KEHRL, J. H. 2008. MyD88 and Trif target Beclin 1 to trigger autophagy in macrophages. *J Biol Chem,* 283**,** 33175-82.

SHI, C. S. & KEHRL, J. H. 2010. TRAF6 and A20 regulate lysine 63-linked ubiquitination of Beclin-1 to control TLR4-induced autophagy. *Sci Signal,* 3**,** ra42.

SHI, C. S., SHENDEROV, K., HUANG, N. N., KABAT, J., ABU-ASAB, M., FITZGERALD, K. A., SHER, A. & KEHRL, J. H. 2012. Activation of autophagy by inflammatory signals limits IL-1beta production by targeting ubiquitinated inflammasomes for destruction. *Nat Immunol,* 13**,** 255-63.

SMITH, J. D. & DE HARVEN, E. 1978. Herpes simplex virus and human cytomegalovirus replication in WI-38 cells. III. Cytochemical localization of lysosomal enzymes in infected cells. *J Virol,* 26**,** 102-9.

SOARES, J. A., LEITE, F. G., ANDRADE, L. G., TORRES, A. A., DE SOUSA, L. P., BARCELOS, L. S., TEIXEIRA, M. M., FERREIRA, P. C., KROON, E. G., SOUTO-PADRON, T. & BONJARDIM, C. A. 2009. Activation of the PI3K/Akt pathway early during vaccinia and cowpox virus infections is required for both host survival and viral replication. *J Virol,* 83**,** 6883-99.

SOGO, J. M., ALMENDRAL, J. M., TALAVERA, A. & VINUELA, E. 1984. Terminal and internal inverted repetitions in African swine fever virus DNA. *Virology,* 133**,** 271-5.

STEFANOVIC, S., WINDSOR, M., NAGATA, K. I., INAGAKI, M. & WILEMAN, T. 2005. Vimentin rearrangement during African swine fever virus infection involves retrograde transport along microtubules and phosphorylation of vimentin by calcium calmodulin kinase II. *J Virol,* 79**,** 11766-75.

SUN, H., JENSON, J., DIXON, L. K. & PARKHOUSE, M. E. 1996. Characterization of the African swine fever virion protein j18L. *J Gen Virol,* 77 (Pt 5)**,** 941-6.

SURVILADZE, Z., STERK, R. T., DEHARO, S. A. & OZBUN, M. A. 2013. Cellular entry of human papillomavirus type 16 involves activation of the phosphatidylinositol 3-kinase/Akt/mTOR pathway and inhibition of autophagy. *J Virol,* 87**,** 2508-17.

SUZUKI, K., KIRISAKO, T., KAMADA, Y., MIZUSHIMA, N., NODA, T. & OHSUMI, Y. 2001. The pre-autophagosomal structure organized by concerted functions of APG genes is essential for autophagosome formation. *EMBO J,* 20**,** 5971-81.

SUZUKI, K. & OHSUMI, Y. 2010. Current knowledge of the pre-autophagosomal structure (PAS). *FEBS Lett,* 584**,** 1280-6.

SZEGEZDI, E., FITZGERALD, U. & SAMALI, A. 2003. Caspase-12 and ER-stress-mediated apoptosis: the story so far. *Ann N Y Acad Sci,* 1010**,** 186-94.

SZEGEZDI, E., LOGUE, S. E., GORMAN, A. M. & SAMALI, A. 2006. Mediators of endoplasmic reticulum stress-induced apoptosis. *EMBO Rep,* 7**,** 880-5.

TAKAMATSU, H. H., DENYER, M. S., LACASTA, A., STIRLING, C. M., ARGILAGUET, J. M., NETHERTON, C. L., OURA, C. A., MARTINS, C. & RODRIGUEZ, F. 2013. Cellular immunity in ASFV responses. *Virus Res,* 173**,** 110-21.

TALLOCZY, Z., VIRGIN, H. W. T. & LEVINE, B. 2006. PKR-dependent autophagic degradation of herpes simplex virus type 1. *Autophagy,* 2**,** 24-9.

THOMAS, K. W., MONICK, M. M., STABER, J. M., YAROVINSKY, T., CARTER, A. B. & HUNNINGHAKE, G. W. 2002. Respiratory syncytial virus inhibits apoptosis and induces NF-kappa B activity through a phosphatidylinositol 3-kinase-dependent pathway. *J Biol Chem,* 277**,** 492-501.

THOREEN, C. C., KANG, S. A., CHANG, J. W., LIU, Q., ZHANG, J., GAO, Y., REICHLING, L. J., SIM, T., SABATINI, D. M. & GRAY, N. S. 2009. An ATP-competitive mammalian target of rapamycin inhibitor reveals rapamycin-resistant functions of mTORC1. *J Biol Chem,* 284**,** 8023-32.

THURSTON, T. L., RYZHAKOV, G., BLOOR, S., VON MUHLINEN, N. & RANDOW, F. 2009. The TBK1 adaptor and autophagy receptor NDP52 restricts the proliferation of ubiquitin-coated bacteria. *Nat Immunol,* 10**,** 1215-21.

TIAN, Y., WANG, M. L. & ZHAO, J. 2019. Crosstalk between Autophagy and Type I Interferon Responses in Innate Antiviral Immunity. *Viruses,* 11.

TUPPURAINEN, E. S., LUBINGA, J. C., STOLTSZ, W. H., TROSKIE, M., CARPENTER, S. T., COETZER, J. A., VENTER, E. H. & OURA, C. A. 2013. Mechanical transmission of lumpy skin disease virus by Rhipicephalus appendiculatus male ticks. *Epidemiol Infect,* 141**,** 425-30.

TUPPURAINEN, E. S., STOLTSZ, W. H., TROSKIE, M., WALLACE, D. B., OURA, C. A., MELLOR, P. S., COETZER, J. A. & VENTER, E. H. 2011. A potential role for ixodid (hard) tick vectors in the transmission of lumpy skin disease virus in cattle. *Transbound Emerg Dis,* 58**,** 93-104.

TUPPURAINEN, E. S., VENTER, E. H., COETZER, J. A. & BELL-SAKYI, L. 2015. Lumpy skin disease: attempted propagation in tick cell lines and presence of viral DNA in field ticks collected from naturally-infected cattle. *Ticks Tick Borne Dis,* 6**,** 134-40.

TYANOVA, S., TEMU, T., SINITCYN, P., CARLSON, A., HEIN, M. Y., GEIGER, T., MANN, M. & COX, J. 2016. The Perseus computational platform for comprehensive analysis of (prote)omics data. *Nat Methods,* 13**,** 731-40.

VLAHOS, C. J., MATTER, W. F., HUI, K. Y. & BROWN, R. F. 1994. A specific inhibitor of phosphatidylinositol 3-kinase, 2-(4-morpholinyl)-8-phenyl-4H-1-benzopyran-4-one (LY294002). *J Biol Chem,* 269**,** 5241-8.

WAKEFIELD, J. S., GALE, J. S., BERRIDGE, M. V., JORDAN, T. W. & FORD, H. C. 1982. Is Percoll innocuous to cells? *Biochem J,* 202**,** 795-7.

WANG, R. C., WEI, Y., AN, Z., ZOU, Z., XIAO, G., BHAGAT, G., WHITE, M., REICHELT, J. & LEVINE, B. 2012. Akt-mediated regulation of autophagy and tumorigenesis through Beclin 1 phosphorylation. *Science,* 338**,** 956-9.

WEIDBERG, H., SHVETS, E., SHPILKA, T., SHIMRON, F., SHINDER, V. & ELAZAR, Z. 2010. LC3 and GATE-16/GABARAP subfamilies are both essential yet act differently in autophagosome biogenesis. *EMBO J,* 29**,** 1792-802.

WILD, P., FARHAN, H., MCEWAN, D. G., WAGNER, S., ROGOV, V. V., BRADY, N. R., RICHTER, B., KORAC, J., WAIDMANN, O., CHOUDHARY, C., DOTSCH, V., BUMANN, D. & DIKIC, I. 2011. Phosphorylation of the autophagy receptor optineurin restricts Salmonella growth. *Science,* 333**,** 228-33.

WILKINSON, P. J., DONALDSON, A. I., GREIG, A. & BRUCE, W. 1977. Transmission studies with African swine fever virus. Infections of pigs by airborne virus. *J Comp Pathol,* 87**,** 487-95.

WILLIAMS, D. B. 2006. Beyond lectins: the calnexin/calreticulin chaperone system of the endoplasmic reticulum. *J Cell Sci,* 119**,** 615-23.

WINDSOR, M., HAWES, P., MONAGHAN, P., SNAPP, E., SALAS, M. L., RODRIGUEZ, J. M. & WILEMAN, T. 2012. Mechanism of collapse of endoplasmic reticulum cisternae during African swine fever virus infection. *Traffic,* 13**,** 30-42.

WIRAWAN, E., VANDE WALLE, L., KERSSE, K., CORNELIS, S., CLAERHOUT, S., VANOVERBERGHE, I., ROELANDT, R., DE RYCKE, R., VERSPURTEN, J., DECLERCQ, W., AGOSTINIS, P., VANDEN BERGHE, T., LIPPENS, S. & VANDENABEELE, P. 2010. Caspase-mediated cleavage of Beclin-1 inactivates Beclin-1-induced autophagy and enhances apoptosis by promoting the release of proapoptotic factors from mitochondria. *Cell Death Dis,* 1**,** e18.

WU, Y. T., TAN, H. L., SHUI, G., BAUVY, C., HUANG, Q., WENK, M. R., ONG, C. N., CODOGNO, P. & SHEN, H. M. 2010. Dual role of 3-methyladenine in modulation of autophagy via different temporal patterns of inhibition on class I and III phosphoinositide 3-kinase. *J Biol Chem,* 285**,** 10850-61.

YAMAMOTO, A., TAGAWA, Y., YOSHIMORI, T., MORIYAMA, Y., MASAKI, R. & TASHIRO, Y. 1998. Bafilomycin A1 prevents maturation of autophagic vacuoles by inhibiting fusion between autophagosomes and lysosomes in rat hepatoma cell line, H-4-II-E cells. *Cell Struct Funct,* 23**,** 33-42.

YAN, L. 2009. Abstract #DDT01-1: MK-2206: A potent oral allosteric AKT inhibitor. *Cancer Research,* 69**,** DDT01-1-DDT01-1.

YANEZ, R. J., RODRIGUEZ, J. M., NOGAL, M. L., YUSTE, L., ENRIQUEZ, C., RODRIGUEZ, J. F. & VINUELA, E. 1995. Analysis of the complete nucleotide sequence of African swine fever virus. *Virology,* 208**,** 249-78.

YANG, Z. & KLIONSKY, D. J. 2009. An overview of the molecular mechanism of autophagy. *Curr Top Microbiol Immunol,* 335**,** 1-32.

YLA-ANTTILA, P., VIHINEN, H., JOKITALO, E. & ESKELINEN, E. L. 2009. 3D tomography reveals connections between the phagophore and endoplasmic reticulum. *Autophagy,* 5**,** 1180-5.

YU, Y. & ALWINE, J. C. 2002. Human cytomegalovirus major immediate-early proteins and simian virus 40 large T antigen can inhibit apoptosis through activation of the phosphatidylinositide 3'-OH kinase pathway and the cellular kinase Akt. *J Virol,* 76**,** 3731-8.

ZHANG, F., MOON, A., CHILDS, K., GOODBOURN, S. & DIXON, L. K. 2010. The African swine fever virus DP71L protein recruits the protein phosphatase 1 catalytic subunit to dephosphorylate eIF2alpha and inhibits CHOP induction but is dispensable for these activities during virus infection. *J Virol,* 84**,** 10681-9.

ZHANG, R., CHI, X., WANG, S., QI, B., YU, X. & CHEN, J. L. 2014. The regulation of autophagy by influenza A virus. *Biomed Res Int,* 2014**,** 498083.

ZHAO, Z., THACKRAY, L. B., MILLER, B. C., LYNN, T. M., BECKER, M. M., WARD, E., MIZUSHIMA, N. N., DENISON, M. R. & VIRGIN, H. W. T. 2007. Coronavirus replication does not require the autophagy gene ATG5. *Autophagy,* 3**,** 581-5.

ZSAK, L., CALER, E., LU, Z., KUTISH, G. F., NEILAN, J. G. & ROCK, D. L. 1998. A nonessential African swine fever virus gene UK is a significant virulence determinant in domestic swine. *J Virol,* 72**,** 1028-35.

ZSAK, L., ONISK, D. V., AFONSO, C. L. & ROCK, D. L. 1993. Virulent African swine fever virus isolates are neutralized by swine immune serum and by monoclonal antibodies recognizing a 72-kDa viral protein. *Virology,* 196**,** 596-602.

Appendix I

Significant E199L interacting proteins (excl. proteasomal proteins)

Human database
Calreticulin
AN1-type zinc finger protein 2A
Glucosidase 2 subunit beta
Protein ERGIC-53
Inhibin beta A chain
Cyclin-dependent kinase inhibitor 1
Serine/threonine-protein phosphatase 2A 65 kDa regulatory subunit A alpha isoform
Large proline-rich protein BAG6
Transitional endoplasmic reticulum ATPase
Breast cancer anti-estrogen resistance protein 1
Heme oxygenase 1
Peptidyl-prolyl cis-trans isomerase FKBP10
Dihydrolipoyllysine-residue succinyltransferase component of 2-oxoglutarate dehydrogenase complex, mitochondrial
Prolyl 4-hydroxylase subunit alpha-1
Endoplasmin
Vesicular integral-membrane protein VIP36
Calnexin
Prolyl 4-hydroxylase subunit alpha-2

African green monkey database
Zinc finger AN1-type containing 2A OS=Chlorocebus sabaeus GN=ZFAND2A PE=4 SV=1
Calreticulin OS=Chlorocebus sabaeus GN=CALR PE=3 SV=1
Cyclin dependent kinase inhibitor 1A OS=Chlorocebus sabaeus GN=CDKN1A PE=4 SV=1
Protein kinase C substrate 80K-H OS=Chlorocebus sabaeus GN=PRKCSH PE=4 SV=1
Growth differentiation factor 15 OS=Chlorocebus sabaeus GN=GDF15 PE=3 SV=1
Inhibin beta A subunit OS=Chlorocebus sabaeus GN=INHBA PE=3 SV=1
Lectin, mannose binding 1 OS=Chlorocebus sabaeus GN=LMAN1 PE=4 SV=1
Peptidylprolyl isomerase OS=Chlorocebus sabaeus GN=FKBP10 PE=4 SV=1
TNF receptor superfamily member 10b OS=Chlorocebus sabaeus GN=TNFRSF10B PE=4 SV=1
Heme oxygenase 1 OS=Chlorocebus sabaeus GN=HMOX1 PE=4 SV=1
Heat shock protein 90 beta family member 1 OS=Chlorocebus sabaeus GN=HSP90B1 PE=3 SV=1
Dihydrolipoamide S-succinyltransferase OS=Chlorocebus sabaeus GN=DLST PE=4 SV=1